NULL FIELD TREATMENT OF ANTENNAS

A thesis presented for the degree of

Doctor of Philosophy

in Electrical Engineering,

in the University of Canterbury,

Christchurch, New Zealand,

by

WONG CHIN TENG, B.E.(Hons.)

1972

ACKNOWLEDGEMENTS

I am especially indebted to my supervisor, Mr R.H.T. Bates, for his guidance, patience and interest throughout this research.

I am grateful to Marian and San for their patience and understanding.

The discussions with and assistance of C.L. Anderson, A. Gulab, J.O. Williamson, F.C. Gair and W.H. Bowen; my colleagues; and the workshop staff of the Electrical Engineering Department have been invaluable.

I am also grateful to the Department of Broadcasting, Malaysia, and especially Inche Dol Ramli, for their interest and support.

I thank the External Aid Division, Ministry of Foreign Affairs, New Zealand and the Malaysian Government for the award of a Colombo Plan scholarship. The financial assistance of the University Grants Committee is gratefully acknowledged.

GLOSSARY

Symbols, notations and abbreviations

The number in brackets indicates the chapter where the symbol as defined is first used. Some of the symbols listed here (and others not listed) are also used to represent other quantities and are defined at the appropriate places in the text.

a	radius cylindrical monopole (1); radius of central cylindrical conductor of end-loaded dipole (4)
A	radii of end-plates of end-loaded dipole (4)
b	radius of circular ring of magnetic current (3)
b_o, b_1	inner and outer radii, respectively, of coaxial line (1)
B	integration constant (1); susceptance of monopole (3)
B_m	measured susceptance (4)
$\overline{B}$	computed mean susceptance (4)
C, C_-, C_+	integration contours in complex γ-plane shown in Fig. 1.5 (1)
C	generatrix of the surface of a body of revolution (1)
C_u	curve parallel to, and beneath, generatrix C (1)
$d = (\chi_1^2 - (b-a)^2)^{\frac{1}{2}}$	defined below eqn III.9 in Appendix III (3)
d	distance of fictitious surface γ from the z-axis in Fig. 4.4 (4)
D_b	difference bound (4)

$D_{p,m}$ Schmidt orthonormalisation coefficients (3)

e, exp exponential function (1)

$\underline{E}$ electric intensity (2)

E_z z-component of electric intensity (1)

$E_z(a,z)$ z-component of electric intensity on a cylindrical surface of radius a (1)

E_z^i z-component of incident electric intensity (1)

F_m expansion coefficients of partial electromagnetic field in the parallel-plate region of an end-loaded dipole driven by a magnetic frill source (4)

G scalar Green's function (2); conductance (3)

$\overline{G}$ computed mean conductance (4)

G_o scalar Green's function for free space (1)

$\underline{\underline{G}}$ dyadic Green's function for free space (2)

h height of thin excitation monopole (Appendix IV)

$h_n^{(2)}$ spherical Hankel function of second kind and integer order n (3)

H dipole semi-height or monopole height (1)

$H_o^{(2)}$ zeroth order Hankel function of second kind (1)

$\underline{H}$ magnetic intensity (2)

$\underline{H}^i$ magnetic intensity incident on an antenna (1)

I_o modified Bessel function of first kind and zeroth order (1)

$I_o(z)$ total longitudinal current on cylindrical antenna (1)

$I(\xi) = 2\pi\rho'(\xi)K(\xi)$ total current along a meridian of an antenna body of rev ution (1)

Im[F] imaginary part of complex quantity F(3)

$\underline{\underline{I}}$ unit dyadic (2)

$j = \sqrt{-1}$ imaginary number (1)

j_n spherical Bessel function of integer order n (3)

J_o Bessel function of zeroth order (1)

$\underline{J}$ applied electric volume current density (2)

$\underline{J}^m$ applied magnetic volume current density (2)

$k = \omega(\mu\varepsilon)^{\frac{1}{2}}$ wavenumber (2)

$k_o = \omega(\mu_o\varepsilon_o)^{\frac{1}{2}}$ free space wavenumber (1)

$k_m = \left(k_o^2 - (\frac{m\pi}{W})\right)^{\frac{1}{2}}$ (4)

K_o, K_1 modified Bessel functions of second kind and orders 0 and 1 respectively (1)

K_m expansion coefficients of $K(\xi)$, which is expanded in a basis (expansion) set of functions $\varphi_m(\xi)$ (3)

$K(\xi)$ electric surface current density flowing along a meridian of an axially symmetric solid dipole (3)

$\underline{K}_s$ electric surface current density (2)

$\underline{K}_s(\xi)$ electric surface current density on generatrix C (4)

$K^{(p)}(\xi)$ superscript denotes "p^{th} derivative of $K(\xi)$ with respect to ξ" (3)

$K_{z,m}(\xi)$ m^{th} Fourier expansion coefficient of the z-component of $\underline{K}_s(\xi)$ (Appendix IV)

$K_{\varphi,m}(\xi)$ m^{th} Fourier expansion coefficient of the φ-component of $\underline{K}_s(\xi)$ (Appendix IV)

ℓ integer number defined by $\ell < \frac{k_o W}{\pi} < \ell+1$ (4)

L half-length of generatrix C (1)

$\underline{L}^{(q)}_{\sigma mn}, \underline{M}^{(q)}_{\sigma mn}, \underline{N}^{(q)}_{\sigma mn}$ spherical vector wavefunctions defined in Appendix I (2)

M number of basis functions $\varphi_m(\xi)$ used in approximati $K(\xi)$ (3); also size of square solution matrix (3)

M_c convergence number defined at end of section 3.5 (3)

M_1 number of basis functions $\varphi_m(\xi)$ used in approximating $K(\xi)$ on end plates (4)

M_2 truncation number of infinite series in eqn (4.21) (4)

O origin of coordinate origin (1)

$O(\|Z\|)$ order of magnitude of normalised determinant $\|Z\|$ (3)

P arbitrary point in space (1)

P_n^1 Legendre function of degree 1 and integer order n (3)

$Q = Q(\rho',\varphi',z')$
$= Q(\eta=0,\varphi',\xi)$ } { arbitrary point on generatrix C of an axially symmetric solid dipole (3)

Q_0,Q_1,Q_2,Q_3 points on generatrix C (3)

$Q(\xi)$ function defined by eqn (3.43) (3)

(r,θ,φ) spherical polar coordinates (3)

$\underline{r}$ position vector of P (1)

$\underline{r}'$ position vector of a point at the applied sources, $\underline{J}$ and $\underline{J}^m$, or on surfaces α, β,β_1,β_2, γ, S_o,S_i,S_1,S_2 S_a and S_p (1)

R distance between points denoted by $\underline{r}$ and $\underline{r}'$

Re[F] real part of complex quantity F (3)

s surface element (1)

S_1 integral function defined in eqn (1.23) (1)

S_0,S_i,S_1,S_2,S_a,S_p fictitious surfaces (2)

t time

T_m Tchebyshev polynomial of integer order m (3)

TEM denotes transverse electromagnetic (1)

TE_{11} refers to transverse electric mode in a coaxial transmission line (1)

u	width of radial transmission line (3)
v	volume element (2)
V_o, V_1, V_2	volume regions (2)
w_n	testing functions defined in Appendix II (3)
$2W$	end-plates separation (4)
(x,y,z)	Cartesian coordinates(1)
y_n	spherical Neumann function of integer order n (2)
Y	admittance (1)
Y_m	measured admittance (4)
$\bar{Y}$	computed mean admittance (4)
Y_o	Neumann function of zeroth order (1)
ζ	distance of magnetic ring source along z-direction (3)
z_n	denotes points along dipole axis inside the dipole (3)
z_p	position, along z-axis, of the perfectly conducting plate in the interior of a hollow cylindrical monopole (5)
Z_o	intrinsic wave impedance, and equals 120 π ohms for free space (1)
$Z(z,\xi)$	kernel of integral equation of first kind (3)
$[Z_{nm}]$	square solution matrix of size M x M and with elements Z_{nm}(3)
$[Z_{nm}]^{-1}$	matrix inverse of $[Z_{nm}]$ (3)
$\|\|Z\|\|$	normalised determinant of $[Z_{nm}]$ defined in section II-2 of Appendix II (3)

α, γ complex variables (1)

α, β, γ fictitious surfaces (2)

β_1, β_2 fictitious surfaces (4)

$\beta = \sqrt{k_o^2 - \alpha^2}$

$\gamma_n = \sqrt{k_o^2 - \left(\frac{\chi_{o,n}}{a}\right)^2}$ (1)

Γ integration contour (1); fictitious surface (5)

δ Dirac delta function (1)

$\varepsilon, \varepsilon_o$ permittivities of arbitrary medium and free space respectively (1)

ε_m Neumann factor, equals 1 when m = 0, and equals 2 when m = 1,2,3,... (2)

ζ integration variable

(η, φ', ξ) local surface coordinates on axially symmetric solid antenna (1)

λ free space wavelength (1)

μ, μ_o permeability of arbitrary medium and free space respectively (1)

ξ tangent to generatrix C (1); also denotes arc-length along C (1)

ξ_2 arc-length between points Q_1 and Q_2 in Fig. 4.4 (4)

$\pi = 3.141592653589793$ (1)

(ρ, φ, z) cylindrical polar coordinates (1)

ρ electric volume charge density (2)

ρ^m magnetic volume charge density (2)

σ conductivity (2)

$\sigma = e$ denotes even φ-variation (cos $m\varphi$) (2)

$= o$ denotes odd φ-variation (sin $m\varphi$) (2)

τ radius of curvature of corners at end of thick solid dipole shown in Fig. 3.7 (3); also radius of curvature of edge of circular end-plates shown in Fig. 4.5 (4)

φ_m basis (expansion) functions for approximating $K(\xi)$ (3)

$\Phi = (\varphi - \varphi')$ (1)

χ_n zeros of zeroth order Neumann function (3)

$\chi_{o,n}$ zeros of zeroth order Bessel function (1)

ψ angle which the normal unit vector $\hat{\eta}$ makes with z-axis (1)

$\Psi(\alpha), \Psi_-(\alpha)$ Fourier transforms defined in eqns (1.9) and (1.10) respectively (1)

ω radian (angular) frequency (1)

$\cup$ union of surfaces (2)

∇ vector gradient operator (1)

$\nabla\wedge$ vector curl operator (1)

$\nabla\cdot$ vector divergence operator (1)

$\hat{x}$ unit vector in x-direction (1)

$\underline{X}$ vector of amplitude X (1)

$|K(\xi)|$ magnitude of $K(\xi)$ (3)

$\underline{/K(\xi)}$ phase of $K(\xi)$ (3)

METHOD 1 defined by eqns (3.21) and (3.34) (3)

METHOD 2 defined by eqns (3.25) and (3.36) (3)

METHOD 1A defined by eqns (VI.1) and (VI.3) of Appendix VI (5)

METHOD 2A defined by eqns (4.13) and (4.17) (4).

TABLE OF CONTENTS

PREFACE

The cylindrical metallic antenna not only has a long and interesting history, but is also a subject of current interest. Until a few years ago there were few treatments of cylindrical antennas with radii greater than one-fiftieth of the free space wavelength (λ). Most of these treatments have used direct numerical methods of solution. An exception is Bach Andersen's method (Bach Andersen, 1968, 1971; Bach Andersen and Yee, 1969), in which the travelling wave theory leads to a simple expression for the admittance of the tubular cylindrical monopole. It is difficult to extend the travelling wave theory to thick antennas with arbitrarily shaped ends.

This thesis is concerned with applying the extended boundary condition to electrically thick antennas. Detailed exposition is restricted to circularly symmetric, symmetrically fed antennas.

The usual extended boundary (or null field) condition states that, when a perfectly conducting closed surface is excited externally (or internally), the total electromagnetic field is zero in the interior (or exterior). The region in which the total field is zero is called a "null field region". The extended boundary condition can be generalised to regions other than those bounded by perfectly conducting surfaces. The generalisation can be made by appealing to Love's field equivalence principle (Collin, 1969) or the vector Hemholtz integral formulas for electromagnetic fields (Stratton, 1941, Section 8.14; Waterman, 1969a, 1971), which postulate fictitious null field regions.

Chapter 1 reviews the literature on electrically thick cylindrical antennas. Previous treatments of solid cylindrical antennas with radii greater than $\lambda/6$ formulate the antenna problem in terms of integral equations involving numerically troublesome double integrals, which can be avoided by applying the extended boundary condition as described herein.

Chapter 2 describes Waterman's (1965, 1969a, 1971) extended integral equation formulation, which is a generalization of the usual extended boundary condition and is applicable to arbitrary diffracting bodies. Here, the formulation is extended to null field regions of arbitrary shape. This has been done to construct "extended" integral equations which lead to practicable numerical solutions for the end-loaded dipoles treated in chapter 4.

In chapter 3, the usual null field condition is applied to symmetrically fed, axially symmetric solid dipoles. The null field region is chosen to coincide with the antenna body. Two essentially distinct methods, METHODS 1 and 2, are developed. METHOD 1 employs the extended boundary condition on the dipole axis. METHOD 2 expands the total electromagnetic field in spherical vector wave functions and then requires it to be zero inside an inscribed sphere in the dipole. Both methods lead to sets of integral equations involving single line integrals with well-behaved nonsingular kernels. The integral equations are solved numerically by the general method of moments (Harrington, 1968, chap.1), with the surface current density expanded in various basis (expansion) sets of functions. The functions in one of the basis sets

have analytic properties suitable for expanding the current density at sharp corners. The two methods lead to practicable numerical solutions for dipoles with length to maximum diameter ratios from about 0.25 to 25, and with maximum diameters of about 2λ. Measurements have been made to check the numerical computations. Both methods are compared computationally with methods previously reported in the literature.

End-loaded dipoles (or monopoles) are examined in chapter 4. Many of the previous calculations of the characteristics of such antennas use assumed current distribution (cf. Wait, 1969b). Rigorously based computations have recently (Kalafus, 1971) been reported for an electrically small end-loaded dipole with a maximum dimension of 0.08λ. Andrews (1968) has used ray-optical techniques to treat dipoles with disc end-plates of diameters greater than a wavelength. In applying the extended integral formulation here, the null field region chosen includes, besides the region occupied by the dipole, a part of the parallel-plate region which lies between the end-plates. A method, called METHOD 2A because of its close correspondence to METHOD 2, is developed in which the total electromagnetic field is expanded in spherical vector wave functions and is then required to be zero inside a sphere in a chosen null field region. Two types of circular end-plates are considered: (1) electrically thick with rounded edges; and (2) electrically thin circular discs. The surface current density on the thick end-plates is obtained in terms of two sets of basis functions. For disc end-plates, a basis set of

Bessel functions, which satisfy the electromagnetic edge conditions at the circular edges of the discs, is used to represent the surface current density. METHOD 2A leads to practicable numerical solutions (denote the dipole semi-height by H and the end-plate radius by A) in the range $H/A < 2$, $A < 0.5\lambda$ for dipoles with thick end-plates, and $0.25 < H/A < 0.4$, $A < 0.4\lambda$ for dipoles with disc end-plates.

Conclusions on the practicability of the formulation as applied in chapters 3 and 4 are drawn in chapter 5, which also gives some suggestions for further research. Two of the antennas suggested for investigation are: (a) the coaxially-fed infinite conical monopole, and (b) the hollow cylindrical monopole with a circular plate short-circuiting the interior anywhere along the length of the monopole. Antenna (a) is of interest because it appears that the broad-band design of the input regions of coaxially fed conical monopoles has not been treated. Antenna (b) has so far been treated for only two cases: viz. the shorting plate is flush with the ground plane on which the monopole is mounted (Chang, 1968a, 1968b), or it is well inside the central conductor of the coaxial line feeding the monopole (Bach Andersen, 1968, 1971; Bach Andersen and Yee, 1969). The procedures for setting up the appropriate integral equations (using the extended integral equation formulation) are outlined in the chapter. Lastly, an analysis in Appendix VI shows that Einarsson's (1963, 1966) method could be suitable for treating the cylindrical monopole radiating into an infinite parallel-plate region.

The computations in chapters 3 and 4 have been carried out on the University of Canterbury IBM 360/44 machine, which has 128 Kbytes of core memory (1 byte = 8 bits). Except for

the standard IBM subroutines, the computer programs used have been written by the author. These programs are in FORTRAN IV. Double precision arithmetic (i.e. 8-byte words) is used in the computations.

CHAPTER 1

REVIEW OF LITERATURE ON THICK CYLINDRICAL ANTENNAS

1.1 INTRODUCTION

In this thesis a thick cylindrical antenna is one in which the radius is greater than 0.02 of the electrical wavelength (λ). When the radius is less than 0.02λ, the antenna is considered to be thin.

Before the advent of high speed electronic computers practically all the success made with cylindrical antennas had been confined to the electrically thin antennas, where small radius approximations greatly reduce the computational effort in obtaining quantitative solutions to the integral equations, e.g. Hallen's equation (reviewed in King, 1956; Hurd, 1969). Recently there has been a growing number of papers presenting quantitative results on thick antennas. The thick antennas (cf. King and Wu, 1967) have become increasingly important in a variety of applications that include broadband antennas, millimetre-wave and microwave monopoles, missiles, and various metal structures used as transmitting and receiving elements, and problems that relate to radio-frequency hazards in rockets.

This review has two motivations. Firstly, there has been no review of literature pertaining to these antennas; only brief references to some of the papers can be found in Bakhrakh et al. (1967), Chang (1968a), Hurd (1969), and Jacobsen and Hurd (1970). Secondly, we will be comparing our contributions (presented in chapter 3) with the existing methods for treating such antennas.

The papers which present quantitative results on the isolated transmitting cylindrical antenna of finite length and radius larger than 0.02λ are Vasil'ev (1959), Gavorun (1962), Einarsson (1963, 1966), Vasil'ev and Seregina (1963), Vasil'ev et al. (1967a, 1967b), Chang (1967, 1968a, 1968b), Otto (1968b), Bach Andersen and Yee (1969), Ting (1969), Hurd (1969), Jacobsen and Hurd (1970), and Bach Andersen (1971). Taken together, the results cover both the hollow and the solid cylinders of arbitrary dimensions. In section 1.2, we review the papers whose methods depend on the cylindrical geometry of the antenna. Section 1.3 concerns papers which use methods applicable to any arbitrary shaped solid antenna body of revolution. For convenience, we have confined the short discussions on the methods used to the perfectly conducting antenna under circularly symmetric, monochromatic (angular frequency ω) excitation, and having induced surface currents which flow longitudinally (on the hollow cylinder) or along the meridians (on the solid body of revolution).

1.2 METHODS DEPENDENT ON CYLINDRICAL GEOMETRY

1.2.1 Travelling Wave Theory

In the travelling wave theory for cylindrical antennas the current on the longitudinal wall is first resolved into an outgoing wave (due to the excitation source), plus an infinite series of waves multiply-reflected from the ends. The problem, then, consists of determining each reflected wave for an incoming wave which has been found previously. For the hollow perfectly conducting tubular dipole fed symmetrically by a delta gap source, Hallen (1961; 1962, chap. 35 and supplement) has obtained a formally exact travelling

wave solution by solving his well-known integral equation by the Wiener-Hopf procedure (Noble, 1958). A simpler derivation can also be found in Einarsson (1963). As the exact solution contains a (N-1)-dimensional integral with complicated integrands for the Nth reflected wave, it has only been evaluated numerically for thin antennas where small radius approximations in the integrands could be made (Hallen, 1962, chap. 35). Earlier (Hallen, 1956), the reflection from the open end of a semi-infinite tube for a current wave (on the outer surface only) coming from infinity had been obtained. In comparing the waves, Hallen (1962, Section 35.7) found that, (a) representing the reflected waves on the finite tube by the reflected wave on the semi-infinite tube was "a very insignificant approximation" (sic.) and (b) at points not too close to the ends the reflected waves could not be distinguished from a wave originating from the delta gap source on an infinite cylinder. This comparison justifies his earlier computations on the current distributions, using the approximations just mentioned (Hallen, 1953; Chen and Keller, 1962). It should be noted that the "end admittance $Y_e^e(0)$", viz. the ratio between the current wave reflected at the end and the corresponding scalar potential wave, for the semi-infinite tube was computed accurately by Hallen (1956) for radii up to 0.07λ.

More recently, the travelling wave theory was applied by Bach Andersen (1968, 1971), and Bach Andersen and Yee (1969) to the cylindrical metallic, dielectric or plasma monopole, which is mounted on an infinite ground plane and excited by an incoming TEM or TE_{11} mode in a coaxial transmission line.

For the perfectly conducting hollow monopole of Fig. 1.1 fed by an incoming TEM mode, an expression for the admittance which took account of the coaxial line-antenna coupling, was derived with approximations similar to those of Hallen's (1953) above. Instead of defining the admittance at the coaxial aperture in the ground plane (cf. King, 1955; Chang and Wu, 1968; Otto, 1965, 1967), Bach Andersen defined it inside the coaxial line at a reference plane some multiples of a half-wavelength from the aperture. By introducing the concept of an "effective gap source" (physically at the end) for each reflected current wave, the coaxial line-antenna coupling became known when the field at the reference plane, due to each effective gap source, was found by means of the reciprocity theorem (Harrington, 1961, Section 3.8).

The expression found is

$$Y = Y_\infty - \frac{2[Y_o^e(H)]^2}{Y_e^e(0) + Y_o^e(2H)} \; ; \qquad (1.1)$$

where H is the length of the monopole; Y_∞ is the admittance of the corresponding infinite antenna; $Y_o^e(z)$ is the wave admittance of the outgoing wave on the outer surface of the infinite cylinder; and $Y_e^e(0)$ is the end admittance of a semi-infinite cylinder when the incident current wave (on the outer surface only) comes from infinity.

It is interesting that this expression can also be obtained by ignoring the coaxial line-antenna coupling. The admittance was computed (Bach Andersen, 1968) by using the asymptotic forms of $Y_o^e(H)$, $Y_o^e(2H)$ and Hallen's (1956) values for $Y_e^e(0)$. It agreed to better than 5% with those obtained from measurements (Bach Andersen, 1968, Fig.6). $Y_e^e(0)$ was

found later (Bach Andersen and Yee, 1969) by ray-optical techniques for monopoles having radii larger than 0.2λ. The conductances calculated (Bach Andersen and Yee, 1969) from the latter $Y_e^e(0)$ for various monopole lengths (H) and radii 0.217λ were compared with the values got by Chang (1968a, 1968b). The comparison showed that the agreement was better than 1% for H = 0.5λ (see Fig. 1.1) and within 10% for H as short as 0.125λ.

It seems unfair for Bach Andersen and Yee (1969) to compare their results with those of Chang's (1968a, 1968b) when there is a physical difference between the monopoles considered (cf. Figs 1.1 and 1.2). The expression (1.1) applies to monopoles whose hollow interior extends into the coaxial line so that the reflected current waves on the inside surface play no part in calculating the strengths of the effective gap sources. Chang, on the other hand, considered the hollow monopole with a perfectly conducting plate across the interior as shown in Fig. 1.2. If the latter monopole were treated by the travelling wave theory the waves inside would be reflected by the plate and lead to a different admittance expression from (1.1). However, if the monopole were thin, long or both, i.e. the waves inside are all exponentially damped, only a small difference would be involved in using (1.1). Since the admittance given by (1.1) can be obtained by ignoring the coaxial-line-antenna coupling, it can be shown that the admittance of Chang's monopole is given by

$$Y = Y_\infty - \frac{2[Y_o^e(H)]^2 Y_e(0)}{Y_e^e(0)[Y_e(0) + Y_o(2H)]} \; ; \qquad (1.2)$$

where $Y_o(z)$ is the wave admittance of the outgoing wave on both surfaces of the infinite cylinder, and $Y_e(0)$ is the end admittance of the semi-infinite cylinder, when the incident wave (on both surfaces) comes from infinity. It appears that no attempt to evaluate $Y_e(0)$ has been made.

Lee and Mittra (1969) derived a modified Wiener-Hopf equation for a semi-infinite solid cylinder when an incident current wave comes from infinity. This equation was solved by pairing the various singularities in the lower half complex plane. The solution led to an approximate expression for the end admittance $\overline{Y}_e^e(0)$ in terms of the end-admittance $Y_e^e(0)$ for the semi-infinite tubular cylinder,

$$\overline{Y}_e^e(0) = Y_e^e(0)\ (S(k_o))^{-1};$$

where $S(k_o)$ was to be determined from an infinite set of algebraic equations. When the solid cylinder is electrically thin ($k_o a \ll 1$), $S(k_o)$ has the simple form

$$S(k_o) \approx 1 + j\,\frac{\pi k_o a}{12} \qquad \text{for} \quad k_o a \ll 1.$$

By using the travelling wave theory and Hallen's (1953) approximations, an expression, which is similar to (1.1), was obtained by Lee and Mittra (1969) for the admittance of a solid dipole, which was symmetrically fed by a unit-amplitude voltage source across a small gap. Numerical results were presented for dipoles with radii $a = 0.04\ k_o^{-1}\lambda$ and lengths between $\lambda/3$ and 5λ.

1.2.2 Integral Equations for the Electric Field

Instead of taking the current as the fundamental unknown, Einarsson (1963) and Hurd (1964) independently employed an integral equation for the longitudinal component

of electric intensity on the infinite cylindrical extension of a tubular antenna (see Fig. 1.3). From this different point of view Einarsson rederived Hallen's (1961) solution and showed that the Fourier transform of the current is the solution of an integral equation of the second kind. The generalisations to off-centre feeding, and passive receiving antennas were also discussed. To obtain the current, Einarsson used a numerical technique. Later, the solid antenna was analysed (Einarsson, 1966) and the current distributions compared in the tubular and solid cylinder cases. Hurd initially derived a variational expression for the admittance of the long thin antenna, from the integral equation. Later (Hurd, 1966), an associated integral equation for the Fourier transform of the electric field was obtained by the Wiener-Hopf procedure. This was solved by an asymptotic technique valid for long antennas, but which worked well for dipole half-lengths as short as $\lambda/3$ and as thick as $\lambda/6$ (Hurd, 1966; Jacobsen and Hurd, 1970). The generalisation to off-centre feeding, non-delta gap sources, and sleeve monopoles were treated by Hurd (1969).

Consider the tubular and the solid cylindrical dipoles, which have the geometry shown in Fig. 1.3, fed symmetrically by a delta gap source, $E_z(a,z) = -\delta(z)$, of angular frequency ω. Einarsson (1963, 1966) obtained the equations for the electric field on the antenna extension of the tubular and the solid cylindrical dipoles, respectively, as

$$I_o(z) = \int_0^\infty E_z(a,H+\zeta)[I_o(z-H-\zeta) + I_o(z+H+\zeta)]d\zeta, \quad |z| \geq H; \quad \text{tubular antenna;} \qquad (1.3)$$

$$I_o^e(z) = \int_0^\infty E_z(a,H+\zeta)[I_o(z-H-\zeta) + I_o^e(z+H+\zeta) + I_o^i(z-H-\zeta)]d\zeta;$$

$$z > H; \quad \text{solid antenna;} \qquad (1.4)$$

$$I_o^e(z) = \frac{jk_o a}{Z_o} \int_\Gamma \frac{\exp(j\alpha z)}{\sqrt{\alpha^2-k_o^2}} \frac{K_1(a\sqrt{\alpha^2-k_o^2})}{K_o(a\sqrt{\alpha^2-k_o^2})} d\alpha \; ; \qquad (1.5)$$

$$I_o^i(z) = \frac{2\pi jk_o a}{Z_o} \sum_{n=1}^{\infty} \frac{\exp\left(-\frac{|z|}{a}\sqrt{\chi_{o,n}^2 - (k_o a)^2}\right)}{\sqrt{\chi_{o,n}^2 - (k_o a)^2}} \; ; \qquad (1.6)$$

$$I_o(z) = I_o^e(z) + I_o^i(z) \; ; \qquad (1.7)$$

where $Z_o \triangleq 120\pi$ ohms; $\chi_{o,n}$ is the n^{th} root of $J_o(\chi) = 0$; the integration contour Γ is shown in Fig. 1.4; and J_o, K_o and K_1 are Bessel and modified Bessel functions. Once $E_z(a,H+\zeta)$, $\zeta \geqslant 0$ is known, the total current $I(z)$ on the antenna can be obtained by straightforward integration. Both equations (1.3) and (1.4) were solved by the same numerical technique, which involved a point-matching procedure to determine the coefficients of a series expansion of the field. The edge singularities of the field at the antenna ends were accounted for by requiring one term of the series to possess the correct edge behaviour. This resulted in having to solve, by matrix methods, a finite system of simultaneous algebraic equations. Current distributions and radiation patterns for both tubular and solid antennas with radii of 0.01λ, 0.033λ, and 0.10λ were presented (Einarsson, 1966). The current distributions were quoted as being accurate to within 0.5%.

The numerical solutions of equations (1.3) and (1.4) become increasingly difficult as the antennas become thicker. As the radius increases, the unknown $E_z(a,H+\zeta)$ decays more

slowly along ζ, so that more series expansion terms are required to approximate it accurately. Since the evaluation of the coefficients of the system of algebraic equations involve semi-infinite integrals and singular quantities, i.e. $I_o^e(z)$ and $I_o^i(z)$ which are singular at $z = 0$, numerical solutions become impracticable for thick ($a > 0.15\lambda$) antennas.

For antennas with the same radii, the number of algebraic equations which have to be solved remains the same for any antenna length H. This represents a significant advantage over other methods that use integral equations in the unknown antenna current (Vasil'ev, 1959; Vasil'ev and Seregina, 1963; Chang, 1967, 1968a, 1968b; Vasil'ev et al., 1967a; Mautz and Harrington, 1969) which involve an increasing number of algebraic equations as the antenna length increases. Another advantage of Einarsson's (1963, 1966) technique is the "insensitiveness" of the antenna current to small errors in the electric field $E_z(a,H+\zeta)$. In other words, a first order error in $E_z(a,H+\zeta)$ is reflected as a second order error in the antenna current (Einarsson, 1966).

Otto (1968b) has generalised Einarsson's (1966) analysis to the monopole fed by a coaxial and a radial transmission line over an infinite ground plane, and the monopole immersed in an homogeneous conducting medium. Instead of solving $E_z(a,H+\zeta)$ directly from equations (1.3) and (1.4), Otto computed the electric field (of unknown constant amplitude) on the antenna axis by integration, from an assumed current distribution. The electric field thus found was modified by a multiplicative factor designed to give the correct singularity at the end of the monopole, and the unknown

amplitude determined by satisfying (1.3) and (1.4) respectively, at the point z = H. This new electric field was then used to obtain the current distribution by simple integration.

For the tubular dipole (as in Fig. 1.3) of length 2H and fed symmetrically by the delta gap source, $E_z(a,z) = -\delta(z)$, $|z| < H$, Hurd (1966) used the Wiener-Hopf procedure (Noble, 1958) to derive an associated integral equation given by

$$f(-\alpha) + \frac{1}{2\pi j}\int_{C_+} \frac{\exp(-j2\gamma H) f(\gamma)\Psi(\gamma)}{(\gamma-\alpha)\Psi_-^2(\gamma)}\, d\gamma$$

$$= \frac{1}{2\pi j}\int_{C_+} \frac{\exp(-j\gamma H)\Psi(\gamma)}{(\gamma-\alpha)\Psi_-(\gamma)}\, d\gamma \ ; \qquad (1.8)$$

where C_+ is the contour shown in Fig. 1.5, and α and γ are complex variables. The quantity $f(-\alpha)$ is the unknown, and is related to the electric field $E_z(a,z)$ on the antenna extension via

$$f(\alpha) = \Psi_-(\alpha)\, e^{j\alpha H}\int_H^\infty e^{-j\alpha z}\, E_z(a,z)dz.$$

$\Psi(\alpha)$ and $\Psi_-(\alpha)$ are explicitly given by,

$$\Psi(\alpha) = \frac{2\pi}{\left[\sqrt{k_o^2-\alpha^2}\; J_o\left(a\sqrt{k_o^2-\alpha^2}\right)\; H_o^{(2)}\left(a\sqrt{k_o^2-\alpha^2}\right)\right]} \ ; \qquad (1.9)$$

$$\Psi_-(\alpha) = \exp\left\{\frac{1}{2\pi j}\int_{C_-} \frac{\ell n[\Psi(\alpha)]}{(\gamma-\alpha)}\, d\gamma\right\}. \qquad (1.10)$$

When $f(\alpha)$ is known, the total current on the antenna can be evaluated from

$$I(z) = I_\infty(z) - \frac{2k_o}{\pi^2 Z_o}\int_\Gamma \Psi(\alpha).\exp[-j\alpha(H-z)].\frac{f(\alpha)}{\Psi_-(\alpha)}\, d\alpha, \ |z| < H; \qquad (1.11)$$

where the contour Γ is shown in Fig. 1.4, and $I_\infty(z)$ is the current on the corresponding infinite tubular antenna.

To take advantage of the exponential terms in (1.8) and (1.11), Hurd deformed the contour C_+ into the branch-cut contour C in Fig. 1.5. In deforming the contour, the poles of $\Psi(\gamma)$, corresponding to the zeros of $J_o(\chi_{o,n})$, were crossed. As the antenna radius was assumed small, and the poles occurred at large negative imaginary values of γ i.e.

$$\gamma_n = \sqrt{k_o^2 - \left(\frac{\chi_{o,n}}{a}\right)^2} \ ,$$

only the first term of the residue series was retained. The next step taken was to express $f(\gamma)$ inside the integral in (1.8) as a Taylor's series about the point $\gamma = k_o$. To determine $f(\gamma)$ at γ_1 and its (N-1) derivatives at $\gamma = k_o$, (N+1) algebraic equations were required. One equation came from setting $\alpha = -\gamma_1$ in (1.8). The others were obtained by first taking the zeroth, first, second,..., (N-1)th derivative of (1.8) with respect to α, and then setting $\alpha = -k_o$. A maximum of four equations was used by Hurd (1966, 1969) and Jacobsen and Hurd (1970), to obtain admittances valid for dipole half-lengths as short as $\lambda/6$ and radii at least up to $\lambda/6$. No accuracy figures were, however, given for these admittance values.

For this method of numerical solution, the integrals which have to be evaluated have one of the three following forms:

$$F_n(H) = \frac{1}{2\pi j} \int_C \exp(-j\gamma H)\Psi(\gamma)(\gamma - k_o)^n d\gamma; \qquad (1.12)$$

$$F_n(2H) = \frac{1}{2\pi j} \int_C \exp(-j2\gamma H)\Psi(\gamma)(\gamma - k_o)^n d\gamma; \qquad (1.13)$$

$$T_n = \frac{1}{2\pi j} \int_{C_-} \frac{\ell n[\Psi(\gamma)]}{(\gamma - k_o)^n} \, d\gamma \, . \qquad (1.14)$$

It is these integrals which have restricted the method to the lengths and radii considered by Hurd and Jacobsen. The comments made on the method used by Einarsson (1963, 1966) apply equally here.

1.2.3 Hallen's Equation and a Particular Numerical Method of Solution

Chang (1967) presented a numerical solution to Hallen's (1938) exact integral equation for the current on tubular cylindrical dipoles. Later (Chang, 1968a, 1968b) the tubular monopole driven by a coaxial line excited in the TEM mode was studied theoretically and experimentally. The integral equation which was derived differed from that of Hallen by an extra source term, which had earlier been obtained by Otto (1965, 1967). Numerical results on the current distributions and admittances were given for monopole lengths and radii of up to 0.5λ. Extension to the hemispherically capped monopole with radius less than 0.15λ was carried out by Ting (1969). The numerical procedure presented by Chang (1967) has also been used by Kao (1970a) to solve the integral equations for the three-dimensional scattering from a circular tube of finite length.

For the tubular monopole shown in Fig. 1.2 with an assumed radial electric field in the coaxial aperture, given by the TEM coaxial line mode, the integral equation for the total current $I(z)$ on the antenna is;

$$\int_0^H I(z') \int_0^\infty H_o^{(2)}(\beta a) J_o(\beta a) \cos\alpha z' \cos\alpha z \, d\alpha \, dz'$$

$$= B \cos k_o z + \frac{j2\pi V}{Z_o \ell n(b_{1/a})} \int_0^z \sin k_o(z-z')$$

$$\times \left\{ \int_0^\infty [H_o^{(2)}(\beta a) - H_o^{(2)}(\beta b_1)] \, J_o(\beta a) \cos\alpha z' \, d\alpha \right\} dz',$$

$$|z| < H \; ; \qquad (1.15)$$

where V is the voltage applied across the aperture; $\beta = \sqrt{k_o^2 - \alpha^2}$; α is a complex variable; and B and I(z) are unknown quantities.

To solve equation (1.15) numerically the antenna length was first divided into N segments. Within each segment the current was approximated by a parabolic distribution. A point-matching procedure was then used to set up (2N+1) algebraic equations for determining the constants B and the current at the centres and end points of the segments. Chang (1967) showed that the $(4N^2+2N)$ matrix coefficients related to the current could be obtained from a linear combination of 12N "moment functions", which have the form,

$$j \int_0^{k_o} \frac{G_s(m,-\alpha)}{-\alpha} J_o^2(\beta a) d\alpha + \int_0^\infty \frac{G_s(m,-j\alpha)}{-j\alpha} J_o^2(a\sqrt{k_o^2 + \alpha^2}) d\alpha; \quad (1.16)$$

where the $G_s(m,\alpha)$ are simple combinations of elementary functions.

The numerical procedure of Chang has two obvious advantages; the more important one being the linear, rather than quadratic, dependence of the number of moment functions on the matrix size. The other concerns the integrable singularity in the kernel of the integral equation, which leads to matrices with strongly dominant diagonals.

Ting (1969) placed a hemispherical cap on the cylinder and added the term

$$\frac{-2\pi}{Z_o} \int_0^z E_{zc}(z') \sin k_o(z-z')dz', \qquad (1.17)$$

to the left hand side of the integral equation (1.15) with $E_{zc}(z')$ being the axial electric field on the outer cylindrical surface, due to the current on the end cap. In order to retain the advantages of Chang's (1967) numerical technique, the end cap current was approximated by a sinusoidal distribution with constant phase. The latter approximation meant that only antennas with radii less than 0.15λ could be treated by Ting's approach. A comparison (Ting, 1969) of the computed and the measured admittances for the monopoles of various lengths and radii 0.051λ and 0.063λ showed that agreement was to better than 10% or 2 millimhos.

1.3 METHODS APPLICABLE TO ANY ANTENNA BODY OF REVOLUTION

The solid, arbitrary shaped body of revolution, of which the solid cylinder is a special case, has been studied as a scatterer by many researchers (e.g. Andreasen, 1965; Waterman, 1965, 1971; Garbacz, 1965). It appears that the transmitting antenna problem was first considered by Albert and Synge (1948), who applied the Lorentz reciprocity relation (cf. Harrington, 1961, Section 3.8) to obtain an exact integral equation for the current. Synge (1948) solved this integral equation by means of a variational technique, and obtained results which were valid for thin cylindrical antennas. By using the Stratton-Chu integral formulae (Stratton, 1941, Section 8.14) for the general electromagnetic

field, Gavorun (1959) obtained two sets of integral equations for the antenna with a surface impedance condition and under arbitrary excitation. One of these sets of equations was derived by using the surface boundary condition which states that the surface current density is the vector cross-product of the surface unit normal vector and the magnetic intensity on the antenna surface. The other set was derived by setting the field zero on the antenna axis inside the antenna body. For the zeroth harmonic of the meridional current on the perfectly conducting antenna, the integral equation was identical to that of Albert and Synge (1948). It was solved numerically for cylindrical antennas with plane ends and radii of less than 0.04λ (Gavorun, 1962). Vasil'ev (1959) also derived the first set of Gavorun's equations for the perfectly conducting antenna, and obtained numerical solutions to hemispherically-capped cylindrical dipoles of radii up to 0.3λ. Later (Vasil'ev and Seregina, 1963), current distributions were given for the thick dipole (radius greater than 0.1λ) with different shapes of end surfaces. On account of the singularity in the kernels of his equations, Vasil'ev et al. (1967a) later treated the antenna by the method of Albert and Synge (1948), using the Lorentz reciprocity relation. In general, this latter method leads to integral equations which have kernels defined by the choice of "auxilliary sources". Unlike Albert and Synge (1948), who chose an elementary electric dipole on the antenna axis, Vasil'ev et al. (1967a) considered rings of electric and magnetic azimuthal, axial and radial currents beneath the antenna surface. They found that the kernels most suited to

their numerical technique of solution correspond to auxiliary sources in the form of magnetic tangential currents. Examples of current distributions were given for thick solid cylinders with rounded corners at the ends. An associated paper (Vasil'ev et al., 1967b) generalised the method to antennas with a surface condition. The method of Albert and Synge (1948) has also been used by Abeyaskere (1972), who carried out numerical computations for thin cylindrical dipoles.

The problem of electromagnetic radiation and scattering from perfectly conducting bodies of revolution has also been considered by Mautz and Harrington (1969). Their integral equations were obtained by requiring the tangential component of the electric intensity be zero on the antenna surface. Numerical results were presented for the sphere and cone-sphere only. Recently (Harrington and Mautz, 1971a,1971b,1972), their method has been used to compute characteristic mode currents and fields for some bodies, viz. sphere, cone-sphere, disc and wires (cf. Garbacz, 1965; Waterman, 1969b,1971; Garbacz and Turpin, 1971). An application of the method of Mautz and Harrington (1969) to electrically small end-loaded dipoles and broadband biconical and "bulb" dipoles can be found in Kalafus (1971).

Consider the solid perfectly conducting antenna body of revolution in Fig. 1.6, where the polar cylindrical coordinates (ρ',φ',z') and surface coordinates (η,φ',ξ) denote the same point on the antenna surface. Under axially symmetric excitation, only the circularly symmetric, meridional current is induced on the surface. By using the Stratton-Chu integral formulae (Stratton, 1941, Section 8.14) and the condition that the field is zero on the part of the z-axis inside the antenna, Gavorun (1959) obtained the

integral equation for the total current $I(\xi)$,

$$\int_C \left\{\left(\frac{\partial^2 G_o}{\partial z^2} + k_o^2 G_o\right) \sin\psi + \frac{\partial^2 G_o}{\partial \rho' \partial z} \cos\psi\right\} I(\xi)\, d\xi$$

$$= -\frac{jk_o 4\pi}{Z_o} E_z^i(\rho, z)\Big|_{\rho=0} ; \qquad (1.18)$$

where C is the generating arc of the antenna; ψ is the angle between the z-axis and the normal to the antenna surface; E_z^i is the longitudinal component of the electric intensity due to the excitation source; and G_o is the free space Green's function $\left(\exp(-jk_oR)/R,\ R = \sqrt{(\rho')^2 + (z-z')^2}\right)$. The equation (1.18) was transformed into one which resembled Hallen's equation (1938),

$$\int_C Z(z,\xi) I(\xi)\, d\xi = A \sin k_o z + B \cos k_o z$$

$$- \frac{jk_o 4\pi}{Z_o} \int_0^z E_z^i(0,\zeta) \sin k_o(z-\zeta)\, d\zeta ; \qquad (1.19)$$

where A and B are unknown integration constants; and the kernel $Z(z,\xi)$ is given by,

$$Z(z,\xi) = G_o \sin\psi + \int_0^z \left(\frac{\partial^2 G_o}{\partial \rho' \partial z} \cos\psi\right)\Big|_{z=\zeta} \sin k_o(z-\zeta)\, d\zeta . \qquad (1.20)$$

Equation (1.19) was solved by a numerical technique developed for the moderately thick solid cylindrical antenna with plane ends. Dividing the antenna length into 2N equal segments, Gavorun (1962), approximated the current within each segment by a second order Lagrangian polynomial distribution. The restriction to moderately thick antennas (radius $< 0.05\lambda$) comes partly from approximating the current at the plane ends by a quadratic distribution. A point-matching procedure gave (2N+1) algebraic equations to determine the current at

the segment end-points from a method of successive approximations. The constants A and B, were found from the boundary condition requiring continuity of charge at the corners. Between 16 to 32 segments per wavelength of the arc length of C (see Fig. 1.6) were taken, giving an accuracy between 1.0% and 0.1% for the results obtained.

Gavorun (1962) chose to use equation (1.19) to carry out his computations on thin and moderately thick cylindrical antennas, because the kernel $Z(z,\xi)$ is sharply peaked and makes the diagonal in the matrix obtained by his numerical procedure strongly dominant. The kernel in equation (1.18), on the other hand, possesses two sharp peaks and is therefore unsuitable for his numerical procedure. As noted by Gavorun, $Z(z,\xi)$ is easy to compute for thin cylindrical antennas because the integral in (1.20) need be performed for the ends only, and contributes negligibly to the total value if the point z is more than a few radii from the ends.

As mentioned in the beginning of this section, Vasil'ev and his co-workers (Vasil'ev, 1959; Vasil'ev and Seregina, 1963; Vasil'ev et al., 1967a) derived their integral equations from the Stratton-Chu formulas and the Lorentz reciprocity relation. For the antenna body of revolution of Fig. 1.6 under axially symmetric excitation, they obtained the respective equations;

$$K(\xi_o) = 2K^i(\xi_o) + k_o\int_C (\rho' \frac{\partial S_1}{\partial \eta} + S_1 \sin \psi)\, K(\xi)d\xi; \quad (1.21)$$

$$0 = 2K^i(\xi_o) + k_o\int_C (\rho' \frac{\partial S_1}{\partial \eta} + S_1 \sin \psi)\, K(\xi)d\xi; \quad (1.22)$$

where $K(\xi)$ represents the unknown surface current density on

the antenna surface; $\hat{\xi}K^i(\xi_o) = \hat{n}\wedge\underline{H}^i(\xi_o)$, and $\underline{H}^i(\xi)$ is the magnetic intensity due to the excitation source. The angle ψ is that between the z-axis and the surface unit normal vector. The point ξ_o, which is described by the coordinates (ρ,φ,z), lies on the generating arc C in equation (1.21) and on the arc C_u parallel to, but beneath, arc C in equation (1.22). S_1 is given by

$$S_1 = \frac{1}{2\pi}\int_0^{2\pi} \frac{\exp(-jk_oR)\ \exp(-j\Phi)}{k_oR}\, d\Phi; \qquad (1.23)$$

where $\Phi = (\varphi-\varphi')$ and $R^2 = (z-z')^2 + \rho^2 + (\rho')^2 - 2\rho\rho'\cos\Phi$. In computing S_1, Vasil'ev chose to use an infinite series expansion of Bessel and hypergeometric functions; the series converging more slowly for small R (Vasil'ev, 1965). The equations (1.21) and (1.22) were solved by the method of subsections, the current within each subsection (or segment) being approximated by a pulse function. As it was found (Vasil'ev, 1959) that the current distributions, at closely spaced points on arc C, for the subsection lengths 0.1λ and 0.05λ agreed to within 2% to 7%, all the results presented used 0.1λ subsection lengths. The figure of 0.1λ was said to limit their method to antennas with generating arc lengths of 10λ and less.

The use of equation (1.22) instead of equation (1.21) represented a reduction in the computational effort, because S_1 given by (1.23) is singular at $\xi_o = \xi$ (i.e. R = 0) in equation (1.21). The kernel in equation (1.22) was still sharply peaked because the separation distance between the arcs C and C_u was chosen to be a small fraction of a

wavelength. This gave a matrix with a strongly dominant diagonal.

By using the conventional vector potential method (Hallen, 1938; King, 1956, chap.1; Andreasen, 1965), Mautz and Harrington (1969) rederived the integral equations obtained previously by Andreasen (1965) for the radiation and scattering from a perfectly conducting body of revolution. The derivation employed the boundary condition that the tangential component of the electric intensity is zero on the perfectly conducting surface. For the body of revolution shown in Fig. 1.6, the integral equation obtained is

$$\hat{n} \wedge \underline{E}^i = \frac{-\hat{n} \wedge}{j4\pi\omega\varepsilon_o} (\nabla\nabla\cdot + k_o^2) \int_C \int_0^{2\pi} \underline{K}_s(\eta=0,\varphi',\xi) \frac{e^{-jk_oR}}{R} \rho' d\varphi' d\xi; \tag{1.24}$$

where $\underline{E}^i$ is the applied electric intensity on the antenna surface, $\underline{K}_s$ is the electric surface current density, the function $\exp(-jk_oR)/R$ is the ordinary free space Green's function, and $R^2 = [(z-z')^2 + \rho^2 + (\rho')^2 - 2\rho\rho'\cos(\varphi-\varphi')]$. Equation (1.24) was solved by the method of subsections using a piecewise linear approximation for the current within each subsection. Current distributions and radiation patterns were presented for the sphere (radius equal to 0.2λ) and the cone-sphere (spherical radius equal to 0.2λ and a 10^o half cone angle) using subsection lengths of 0.03λ and 0.07λ respectively. No quantitative measure of the accuracy of their results was, however, given.

Like Vasil'ev's equation (Vasil'ev, 1959; Vasil'ev and Seregina, 1963), which is given by equation (1.21), equation (1.24) involves numerically troublesome double integrals, and a kernel which is singular when R = 0.

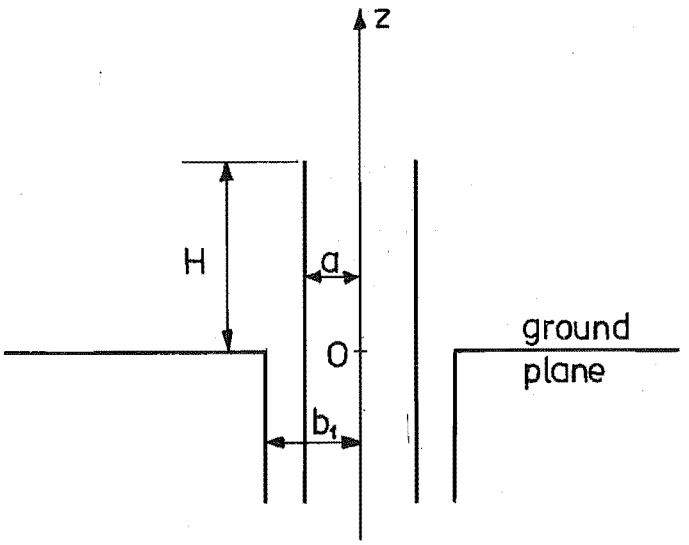

Fig. 1.1: Tubular monopole fed by a coaxial line.

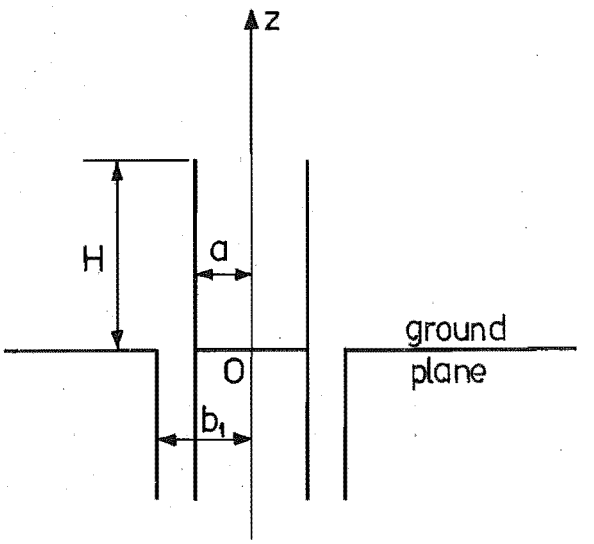

Fig. 1.2: Tubular monopole with a perfectly conducting plate across the interior and driven by a coaxial line.

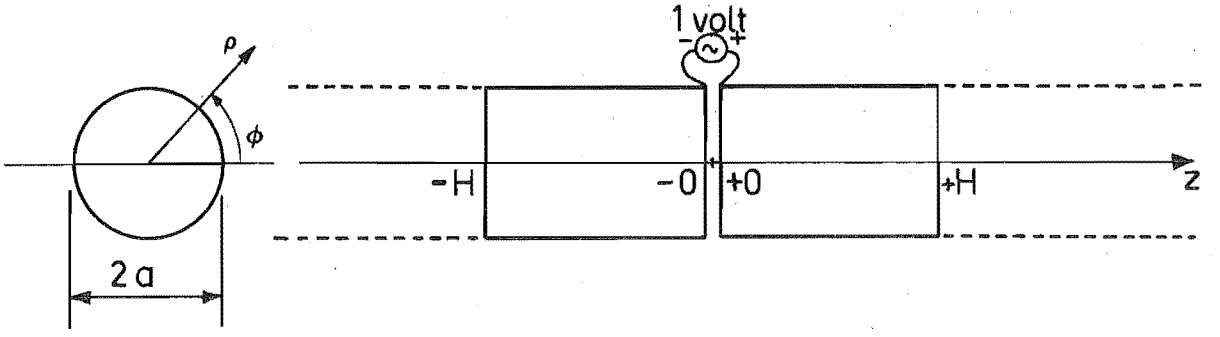

Fig. 1.3: Centre-fed cylindrical dipole antenna. Dashes denote infinite cylindrical extension of antenna.

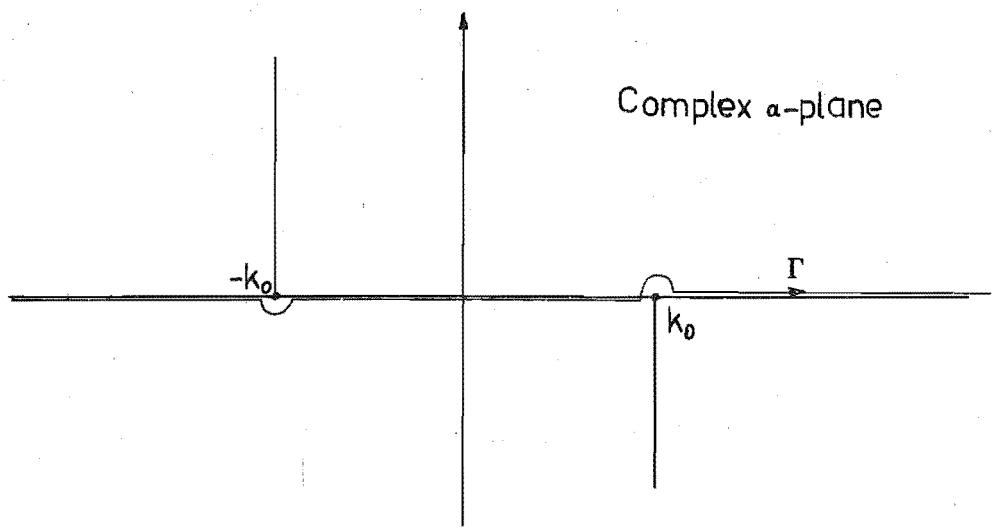

Fig. 1.4: The integration contour Γ in the complex α-plane.

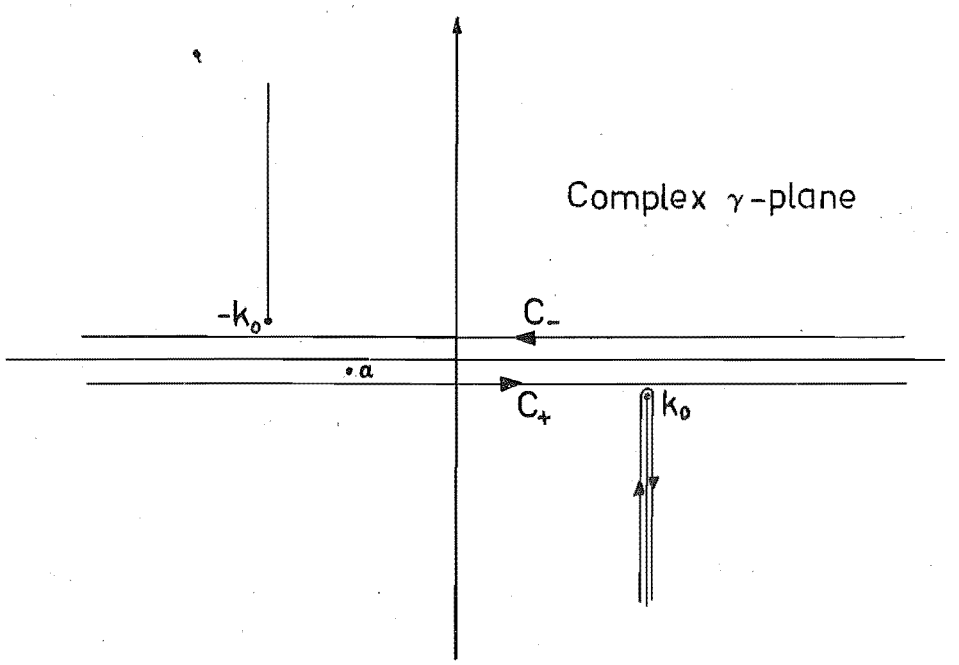

Fig. 1.5: The integration contours C_+, C_- and C in the complex γ-plane.

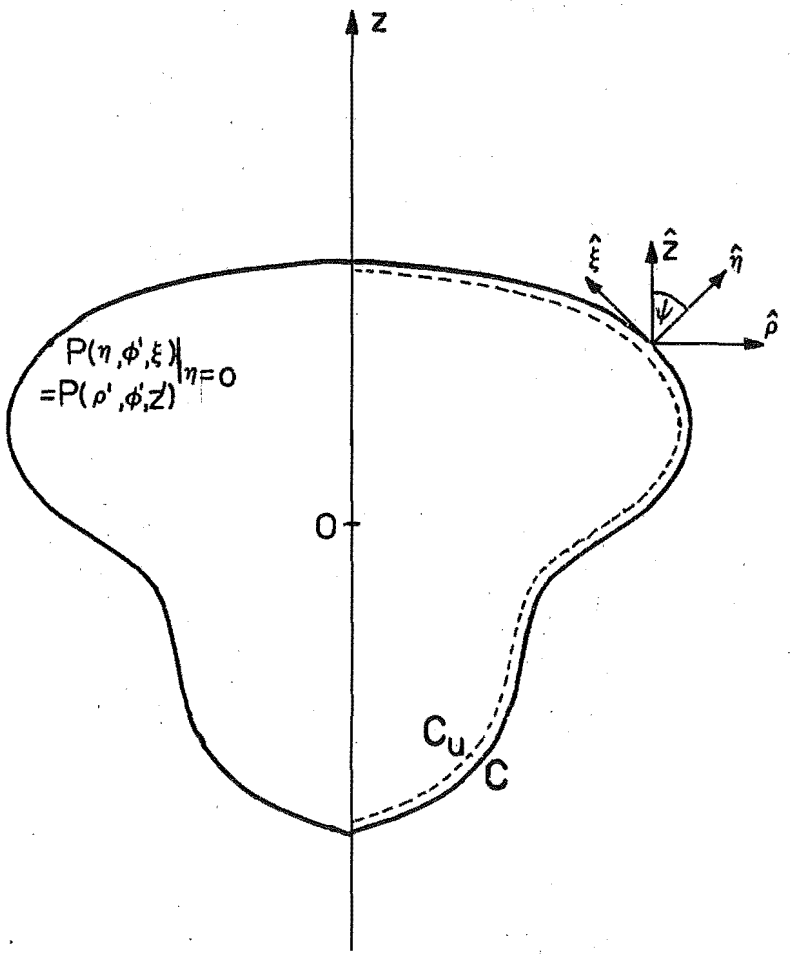

Fig. 1.6: A body of revolution with generating arc C. (ρ,φ,z) are cylindrical polar and (η,φ',ξ) are local surface coordinates.

CHAPTER 2

THE EXTENDED INTEGRAL EQUATION FORMULATION

2.1 INTRODUCTION

In the integral equation formulation of electromagnetic problems there are sometimes null-field regions, i.e. regions in which the field is zero. These occur when perfectly conducting bodies are involved. Examples are the null field inside a solid body which is illuminated externally, and that outside a waveguide. They also occur as a consequence of using the vector Helmholtz integral formula for the field (Stratton, 1941, Section 8.14; Mentzer, 1955, Chap. 2; Honl et al., 1961, p.240; Jones, 1964, Section 1.26) in reformulating the problems as integral equations. Love's field equivalence principle (Love, 1901; Harrington, 1961, Section 3.5; Collin, 1969) in fact postulates null-field regions.

Although these regions have been known for a long time, it was not until Waterman (1965, 1969a, 1969b, 1971) pointed out the computational advantages related to the extended boundary condition, i.e. the null field in these regions, that they have become increasingly used. The extended integral equation formulation, which employs the extended boundary condition explicitly, has been applied to the scattering from perfectly conducting and dielectric bodies of revolution (Gavorun, 1959, 1962; Waterman, 1965, 1969a, 1971; Hizal et al., 1970; Gardner, 1969), perfectly conducting cylinders of arbitrary cross-section (Bates, 1968; Hunter, 1972) and deformed

infinite wedges (Hunter and Bates, 1970, 1972). Its application to the determination of waveguide characteristics has been carried out by Bates (1969) and Ng and Bates (1972). Corresponding extended boundary conditions have also been used by Smythe (1956, 1960) in electrostatic potential calculations, and by Copley (1967), Schenck (1968) and Fenlon (1969) in acoustic radiation and scattering problems.

The integral equations which were derived from the Lorentz reciprocity relation by Albert and Synge (1948), Sinclair (1959), Vasil'ev et al. (1967a,b), Avetisyan (1970) and Abeyaskere (1972) are not only identical to, but also involve essentially the same mathematical analysis as those obtained by the present approach (cf. Vasil'ev et al., 1967a).

The formulation is presented in this chapter for the sake of convenient reference in later chapters, and also to indicate the main outline of its application to the solid cylindrical antenna, and the circular end-loaded dipole. It can be found, in parts, in any comprehensive book on electromagnetic theory (Stratton, 1941, Chap. 8; Mentzer, 1955, Chap. 2; Honl et al., 1961, p.238-243). It is an extended form of Huygen's principle, and appears to be first developed by Love (1901). In section 2.2 the formulation of the equations for the radiation from the non-conducting and perfectly conducting solid antennas is presented. The formulation is modified in section 2.3 to highly indented antenna bodies. The last section, 2.4, shows the conversion of the equations in sections 2.2 and 2.3, which use the scalar Green's function, into ones which use the dyadic Green's function.

2.2 FORMULATION FOR RADIATION PROBLEMS

Let V be a region of space bounded internally by the surface S_i and externally by S_o (see Fig. 2.1). The surface S_i represents the boundary of a 'foreign object' in the total region enclosed by S_o. The medium in V is assumed to be linear, homogeneous, isotropic, of zero conductivity ($\sigma = 0$), of permittivity ε, and of permeability μ. Within V the applied densities of electric and magnetic currents $\underline{J}$ and $\underline{J}^m$ are varying monochromatically (radian frequency ω). The field intensities $\underline{E}$ and $\underline{H}$ in V satisfy Maxwell's field equations,

$$\begin{aligned} \nabla \wedge \underline{E} + j\omega\mu\underline{H} &= -\underline{J}^m, \qquad \nabla \cdot \underline{H} = \frac{\rho^m}{\mu}, \\ \nabla \wedge \underline{H} - j\omega\varepsilon\underline{E} &= \underline{J}, \qquad \nabla \cdot \underline{E} = \frac{\rho}{\varepsilon}, \end{aligned} \tag{2.1}$$

where the time harmonic factor $\exp(j\omega t)$ is suppressed, and ρ and ρ^m are electric and magnetic volume charge densities associated with $\underline{J}$ and $\underline{J}^m$ by the equations of continuity,

$$\nabla \cdot \underline{J} + j\omega\rho = 0, \qquad \nabla \cdot \underline{J}^m + j\omega\rho^m = 0. \tag{2.2}$$

The corresponding vector Helmholtz equations for $\underline{E}$ and $\underline{H}$ are

$$\begin{aligned} \nabla \wedge \nabla \wedge \underline{E} - k^2\underline{E} &= -j\omega\mu\underline{J} - \nabla \wedge \underline{J}^m, \\ \nabla \wedge \nabla \wedge \underline{H} - k^2\underline{H} &= -j\omega\mu\underline{J}^m + \nabla \wedge \underline{J}, \end{aligned} \tag{2.3}$$

where $k = \omega(\mu\varepsilon)^{\frac{1}{2}}$ is the wavenumber or propagation constant. By applying the vector analogue of the Green's theorem to the field equations, Stratton (1941, Sect. 8.14) obtained the vector Helmholtz integral formula for the field intensities at an interior point of V in terms of the values of $\underline{E}$ and $\underline{H}$ over

the enclosing surfaces S_i and S_o (cf. Jones, 1964, Sect. 1.26). Stratton and various authors (Mentzer, 1955, Sect. 2.2; Honl et al., 1961, p.240) have shown that the same formula gives a 'zero' field at points outside V. Thus,

$$\left.\begin{matrix}\underline{E}(\underline{r}) \\ 0\end{matrix}\right\} = \frac{(\nabla\nabla\cdot + k^2)}{j4\pi\omega\varepsilon}\int_V \underline{J}(\underline{r}')G\,dv - \frac{\nabla\wedge}{4\pi}\int_V \underline{J}^m(\underline{r}')G\,dv$$

$$- \frac{(\nabla\nabla\cdot + k^2)}{j4\pi\omega\varepsilon}\int_{S_o+S_i} [\hat{n}_+\wedge \underline{H}_+(\underline{r}')]G\,ds$$

$$- \frac{\nabla\wedge}{4\pi}\int_{S_o+S_i} [\hat{n}_+\wedge \underline{E}_+(\underline{r}')]G\,ds, \qquad (2.4a)$$

$$\left.\begin{matrix}\underline{H}(\underline{r}) \\ 0\end{matrix}\right\} = \frac{\nabla\wedge}{4\pi}\int_V \underline{J}(\underline{r}')G\,dv + \frac{(\nabla\nabla\cdot + k^2)}{j4\pi\omega\mu}\int_V \underline{J}^m(\underline{r}')G\,dv$$

$$- \frac{\nabla\wedge}{4\pi}\int_{S_o+S_i} [\hat{n}_+\wedge \underline{H}_+(\underline{r}')]G\,ds$$

$$+ \frac{(\nabla\nabla\cdot + k^2)}{j4\pi\omega\mu}\int_{S_o+S_i} [\hat{n}_+\wedge \underline{E}_+(\underline{r}')]G\,ds, \qquad (2.4b)$$

$$\underline{r} \quad \begin{cases}\text{in } V \\ \text{outside } V\end{cases},$$

where $\underline{r}'$ is the position vector of the source points, $\hat{n}_+$ is the unit normal vector on S_i or S_o and directed out of V (see Fig. 2.1), $\underline{E}_+$ and $\underline{H}_+$ are the field intensities lying on the negative side of S_o or S_i with respect to $\hat{n}_+$, and $G = G(k,\underline{r},\underline{r}') = \exp(-jk|\underline{r}-\underline{r}'|)/|\underline{r}-\underline{r}'|$ is the usual scalar Green's function in an infinite domain.

In a radiation problem, the particular antenna occupies the region V_i enclosed by S_i and the region V is free space with $k = k_o = \omega(\mu_o\varepsilon_o)^{\frac{1}{2}}$. The field intensities are assumed to satisfy the radiation conditions at infinity, i.e. the field

behaves like an outgoing electromagnetic wave and the surface integrals over S_o in (2.4a,b) vanish as S_o tends to infinity. (2.4a,b) become

$$\left.\begin{matrix}\underline{E}(\underline{r}) \\ 0\end{matrix}\right\} = \frac{(\nabla\nabla\cdot + k_o^2)}{j4\pi\omega\varepsilon_o}\int_V \underline{J}(\underline{r}')G_o dv - \frac{\nabla\wedge}{4\pi}\int_V \underline{J}^m(\underline{r}')G_o dv$$
$$- \frac{(\nabla\nabla\cdot + k_o^2)}{j4\pi\omega\varepsilon_o}\int_{S_i} [\hat{n}_+\wedge \underline{H}_+(\underline{r}')]G_o ds$$
$$- \frac{\nabla\wedge}{4\pi}\int_{S_i} [\hat{n}_+\wedge \underline{E}_+(\underline{r}')]G_o ds, \qquad (2.5a)$$

$$\left.\begin{matrix}\underline{H}(\underline{r}) \\ 0\end{matrix}\right\} = \frac{\nabla\wedge}{4\pi}\int_V \underline{J}(\underline{r}')G_o dv + \frac{(\nabla\nabla\cdot + k_o^2)}{j4\pi\omega\mu_o}\int_V \underline{J}^m(\underline{r}')G_o dv$$
$$- \frac{\nabla\wedge}{4\pi}\int_{S_i} [\hat{n}_+\wedge \underline{H}_+(\underline{r}')]G_o ds$$
$$+ \frac{(\nabla\nabla\cdot + k_o^2)}{j4\pi\omega\mu_o}\int_{S_i} [\hat{n}_+\wedge \underline{E}_+(\underline{r}')]G_o ds, \qquad (2.5b)$$

$$\underline{r} \quad \left\{\begin{matrix}\text{in } V \\ \text{in } V_i\end{matrix}\right. ,$$

where $G_o = G(k_o,\underline{r},\underline{r}')$. Since (2.5a) and (2.5b) can be obtained from each other by (2.1), they represent, with $\underline{r}$ in V_i, only a single extended integral equation to determine the two unknowns $\hat{n}_+\wedge \underline{E}_+$ and $\hat{n}_+\wedge \underline{H}_+$ on S_i. An extra condition or integral equation or both, required to determine these two unknowns uniquely, can be obtained by a consideration of the electromagnetic problem inside the antenna body V_i.

When the antenna is a source-free non-conducting body with $k = k_i = \omega(\mu_i\varepsilon_i)^{\frac{1}{2}}$, the field intensities $\underline{E}_i$ and $\underline{H}_i$ in V_i are given by formulas similar to (2.4a,b),

$$\left.\begin{matrix}\underline{E}_i(\underline{r}) \\ 0\end{matrix}\right\} = -\frac{(\nabla\nabla\cdot + k_i^2)}{j4\pi\omega\varepsilon_i}\int_{S_i}[\hat{n}_- \wedge \underline{H}_-(\underline{r}')]G_i\,ds$$

$$-\frac{\nabla\wedge}{4\pi}\int_{S_i}[\hat{n}_- \wedge \underline{E}_-(\underline{r}')]G_i\,ds, \qquad (2.6a)$$

$$\left.\begin{matrix}\underline{H}_i(\underline{r}) \\ 0\end{matrix}\right\} = -\frac{\nabla\wedge}{4\pi}\int_{S_i}[\hat{n}_- \wedge \underline{H}_-(\underline{r}')]G_i\,ds$$

$$+\frac{(\nabla\nabla\cdot + k_i^2)}{4\pi j\omega\mu_i}\int_{S_i}[\hat{n}_- \wedge \underline{E}_-(\underline{r}')]G_i\,ds, \qquad (2.6b)$$

$$\underline{r} \quad \begin{cases}\text{in} & V_i \\ \text{in} & V\end{cases},$$

where $G_i = G(k_i,\underline{r},\underline{r}')$, $\hat{n}_- = -\hat{n}_+$ (see Fig. 2.1); and $\underline{E}_-$ and $\underline{H}_-$ are the field intensities lying on the surface just inside S_i. Surface boundary conditions (Jones, 1964, Sect. 1.21) require that the tangential components of the field be continuous across S_i so that

$$\hat{n}_+ \wedge (\underline{E}_+ - \underline{E}_-) = 0, \quad \hat{n}_+ \wedge (\underline{H}_+ - \underline{H}_-) = 0. \qquad (2.7)$$

The two sets of dual integral equations for solving the radiation from a non-conducting antenna body are obtained from (2.5a,b), (2.6a,b) and (2.7) as

$$0 = \frac{(\nabla\nabla\cdot + k_o^2)}{j4\pi\omega\varepsilon_o}\int_V \underline{J}(\underline{r}')G_o\,dv - \frac{\nabla\wedge}{4\pi}\int_V \underline{J}^m(\underline{r}')G_o\,dr$$

$$+\frac{(\nabla\nabla\cdot + k_o^2)}{j4\pi\omega\varepsilon_o}\int_{S_i}[\hat{n}\wedge\underline{H}_+(\underline{r}')]G_o\,ds$$

$$+\frac{\nabla\wedge}{4\pi}\int_{S_i}[\hat{n}\wedge\underline{E}_+(\underline{r}')]G_o\,ds, \qquad \underline{r}\text{ in } V_i; \qquad (2.8a)$$

$$0 = -\frac{(\nabla\nabla\cdot + k_o^2)}{j4\pi\omega\varepsilon_i}\int_{S_i}[\hat{n}\wedge \underline{H}_+(\underline{r}')]G_i\,ds$$

$$-\frac{\nabla\wedge}{4\pi}\int_{S_i}[\hat{n}\wedge \underline{E}_+(\underline{r}')]G_i\,ds, \qquad \underline{r} \text{ in } V\ ; \tag{2.8b}$$

and

$$0 = \frac{\nabla\wedge}{4\pi}\int_V \underline{J}(\underline{r}')G_o\,dv + \frac{(\nabla\nabla\cdot + k_o^2)}{j4\pi\omega\mu_o}\int_V \underline{J}^m(\underline{r}')G_o\,dv$$

$$+\frac{\nabla\wedge}{4\pi}\int_{S_i}[\hat{n}\wedge \underline{H}_+(\underline{r}')]G_o\,ds - \frac{(\nabla\nabla\cdot + k_o^2)}{j4\pi\omega\mu_o}\int_{S_i}[\hat{n}\wedge \underline{E}_+(\underline{r}')]G_o\,ds,$$

$$\underline{r} \text{ in } V_i; \tag{2.9a}$$

$$0 = -\frac{\nabla\wedge}{4\pi}\int_{S_i}[\hat{n}\wedge \underline{H}_+(\underline{r}')]G_i\,ds + \frac{(\nabla\nabla\cdot + k_i^2)}{j4\pi\omega\mu_i}\int_{S_i}[\hat{n}\wedge \underline{E}_+(\underline{r}')]G_i\,ds,$$

$$\underline{r} \text{ in } V\ ; \tag{2.9b}$$

where $\hat{n} = -\hat{n}_+ = \hat{n}_-$ is the unit normal vector on S_i pointing into V. By using the extended boundary condition only, Mentzer (1955, Sect. 2.2.2) has proved that the solution to both (2.8a,b) and (2.9a,b) is unique. (2.8a,b) and (2.9a,b) have been used by Waterman (1969a) for the scattering from dielectric obstacles.

When the antenna is perfectly conducting, the field intensities in V_i are physically zero, $\hat{n}_+\wedge \underline{E}_+ \equiv 0$ on S_i, and the induced electric surface current density on S_i is given by

$$\underline{K}_s = -\hat{n}_+\wedge \underline{H}_+ = \hat{n}\wedge \underline{H}_+. \tag{2.10}$$

$\underline{K}_s$ is then determined from (cf. 2.5a,b)

$$0 = \frac{(\nabla\nabla\cdot + k_o^2)}{4\pi j\omega\varepsilon_o}\int_V \underline{J}(\underline{r}')G_o dv - \frac{\nabla\wedge}{4\pi}\int_V \underline{J}^m(\underline{r}')G_o dv$$

$$+ \frac{(\nabla\nabla\cdot + k_o^2)}{4\pi j\omega\varepsilon_o}\int_{S_i} K_s(\underline{r}')G_o ds, \qquad \underline{r} \text{ in } V_i; \quad \text{or} \qquad (2.11a)$$

$$0 = \frac{\nabla\wedge}{4\pi}\int_V \underline{J}(\underline{r}')G_o dv + \frac{(\nabla\nabla\cdot + k_o^2)}{j4\pi\omega\mu_o}\int_V \underline{J}^m(\underline{r}')G_o dv$$

$$+ \frac{\nabla\wedge}{4\pi}\int_{S_i} \underline{K}_s(\underline{r}')G_o dv, \qquad \underline{r} \text{ in } V_i; \qquad (2.11b)$$

Both (2.11a) and (2.11b) lead to a unique solution (Mentzer, 1955, Sect. 2.2.2; Waterman, 1965) and have been used to treat the scattering from perfectly conducting obstacles (Gavorun, 1959, 1962; Waterman, 1965, 1971; Vasil'ev et al., 1967a; Bates, 1968; Gardner, 1969; Hunter and Bates, 1970, 1972; Hunter, 1972) and the radiation from perfectly conducting bodies of revolution(Albert and Synge, 1948; Gavorun, 1959, 1962; Vasil'ev et al., 1967a; Abeyaskere, 1972).

It is interesting to compare (2.11a,b) with the corresponding equations obtained by imposing just the surface boundary conditions on S_i (cf. Harrington, 1968, Chapters 3, 4 and 5). These surface equations (as contrasted with extended ones in (2.11a,b)) are just (2.11a,b) with the position vector $\underline{r}$ on S_i, and have singular kernels because G_o is singular at $\underline{r} = \underline{r}'$. Their solutions are also non-unique at frequencies for which resonant modes exist in the region V_i (with the same medium as in V and bounded by a perfectly conducting surface S_i). For clarity, rewrite (2.11a) as

$$-\frac{(\nabla\nabla\cdot + k_o^2)}{j4\pi\omega\varepsilon_o}\int_{S_i} \underline{K}_s(\underline{r}')G_o dv = \underline{E}^i(\underline{r}), \quad \underline{r} \text{ in } V_i; \qquad (2.12)$$

$$-\frac{(\nabla\nabla\cdot + k_o^2)}{j4\pi\omega\varepsilon_o}\int_{S_i} \underline{K}_s(\underline{r}')G_o\,dv = \underline{E}^i(\underline{r}), \quad \underline{r} \text{ on } S_i; \tag{2.13}$$

where $\underline{E}^i(\underline{r})$ are the volume integrals in (2.11a). The homogeneous part of (2.13) is also the surface equation for determining the resonant frequencies and modes that can exist in V_i. As (2.13) does not state explicitly that the field is zero on V_i, the resulting solution is non-unique at these resonant frequencies. In contrast, (3.12) requires a null field in V_i, thus suppressing the resonant modes. Schenck (1969), when reviewing the corresponding equations for acoustic radiation and scattering problems, forced the resonant or characteristic modes to vanish by supplementing the surface equations with those of the extended type.

Extended integral equations for determining the characteristic frequencies and modes of a volume region V_i with $k = k_i = \omega(\mu_i\varepsilon_i)^{\frac{1}{2}}$ and bounded by a perfectly conducting surface S_i are

$$(\nabla\nabla\cdot + k_i^2)\int_{S_i} \underline{K}_s(\underline{r}')G_i\,ds = 0, \quad \underline{r} \text{ outside } V_i; \tag{2.14a}$$

$$\nabla\wedge\int_{S_i} \underline{K}_s(\underline{r}')G_i\,ds = 0, \quad \underline{r} \text{ outside } V_i. \tag{2.14b}$$

These are obtained directly from (2.6a,b) with $\hat{n}\wedge\underline{E}(\underline{r}') = 0$ on S_i and have been applied to waveguides of arbitrary cross-section by Bates (1969), and Ng and Bates (1972).

The extended boundary condition does not have to be applied everywhere in the null-field regions to obtain unique solutions to the equations. It can be applied on a line segment (Gavorun, 1959, 1962), a closed surface

(Vasil'ev et al., 1967a,b) or over a finite volume (Waterman, 1965). For waveguides, Bates (1969) has shown that the extended boundary condition need be applied to a small null field region, the area of which is not infinitesimal. The proof is based on an analytic continuation argument and is summarised by the theorem (Morse and Feshbach, 1953, p.390) which states that " if a function is analytic in a region and vanishes along any arc of a continuous curve in this region, then it must vanish identically in this region" (sic).

2.3 EQUATIONS FOR INDENTED ANTENNAS

For certain antenna problems, e.g. the hollow cylindrical dipole with open ends discussed in chapter 1 and the very thin linear dipole end-loaded with circular flat discs, the extended integral equations of section 2.2 become very similar to the surface ones. These antennas can, however, be treated differently from the straightforward procedure in section 2.2 where the surface S_i coincides with the antenna surface.

Consider the highly indented perfectly conducting antenna shown in Fig. 2.2. It is immersed in free space and excited by the applied electric and magnetic current densities $\underline{J}$ and $\underline{J}^m$ respectively. Fictitious surfaces α, β, and γ are chosen as shown in Fig. 2.2 and S_o recedes to infinity. The free space region V_1 is bounded by the union of the open surfaces α and γ (i.e. $\alpha \cup \gamma$) and V_o by $\beta \cup \gamma$ and S_o. Both V_o and V_1 share a common open surface γ, across which the field is continuous. Since the tangential components of the electric intensity are zero on $\alpha \cup \beta$, the extended dual

integral equations for the two regions V_o and V_1 are, from (2,5a,b) and (2.6a,b),

$$0 = \frac{(\nabla\nabla\cdot + k_o^2)}{j4\pi\omega\varepsilon_o}\int_{V_o} \underline{J}(\underline{r}')G_o dv - \frac{\nabla\wedge}{4\pi}\int_{V_o} \underline{J}^m(\underline{r}')G_o dv$$

$$- \frac{(\nabla\nabla\cdot + k_o^2)}{j4\pi\omega\varepsilon_o}\int_{\beta\cup\gamma}[\hat{n}_o\wedge \underline{H}_o(\underline{r}')]G_o ds$$

$$- \frac{\nabla\wedge}{4\pi}\int_{\gamma}[\hat{n}_o\wedge \underline{E}_o(\underline{r}')]G_o dv, \qquad \underline{r} \text{ in } V_1 \cup V_2; \tag{2.15a}$$

$$0 = \frac{(\nabla\nabla\cdot + k_o^2)}{j4\pi\omega\varepsilon_o}\int_{\alpha\cup\gamma}[\hat{n}_1\wedge \underline{H}_1(\underline{r}')]G_o ds$$

$$- \frac{\nabla\wedge}{4\pi}\int_{\gamma}[\hat{n}_1\wedge \underline{E}_1(\underline{r}')]G_o ds, \qquad \underline{r} \text{ in } V_o \cup V_2; \tag{2.15b}$$

and

$$0 = \frac{\nabla\wedge}{4\pi}\int_{V_o} \underline{J}(\underline{r}')G_o dv + \frac{(\nabla\nabla\cdot + k_o^2)}{j4\pi\omega\mu_o}\int_{V_o} \underline{J}^m(\underline{r}')G_o dv$$

$$- \frac{\nabla\wedge}{4\pi}\int_{\beta\cup\gamma}[\hat{n}_o\wedge H_o(\underline{r}')]G_o ds$$

$$+ \frac{(\nabla\nabla\cdot + k_o^2)}{j4\pi\omega\mu_o}\int_{\gamma}[\hat{n}_o\wedge \underline{E}_o(\underline{r}')]G_o dv, \quad \underline{r} \text{ in } V_1 \cup V_2; \tag{2.16a}$$

$$0 = -\frac{\nabla\wedge}{4\pi}\int_{\alpha\cup\gamma}[\hat{n}_1\wedge \underline{H}_1(\underline{r}')]G_o ds$$

$$+ \frac{(\nabla\nabla\cdot + k_o^2)}{j4\pi\omega\mu_o}\int_{\gamma}[\hat{n}_1\wedge \underline{E}_1(\underline{r}')]G_o ds, \quad \underline{r} \text{ in } V_o \cup V_2, \tag{2.16b}$$

where $\hat{n}_o$, $\hat{n}_1$ are the respective unit normal vectors on $\beta \cup \gamma$ and $\alpha \cup \gamma$ with $\hat{n}_o$ directed out of V_o and $\hat{n}_1$ out of V_1 (see Fig. 2.2); $\underline{E}_o$, $\underline{H}_o$ and $\underline{E}_1$, $\underline{H}_1$ are the electric and magnetic intensities in the respective regions V_o and V_1.

$$\underline{E}_o = \underline{E}_1 \quad , \quad \underline{H}_o = \underline{H}_1, \quad \underline{r}' \text{ on } \gamma;$$

$$\underline{K}_s = -\hat{n}_o \wedge \underline{H}_o \ , \quad \underline{r}' \text{ on } \beta; \text{ and} \tag{2.17}$$

$$\underline{K}_s = -\hat{n}_1 \wedge \underline{H}_1 \ , \quad \underline{r}' \text{ on } \alpha$$

where $\underline{K}_s$ is the electric surface current density on the highly indented antenna surface. (2.17) together with either (2.15a,b) or (2.16a,b) are sufficient to determine $\underline{K}_s$ uniquely.

A simplification to the equations occurs if the surface $\alpha \cup \gamma$ can be subdivided into parts coinciding with parts of coordinate surfaces of a coordinate system in which the vector Helmholtz wave equation (2.3) is separable (Schelkunoff, 1952, Sect. 2.2; Morse and Feshbach, 1953, Chap.5 and p.1767, Hunter and Bates,1970). The standard method of separation of variables then leads to a series expansion of orthogonal wavefunctions, with undetermined coefficients, for the field in V_1 and specifies the relation between $\underline{E}_1$ and $\underline{H}_1$ explicitly. The latter relation and (2.17) means that either (2.15a) or (2.16a) is sufficient to determine the single unknown $\hat{n}_o \wedge \underline{H}_o$ on $\beta \cup \gamma$ since $\hat{n}_o \wedge \underline{E}_o$ is now known in terms of $\hat{n}_o \wedge \underline{H}_o$ on γ. We defer the details to Chapter 4 where end-loaded cylindrical dipoles are treated specifically.

2.4 EQUATIONS USING THE DYADIC GREEN'S FUNCTION

The dyadic Green's function in an infinite domain is given by (Morse and Feshbach, 1953, p.1778; Collin, 1969, Sect. 2.6)

$$\underline{\underline{G}} = \underline{\underline{G}}(k,\underline{r},\underline{r}') = \underline{\underline{I}}\, G(k,\underline{r},\underline{r}') \tag{2.18}$$

where $\underline{\underline{I}} = \hat{x}\hat{x} + \hat{y}\hat{y} + \hat{z}\hat{z}$ is the unit dyadic. Since a dot product of a vector $\underline{F}$ with $\underline{\underline{I}}$ gives $\underline{F}.\underline{\underline{I}} = \underline{F}$, the scalar Green's function $G(k,\underline{r},\underline{r}')$ in the equations in sections 2.2 and 2.3 can be replaced by $\cdot\underline{\underline{G}}$. As an illustration (2.11b) is rewritten as

$$0 = \frac{\nabla\wedge}{4\pi}\int_V \underline{J}(\underline{r}').\underline{\underline{G}}_o dv + \frac{(\nabla\nabla. + k_o^2)}{j4\pi\omega\mu_o}\int_V \underline{J}^m(\underline{r}').\underline{\underline{G}}_o dv$$

$$+ \frac{\nabla\wedge}{4\pi}\int_{S_i} \underline{K}_s(\underline{r}').\underline{\underline{G}}_o ds, \qquad \underline{r} \text{ in } V_i. \tag{2.19}$$

It is introduced because the expansion of $\underline{\underline{G}}$ in vector spherical wavefunctions (Morse and Feshbach, 1953, p.1875) is convenient for enforcing the extended boundary condition on spherical surfaces inside the null field regions (Waterman, 1965, 1969a, 1969b, 1971). The analysis is carried out on (2.19). With reference to Appendix I, the expansion of $\underline{\underline{G}}_o$ in spherical coordinates (r,θ,φ) is

$$\underline{\underline{G}}_o = \underline{\underline{G}}(k_o,\underline{r},\underline{r}') = \frac{-jk_o}{\pi}\sum_{n=0}^{\infty}\frac{(2n+1)}{n(n+1)}\sum_{m,\sigma}\varepsilon_m\frac{(n-m)!}{(n+m)!}$$

$$\times\Big[\underline{M}^{(1)}_{\sigma mn}(k_o\underline{r}_<)\underline{M}^{(4)}_{\sigma mn}(k_o\underline{r}_>) + \underline{N}^{(1)}_{\sigma mn}(k_o\underline{r}_<)\underline{N}^{(4)}_{\sigma mn}(k_o\underline{r}_>)$$

$$+ n(n+1)\,\underline{L}^{(1)}_{\sigma mn}(k_o\underline{r}_<)\,\underline{L}^{(4)}_{\sigma mn}(k_o\underline{r}_>)\Big], \tag{2.20}$$

where $r_<$, $r_>$ are respectively the lesser or greater of r, r'; ε_m is the Neumann factor; m goes from 0 to n; σ is e (for even modes) or o (for odd modes); and the vector functions $\underline{M}$, $\underline{N}$ and $\underline{L}$ are defined in Appendix I. Substituting (2.20) into (2.19) and from the properties of $\underline{M}$, $\underline{N}$ and $\underline{L}$, gives

$$0 = \frac{-jk_o^2}{4\pi^2} \sum_{n=0}^{\infty} \frac{(2n+1)}{n(n+1)} \sum_{m,\sigma} \varepsilon_m \frac{(n-m)!}{(n+m)!} \left\{ A^{(4)}_{\sigma mn} \underline{M}^{(1)}_{\sigma mn}(k_o\underline{r}) + B^{(4)}_{\sigma mn} \underline{N}^{(1)}_{\sigma mn}(k_o\underline{r}) \right\} ; \quad (2.21)$$

$$A^{(4)}_{\sigma mn} = \int_V \underline{J}(\underline{r}').\underline{N}^{(4)}_{\sigma mn}(k_o\underline{r}')dv + \frac{k_o}{j\omega\mu_o} \int_V \underline{J}^m(\underline{r}').\underline{M}^{(4)}_{\sigma mn}(k_o\underline{r}')dv + \int_{S_i} \underline{K}_s(\underline{r}').\underline{N}^{(4)}_{\sigma mn}(k_o\underline{r}')ds; \quad (2.22a)$$

$$B^{(4)}_{\sigma mn} = \int_V \underline{J}(\underline{r}').\underline{M}^{(4)}_{\sigma mn}(k_o\underline{r}')dv + \frac{k_o}{j\omega\mu_o} \int_V \underline{J}^m(\underline{r}').\underline{N}^{(4)}_{\sigma mn}(k_o\underline{r}')dv + \int_{S_i} \underline{K}_s(\underline{r}').\underline{M}^{(4)}_{\sigma mn}(k_o\underline{r}')ds. \quad (2.22b)$$

The coordinate origin 0 is inside V_i; r is less than the least value of r'; and r' refers to points on the antenna surface S_i (see Fig. 2.1). Since $\underline{M}^{(1)}_{\sigma mn}$ and $\underline{N}^{(1)}_{\sigma mn}$ are orthogonal over a constant spherical surface for any index triplet (σ,m,n), $A^{(4)}_{\sigma mn}$ and $B^{(4)}_{\sigma mn}$ are identically zero,

$$\int_{S_i} \underline{K}_s(\underline{r}').\underline{N}^{(4)}_{\sigma mn}(k_o\underline{r}')ds = -\int_V \underline{J}(\underline{r}').\underline{N}^{(4)}_{\sigma mn}(k_o\underline{r}') + \frac{k_o}{j\omega\mu_o} \underline{J}^m(k_o\underline{r}').\underline{M}^{(4)}_{\sigma mn}(k_o\underline{r}')dv, \quad (2.23a)$$

$$\int_{S_i} \underline{K}_s(\underline{r}').\underline{M}^{(4)}_{\sigma mn}(k_o\underline{r}')ds = -\int_V \underline{J}(\underline{r}').\underline{M}^{(4)}_{\sigma mn}(k_o\underline{r}') + \frac{k_o}{j\omega\mu_o} \underline{J}^m(k_o\underline{r}').\underline{N}^{(4)}_{\sigma mn}(k_o\underline{r}')dv . \quad (2.23b)$$

(2.23a,b) are an infinite set of non-singular integral equations for solving the surface currents $\underline{K}_s$, and corresponds to Waterman's (1965, 1971) equation for the scattering from a

perfectly conducting solid body.

Another advantage of expressing the free space dyadic function $\underline{\underline{G}}$ in vector spherical wavefunctions is the ease with which the radiation pattern of an arbitrarily shaped antenna can be computed. Consider again the integral equation (2.11b), which applies to a perfectly conducting solid antenna body V_i excited by the applied electric and magnetic current densities $\underline{J}$ and $\underline{J}^m$ respectively. It is obtained from equation (2.5b) where the observation point, denoted by the position vector $\underline{r}$, is taken inside the body V_i. If the observation point were taken on an infinite spherical surface outside V_i, (2.5b), and correspondingly (2.11b), give the magnetic intensity in the radiation zone, i.e.

$$\underline{H}(\underline{r}) = \frac{\nabla\wedge}{4\pi}\int_V \underline{J}(\underline{r}')G_o dv + \frac{\nabla\nabla\cdot + k_o^2}{j4\pi\omega\mu_o}\int_V \underline{J}^m(\underline{r}')G_o dv$$

$$+ \frac{\nabla\wedge}{4\pi}\int_{S_i} \underline{K}_s(\underline{r}')G_o ds. \qquad (2.24)$$

When the scalar Green's function G_o is replaced by its dyadic form expressed in vector spherical wavefunctions, viz. as in (2.20), equation (2.24) becomes

$$\underline{H}(\underline{r}) = \frac{-jk_o^2}{4\pi^2}\sum_{n=0}^{\infty}\frac{(2n+1)}{n(n+1)}\sum_{m,\sigma}\varepsilon_m\frac{(n-m)!}{(n+m)!}\Big\{A^{(1)}_{\sigma mn}\underline{M}^{(4)}_{\sigma mn}(k_o\underline{r})$$

$$+ \underline{B}^{(1)}_{\sigma mn}\underline{N}^{(4)}_{\sigma mn}(k_o\underline{r})\Big\}\ ; \qquad (2.25)$$

$$A^{(1)}_{\sigma mn} = \int_V \underline{J}(\underline{r}').\underline{N}^{(1)}_{\sigma mn}(k_o\underline{r}')dv$$

$$+ \frac{k_o}{j\omega\mu_o}\int_V \underline{J}^m(\underline{r}').\underline{M}^{(1)}_{\sigma mn}(k_o\underline{r}')dv + \int_{S_i}\underline{K}_s(\underline{r}').\underline{N}^{(1)}_{\sigma mn}(k_o\underline{r}')ds; \qquad (2.26a)$$

$$B^{(1)}_{\sigma mn} = \int_V \underline{J}(\underline{r}').\underline{M}^{(1)}_{\sigma mn}(k_o\underline{r}')dv + \frac{k_o}{j\omega\mu_o}\int_V \underline{J}^m(\underline{r}').\underline{N}^{(1)}_{\sigma mn}(k_o\underline{r}')dv$$

$$+ \int_{S_i} \underline{K}_s(\underline{r}').\underline{M}^{(1)}_{\sigma mn}(k_o\underline{r}')ds. \qquad (2.26b)$$

The coefficients, $A^{(1)}_{\sigma mn}$ and $B^{(1)}_{\sigma mn}$, are related to the $A^{(4)}_{\sigma mn}$ and $B^{(4)}_{\sigma mn}$ in (2.22a,b) by the relations between the vector functions,

$$\underline{M}^{(4)}_{\sigma mn} = \underline{M}^{(1)}_{\sigma mn} - j\,\underline{M}^{(2)}_{\sigma mn}; \quad \underline{N}^{(4)}_{\sigma mn} = \underline{N}^{(1)}_{\sigma mn} - j\,\underline{N}^{(2)}_{\sigma mn}; \qquad (2.27)$$

as given in Appendix I. The radially dependent functions in $\underline{M}^{(1)}_{\sigma mn}$ and $\underline{N}^{(1)}_{\sigma mn}$ are spherical Bessel functions whilst those in $\underline{M}^{(2)}_{\sigma mn}$ and $\underline{N}^{(2)}_{\sigma mn}$ are spherical Neumann functions. As the $A^{(1)}_{\sigma mn}$ and $B^{(1)}_{\sigma mn}$ are automatically computed in the process of solving the integral equations (2.23a,b) for the unknown antenna surface currents, the radiation pattern as given by equation (2.25) is straightforwardly obtained.

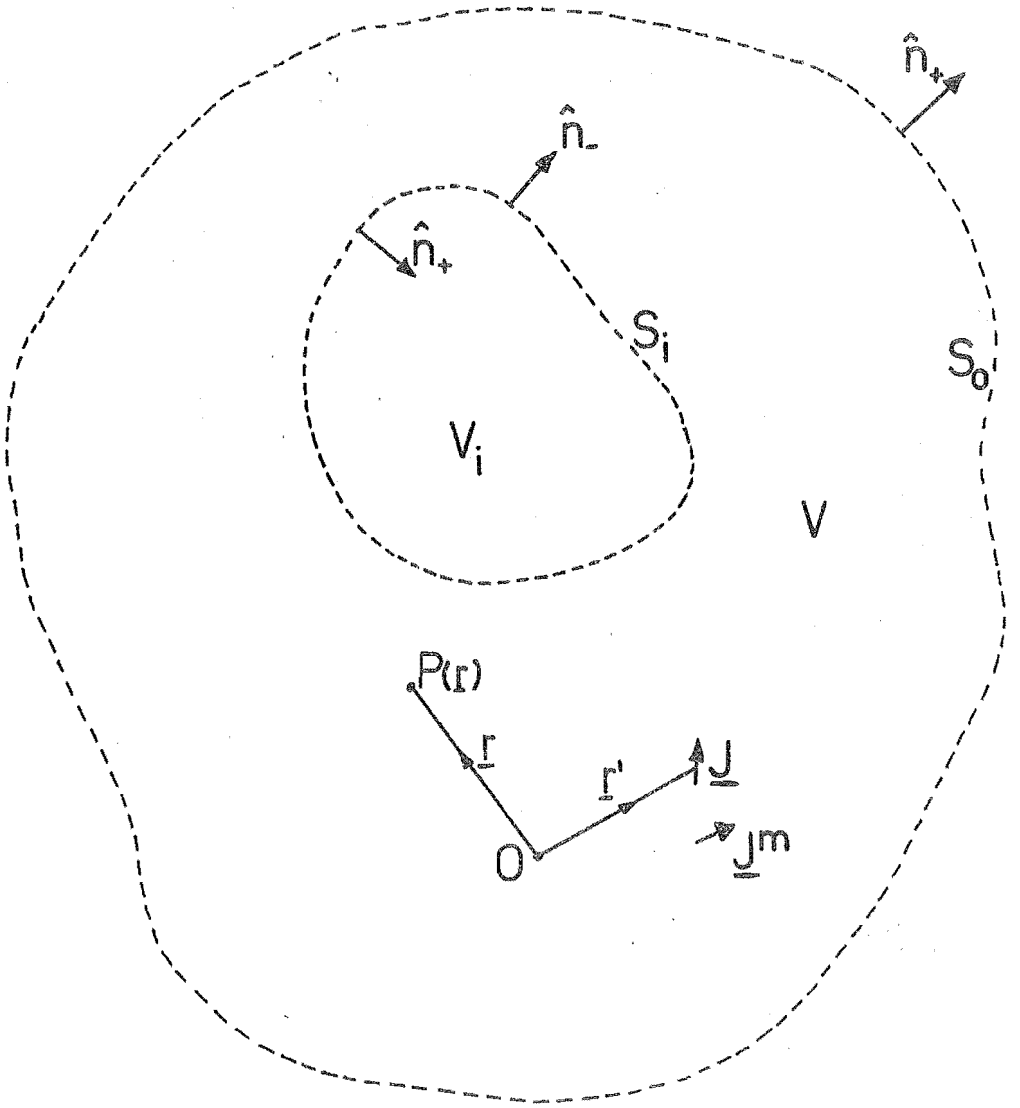

Fig. 2.1: A region of space V bounded internally and externally by closed fictitious surfaces S_i and S_o respectively. $\underline{J}$ and $\underline{J}^m$ are applied electric and magnetic current densities respectively.

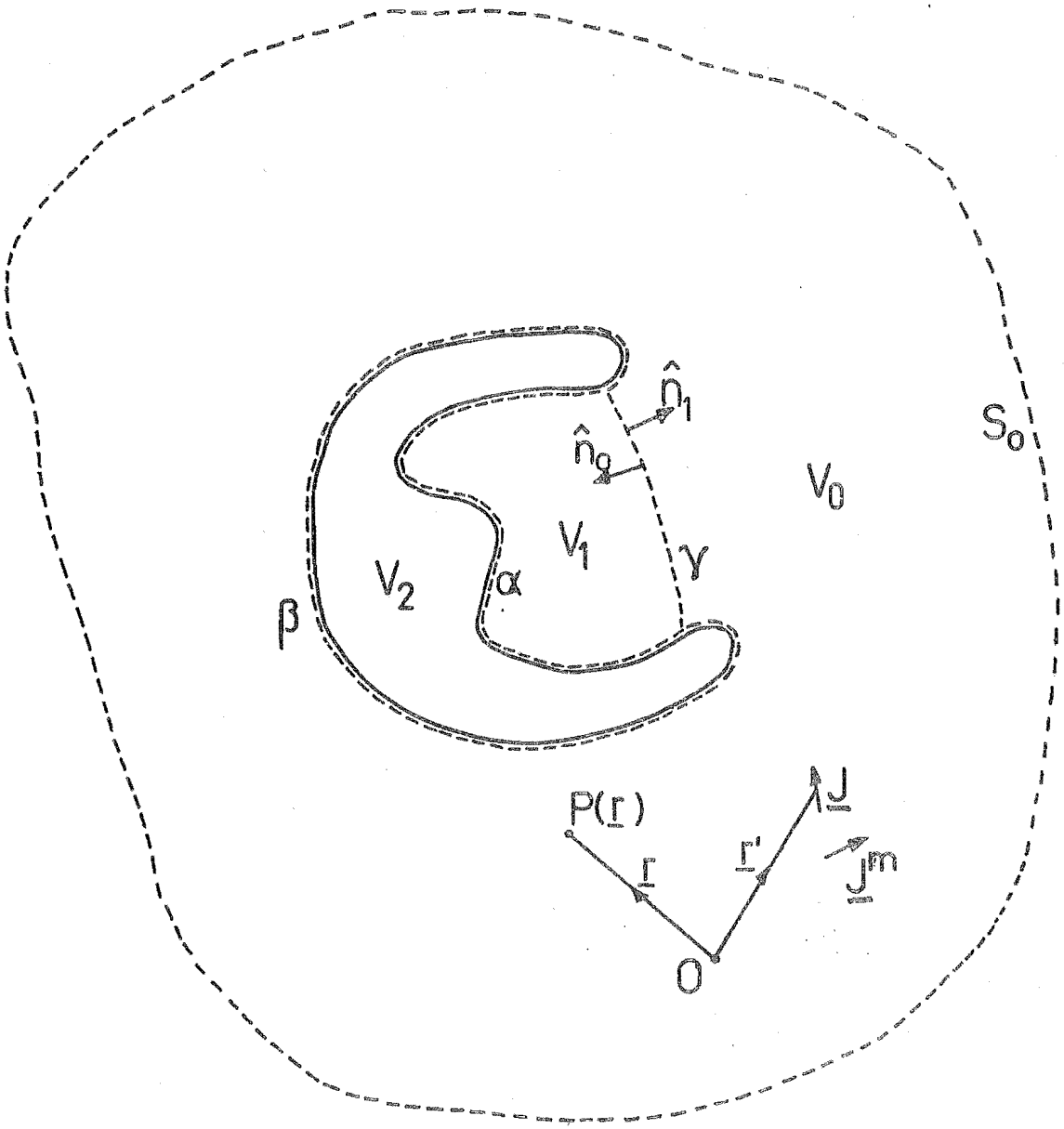

Fig. 2.2: The indented antenna occupying volume V_2, and the fictitious surfaces α, β, γ and S_o.

CHAPTER 3

APPLICATION OF EXTENDED INTEGRAL EQUATION FORMULATION TO THICK, SOLID DIPOLE ANTENNAS

3.1 INTRODUCTION

The extended integral equation formulation that is described in chapter 2 is applied here to the electrically thick, perfectly conducting solid dipole antenna. In section 3.2, the axially symmetric monopole mounted on a ground plane and fed by a coaxial transmission line is converted, by Love's field equivalence principle and image theory, into a dipole antenna which is symmetrically driven by a circular frill, or a circumferential band, of magnetic currents. Because the frill and the band of magnetic currents can be considered as being made of rings of magnetic current, the dipole antenna treated in later sections is defined in section 3.2.1 as that driven by a ring of magnetic current. Section 3.3 reduces the relevant extended integral equations in Chapter 2 to ones which apply directly to the dipole antenna. The numerical method of solving the integral equations, obtained by setting the field zero in a spherical region, or on the central axis, inside the dipole, is discussed in section 3.4 and Appendix II. Computational considerations and numerical results obtained are discussed in sections 3.5 and 3.6 respectively. Lastly, section 3.7 gives a comparison of the methods presented in this chapter with those reviewed in chapter 1.

3.2 THE DIPOLE ANTENNA PROBLEM

Equivalent dipole antennas of the two axially symmetric, perfectly conducting solid monopoles shown in Figs 3.2a and 3.3a, where they are mounted on a perfectly conducting ground plane and fed by a co-axial line, can be developed by the use of Love's field equivalence principle (Love, 1901; Harrington, 1961, Sect. 3.5; Otto, 1967, 1968b; Wallenberg and Harrington, 1969) and image theory.

Consider, firstly, the monopole antenna in Fig. 3.2a which is excited by an incoming TEM field in the coaxial line. The excitation has angular frequency ω. (The time factor $\exp(j\omega t)$ is suppressed throughout this chapter.) Let the surface S_a envelop the monopole and S_p lie on the infinite ground plane. Because of the circular symmetry of the antenna and the excitation source, the only non-zero field components in polarcylindrical coordinates (see Fig. 3.1) are E_ρ, E_z and H_φ. Boundary conditions require that the tangential component of the electric intensity be zero on S_a and S_p except at the coaxial aperture at $z = 0$, $b_o < \rho < b_1$, where b_o and b_1, respectively, are the inner and outer radii of the coaxial line. The use of Love's equivalence principle (Harrington, 1961, Sect. 3.5) for the field above ground leads to an identical monopole which is mounted on a complete ground plane and excited by a circular frill of magnetic currents $\underline{J}^m$ (see Fig. 3.2b).

$$\underline{J}^m = -\hat{n} \wedge \underline{E} = -\hat{\varphi}\, E_\rho(\rho,\varphi,0) \quad ; \quad b_o < \rho < b_1 \tag{3.1}$$

where $\hat{n}$ is the unit normal vector to S_a and S_p in Fig. 3.2a. From image theory, the field above ground is the same as that

of the dipole antenna in Fig. 3.2c excited by the magnetic frill source,

$$\underline{J}^{m}(\rho,\varphi,0) = -\hat{\varphi}\ 2E_{\rho}(\rho,\varphi,0) \quad ; \quad b_o < \rho < b_1. \tag{3.2}$$

The equivalence of the dipole antenna in Fig. 3.2c to the coaxially driven monopole in Fig. 3.2a is exact when E_ρ is known. The exact form of E_ρ, however, can be obtained only by solving the complete antenna-coaxial line problem. In only the antennas shown in Figs 3.4 and 3.5 has the complete problem been analysed (Papadopoulos, 1960; Wu, 1962, 1963; Otto, 1967). Figs 3.4 and 3.5 show monopoles which are respectively the infinite and finite extensions of the inner conductor of the coaxial line. The monopole in Fig. 3.5 radiates into an infinite parallel-plate region. Papadopoulos (1960) analysed the infinite monopole and obtained an infinite set of equations by matching the fields in the coaxial aperture. This set of equations was solved by truncation to yield a result for electrically small apertures. The results obtained disagree with those of Bach Andersen (1968). Both monopoles in Fig. 3.4 and 3.5 were considered by Wu (1962, 1963) and Otto (1967). Wu (1962, 1963) derived an integral equation for E_ρ in the aperture. The equation was later solved approximately for small coaxial radii ($b_1 \ll \lambda$) and/or aperture widths ($b_1-b_o \ll \lambda$) (Chang and Wu, 1968; Kao, 1971). Otto (1967) found that the admittance, which would be measured in the line by conventional slotted-line techniques, was related to the integrals of the tangential fields in the aperture,

$$Y = \frac{2\pi}{\ell n(b_1/b_o)} \frac{\int_{b_o}^{b_1} H_\varphi(\rho,\varphi,0)d\rho}{\int_{b_o}^{b_1} E_\rho(\rho,\varphi,0)d\rho} \tag{3.3}$$

By taking E_ρ in (3.3) to be

$$E_\rho(\rho,\varphi,0) = \frac{V}{\rho \ell n(b_1/b_o)} \quad , \quad b_o < \rho < b_1 \tag{3.4}$$

where V is the applied voltage across the line, Otto (1967, 1969) computed the admittance values by using (3.3). These values agreed to within 1 millimho with those measured by Rama Rao (1965) for the antenna in Fig. 3.5.

The ρ dependence in (3.4) is the same as that of the dominant TEM field in the line. Equation (3.4) has been used by Otto (1965, 1967, 1968b), Chang (1968a) and Ting (1969) to treat monopoles of finite dimensions. Although Bach Andersen (1968) accounted for the antenna-coaxial line coupling when the monopole in Fig. 1.1 is a hollow cylinder, the admittance expression, given by equation (1.1), is in terms of the admittance of the associated infinite monopole, which has been solved approximately only (Papadopoulos, 1960; Wu, 1962; Otto, 1967; Chang and Wu, 1968).

Choosing E_ρ in (3.2) to be that in (3.4), the magnetic frill source becomes

$$\underline{J}^m(\rho,\varphi,0) = -\hat{\varphi} \frac{2V}{\rho \ell n(b_1/b_o)} \tag{3.5}$$

The dipole antenna in Fig. 3.2c excited by the frill source given by (3.5) is then an approximate equivalent problem for the monopole antenna in Fig. 3.2a.

For the monopole antenna shown in Fig. 3.3a, where the outer diameter of the coaxial line is smaller than the diameter of the base of the monopole and the gap height is electrically small ($u \ll \lambda$), the application of Love's equivalence principle and the image theory leads to the dipole antenna shown in Fig. 3.3c. The source exciting the dipole antenna is a circumferential band of magnetic currents

$$\underline{J}^m(a,\varphi,z) = +\hat{\varphi}\, E_z(a,\varphi,z) \; ; \qquad |z| < u \tag{3.6}$$

A first approximation to E_z in (3.6) is the field which has a uniform z-variation in the circumferential gap at $\rho = a$, $|z| < u$ (Otto, 1968b),

$$E_z(a,\varphi,z) = -\frac{V}{u} \quad , \qquad |z| < u,$$

So that (3.6) becomes

$$\underline{J}^m(a,\varphi,z) = -\hat{\varphi}\,\frac{V}{u} \quad , \qquad |z| < u, \tag{3.7}$$

where V is the voltage across the circumferential gap at $\rho = a$, $0 < z < u$.

3.2.1 The Magnetic Ring Source

Thin cylindrical antennas have been generally analysed on the basis of Hallen's integral equation, which is exact for the tubular dipole driven by a delta gap source (see section 1.2.2). Otto (1965) pointed out that Hallen's equation was incorrect when used for the antenna configurations shown in Figs 3.2a and 3.3a, and the requisite modifications were easily obtained when equivalent fictitious magnetic current sources were used. Later Otto (1968a) described the general representations of excitation

sources in antenna problems by distributions of magnetic currents. In comparison with the surface vector potential method (Hallen, 1938; King and Wu, 1967) and the Green's function approach (Wu, 1962; Chang, 1968a), the use of distributions of magnetic currents, albeit fictitious, lead to a simpler formulation to the antenna problem (Otto, 1967; Harrington, 1961, Sect. 8.6).

The magnetic frill and band sources in (3.5) and (3.7) can be considered as being made up of rings of magnetic current,

$$\underline{J}^m_{ring}(b,\varphi,\zeta) = -\hat{\varphi}\ \delta(\rho-b)\delta(z-\zeta) \tag{3.8}$$

where δ is the Dirac delta function, such that (3.5) and (3.7) become

$$\underline{J}^m_{frill}(\rho,\varphi,0) = \frac{+2V}{\ell n(b_1/b_o)} \int_{-\infty}^{\infty}\int_{b_o}^{b_1} \frac{\underline{J}^m_{ring}(b,\varphi,\zeta)}{b}\, dbd\zeta, \quad z = 0 \tag{3.9}$$

$$\underline{J}^m_{band}(a,\varphi,z) = + \frac{V}{u} \int_{-u}^{u}\int_{0}^{\infty} \underline{J}^m_{ring}(b,\varphi,\zeta)dbd\zeta, \quad |z| < u, \ \rho = a. \tag{3.10}$$

It can also be shown that the delta gap source (see section 1.2.2) is just two magnetic ring sources, one on the inner and the other on the outer surface of the hollow cylindrical dipole. Since the usual excitation sources, i.e. the magnetic frill and band and the delta gap, can be built up from ring sources, the methods of solution of axially symmetric antennas with circularly symmetric excitation can be studied with respect to the magnetic ring source.

3.2.2 Dipole Antenna Driven by Magnetic Ring Sources

The dipole antenna to be treated in later sections of this chapter is that shown in Fig. 3.6. It is an axially symmetric perfectly conducting solid dipole immersed in free space symmetrically excited by a magnetic ring source, (see (3.8))

$$\underline{J}^{m}_{ring}(b,\varphi,\mathfrak{z}) = -\hat{\varphi}\ \delta(\rho-b)\delta(z), \qquad \mathfrak{z} = 0 \tag{3.11}$$

which corresponds to those used for the magnetic frill source in (3.9). In Fig. 3.6, (x,y,z), (ρ,φ,z) and (η,φ',ξ) are respectively Cartesian, cylindrical polar and local surface coordinates. The surface of the dipole, S, is formed by rotating the curve C, which is even about the x y-plane, about the z-axis. The symbol ξ denotes also the arc length along curve C such that ξ = -L, 0, L respectively at the points Q_1, Q_2, Q_3 on C.

The field has the properties: (i) it is circularly symmetric, i.e. no φ-variation; (ii) only the E_ρ, E_z and H_φ components are non-zero; (iii) $\hat{\eta} \wedge \underline{E} \equiv 0$ on the surface of, and inside, the antenna; (iv) E_ρ and H_φ are zero everywhere on the z-axis, and (v) it possesses image symmetry about the xy-plane. From these properties, the electric surface current density given by $\underline{K}_s(\xi) = \hat{\eta} \wedge \underline{H}$ on the antenna surface S satisfies the relations

$$\underline{K}_s(\xi) = \hat{\xi}\ K(\xi),$$

$$K(-\xi) = K(\xi). \tag{3.12}$$

$$K^{(2p-1)}(0) = 0, \qquad p = 1,2,\ldots \tag{3.13}$$

$$K(\pm L) = 0, \tag{3.14}$$

where $K^{(p)}(\xi)$ means the p^{th} derivative of $K(\xi)$. When the ring source is electrically close ($b-a \ll \lambda$) to the dipole surface, $K(\xi)$ has a rapidly varying behaviour in the neighbourhood of $\xi = 0$ (see Appendix III). The total current $I(\xi)$ is defined by

$$I(\xi) = 2\pi\rho'(\xi)K(\xi) \tag{3.15}$$

where ρ' is the radial distance, from the z-axis, of the point denoted by ξ on C.

3.3 INTEGRAL EQUATIONS

The extended integral equations (2.11a,b) in section 2.1 apply directly to the dipole antenna problem stated in section 3.2.2 and shown in Fig. 3.6, and become

$$\frac{(\nabla\nabla\cdot + k_o^2)}{j\omega\varepsilon_o} \int_S \hat{\xi} K(\xi) G_o(k_o, \underline{r}, \underline{r}') ds = -\nabla \wedge \int_0^{2\pi} \hat{\varphi}' G_b(k_o, \underline{r}) b d\varphi', \tag{3.16}$$

$$\nabla \wedge \int_S \hat{\xi} K(\xi) G_o(k_o, \underline{r}, \underline{r}') ds = \frac{(\nabla\nabla\cdot + k_o^2)}{j\omega\mu_o} \int_0^{2\pi} \hat{\varphi}' G_b(k_o, \underline{r}) b d\varphi', \tag{3.17}$$

where $k_o = \omega(\mu_o\varepsilon_o) = 2\pi/\lambda$ is the free space wavenumber; $G_b = \exp(jk_oR_b)/R_b$, $R_b^2 = z^2 + \rho^2 + b^2 - 2\rho b\cos(\varphi-\varphi')$; $\underline{r}'$ is the position vector of any point, $Q(\rho',\varphi',z') = Q(0,\varphi',\xi)$, on the dipole surface; and $\underline{r}$ refers to any point, $P(\rho,\varphi,z)$, inside the antenna body. Note that (3.16) and (3.17) correspond to setting the electric and the magnetic intensity, respectively, to zero inside the antenna body.

Performing the vector operations in (3.16) and (3.17), the φ-component of (3.16) and the ρ- and z-components of (3.17) are found to be identically zero on both sides of the

equations because of the φ' integration. The remaining components reduce to,

$$\frac{1}{j\omega\varepsilon_o}\int_{-L}^{L} K(\xi)\left\{\rho'\int_0^{2\pi} -\cos\Phi\cos\psi\left[\frac{\partial}{\partial\rho}\,\frac{1}{\rho}\,\frac{\partial}{\partial\rho}\,(\rho G_o) + k_o^2 G_o\right]\right.$$

$$\left. + \cos\psi\,\frac{\partial}{\partial\rho}\,\frac{1}{\rho}\,\frac{\partial}{\partial\varphi}\,(G_o\sin\Phi) + \sin\psi\,\frac{\partial^2}{\partial\rho\partial z}\,G_o\,d\varphi'\right\}\,d\xi$$

$$= b\int_0^{2\pi}\cos\Phi\,\frac{\partial G_b}{\partial z}\,d\varphi'; \qquad (3.18)$$

$$\frac{1}{j\omega\varepsilon_o}\int_{-L}^{L} K(\xi)\,\left\{\rho'\int_0^{2\pi}\sin\psi\left[\frac{\partial^2}{\partial z^2}\,G_o + k_o^2 G_o\right]\right.$$

$$\left. - \cos\Phi\,\frac{\cos\psi}{\rho}\,\frac{\partial^2}{\partial z\partial\rho}(\rho G_o) + \frac{\cos\psi}{\rho}\,\frac{\partial^2}{\partial z\partial\varphi}(G_o\sin\Phi)d\varphi'\right\}\,d\zeta$$

$$= b\int_0^{2\pi} -\frac{\cos\Phi}{\rho}\,\frac{\partial}{\partial\rho}(\rho G_b) + \frac{1}{\rho}\,\frac{\partial}{\partial\rho}(G_b\sin\Phi)\,d\varphi'; \qquad (3.19)$$

$$\int_{-L}^{L} K(\xi)\,\left\{\rho'\int_0^{2\pi} -\cos\Phi\cos\psi\,\frac{\partial G_o}{\partial z} - \sin\psi\,\frac{\partial G_o}{\partial\rho}\,d\varphi'\right\}d\zeta$$

$$= \frac{b}{j\omega\mu_o}\int_0^{2\pi}\frac{1}{\rho^2}\,\frac{\partial}{\partial\varphi}\,\frac{\partial}{\partial\rho}(\rho G_b\sin\Phi) + \frac{1}{\rho^2}\,\frac{\partial^2}{\partial\varphi^2}(G_b\cos\Phi)\,d\varphi'; \qquad (3.20)$$

where $G_o = G(k_o,\underline{r},\underline{r}')$, $\Phi = (\varphi-\varphi')$, and ψ is the angle which $\hat{n}$ at $Q(0,\varphi',\xi)$ makes with the z-axis. Eqns (3.18) to (3.20) have previously been obtained by Vasil'ev et al. (1967a), and the left hand side of (3.20) is identical to (1.22) in section 1.2.

If $P(\rho,\varphi,z)$ is taken on the z-axis, (3.18) and (3.20) are identically zero and (3.19) becomes,

$$\frac{1}{j\omega\varepsilon_o}\int_{-L}^{L} K(\xi)\,\left\{\rho'\sin\psi\left[\frac{\partial^2}{\partial z^2}\,G_o + k_o^2 G_o\right] + \rho'\cos\psi\,\frac{\partial^2 G_o}{\partial z\,\partial\rho'}\right\}_{\rho=0} d\zeta$$

$$= -b^2\,\frac{e^{-jk_oR_o}}{R_o^2}\,\left[jk_o + \frac{1}{R_o}\right], \qquad (3.21)$$

where $R_o^2 = z^2 + b^2$. This equation, 3.21, was derived by Albert and Synge (1948) using the Lorentz reciprocity relation (Harrington, 1961, Sect. 3.8) and by Gavorun (1959, 1962) (cf. equation 1.18 in section 1.2) through requiring the z-component of the electric intensity be zero on the z-axis inside the dipole. Richmond (1965) has also used (3.21) to treat the scattering from thin, straight cylinders.

By considering (3.19) and (3.21) as differential equations in z, they can be transformed into

$$\int_{-L}^{L} K(\xi) \left\{ \rho' \int_0^{2\pi} G_o \sin\psi + \int_0^z \left[-\cos\Phi \frac{\cos\psi}{\rho} \frac{\partial^2}{\partial z \partial \rho}(\rho G_o) + \frac{\cos\psi}{\rho} \frac{\partial^2}{\partial z \partial \varphi}(G_o \sin\Phi) \right]_{z=\zeta} \sin k_o(z-\zeta) d\zeta d\varphi' \right\} d\xi$$

$$= B \cos k_o z + j\omega\varepsilon_o \int_0^z E_z^i(\rho, \varphi, \zeta) \sin k_o(z-\zeta) d\zeta, \qquad (3.22)$$

$$\int_{-L}^{L} K(\xi) \left\{ \rho' G_o \sin\psi + \rho' \int_0^z \left[\cos\psi \frac{\partial^2 G_o}{\partial z \partial \rho'} \right]_{z=\zeta} \sin k_o(z-\zeta) d\zeta \right\}_{\rho=0} d\xi$$

$$= B \cos k_o z + j\omega\varepsilon_o \int_0^z E_z^i(0, \varphi, \zeta) \sin k_o(z-\zeta) d\zeta, \qquad (3.23)$$

where $E_z^i(\rho, \varphi, z)$ and $E_z^i(0, \varphi, z)$ are respectively the right hand sides of (3.19) and (3.21). (3.23) is the integral equation which Gavorun (1962) used to obtain numerical results for the moderately thick ($a < 0.05\lambda$) cylindrical dipole (cf. equation 1.19 in section 1.2).

In section 2.4, the free space dyadic Green's function $\underline{\underline{G}}_o$ and its expansion in vector spherical wave function, which are described in Appendix I, were introduced. They were applied to equation (2.11b) giving an infinite set of

integral equations (2.23a,b) for the surface current density on the arbitrary shaped antenna. For the dipole antenna considered at present, (2.23a,b) are directly applicable and are reduced to

$$\int_{-L}^{L} K(\xi) \left\{ \hat{\xi} \cdot \underline{N}_{eon}^{(4)}(k_o \underline{r}') \rho' \right\} d\xi = \frac{k_o b}{j\omega\mu_o} P_n^1(0), \quad n = 0,1,2,3,\ldots \tag{3.24}$$

where $\underline{N}_{eon}^{(4)}$ is given in Appendix I (cf. Morse and Feshbach, 1953, p.1865), and $P_n^1(x)$ is the associated Legendre function of order n and degree 1. However, (3.24) can be further reduced because of condition (3.14), i.e. $K(-\xi) = K(\xi)$, and that $P_n^1(0) = 0$ when n is an even integer. From the properties of $\underline{N}_{eon}^{(4)}(k_o \underline{r}')$, (3.24) becomes

$$\int_{0}^{L} K(\xi) \left\{ \hat{\xi} \cdot \underline{N}_{eon}^{(4)}(k_o \underline{r}') \rho' \right\} d\xi = \frac{k_o b}{2j\omega\mu_o} P_n^1(0), \quad n = 1,3,5,\ldots \tag{3.25}$$

When the dipole surface S in Fig. 3.6 is a constant spherical one, eqns (3.24) and (3.25) lead to an exact series solution for the surface current density. If (a,θ',φ') are spherical polar coordinates referring to points on the constant spherical surface of radius a, then

$$\underline{N}_{eon}^{(4)}(k_o \underline{r}') = - \hat{\theta} \frac{1}{k_o a} [h_n^{(2)}(k_o a) + k_o a \, h_n^{(2)\prime}(k_o a)] P_n^1(\cos\theta')$$

$$\rho' = a \sin\theta'; \quad \hat{\xi} = - \hat{\theta}; \quad \xi = a \left(\frac{\pi}{2} - \theta'\right)$$

where $h_n^{(2)}(ka)$ and $h_n^{(2)\prime}(ka)$ are the spherical Hankel function, and its derivative, of the second kind and order n. Equation (3.25) now becomes

$$\frac{a^2}{k_o}[h_n^{(2)}(k_o a) + k_o a h_n^{(2)\prime}(k_o a)] \int_0^{\pi/2} K(\theta') P_n^1(\cos\theta') \sin\theta' d\theta'$$

$$= \frac{k_o b}{2j\omega\mu_o} P_n^1(0), \qquad n = 1,3,5,\ldots \tag{3.26}$$

Expanding $K(\theta')$ in terms of a series of the Legendre functions $P_m^1(\cos\theta')$,

$$K(\theta') = \sum_{m=1,3,5}^{\infty} K_m P_m^1(\cos\theta') \tag{3.27}$$

the orthogonal properties of $P_m^1(\cos\theta')$ (Abramowitz and Stegun, 1965, chap. 8) lead (3.26) to be

$$\frac{a^2}{k_o}\left[h_n^{(2)}(k_o a) + k_o a\, h_n^{(2)'}(k_o a)\right] \frac{n(n+1)}{(2n+1)} \delta_{mn} K_m = \frac{k_o b}{2j\omega\mu_o} P_n^1(0), \qquad n = 1,3,5\ldots$$

where $\delta_{mn} = 1$ when $m = n$ and 0 when $m \neq n$. The exact series solution for the surface current density is

$$K(\theta') = \sum_{m=1,3,5}^{\infty} \frac{(2m+1)}{m(m+1)} \frac{k_o^2 b\, P_m^1(0)}{2j\omega\mu_o a^2\left[h_m^{(2)}(k_o a) + k_o a\, h_m^{(2)'}(k_o a)\right]} \cdot P_m^1(\cos\theta'). \tag{3.28}$$

3.3.1 Radiation Pattern and Admittance

It has been mentioned in section 2.4 that, when the surface currents are determined from the extended integral equations (obtained by using the dyadic Green's function), the antenna radiation pattern can be evaluated from a rapidly convergent series. With reference to (2.25) and (2.26a,b), the pattern for the dipole antenna in Fig. 3.6 is given by,

$$\underline{H}(\underline{r}) = \frac{-jk_o^2}{4\pi^2} \sum_{n=1,3,5}^{\infty} \frac{(2n+1)}{n(n+1)} A_{eon}^{(1)} \underline{M}_{eon}^{(4)}(k_o\underline{r}'),$$

$$= \frac{-jk_o^2}{4\pi^2}\left[\sum_{n=1,3,5}^{\infty} \frac{(2n+1)}{n(n+1)} A_{eon}^{(1)} j^{n+1} P_n^1(\cos\theta')\right] \frac{e^{-jk_o r}}{r}\hat{\phi}. \tag{3.29}$$

$$A_{eon}^{(1)} = \frac{2\pi k_o b}{j\omega\mu_o} P_n^1(0) + 4\pi \int_0^L K(\xi)\left\{\hat{\xi}.\underline{N}_{eon}^{(1)}(k_o\underline{r}')\rho'\right\} d\xi \tag{3.30}$$

Note that the integral in (3.30) has been evaluated in the process of solving (3.25) for the surface currents.

With reference to the coaxial line driven monopole shown in Fig. 3.2a and the assumed distribution of E_ρ in the coaxial aperture (as given by (3.4)), admittance expressions that have been used in the literature are

$$Y = \frac{2\pi a}{V} H_\varphi(a,\varphi,0) = \frac{2\pi a}{V} K(\xi=0) \; ; \tag{3.31}$$

$$Y = \frac{2\pi}{V \ell n(b_1/b_o)} \int_{b_o}^{b_1} H_\varphi(\rho,\varphi,0)\, d\rho. \tag{3.32}$$

Equation (3.31) is found in Chang (1968a) and Ting (1969) and (3.32) in Otto (1967, 1968b) (cf. equation (3.3)). Of the two expressions, (3.32) is more accurate than (3.31) because the admittance has been shown to be correctly given by (3.3) (Otto, 1967). Equation (3.32) is, however, easy to implement only if H_φ in (3.32) can be evaluated without necessitating a numerical integration over the surface currents on the monopole. Examples where (3.32) is implemented easily are (a) the monopole is a hollow or solid cylinder with plane ends and the antenna problem is solved by a Fourier transform method (Otto, 1967, 1968b); and (b) the antenna in Fig. 3.5 and the end-loaded dipole (considered in Chapter 4) for which the field in the parallel plate region can be expanded in cylindrical wave functions (Otto, 1967).

3.4 NUMERICAL SOLUTION OF INTEGRAL EQUATIONS

The dipole antenna problem shown in Fig. 3.6 and reformulated as integral equations, (3.18) to (3.25), has an exact solution only if the antenna surface S, which is of finite dimensions, coincides with a constant spheroidal

surface (Schelkunoff, 1952, Chapters 2 and 3; King, 1956, p.5). For the non-spheroidal antenna, the integral equations, (3.18) to (3.25) can be solved numerically by the general method of moments outlined in Appendix II (Harrington, 1968, Chapter 1; Morse and Feshbach, 1953, Sect. 8.3). Equations (3.18) to (3.23) can be rewritten as

$$\int_{-L}^{L} Z(\zeta,\xi)\, K(\xi)\, d\xi = B(\zeta), \quad \zeta_0 < \zeta < \zeta_1 \qquad (3.33)$$

where $Z(\zeta,\xi)$ represent the expressions in braces in, and the $B(\zeta)$ are the right hand sides of, the equations, and ζ is any arc with end points ζ_0 and ζ_1 chosen appropriately for the particular equation. Equation (3.33) has the same form as equation (II-1) in Appendix II.

By using a point-matching procedure with piece-wise parabolic approximation to $K(\xi)$, Gavorun (1962) has obtained numerical solutions to (3.23) valid for moderately thick ($a < 0.05\lambda$) cylindrical dipoles with plane ends. The same numerical technique, but with piece-wise constant approximation to $K(\xi)$, was used by Vasil'ev et al. (1967a) to obtain results from (3.20) for any smooth solid antenna body of revolution.

The author has chosen to study the computational value of integral equations (3.21) and (3.25) for treating thick solid cylindrical dipoles because the kernels involve simple functions only. By using a point-matching procedure, equation (3.21) becomes

$$\int_0^L Z_n(\xi)\, K(\xi)\, d\xi = B_n,\ n = 1,2,3,\ldots,N;\ \text{METHOD 1} \tag{3.34}$$

$$\left.\begin{aligned} Z_n(\xi) &= Z(z,\xi) + Z(z,-\xi), \\ B_n &= -j\omega\varepsilon_o b^2 \frac{e^{-jk_oR_o}}{R_o^2}\left(jk_o + \frac{1}{R_o}\right), \end{aligned}\right\} \quad z = z_n; \tag{3.35}$$

where $R_o^2 = z^2 + b^2$ and $Z(z,\xi)$ is the expression in braces in (3.21). Equation (3.25) already has the same form as (3.34) so that

$$\int_0^L Z_n(\xi)\, K(\xi)\, d\xi = B_n,\ n = 1,2,3,\ldots,N;\ \text{METHOD 2} \tag{3.36}$$

$$\left.\begin{aligned} Z_n(\xi) &= \hat{\xi}.\underline{N}_{eoq}^{(4)}(k_o\underline{r}')\rho', \\ B_n &= \frac{k_o b}{2j\omega\mu_o} P_q^1(0) \quad , \end{aligned}\right\} \quad q = 2n-1\ ; \tag{3.37}$$

To solve for the unknown surface current density $K(\xi)$ in either (3.34) or (3.36), $K(\xi)$ is first assumed to be approximated by a finite number M of basis or expansion functions $\varphi_m(\xi | o < \xi < L)$, i.e.

$$K(\xi) = \sum_{m=1}^{M} K_m\, \varphi_m(\xi), \tag{3.38}$$

where the K_m are unknown expansion coefficients. Substituting (3.38) into equation (3.34) or (3.36) then gives

$$\sum_{m=1}^{M} Z_{nm}K_m = B_n, \quad n = 1,2,3,\ldots,M; \tag{3.39}$$

$$Z_{nm} = \int_0^L Z_n(\xi)\, \varphi_m(\xi)\, d\xi\ ; \tag{3.40}$$

which is a system of linear algebraic equations for the members of $\{K_m\}$. By choosing $n = 1,2,3,\ldots,M$, the matrix equation

$$[Z_{nm}][K_m] = [B_n],\ m = 1,2,3,\ldots,M;\ n = 1,2,3,\ldots,M; \tag{3.41}$$

can be written for (3.39). $[Z_{nm}]$ is a square matrix with an inverse $[Z_{nm}]^{-1}$ if it is not singular. The matrix solution to (3.41) is then

$$[K_m] = [Z_{nm}]^{-1}[B_n]. \tag{3.42}$$

To determine whether numerical convergence is occurring, the procedure adopted is to increase M in (3.38) until, at a number of closely spaced points in the interval $0 < \xi < L$, the surface currents display negligible change with increasing M.

When the magnetic ring source (see Fig. 3.3) is electrically close ($b-a < 0.05\lambda$) to the dipole surface, $K(\xi)$ is rapidly varying in the neighbourhood of $\xi = 0$. A rapidly varying term, which has the approximate form of this behaviour of $K(\xi)$, is obtained by a physical-optics analysis in Appendix III. This term is given by (III-9) in Appendix III as

$$Q(\xi) = \frac{-jk_o}{2Z_o} Y_o\left(k_o\sqrt{\xi^2+(b-a)^2}\right) \frac{\left[1 + \sin(\frac{\pi}{2} + \frac{2\pi}{d})\right]}{2},$$

$$0 < \xi < d < H-\tau; \tag{3.43}$$

where $d^2 = \chi_1^2 - (b-a)^2$, χ_1 is the first zero of $Y_o(\chi_n) = 0$, and Y_o is the zeroth order Neumann function. The subtraction of $Q(\xi)$ from $K(\xi)$ can sometimes improve numerical convergence. Writing

$$\begin{aligned} \bar{K}(\xi) &= K(\xi) - Q(\xi), \quad 0 < \xi < d < H-\tau; \\ &= K(\xi) \qquad , \quad d < \xi < L \qquad ; \end{aligned} \tag{3.44}$$

equation (3.34) or (3.36) becomes

$$\int_0^L Z_n(\xi)\, \bar{K}(\xi)\, d\xi = B_n + \int_0^L Z_n(\xi)\, Q(\xi)\, d\xi. \tag{3.45}$$

If the right hand side of (3.45) is rewritten as B_n, then (3.45) has the same form as equations (3.34) and (3.36), and $\bar{K}(\xi)$ can be solved for by the moment method described to solve (3.34) and (3.36).

3.4.1 Dipole Antenna Configuration

The configuration of the solid cylindrical dipole, for which numerical results are presented in section 3.6, is shown in Fig. 3.7. The dipole is of radius a and semi-height H. The corners at the ends are rounded, with τ being the radius of curvature.

3.4.2 Choice of Basis Functions

The surface current density $K(\xi)$ over the interval $0 < \xi < L$ in Fig. 3.7 is approximated by a finite number M of basis functions (see eqn. (3.38)). In Table 3.1, six sets of basis functions, $\{\varphi_m(\xi): 0 < \xi < L;\ m = 1,2,3,\ldots,M\}$, together with their functional forms, are listed. The members of all six sets of basis functions are zero at $\xi = L$, i.e. $\varphi_m(L) = 0$, so that condition (3.14) is automatically satisfied when these basis functions are used to approximate $K(\xi)$.

Form number 3, the wedge Bessel function, has been chosen to approximate the current on dipoles with sharp corners ($\tau = 0$). If the factors a and $(L-\xi)$ are removed, for $\xi < H$ and $\xi > H$ respectively, then $\varphi_m(\xi)$ is one of the wave-functions exactly applicable to a 90° wedge (Jones, 1964, Sect. 9.2). The aforementioned factors appear to be the simplest way of accounting for the cylindrical curvature of the dipole.

Form number 6, the orthonormalised Schmidt function, is used with METHOD 1 only. It is constructed from the $Z_n(\xi)$ functions, given in (3.37), by Schmidt's orthogonalisation procedure (Morse and Feshbach, 1953, Sect. 8.3; Faddeeva, 1959, Sect. 1.2). When the coefficients $D_{p,n}$ in Table 3.1 are found by the procedure, the orthonormal properties of the Schmidt functions make the matrix inversion in (3.42) trivial, and give

$$K_p = \sum_{n=1}^{p} D_{p,n} B_n. \qquad (3.46)$$

3.5 COMPUTATIONAL CONSIDERATIONS

The computer available at the University of Canterbury is an IBM 360/44 with a core storage of 128 Kbytes which permits double-precision arithmetic in 8-byte or 64-bit words.

Four programmes have been written in Fortran IV to cover all six sets of basis functions $\varphi_m(\xi)$ listed in Table 3.1. The first applies to the Fourier sine, Tchebyschev polynomial and Wedge Bessel functions used; the second to the Lagrange collocation polynomial; the third to the triangle functions; and the last to the Schmidt functions. The first three programmes are used in both METHODS 1 and 2, and each is organised into two separate phases. The first phase evaluates the elements of the matrix $[Z_{nm}]$ for any specified dipole configuration in Fig. 3.7, and the other computes and outputs the current distributions, admittances, and/or radiation patterns for different excitation sources applied to the dipole antenna.

The M x M matrix elements Z_{nm}, given by (3.40), are evaluated in the first phase of each program by numerical integration. The following procedure is adopted to evaluate the Z_{nm} to an accuracy which ensures that the unknown expansion coefficients K_m for different excitation sources are computed to better than 1%. First the integrals of Z_{nm}, given in (3.40), are integrated by the extended Simpson's quadrature rule to two significant figures and the resulting matrix is inverted to give a column vector $[K_m]_2$ for a particular ring source excitation. The subscript 2 attached to $[K_m]$ denotes the accuracy of the integration. The integration accuracy is then increased to three significant figures and the corresponding $[K_m]_3$ obtained. If the elements of $[K_m]_3$ agree with those of $[K_m]_2$ to within 1%, the procedure is stopped and the Z_{nm}, which are accurate to three significant figures, are now acceptable for use in phase two of the programme. Otherwise, the integration accuracy is increased to 4, then 5, 6 and 7 significant figures until two consecutive vectors of $[K_m]$ satisfy the 1% test.

If intermediate integration quantities are stored in the procedure just described, the CPU time required to evaluate $[Z_{nm}]$ is greatly reduced but then the largest size of $[Z_{nm}]$ is restricted to at most 15, which means that the dimensions, a and H, of the dipole antenna in Fig. 3.7 must be less than λ, otherwise numerical convergence is not achieved. METHODS 1 and 2 are thus examined computationally in relation to dipole antennas with $H \leqslant \lambda$ and $a \leqslant \lambda$.

A measure of the rate of numerical convergence is the "convergence number" M_c, defined as that $M = M_c$ for which the

surface current values on $0 < \xi < L$ agree to within 3% of those obtained when $M = M_c+1$ and $M = M_c+2$.

A numerical solution in either METHOD 1 or 2 is defined as practicable for a specific dipole antenna if:

(a) the current distributions obtained with increasing M converges, and the convergence number $M < 30L/\lambda$; and

(b) the corresponding matrices $[Z_{nm}]$ are sufficiently well-conditioned so that the Z_{nm} need be evaluated to at most seven significant figures.

3.6 NUMERICAL RESULTS

3.6.1 General Discussion

Computations in METHOD 1 have been performed with the Fourier sine, Tchebyshev and wedge Bessel basis functions only (see Table 3.1). The following comments apply to these computations.

(i) The computational usefulness of these three sets of basis functions are compared in Table 3.2, which applies to the half-wave dipole antenna with $a = \lambda/20$ and $\tau = 0$. The order of the normalized determinant $||Z||$, defined by (II-12) in Appendix II, at $M = 7$ is 10^{-2}, 10^{-2} and 10^{-13} respectively for the sine, Tchebyshev and wedge Bessel functions. Because of the smallness of $||Z||$ numerical solutions using the wedge Bessel functions are much less practicable than the other two sets (see Tables 3.7 and 3.8 also). Table 3.2 also shows that comparatively fewer terms of φ_m are needed to approximate $K(\xi)$ accurately when $(b-a) = \lambda$ than when $(b-a) = \lambda/100$. In the computations which use the sine functions and where

the ring source is at (b-a) = $\lambda/100$, numerical convergence is poor unless a rapidly varying term $Q(\xi)$ (see eqn (3.43)) is subtracted out. Note that the subtracting out of this rapidly varying term does not always improve the convergence sufficiently to overcome difficulties associated with ill-conditioned matrices $[Z_{nm}]$ or for M_c to be less than 15.

(ii) For a series of dipole antennas which have the same H/a ratios but different radii, numerical solution becomes increasingly impracticable with increasing a. There are two reasons for this. Firstly, the $||Z||$ with increasing M fall off more rapidly. This is illustrated by Table 3.3, which applies to the two dipoles H/a = 4, a = $\lambda/16$ and a = $\lambda/4$. Secondly, the convergence numbers M_c increase because $K(\xi)$ is to be approximated over a longer interval $0 < \xi < L$. For the two antennas with a = $\lambda/16$ and a = $\lambda/4$ in Table 3.3, M_c is 3 and 7 respectively, when the magnetic ring source is at (b-a) = λ.

(iii) With an upper limit of seven significant figures in evaluating Z_{nm} (Section 3.5), $||Z||$ as small as 10^{-18} can be handled. This is demonstrated by Table 3.4 which shows the convergence of the first three expansion coefficients of $K(\xi)$ on the dipole antenna H = λ, a = $\lambda/4$, τ = $\lambda/10$ and (b-a) = λ.

As the spherical (H = a = τ) dipole can be solved exactly by METHOD 2, dipole antennas with H = a and τ varying are chosen to compare the computational usefulness of the various basis functional sets listed in Table 3.1. The convergence numbers M_c shown in Table 3.5 for each of the basis functional forms, apply to dipoles with H = a = $\lambda/4$,

varying τ, and magnetic ring sources at $(b-a) = \lambda/100$ and $(b-a) = \lambda$. Table 3.5 and the computations performed to construct it are discussed below:

(i) The triangle and the orthonormalised Schmidt functions are only satisfactory when the dipole is close to being a sphere. This is demonstrated in Fig. 3.8 where the current distributions are obtained by using the Schmidt functions with different values of M. When τ is nearly the same as H, the numerical convergence is rapid, but it falls off rapidly with decreasing τ. This also applies to the triangle functions. Other computations show that the convergence is even slower when $H \neq a$.

(ii) When the ring source is further than $\lambda/20$ $(b-a > \lambda/20)$ from the dipole surface, the convergence is rapid for the Fourier sine, wedge Bessel, Tchebyshev and Lagrange polynomial basis functions, and it is little affected by decreasing τ(see Table 3.5). In the case where $\tau = 0$, the differences between the surface current distributions obtained with the sine, Tchebyshev and Lagrange functions and that obtained with the wedge Bessel functions are only noticeable in the neighbourhood of the 90° corner. These differences, expressed as a percentage of the maximum surface current value on the dipole, are shown in Fig. 3.9 for the dipole with $H = a = \lambda/4$, $\tau = 0$ and $(b-a) = \lambda$. $M = 10$ is used in computing the results in Fig. 3.9.

(iii) When the ring source is a small electrical distance $(b-a < \lambda/20)$ from the dipole surface, the surface current is rapidly varying in the neighbourhood of $\xi = 0$ (see Appendix III). This behaviour is illustrated in Fig. 3.10,

which applies to the half-wave dipole H = a = $\lambda/4$, $\tau = \lambda/10$ and ring sources at (b-a) = $\lambda/100$ and (b-a) = λ. The imaginary part of the current rises rapidly near $\xi = 0$ when (b-a) = $\lambda/100$. As shown in Table 3.5, this behaviour makes numerical convergence slower, i.e. the convergence numbers M_c when (b-a) = $\lambda/100$ are larger than when (b-a) = λ. Note that Table 3.5 shows that numerical solutions are still practicable when the wedge Bessel, Tchebyshev or Lagrange polynomials are used. However, when the Fourier sine functions are used, numerical convergence is poor for the dipoles with $\tau = \lambda/4$ and $\tau = \lambda/10$ in Table 3.5 unless the rapidly varying term, $Q(\xi)$ given in (3.43), is subtracted out. For the other two dipoles with $\tau = \lambda/25$ and $\tau = 0$ in Table 3.5, numerical convergence does not occur, even on subtracting out $Q(\xi)$, when the Fourier sine functions are used. Further discussion on this point is postponed to section 3.6.2.

(iv) When $M = M_c + 2$ is less than 15, the current distributions computed with $M = M_c$ to M = 15 agree to within 2% of the maximum value on $0 < \xi < L$. The convergence of the first expansion coefficient K_1 is shown in Table 3.6 for the dipole antenna with H = a = $\lambda/4$, $\tau = 0$ and (b-a) = $\lambda/100$.

3.6.2 Dependence on H/a

Two series of dipoles, one having H = $\lambda/4$ and varying a and the other a = $\lambda/4$ and varying H, are chosen to illustrate the range of H/a for which numerical solutions using METHODS 1 and 2 are practicable. The associated normalised determinants, $||Z||$ with N = M = 7, and convergence numbers M_c with ring sources at (b-a) = $\lambda/100$ and (b-a) = λ, are

shown in Tables 3.7 and 3.8 respectively for these two series of dipoles. The tables show that METHODS 1 and 2 are practicable in different ranges of H/a ratios, namely $1.0 < H/a < 25$ and $0.25 < H/a < 2.0$ respectively. They are inconvenient to use in the respective ranges $H/a < 1.0$ and $8.0 < H/a < 0.25$ because the ill-conditioned matrices, indicated by small normalised determinants, necessitate protracted computer evaluations for the matrix elements.

When METHOD 2 is used in the range $2.0 < H/a < 8.0$, the matrices $[Z_{nm}]$ are still well-conditioned enough for accurate computation to be performed conveniently, but numerical solutions diverge with increasing M if the ring source is close to the dipole antenna. This is clearly illustrated in Table 3.9, which applies to dipoles with fixed lengths $H = \lambda/4$, $\tau = 0.1a$, and varying radius. The table shows that, as a/λ decreases, numerical convergence occurs only if the ring source is sufficiently far away.

From Tables 3.7 and 3.8, it is concluded that the Tchebyshev polynomial basis function, number 2 in Table 3.1, leads to practicable numerical solutions over the widest range of H/a and a/λ.

3.6.3 CPU Time

Table 3.10 shows approximate CPU times required to compute the current distributions on the half-wave dipoles of varying radii and excited by a magnetic ring source at $(b-a) = \lambda/100$. These CPU times are calculated on the basis of a matrix size M which is equal to the convergence numbers M_c given in Table 3.7. Table 3.10 shows that, for METHOD 1, CPU time decreases and then increases as a/λ is increased.

For dipoles with electrically small radii ($a/\lambda < 0.05$), the kernel $Z(z,\xi)$ (see eqn 3.21 and 3.25) is rapidly varying when the points denoted by z and ξ are closest together so that numerical integration becomes protracted. The CPU times are larger for the larger a/λ because of the decreasing magnitude of the normalised determinant $||Z||$ (see Table 3.7). For METHOD 2, Table 3.10 shows that CPU time increases as the radius a/λ increases from 0.15 to 1.0. This increase in CPU time is due to the larger M_c needed to obtain accurate current distributions and the smaller magnitude of the associated normalised determinants $||Z||$ (see Table 3.7).

3.6.4 Current Distributions and Radiation Patterns

It is interesting to compare the current distributions on a particular dipole for several ring sources situated at different, but small, electrical distances from the dipole surface. Those shown in Fig. 3.11 are based on computations using 7 Tchebyshev functions in METHOD 1, and apply to the full-wave dipole $H = \lambda/2$, $a = \tau = 0.085\lambda$ driven by a ring source at $b/a = 1.05$, 1.1, or 1.5. Also shown in the figure is the current distribution obtained by exciting the same dipole with a magnetic frill source having dimensions $b_1/b_o = b_1/a = 1.219$. The real parts of all the distributions agree to within 2% overall and the imaginary parts differ noticeably only in the neighbourhood of $\xi = 0$. The two distributions which have been obtained with the ring source at $b/a = 1.1$ and the frill source ($b_1/a = 1.219$) differ by less than 1.5% overall. These results concur with the observation (Bach Andersen, 1968; Otto, 1969) that the conductance of a monopole is much less sensitive to small

changes in the feeding conditions than susceptance.

Some representative radiation patterns, which are obtained by using (3.29), and current distributions on half-wave dipoles are shown in Figs 3.12 and 3.13, where Fourier sine and Tchebyshev basis functions have been used in METHOD 2.

3.6.5 Comparison with Published Results

In this section the results obtained by the present two methods are compared with those published by Vasil'ev (1959), Einarsson (1966) and Ting (1969). Fig. 3.14 compares the normalised surface current density on a hemispherically-capped dipole obtained by Vasil'ev (1959) and that obtained by METHOD 1 using Tchebyshev polynomial basis functions. Two factors make the comparison a qualitative one only. First, the graph given by Vasil'ev is small, viz. about one-tenth of the size in Fig. 3.14. The second concerns the different excitation sources used; Vasil'ev's dipole is fed by an applied voltage across a circumferential slot, of undefined width, in the dipole surface whilst the author uses a ring source at $(b-a) = \lambda/100$.

Einarsson's (1966) results apply to solid dipoles with plane ends and fed symmetrically by a delta gap source. For an exact comparison with his results a ring source at $b = a$ would have to be used in the author's computations. But the computations are inconvenient when $b = a$ because the surface current density is infinite at $\xi = 0$ (see Fig. 3.7). Instead a ring source at $(b-a) = \lambda/100$ is used. The results are compared in Figs 3.15 and 3.16, which show agreement to within 2% and 4 degrees respectively for the magnitude and

phase over most of the interval $0 < \xi < L = 0.33\lambda$ and $L = 0.60\lambda$. The differences are large in the neighbourhood of $\xi = 0$ only. METHOD 1 and 7 Tchebyshev basis functions has been used in the computations.

Ting (1969) treated the hemispherically-capped monopole which is mounted on a ground plane and fed by a coaxial line (see Fig. 3.17a). Using Tchebyshev basis functions in METHOD 1 and a magnetic frill source (cf. eqn (3.5)) with $b_o = a$, admittances defined by (3.31) are computed for the equivalent dipole antenna shown in Fig. 3.17b. Admittance expression (3.31) has been used in preference to (3.32), because (3.32) involves a numerically troublesome double integral over the surface of the dipole. The admittance values are compared with Ting's (1969) in Fig. 3.18. The agreement is to better than 2 millimhos overall.

3.6.6 Comparison with Experimental Results

The normal component of the electric intensity on a thick monopole, with sharp corners ($\tau = 0$) and mounted on a ground plane, has been measured. The experimental technique and the associated computations are described in Appendix IV. Fig. 3.19 compares the measured and computed values, and shows that agreement is within 2.5% for the magnitudes and 8^o for the phases.

3.7 COMPARISON WITH EXISTING METHODS

Of the methods which are reviewed in Chapter 1 only those of Vasil'ev (1959; Vasil'ev and Seregina, 1963), Einarsson (1966), Vasil'ev et al., (1967a), Mautz and Harrington (1969, 1971a,b) and Ting (1969) apply to the thick

solid cylindrical antenna, With reference to the cylindrical dipole shown in Fig. 3.7, the major features of these methods and METHODS 1 and 2 in this chapter are shown in Table 3.11.

The first three methods in Table 3.11 are only applicable to antennas with cylindrical geometry and in Einarsson's (1966) the ends must be plane ($\tau = 0$). For long ($H \gg \lambda$) cylindrical antennas with plane ends, Einarsson's (1966) technique is superior to the others because the size M of the solution matrix $[Z_{nm}]$ remains the same for any H (cf. section 1.2.2). For example, M is 7-8 when $a/\lambda < 0.15$ for H/λ = 0.23, 0.50 and 0.75 (Einarsson, 1966). The other methods, including METHODS 1 and 2, use integral equations in the unknown current density $K(\xi)$, and so require larger matrix sizes as the dipole length is increased.

Though applicable over a wider range of H/a and a/λ than METHODS 1 and 2, the techniques of Vasil'ev and his colleagues (Vasil'ev, 1959; Vasil'ev and Seregina, 1963; Vasil'ev et al., 1967a) and Mautz and Harrington (1969, 1971a,b) involve numerically troublesome double integrals, and are unsuitable for examining surface currents near sharp edges on antennas.

None of the papers pertaining to the methods, numbered as 1 to 6 in Table 3.11, give sufficient information to make a comparison of CPU times with METHODS 1 and 2.

Table 3.1: Basis functions $\varphi_m(\xi)$ used for expanding $K(\xi)$ in eqn (3.38).

Identification number of basis function	Name of basis function	Functional form of basis function	Remarks
1	Fourier sine function	$\sin([2m-1]\pi[L-\xi]/L)$	Equation (3.13) satisfied automatically by $\sum_{m=1}^{M} K_m \varphi_m(\xi)$
2	Tchebyshev polynomial	$T_{2m-1}\left(\frac{L-\xi}{L}\right) =$ $\cos([2m-1]\arccos([L-\xi]/L))$	Extra constraints placed on $\{K_m\}$, during numerical evaluation, to satisfy equation (3.13)
3	Wedge Bessel function	$a\, J_{2(m-1)/3}(k_o[H-\xi])$, $\xi < H$ $(-)^{m-1}[L-\xi]J_{2(m-1)/3}(k_o[\xi-H])$, $\xi > H$	ditto Also, only used for $\tau = 0$
Define a set $\{\xi_n \mid 1 \leq n \leq M;\ 0 \leq \xi_n \leq L;\ \xi_{n+1} > \xi_n\}$ of points along C.			
4	Lagrange collocation polynomial	$\prod_{n=1}^{m-1} \frac{\xi-\xi_n}{\xi_m-\xi_n} \prod_{n=m+1}^{M} \frac{\xi-\xi_n}{\xi_m-\xi_n}$	ditto Also, K_M set to zero during evaluation to satisfy eqn. (3.14).
Define a set $\{\xi_n\}$ as above for 4. Define another set $\{\Omega_p(\xi) \mid 0 \leq p \leq M;\ \Omega_o = \Omega_M = 0; \Omega_p = 1, \xi_p \leq \xi \leq \xi_{p+1}; \Omega_p = 0, \xi_p \geq \xi \geq \xi_{p+1}\}$ of functions.			
5	Triangle function	$\left(\frac{\xi-\xi_{m-1}}{\xi_m-\xi_{m-1}}\right)\Omega_{m-1} + \left(1-\frac{\xi-\xi_m}{\xi_{m+1}-\xi_m}\right)\Omega_m$	K_M set to zero during evaluation to satisfy eqn. (3.14)
6	Orthonormalised Schmidt function	$\sum_{p=1}^{m} D^*_{m,p}[\hat{\xi}.\underline{N}^{(4)}_{eo(2p-1)}(k_o\underline{r}')]^*$; $D_{m,p}$ are Schmidt's orthonormalization coefficients	Equations (3.13) satisfied automatically by $\sum_{m=1}^{M} K_m \varphi_m(\xi)$. The asterisk denotes "complex conjugate of".

Table 3.2: Order of magnitude of normalised determinants $||Z||$ and convergence numbers M_c for dipole H = $\lambda/4$, a = $\lambda/20$ and τ = 0. METHOD 1 used.
* denotes that the rapidly varying term $Q(\xi)$, given in (3.43), has been subtracted out.

Basis functions $\{\varphi_m\}$ as in Table 3.1	Sine	Tchebyshev	Wedge Bessel
$O(\|\|Z\|\|)$ with M = 7	10^{-2}	10^{-2}	10^{-13}
M_c when (b-a) = $\lambda/100$	*5	6	-
M_c when (b-a) = λ	3	3	3

Table 3.3: Order of magnitude of normalised determinant $||Z||$ with increasing M for two dipoles having the same H/a ratio. Fourier sine basis functions used in METHOD 1.

Dipole antenna dimensions as in Fig. 3.7 / M	H = $\lambda/4$, a = $\lambda/16$, τ = H/10	H = λ, a = $\lambda/4$, τ = H/10
2	10^{0}	10^{0}
4	10^{-1}	10^{-1}
6	10^{-1}	10^{-3}
8	10^{-2}	10^{-5}
10	10^{-4}	10^{-7}
12	10^{-7}	10^{-11}
14	10^{-11}	10^{-16}

Table 3.4: Convergence of first three expansion coefficients for surface current density $K(\xi)$ on dipole $H = \lambda$, $a = \lambda/4$, $\tau = \lambda/10$, and $(b-a) = \lambda$. Fourier sine basis functions used in METHOD 1.

M	Order of magnitude of $\|\|Z\|\|$	Modulus of expansion Coefficients		
		$\|K_1\|$	$\|K_2\|$	$\|K_3\|$
3	10^{-1}	0.07256	0.05709	0.02175
4	10^{-1}	0.07166	0.05780	0.02105
5	10^{-2}	0.07130	0.05782	0.01983
6	10^{-3}	0.07114	0.05778	0.01939
7	10^{-4}	0.07109	0.05774	0.01957
8	10^{-5}	0.07108	0.05773	0.01986
9	10^{-6}	0.07107	0.05775	0.01999
10	10^{-7}	0.07106	0.05778	0.01997
11	10^{-9}	0.07105	0.05780	0.01991
12	10^{-11}	0.07104	0.05781	0.01991
13	10^{-13}	0.07104	0.05780	0.01998
14	10^{-16}	0.07103	0.05780	0.02002
15	10^{-18}	0.07103	0.05780	0.02002

Table 3.5: Convergence numbers M_c in METHOD 2 for dipoles H = a = $\lambda/4$ and varying τ.
* denotes that the rapidly varying term $Q(\xi)$ given in (3.43) has been subtracted out.
D denotes divergent numerical solution.

Basis functions $\{\varphi_m\}$ as in Table 3.1	Sine		Tchebyshev		Wedge Bessel		Schmidt		Lagrange		Triangle	
τ/λ \ $(b-a)/\lambda$	.01	1.0	.01	1.0	.01	1.0	.01	1.0	.01	1.0	.01	1.0
0.25	>15	2	6	3	-	-	Exact	Exact	6	3	11	4
0.10	*7	2	7	3	-	-	15	13	6	3	>15	6
0.025	D	2	8	3	-	-	-	-	7	4	D	7
0.00	D	2	8	3	7	3	-	-	7	4	-	-

Table 3.6: Convergence of first expansion coefficient K_1 in eqn (3.38) for dipole $H = a = \lambda/4$, $\tau = 0$, and $(b-a) = \lambda/100$. METHOD 2 used.

Basis functions $\{\varphi_m\}$ as in Table 3.1 / M	Tchebyshev	Wedge Bessel	Lagrange
5	0.1559 + j0.0740	0.04670 - j0.04320	0.1504 + j0.1584
6	0.1535 + j0.0718	0.04908 - j0.04285	0.1540 + j0.1674
7	0.1551 + j0.0728	0.04888 - j0.06129	0.1510 + j0.1742
8	0.1549 + j0.0745	0.04765 - j0.06117	0.1493 + j0.1776
9	0.1548 + j0.0746	0.04724 - j0.05004	0.1507 + j0.1787
10	0.1548 + j0.0746	0.04774 - j0.05018	0.1518 + j0.1800
11	0.1547 + j0.0750	0.04757 - j0.05390	0.1504 + j0.1809
12	0.1549 + j0.0749	0.04753 - j0.05388	0.1496 + j0.1809

Table 3.7: Order of magnitude of normalised determinant $\|Z\|$ with M = 7, and convergence numbers M_c when (b-a) = λ/100 and λ, for dipoles H = λ/4 and varying a.
* denotes that the rapidly varying term Q(ξ) given in (3.43) has been subtracted out.
D denotes divergent numerical solution.

Method used as in eqns 3.34-3.37	METHOD 1			METHOD 2			
Basis functions $\{\varphi_m\}$ as in Table 3.1	sine	Tchebyshev	Wedge Bessel	sine	Tchebyshev	Wedge Bessel	Lagrange
a/λ \ τ/a	0.1	0.1	0.0	0.1	0.1	0.0	0.1
O(‖Z‖) Order of magnitude of normalised determinant ‖Z‖ with M = 7							
0.01	10^{-2}	10^{-4}	10^{-11}				
0.02	10^{-2}	10^{-3}	10^{-12}	10^{-13}	10^{-13}		10^{-21}
0.05	10^{-2}	10^{-2}	10^{-13}	10^{-10}	10^{-10}	10^{-16}	10^{-12}
0.15	10^{-6}	10^{-7}	10^{-18}	10^{-4}	10^{-4}	10^{-10}	10^{-3}
0.25	10^{-11}	10^{-13}		10^{-1}	10^{-1}	10^{-5}	10^{-4}
0.35	10^{-15}	10^{-17}		10^{-2}	10^{-2}	10^{-4}	10^{-8}
0.50	10^{-18}	10^{-22}		10^{-4}	10^{-4}	10^{-6}	10^{-11}
1.00				10^{-7}	10^{-5}	10^{-9}	10^{-15}
Convergence number M_c when ring source is at (b-a) = λ/100							
0.01	*7	6	see section 3.6,	D	D	D	D
0.02	*6	6	ditto	D	D	D	D
0.05	*5	6	ditto	D	D	D	D
0.15	*5	6	ditto	D	5	D	D
0.25	*4			D	8	10	7
0.35				*8	8	9	8
0.50				*8	11	11	12
1.00				*11			
Convergence number M_c when ring source is at (b-a) = λ							
0.01	6	6	5	D	D	D	D
0.02	3	4	4	D	D	D	D
0.05	3	2	3	2	4	4	4
0.15	3	4		2	4	4	3
0.25	4	4		2	3	3	4
0.35	5			3	5	4	5
0.50				6	8	7	7
1.00				9			

Table 3.8: Order of magnitude of normalised determinant $\|Z\|$ with M = 7, and convergence numbers M_c when (b-a) = λ/100 and λ, for dipoles a = λ/4 and varying H.
*denotes that the rapidly varying term Q(ξ) given in (3.43) has been subtracted out.
D denotes divergent numerical solution.

Method used as in eqns 3.34 - 3.37	METHOD 1			METHOD 2			
Basis functions $\{\varphi_m\}$ as in Table 3.1	sine	Tchebyshev	Wedge Bessel	sine	Tchebyshev	Wedge Bessel	Lagrange
H/λ \ τ/H	0.1	0.1	0.0	0.1	0.1	0.0	0.1
O($\|Z\|$) Order of magnitude of normalised determinant $\|Z\|$ with M = 7							
1.00	10^{-3}	10^{-4}	10^{-10}	10^{-8}	10^{-7}		10^{-9}
0.50	10^{-7}	10^{-7}	10^{-15}	10^{-6}	10^{-4}	10^{-10}	10^{-4}
0.35	10^{-9}	10^{-10}		10^{-4}	10^{-3}	10^{-8}	10^{-2}
0.25	10^{-11}	10^{-13}		10^{-1}	10^{-1}	10^{-5}	10^{-4}
0.10				10^{-5}	10^{-6}	10^{-9}	10^{-12}
0.05				10^{-9}	10^{-8}	10^{-15}	10^{-18}
0.025				10^{-10}			
Convergence number M_c when ring source is at (b-a) = λ/100							
1.00	see section 3.6.1	12	see section 3.6.1	D	D	D	D
0.50	ditto	5		D	7	D	D
0.35	ditto	5		D	6	D	6
0.25	*4			D	8	10	7
0.10				10	4	9	5
0.05				11	7	7	7
0.025							
Convergence number M_c when ring source is at (b-a) = λ							
1.00	7	10	see section 3.6.1	8	8		8
0.50	5	5		5	5	6	6
0.35	4	4		3	3	5	5
0.25	4	4		2	3	3	4
0.10				4	3	4	3
0.05				5	3	5	5
0.025				5			

Table 3.9: Convergence numbers M_c for dipole H = $\lambda/4$, τ/a = 0.1 and varying a. Tchebyshev polynomial basis functions used in METHOD 2.
D denotes divergent numerical solution.

a/λ \ (b-a)/λ	0.01	0.10	0.25	1.00
0.03	D	D	D	4
0.05	D	D	4	4
0.10	D	4	4	4
0.15	5	5	5	4

Table 3.10: Approximate CPU time (in minutes) required to compute current distributions on the halfwave dipoles of varying radii to 3% accuracy.
Note: other information related to these dipoles is given in Table 3.7.

Method used as in eqns 3.34-3.37	METHOD 1		METHOD 2			
Basis function $\{\varphi_m\}$ as in Table 3.1	Sine	Tchebyshev	Sine	Tchebyshev	Wedge Bessel	Lagrange
a/λ \ τ/a	0.1	0.1	0.1	0.1	0.0	0.1
0.01	1½	1½				
0.02	1¼	1¼				
0.05	¾	¾				
0.15	¾	¾		1		
0.25	1½			1½	2¼	1
0.35			2	1½	2	1
0.50			3	4	5½	2
1.00			11			

Table 3.11: Major features of methods which are applicable to the thick dipole antenna shown in Fig. 3.7.
† denotes that the figure has been estimated.
N denotes the number of basis functions required to give the surface current density to a prescribed accuracy.

Identification number	Reference or method	Integral equation	Surface, or extended, boundary condition used	Moment method of numerical solution (Appendix II)			Dipole dimensions for which method is practicable	Remarks
				Testing function	Basis function	Form of matrix element Z_{nm}		
1	Einarsson (1966)	(1.4)	surface	Dirac delta	power series	infinite integral with singular integrand	$a/\lambda < 0.15^{\dagger}$	Only 7 to 8 basis functions required for cylindrical dipole of $a \leqslant \lambda/10$ and any H for 0.5% accuracy.
2	Ting (1969)	(1.15) & (1.17)	surface	Dirac delta	parabolic	infinite integral with singular integrand	$a/\lambda < 0.15$	Applicable to hemispherically-capped cylindrical antennas only.
3	Gavorun (1962)	(1.19)	extended	Dirac delta	parabolic	finite integral with simple integrand	$a/\lambda < 0.15^{\dagger}$	Applicable to cylindrical antennas only. $N = 16L/\lambda$ to $32L/\lambda$ for 1% accuracy in $K(\xi)$.
4	Vasil'ev (1959), Vasil'ev & Seregina (1963)	(1.21)	surface	Dirac delta	pulse	double integrals with singular integrand	any a and H, $\tau > \lambda/10$	$N = 10L/\lambda$ for 2-7% accuracy in $K(\xi)$.
5	Vasil'ev et al. (1967a)	(1.22)	extended	ditto	ditto	double integrals with simple integrand	ditto	ditto
6	Mautz and Harrington (1969, 1971a, b)	(1.24)	surface	pulse or triangle	pulse or triangle	double integrals with singular integrand	any a and H	
7	METHOD 1 (chap.3)	(3.21), (3.34) & (3.35)	extended	Dirac delta	sine, Tchebyshev, wedge Bessel	finite integral with simple integrand	$1 < H/a < 25$, $a < \lambda/4$; $2 < H/a < 25$, $\lambda/4 < a < \lambda/2$	When $\tau = 0$, the edge conditions on $K(\xi)$ are satisfied exactly by the wedge Bessel functions.
8	METHOD 2 (chap.3)	(3.25), (3.36) & (3.37)	extended	vector spherical wave	ditto, & Lagrange	ditto	$0.25 < H/a < 2.0$	$N \approx 15L/\lambda$ for 3% accuracy in $K(\xi)$

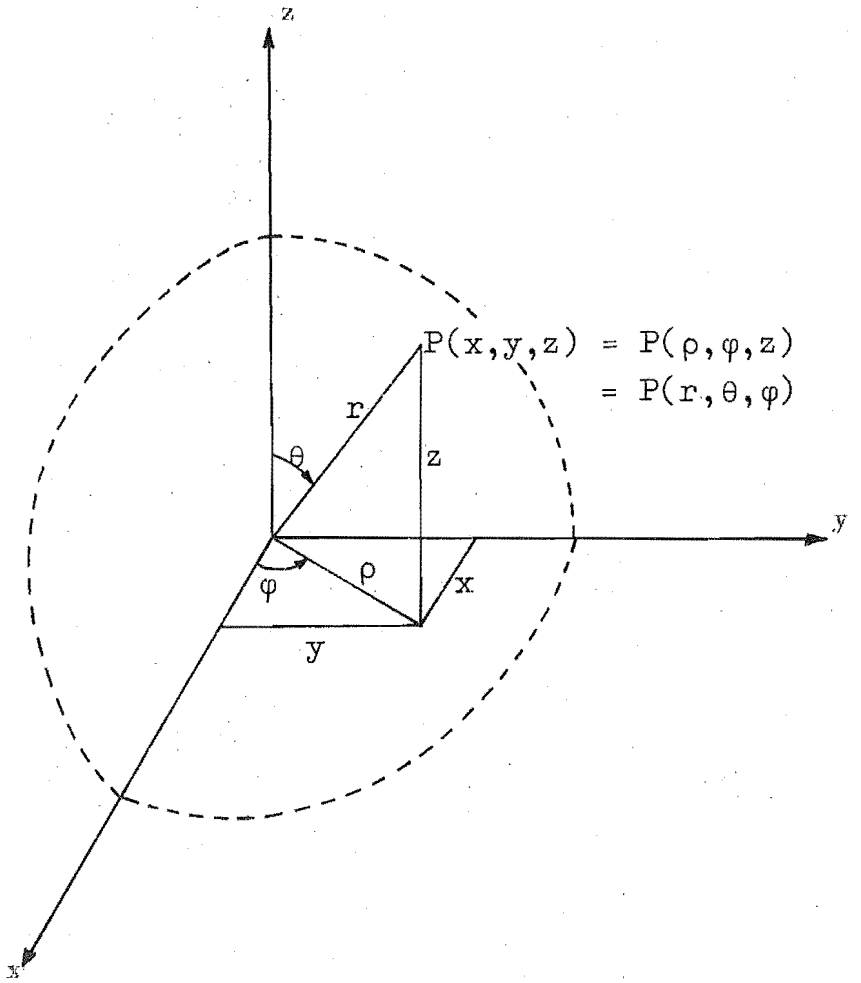

Fig. 3.1: Cartesian, cylindrical and spherical polar coordinate systems.

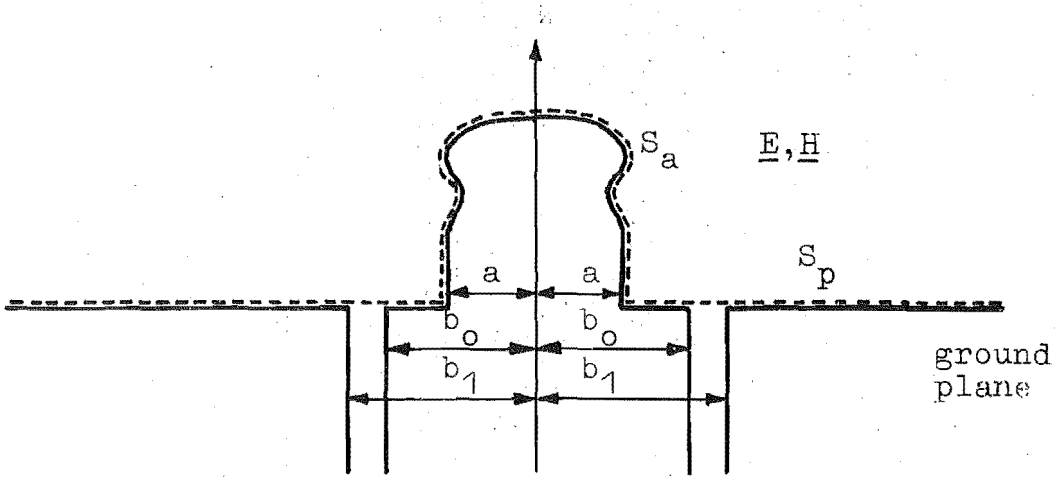

Fig. 3.2a: Axially symmetric monopole mounted on a ground plane and fed by a coaxial line, whose inner radius b_o is greater than a.

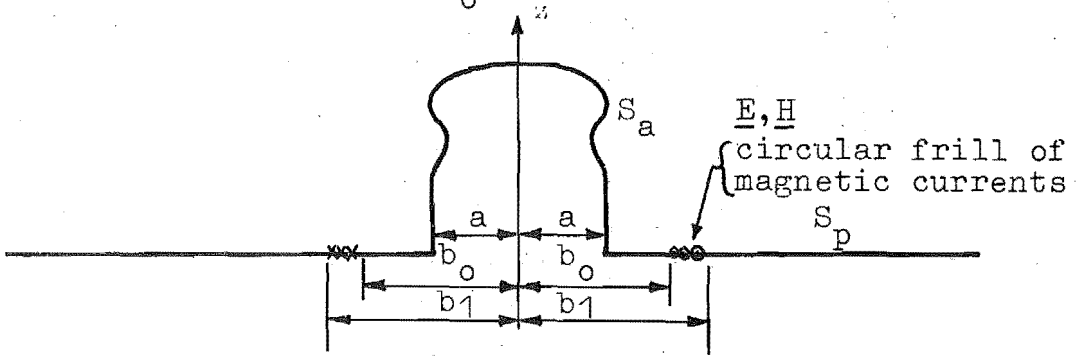

Fig. 3.2b: Monopole antenna equivalent to that shown in Fig. 3.2a

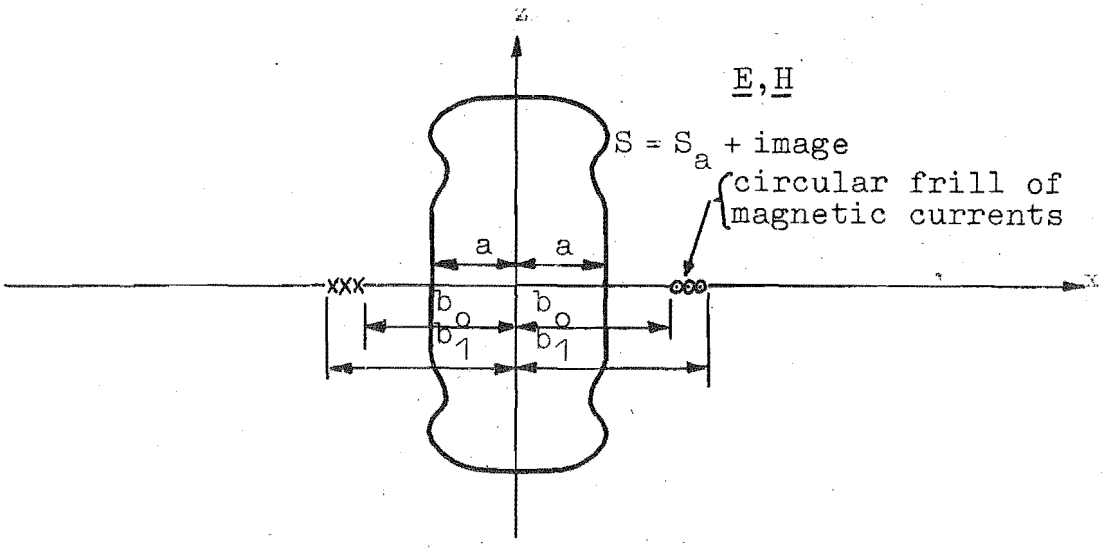

Fig. 3.2c: Dipole antenna equivalent to that shown in Fig. 3.2a.

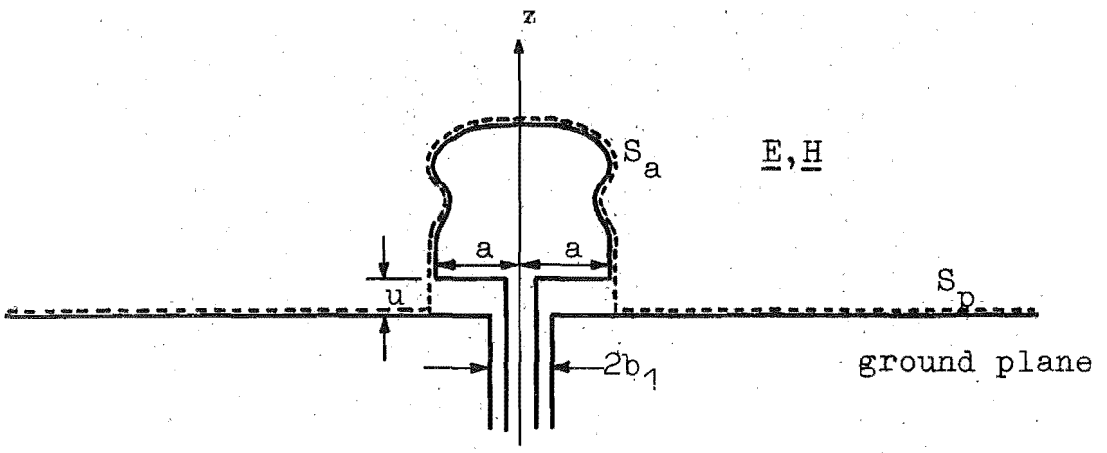

Fig. 3.3a: Axially symmetric monopole mounted on a ground plane and fed by a coaxial line, whose outer radius b_1 is less than a.

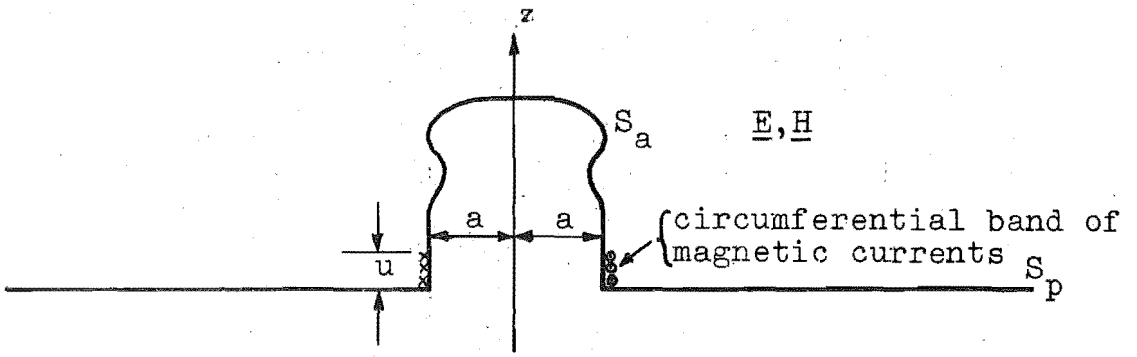

Fig. 3.3b: Monopole antenna equivalent to that shown in Fig. 3.3a.

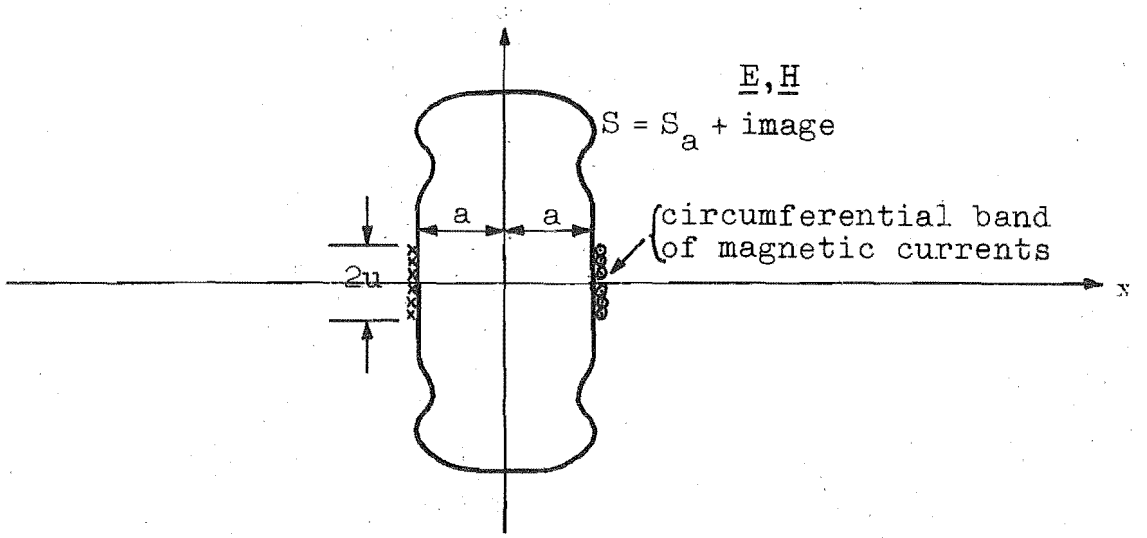

Fig. 3.3c: Dipole antenna equivalent to that shown in Fig. 3.3a.

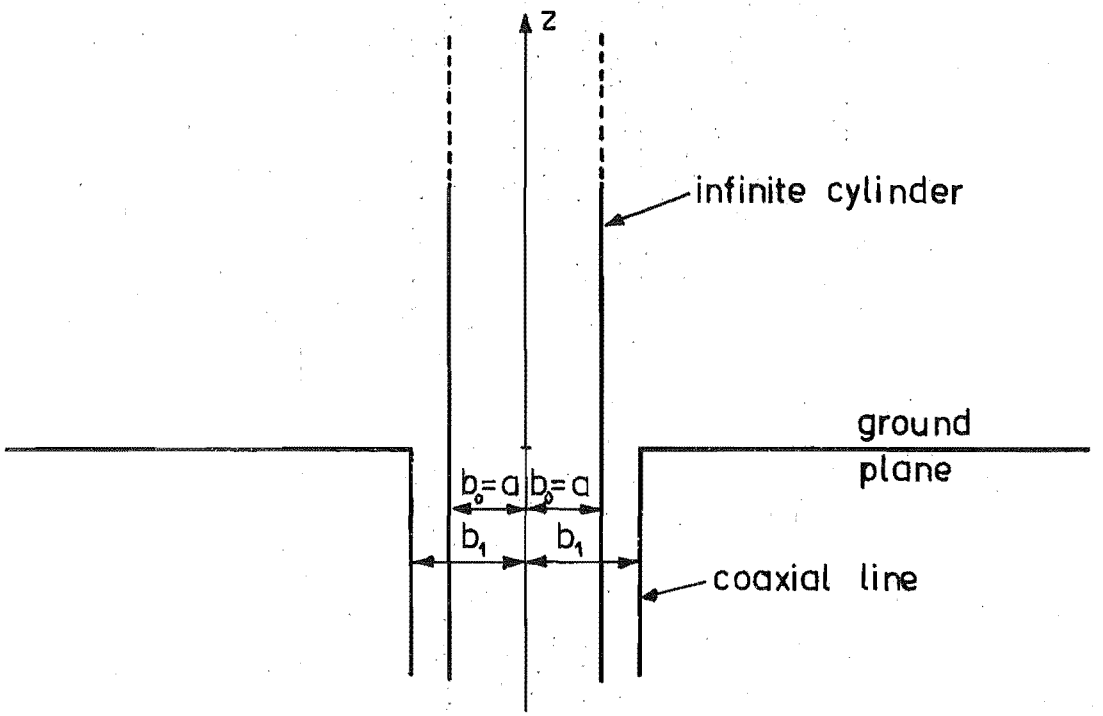

Fig. 3.4: Infinite cylindrical monopole driven by a coaxial line.

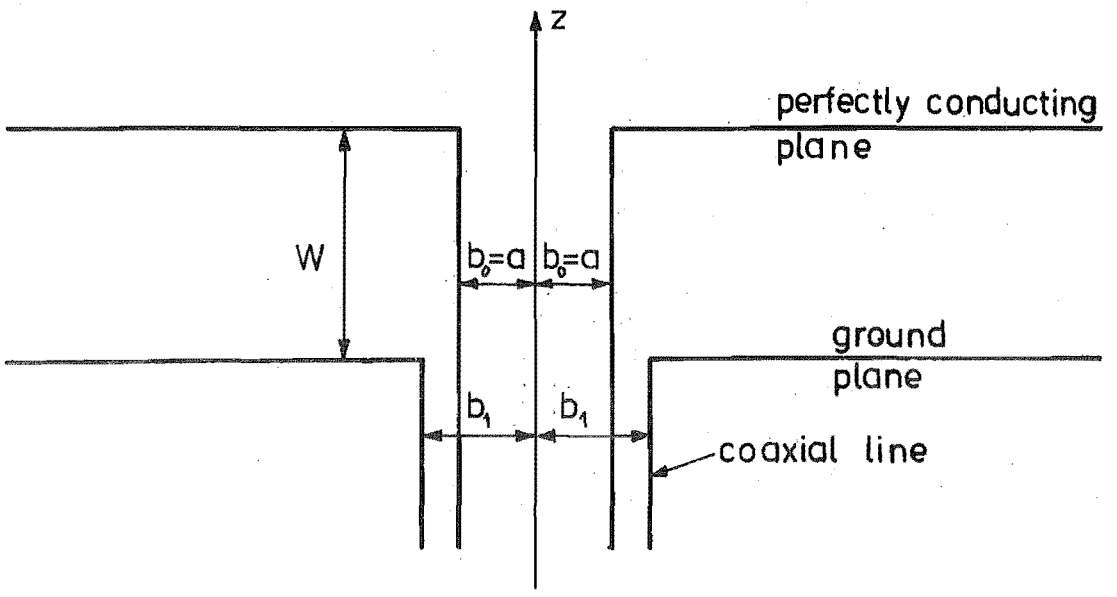

Fig. 3.5: Cylindrical monopole in an infinite parallel-plate region driven by a coaxial line.

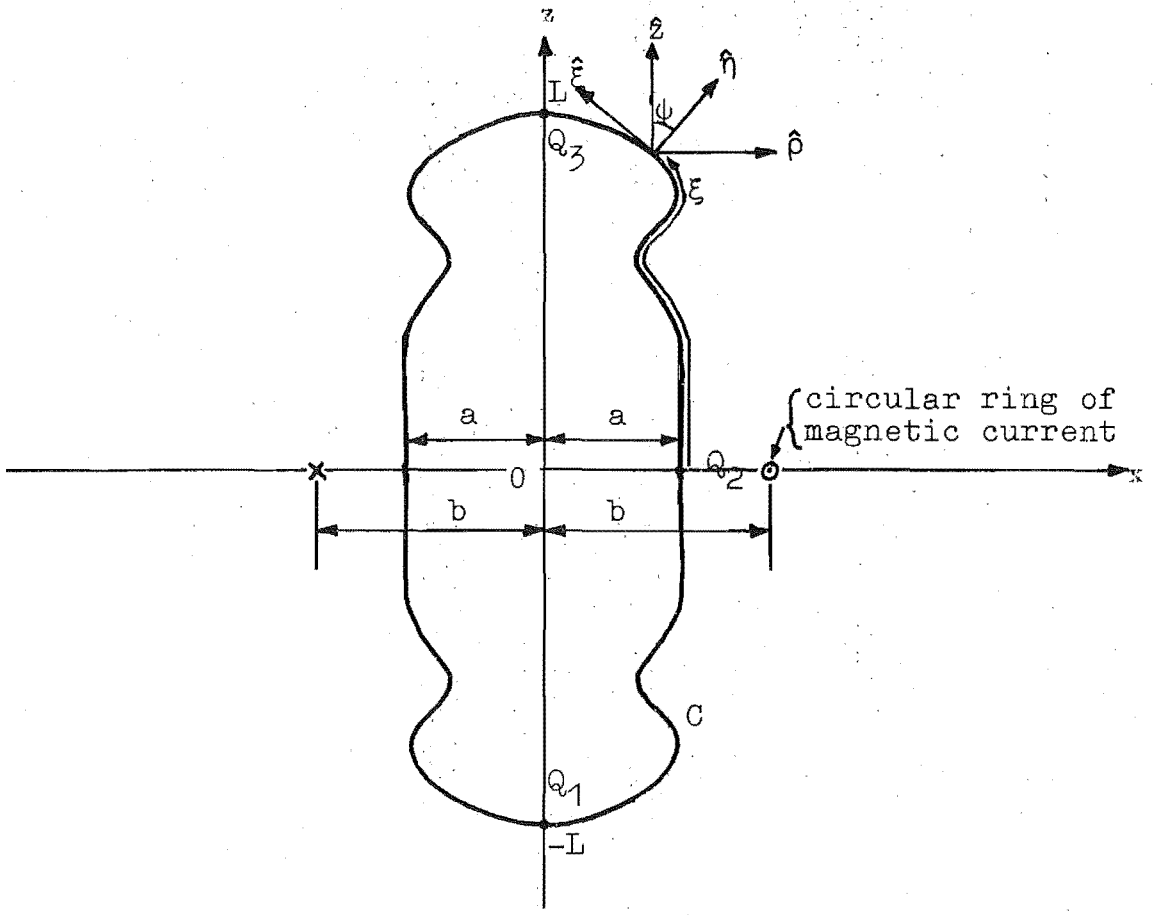

Fig. 3.6: Axially symmetric dipole driven by a magnetic ring source.
C is the generatrix of the dipole.
L is the length of arc from Q_2 to Q_3.

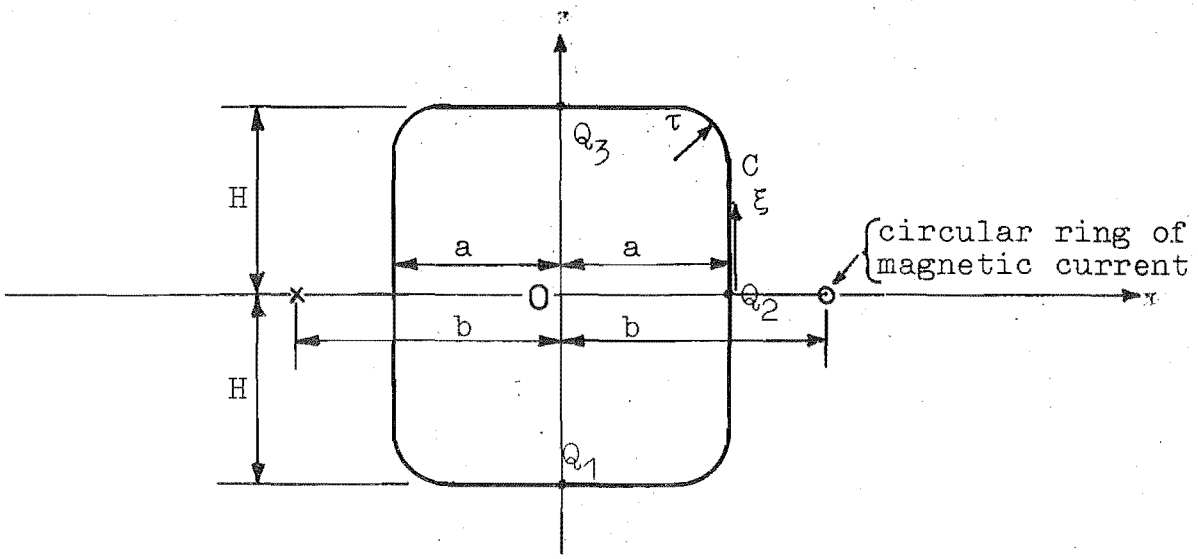

Fig. 3.7: Particular dipole configuration to which the results of section 3.6 apply.
H = semi-height; a = radius; τ = radius of curvature of corner; $L = H + a - 2\tau + \pi\tau/2$; and b = radius of magnetic ring source.

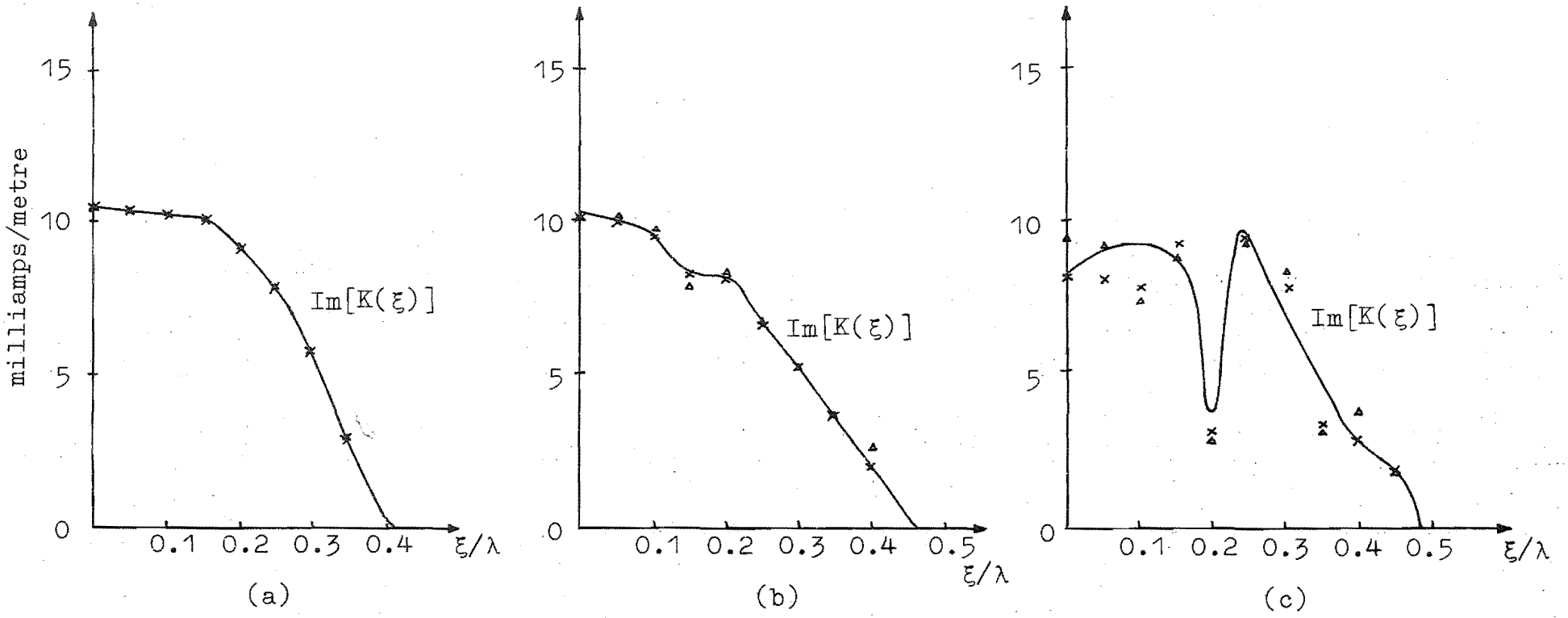

Fig. 3.8: Numerical convergence of imaginary part of surface current density $K(\xi)$, computed by using Schmidt orthonormalised functions in METHOD 2, on a dipole of $H = a = \lambda/4$, $(b-a) = \lambda$ and (a) $\tau = 0.22\lambda$; (b) $\tau = 0.10\lambda$; and (c) $\tau = 0.025\lambda$.
Legend: ▲▲▲▲ M = 9; ×××× M = 12; and ——— M = 15.

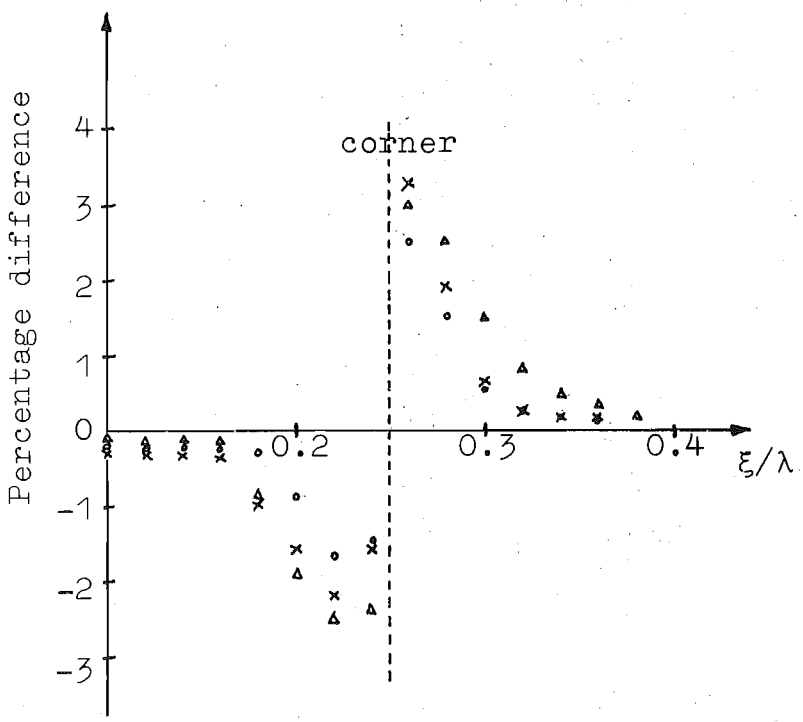

Fig. 3.9: Percentage difference of $K^1(\xi)$, $K^2(\xi)$, $K^3(\xi)$ and $K^4(\xi)$ near sharp corner (τ = 0) of dipole H = a = $\lambda/4$ and (b-a) = λ. METHOD 2 used. Superscripts on $K(\xi)$ indicate which set of basis functions, as numbered in Table 3.1, is used in eqn (3.37). "Re" denotes "real part of".

Legend: .... $\mathrm{Re}[K^1(\xi) - K^3(\xi)]/\mathrm{Max.Re}[K^3(\xi)]$;

^^^^ $\mathrm{Re}[K^2(\xi) - K^3(\xi)]/\mathrm{Max.Re}[K^3(\xi)]$;

×××× $\mathrm{Re}[K^4(\xi) - K^3(\xi)]/\mathrm{Max.Re}[K^3(\xi)]$.

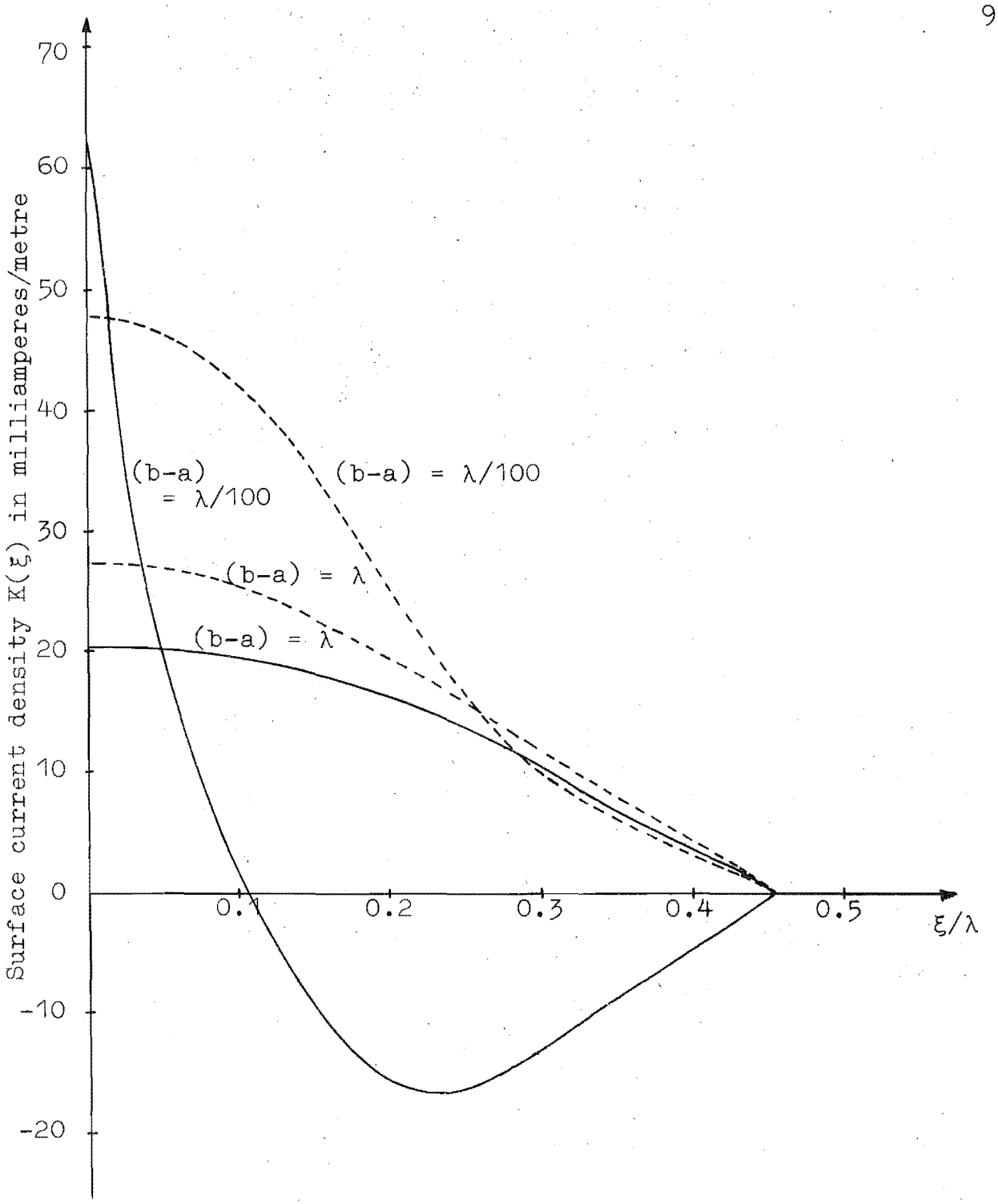

Fig. 3.10: Behaviour of surface current density K(ξ) with varying position of magnetic ring sources. Applies to dipole of H = a = λ/4, τ = λ/10 and with (b-a) = λ/100 and (b-a) = λ. 10 Lagrange polynomial basis functions used in METHOD 2. Legend: ---- real part; and —— imaginary part.

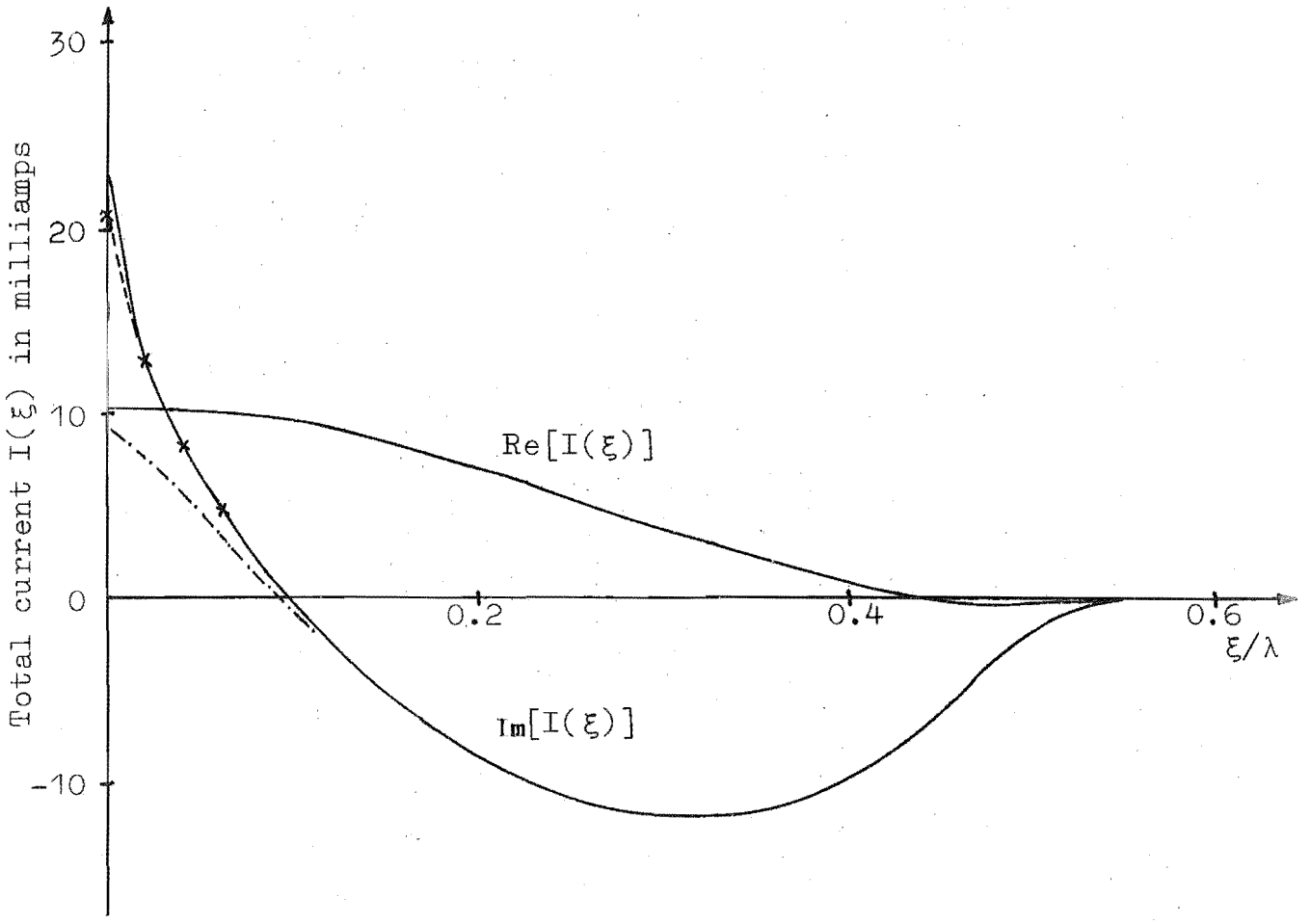

Fig. 3.11: Total current $I(\xi)$ on dipole $H = \lambda/2$, $\tau = a = 0.085\lambda$ for various magnetic ring sources and a magnetic frill source. Seven Tchebyshev polynomial functions used in METHOD 1.

Legend: ——— $b/a = 1.05$; ----- $b/a = 1.10$; -·-·-·- $b/a = 1.50$; and ×××× $b_1/b_o = b_1/a = 1.219$.

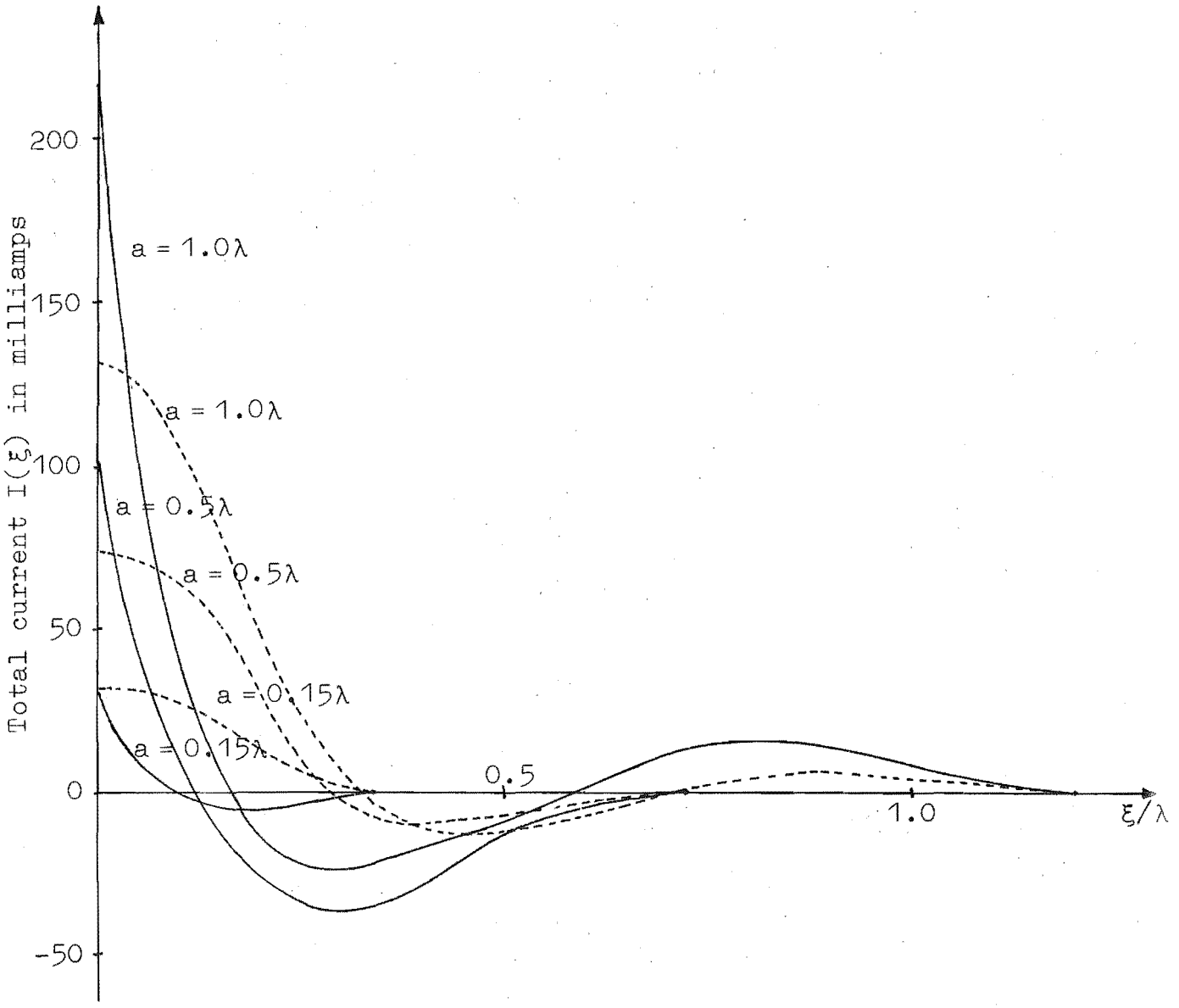

Fig. 3.12: Total current I(ξ) on half-wave dipoles H = λ/4; a = 0.15λ, a = 0.50λ, a = 1.0λ; τ/a = 0.1 with magnetic ring source at (b-a) = λ/100. 7 Tchebyshev polynomial functions used in METHOD 2 for dipole with a = 0.15λ; and 10 and 12 sine functions used in METHOD 2 respectively for dipoles a = 0.50λ and a = 1.0λ.
Legend: ----- real part; and ——— imaginary part.

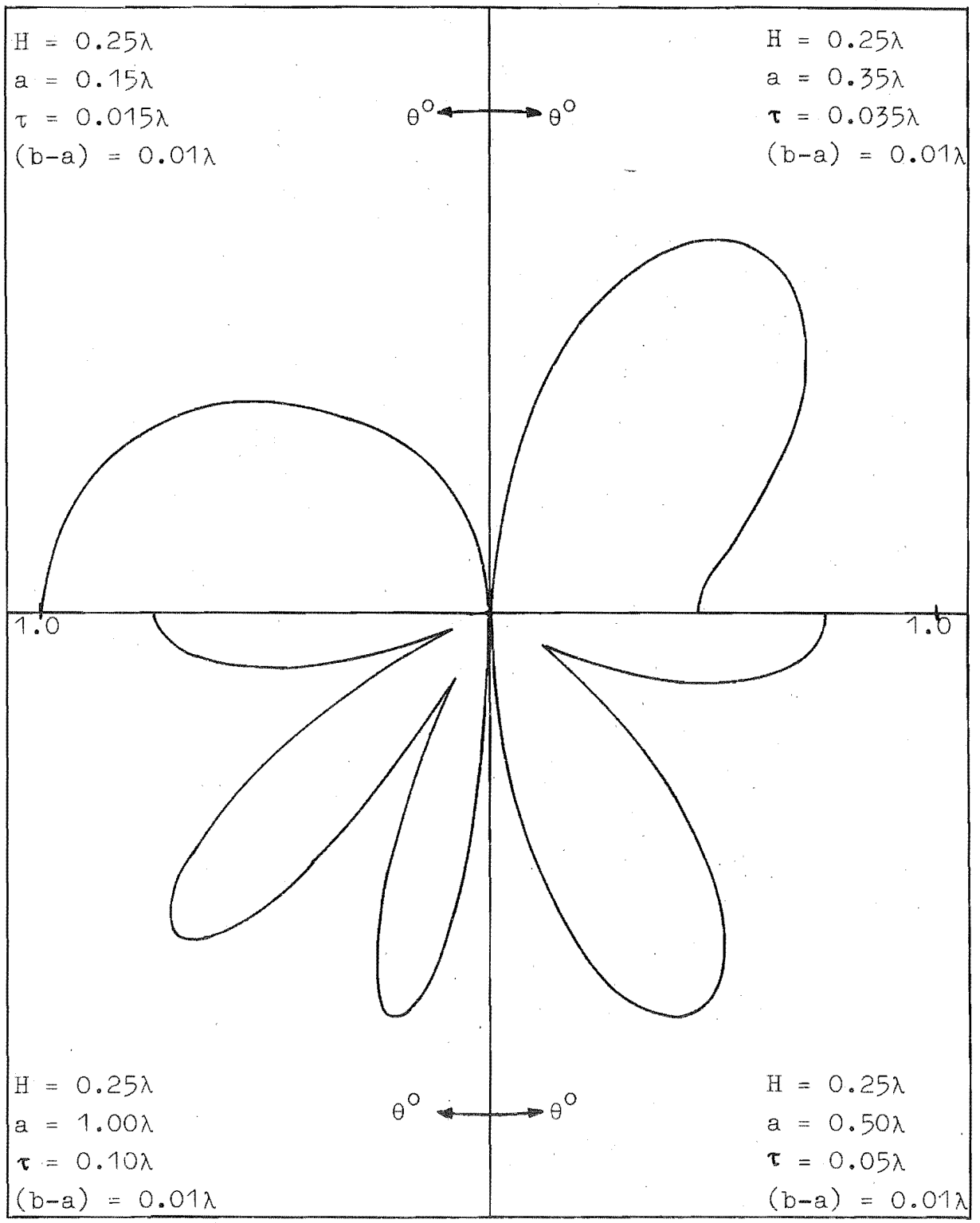

Fig. 3.13: Radiation patterns of four half-wave dipoles when the magnetic ring source is 0.01λ from the dipole surface. METHOD 2 used in the computations.

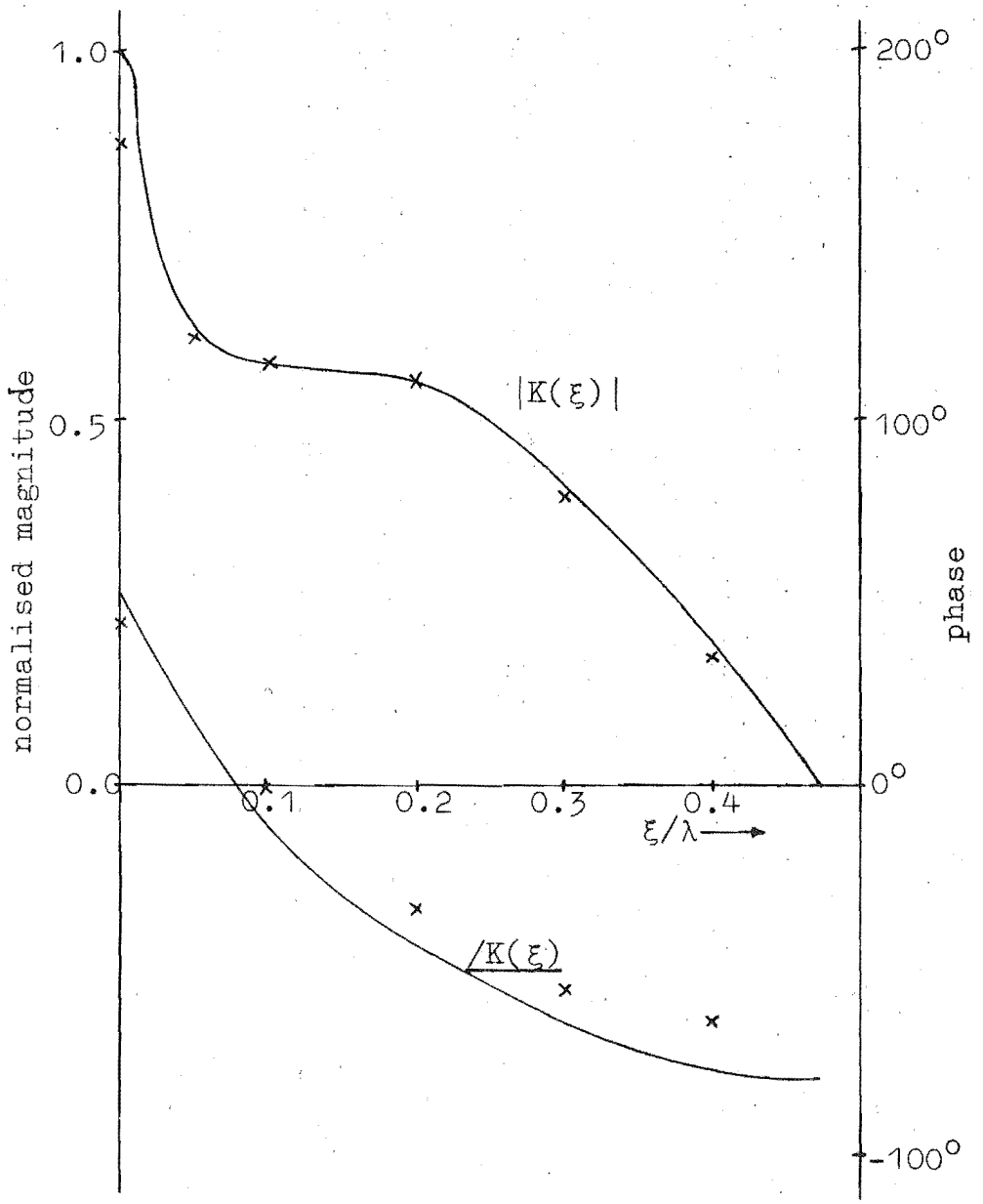

Fig. 3.14: Surface current density K(ξ) on dipole H = 0.3935λ, τ = a = 0.1435λ.
Legend: —— computed by METHOD 1 using 5 Tchebyshev polynomial functions with (b-a) = λ/100; and ×××× computed by Vasil'ev (1959).

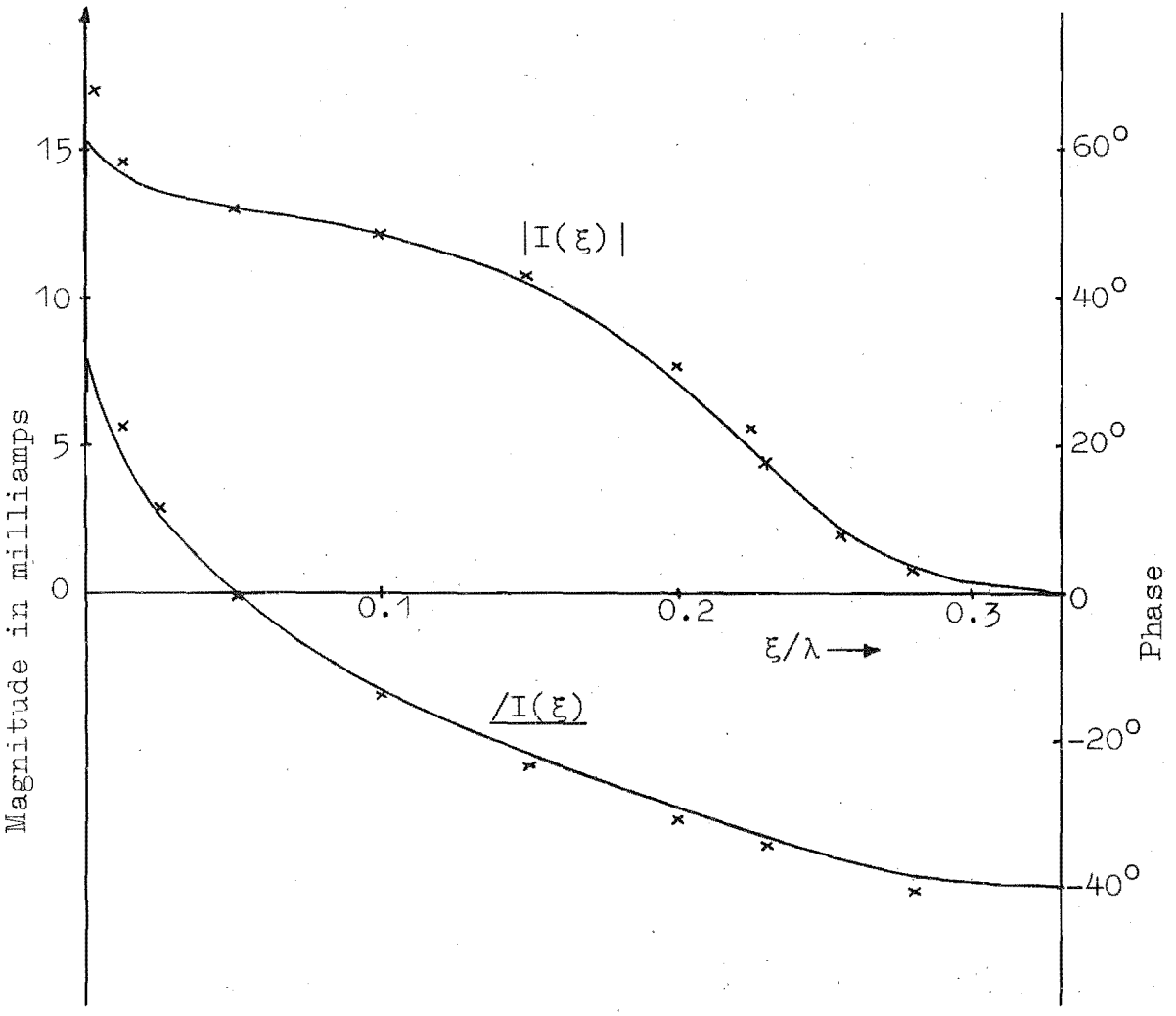

Fig. 3.15: Total current $I(\xi)$ on cylindrical dipole $H = 0.23\lambda$, $a = 0.10\lambda$, and $\tau = 0$. Legend: ——— computed by METHOD 1 using 7 Tchebyshev polynomial functions with $(b-a) = \lambda/100$; and ×××× computed by Einarsson (1966).

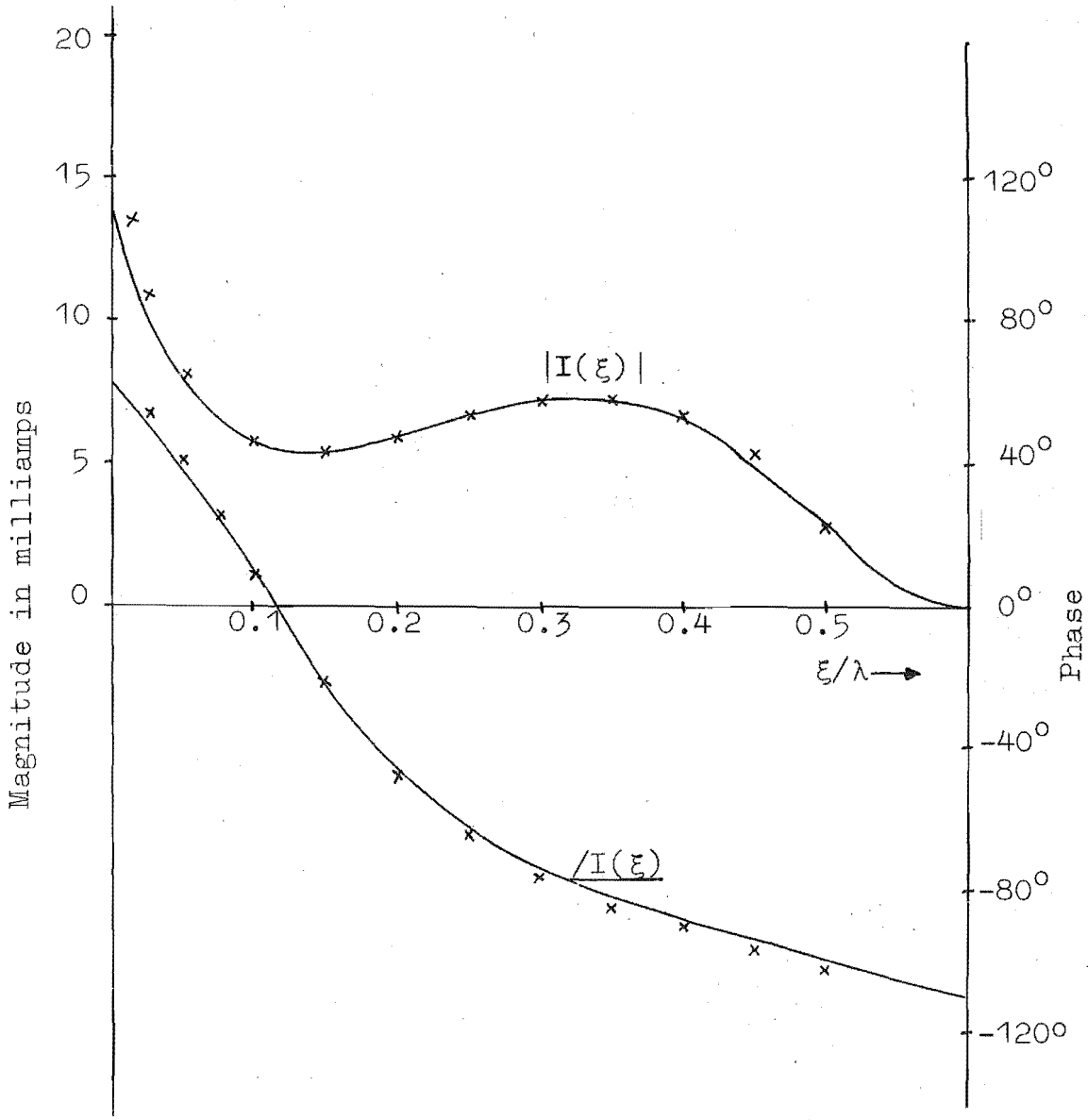

Fig. 3.16: Total current $I(\xi)$ on cylindrical dipole $H = 0.50\lambda$, $a = 0.10\lambda$, and $\tau = 0$. Legend: ——— computed by METHOD 1 using 7 Tchebyshev polynomial functions with $(b-a) = \lambda/100$; and ×××× computed by Einarsson (1966).

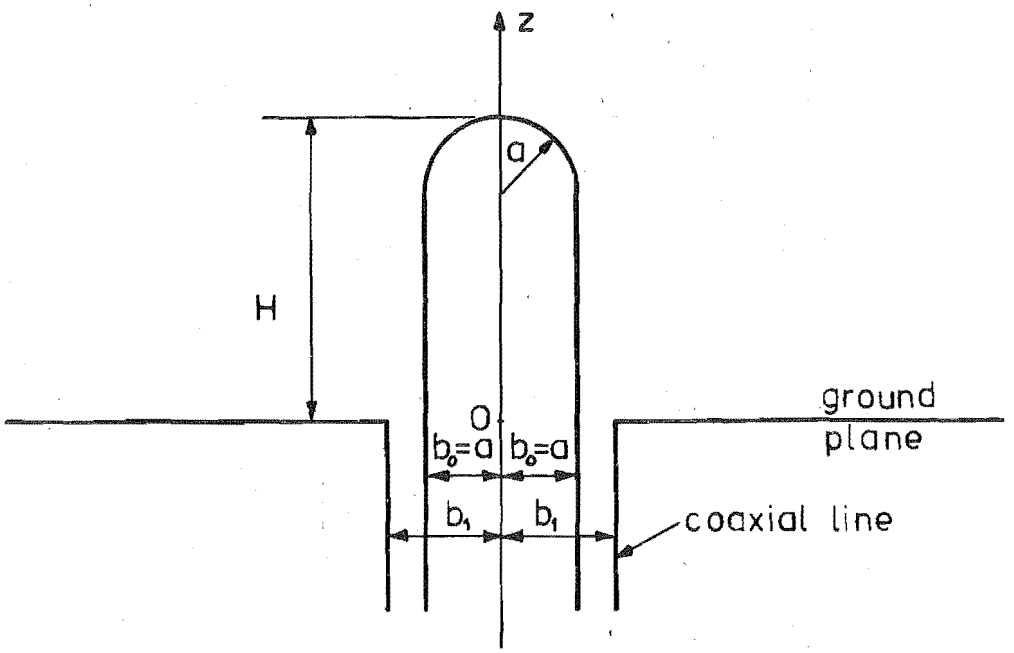

Fig. 3.17a: Hemispherically-capped cylindrical monopole driven by a coaxial line.

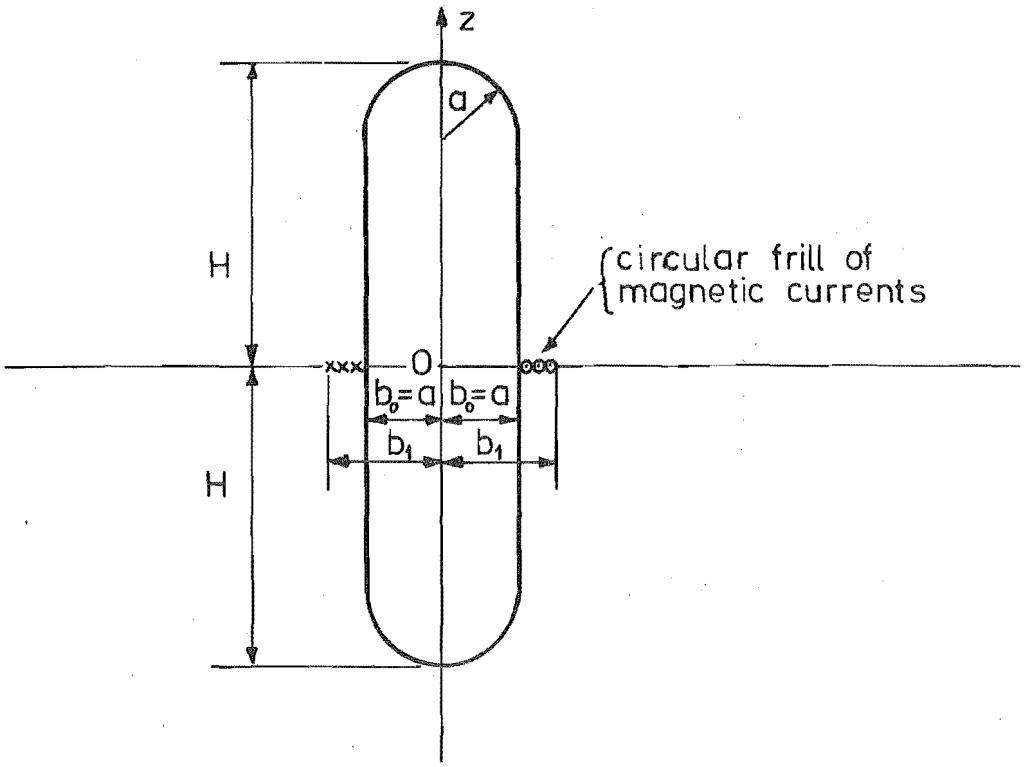

Fig. 3.17b: Hemispherically-capped cylindrical dipole equivalent to that shown in Fig. 3.17a.

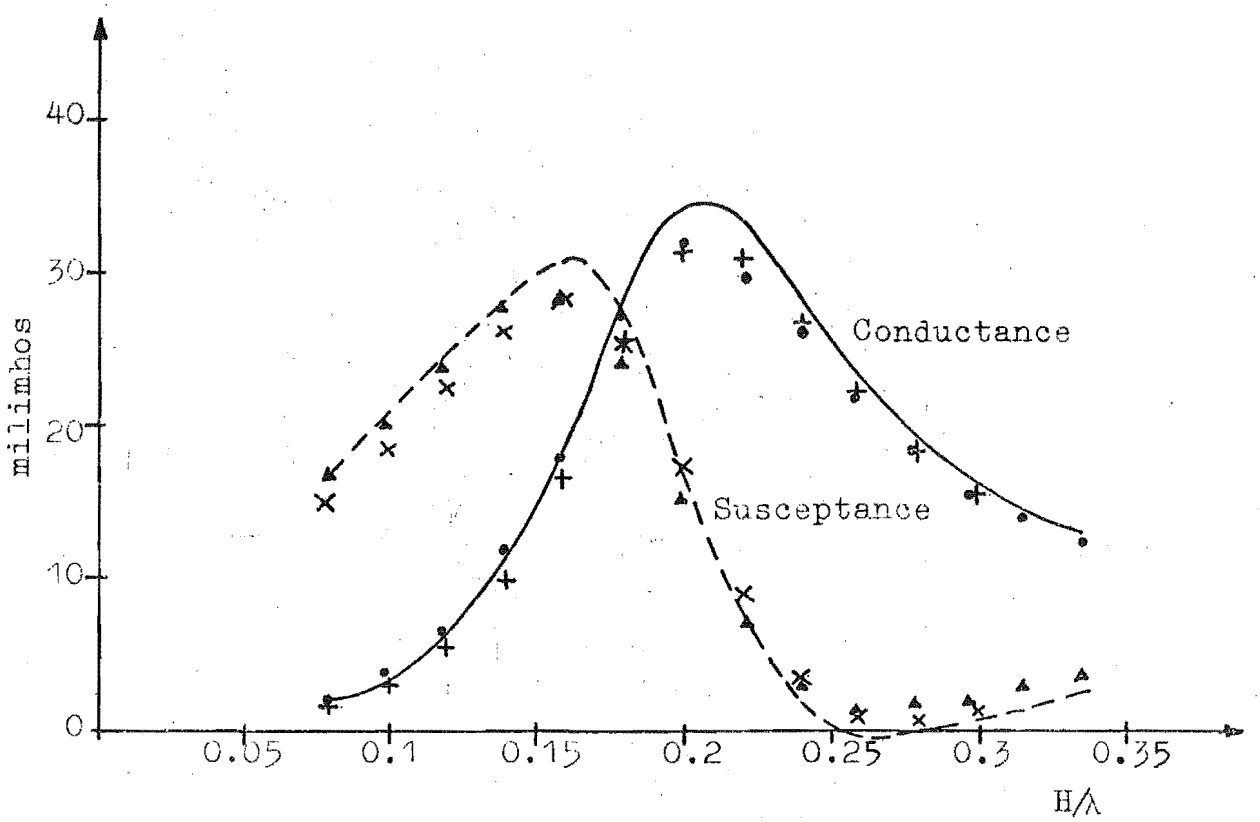

Fig. 3.18: Admittance of a hemispherically-capped cylindrical monopole (τ = a = 0.063λ) driven by a coaxial line $b_1/b_o = b_1/a = 2.0$.
Legend: ——— and ----- computed, •••• and ▲▲▲▲ measured by Ting (1969); and ++++ and ×××× computed using Tchebyshev polynomial functions in METHOD 2.

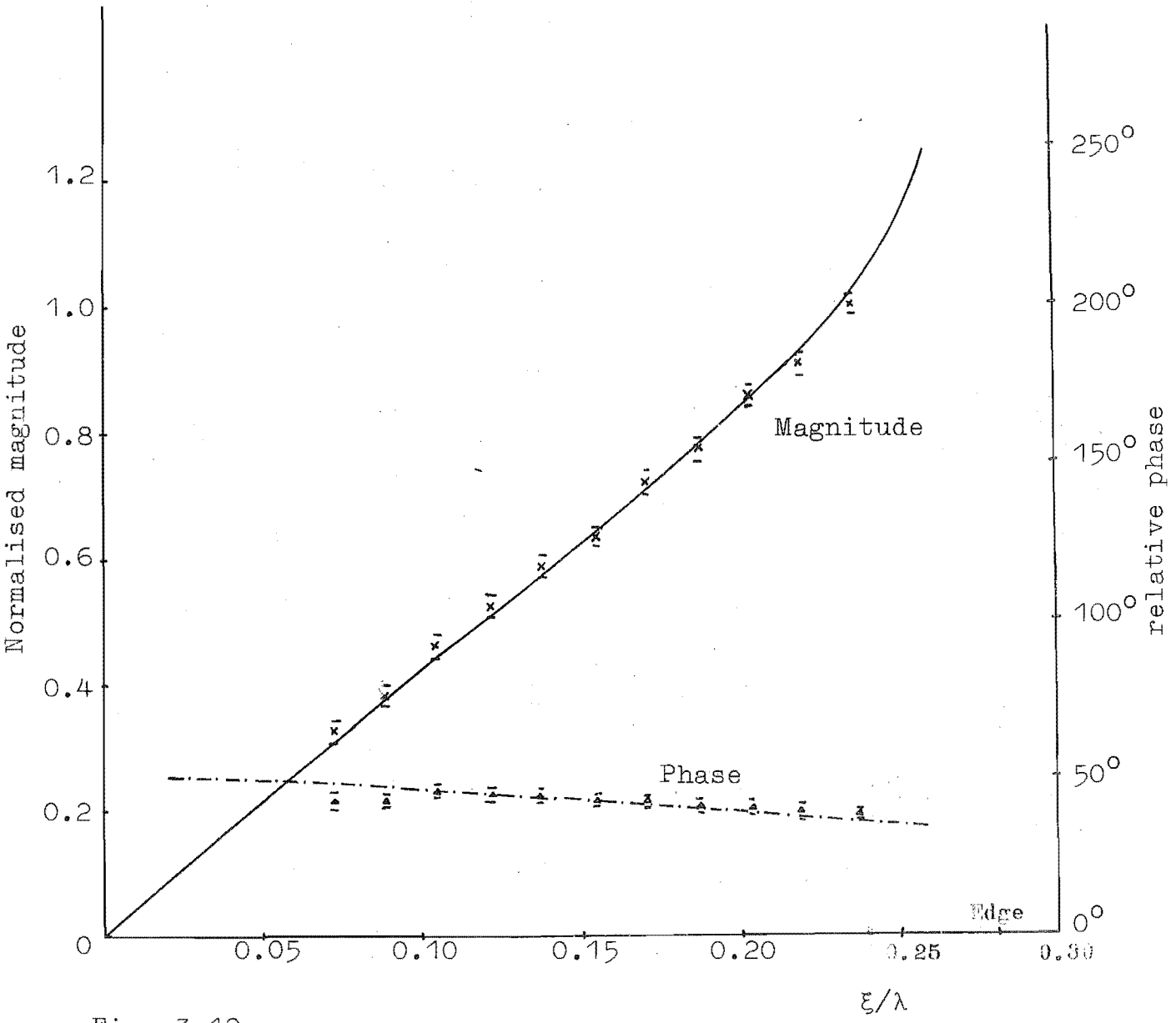

Fig. 3.19:
The normal component of electric intensity on a thick monopole H = 0.28 λ, a = 0.17λ , τ = 0 described in Appendix IV. METHOD 2 used in computations.

Legend: Normalised magnitude, ——— computed, ×××× inferred from measurements; relative phase, -·-·-·- computed, ▲▲▲▲ inferred from measurement; and ⊼ ⊼ are measurement error bars.

CHAPTER 4

APPLICATION OF THE EXTENDED INTEGRAL EQUATION FORMULATION TO END-LOADED DIPOLE ANTENNAS

4.1 INTRODUCTION

In this chapter the extended integral equations for "indented" antennas, derived in section 2.3 of chapter 2, are used to develop accurate computational treatments of end-loaded dipole antennas. Most calculations of the characteristics of end-loaded dipoles use assumed current distributions (cf. Wait, 1959; Hansen and Larsen, 1962; Watt, 1967, Sect. 2.3; Wait, 1969b). Recently, Kalafus (1971) used a method of Mautz and Harrington (1969) to compute the current distribution on an electrically small end-loaded dipole with maximum dimension of 0.08λ. When the dipoles are end-loaded with circular discs of diameters greater than a wavelength, ray-optical techniques have been used by Andrews (1968). When the dipoles are radiating into infinite parallel-plate regions (Otto, 1967), the fields and currents have been elucidated in closed form (Levin, 1959; Wu, 1963, Rama Rao, 1965; Otto, 1967). It is worthwhile noting that Galejs (1964) has given accurate numerical solutions for the end-loaded biconical antenna.

A further interest in obtaining accurate computational methods of treating end-loaded dipoles arises from their usefulness as calibration antennas for wideband antenna ranges (Ross and Fenster, 1968).

Section 4.2 shows that the problem of an end-loaded dipole symmetrically excited by a circular frill of magnetic currents is equivalent to a top-loaded monopole mounted on a ground plane and fed by a coaxial line. The integral equations in section 2.3 and the expressions derived in Appendix V for the fields in the parallel-plate region, are introduced in section 4.3 to develop specific integral equations directly applicable to the end-loaded dipole antenna problem. Otto's (1967) expression for the monopole admittance is used in section 4.3.1 to obtain the top-loaded monopole admittance. The numerical technique of solution is dealt with in section 4.4. Sections 4.5 and 4.6 respectively discuss the computational considerations and numerical and experimental results obtained. A comparison is made with Kalafus's (1971) method in section 4.7.

4.2 THE END-LOADED DIPOLE ANTENNA PROBLEM

Consider the perfectly conducting, top-loaded, linear monopole (shown in Fig. 4.2a) which is mounted on a perfectly conducting ground plane and driven by a coaxial line. The coaxial line is excited in its TEM mode at angular frequency ω. The antenna is immersed in free space (permittivity ε_o and permeability μ_o). Let a surface S_a envelop the monopole and the top-plate, and another surface S_p lie over the ground plane and coaxial aperture. The circular symmetry of the monopole and the excitation source requires that the electromagnetic field around the monopole and inside the coaxial line be circularly symmetric. Also, the only non-zero field components, in cylindrical polar coordinates (ρ,φ,z) (see Fig. 4.1), are E_ρ, E_z and H_φ.

The problem posed by the end-loaded dipole antenna (Fig. 4.2b) driven by a magnetic frill source is equivalent to that posed by the top-loaded monopole in Fig. 4.2a. The procedure for establishing equivalence is described in full in section 3.2 of chapter 3. The magnetic frill source is given by

$$\underline{J}^m(\rho,\varphi,0) = -\hat{\varphi}\, 2\, E_\rho(\rho,\varphi,0), \qquad a = b_o < \rho < b_1 \tag{4.1}$$

where E_ρ in (4.1) is the radial component of the electric intensity in the coaxial aperture in the ground plane. The time-harmonic factor $\exp(j\omega t)$ is suppressed throughout. By taking E_ρ in (4.1) to be

$$E_\rho = \frac{V}{\rho\, \ell n(b_1/a)}, \qquad a = b_o < \rho < b_1 \tag{4.2}$$

where V is the voltage across the coaxial line, the frill source becomes

$$\underline{J}^m(\rho,\varphi,0) = \frac{-\hat{\varphi}\, 2\, V}{\rho\, \ell n(b_1/a)}\,. \tag{4.3}$$

The rationale for taking E_ρ to be given by (4.2) has been discussed in section 3.2.

The end-loaded dipole antenna of Fig. 4.2b is shown again in Fig. 4.3 to introduce some symbols which are to be used in later sections of this chapter. The antenna surface S is formed by rotating the curve C, which possesses image symmetry about the xy-plane, about the z-axis. The curve C has a total length of 2L, the points Q_o and Q_3 as end points, and Q_1 as mid-point. On S a local coordinate system (η,φ',ξ) is defined as shown in Fig. 4.3. The symbol ξ is also used to denote the arc length along the curve C and is measured from the mid-point Q_1 so that the values of ξ at the points Q_o and Q_3 are respectively -L and L.

The electromagnetic field has the following properties: (i) it is circularly symmetric, i.e. no φ-variation; (ii) only the E_ρ, E_z and H_φ components are non-zero; (iii) $\hat{\eta} \wedge \underline{E} \equiv 0$ on the surface of, and inside, the antenna; (iv) E_ρ and H_φ are zero everywhere on the z-axis; and (v) the field possesses image symmetry about the xy-plane. From these properties of the field, the electric surface current density given by $\underline{K}_s(\xi) = \hat{\eta} \wedge \underline{H}$ on S satisfies the relations

$$\underline{K}_s(\xi) = \hat{\xi}\, K(\xi);$$

$$K(-\xi) = K(\xi); \tag{4.4}$$

$$K^{(2p-1)}(0) = 0, \quad p = 1,2,3,\ldots; \tag{4.5}$$

$$K(\pm L) = 0; \tag{4.6}$$

where $K^{(p)}(\xi)$ means the p^{th} derivative of $K(\xi)$. Because the magnetic frill source in (4.3) can be considered as made of rings of magnetic current (see section 3.2.1), the analysis in Appendix III indicates that $K(\xi)$ has a rapidly varying behaviour in the neighbourhood of $\xi = 0$ when the width of the coaxial aperture (b_1-a) is electrically small. The total current $I(\xi)$ is defined by

$$I(\xi) = 2\pi\rho'(\xi)\, K(\xi) \tag{4.7}$$

where ρ' is the radial distance, from the z-axis, of the point denoted by ξ on C.

4.3 THE EXTENDED INTEGRAL EQUATIONS

The extended integral equations (2,11a,b) are used in chapter 3 to develop METHODS 1 and 2 for treating the thick cylindrical dipole antenna in Fig. 3.7. Computations in chapter 3 show that METHODS 1 and 2 are practicable in the ranges $1 < H/a < 25$ and $0.25 < H/a < 2.0$ respectively, where H and a are respectively the thick dipole semi-height and radius (see Fig. 3.7). In the present problem of the end-loaded dipole antenna, where H is the antenna semi-height and a is the radius of the central (electrically thin $a < 0.02\lambda$) dipole, H/a is much larger than 2, which precludes the use of METHOD 2. METHOD 1 is yet to be applied to the end-loaded dipole antenna, and is suggested for future research in section 5.3. It is now shown that equations (2.15a,b) and (2.16a,b), which were derived for the highly indented antenna in section 2.3, lead to practicable numerical solutions. In order to apply (2.15a,b) to the end-loaded dipole antenna, fictitious surfaces α, β_1, β_2 and γ are introduced. Consider the dipole antenna shown in Fig. 4.4. It is the same as that in Figs. 4.2b and 4.3, except that four fictitious surfaces α, β_1, β_2 and γ are drawn. V_2 is the region occupied by the dipole body and is bounded by the union of the surfaces α, β_1 and β_2 (i.e. $\alpha \cup \beta_1 \cup \beta_2$). V_1 is the annular or the parallel plate region bounded by the closed surface $\alpha \cup \gamma$. V_o constitutes the remainder of space. The open cylindrical surface γ, which is a distance d from the z-axis, meets with the curve C at the point Q_2, which is a distance $\xi = \xi_2$ from the mid-point Q_1 of curve C. By letting the surface β be $\beta_1 \cup \beta_2$, equation (2.15a) of section 2.3 can be written for the end-loaded dipole antenna in Fig. 4.4 as

$$0 = \frac{(\nabla\nabla\cdot + k_o^2)}{j4\pi\omega\varepsilon_o}\left\{\int_\beta \hat{\xi}\ K(\xi)\ G_o\ ds + \int_\gamma \hat{z}\ H_\varphi(\underline{r}')\ G_o\ ds\right.$$

$$\left. - \frac{\nabla\wedge}{4\pi}\int_\gamma \hat{\varphi}\ E_z(\underline{r}')\ G_o\ ds, \qquad \underline{r} \text{ in } V_1\ \ V_2\right. \tag{4.8}$$

where $k_o = \omega(\mu_o\varepsilon_o)^{\frac{1}{2}}$ is the free space wavenumber, $\underline{r}'$ is the position vector of any point $Q(\rho',\varphi',z')$ on the surface $\beta \cup \gamma$; $\underline{r}$ refers to any point $P(\rho,\varphi,z)$ in volume regions V_1 and V_2; and $G_o = G(k_o,\underline{r},\underline{r}')$ is the scalar Green functions for free space. On the common surface between V_1 and V_o the tangential field components E_z and H_ρ can be specified in terms of one set of unknowns $\{F_m\}$. This specific relation between E_z and H_φ is obtained in Appendix V, where cylindrical wave functions are used to represent the field in the parallel plate region V_1 completely. From equations (V.34) and (V.35) in Appendix V, E_z and H_φ on surface γ are given by

$$E_z(\rho=d,\varphi,z)$$

$$= \frac{-2}{\ell n(b_1/a)}\left\{\begin{array}{l}\sum_{m=0}^{\ell} F_m U_o(k_m d)\cos(\frac{m\pi z}{W}) + \sum_{m=\ell+1}^{\infty} F_m V_o(k_m d)\cos(\frac{m\pi z}{W}) \\ \\ + F^i(d,\varphi,z)\end{array}\right\};$$

(4.9)

$$H_\varphi(\rho=d,\varphi,z)$$

$$= \frac{-2j\omega\varepsilon_o}{\ell n(b_1/a)}\left\{\begin{array}{l}\sum_{m=0}^{\ell} \frac{F_m}{k_m} U_1(k_m d)\cos(\frac{m\pi z}{W}) + \sum_{m=\ell+1}^{\infty} \frac{F_m}{|k_m|} V_1(k_m d)\cos(\frac{m\pi z}{W}) \\ \\ + G^i(d,\varphi,z)\end{array}\right\};$$

(4.10)

$$F^i(d,\varphi,z) = \frac{-j\pi V}{8W}\sum_{m=0}^{\ell} \varepsilon_m U_o(k_m b_1)\ H_o^{(2)}(k_m d)\cos(\frac{m\pi z}{W})$$

$$+ \frac{V}{W}\sum_{m=\ell+1}^{\infty} V_o(k_m b_1)\ K_o(|k_m|d)\cos(\frac{m\pi z}{W}); \tag{4.11}$$

$$G^i(d,\varphi,z) = \frac{-j\pi V}{8W} \sum_{m=0}^{\ell} \varepsilon_m U_o(k_m b_1)\, H_1^{(2)}(k_m d)\cos\left(\frac{m\pi z}{W}\right)$$

$$- \frac{V}{W} \sum_{m=\ell+1}^{\infty} V_o(k_m b_1)\, K_1(|k_m| d)\cos\left(\frac{m\pi z}{W}\right); \qquad (4.12)$$

where $k_m^2 = k_o^2 - (\frac{m\pi}{W})^2$; $\ell < \frac{k_o W}{\pi} < \ell+1$; U_o, U_1, V_o and V_1 are defined by (V.29) and (V.30) in Appendix V; $H_o^{(2)}$ and $H_1^{(2)}$ are respectively the zeroth and first order Hankel functions of the second kind; and K_o and K_1 are respectively the zeroth and first order modified Bessel functions of the second kind.

An integral equation can be obtained by replacing the scalar Green's function in equation (4.8) with its dyadic form, expressed in vector spherical wave functions. Alternatively, it can be obtained from (2.23a). Note that (2.23b) is not applicable because both sides of the equation become identically zero when applied for the present dipole problem. After some manipulation the following equation, which is similar to that of METHOD 2 in chapter 3 (see eqn (3.25)), is obtained

$$\int_{\xi_2}^{L} Z_n(\xi)\, K(\xi)\, d\xi + \sum_{m=0}^{\infty} Q_{nm} F_m = B_n, \qquad n = 1,2,3,\ldots;$$

METHOD 2A (4.13)

$$Z_n(\xi) = \hat{\xi} \cdot \underline{N}^{(4)}_{eop}(k_o\underline{r}')\rho' ;$$

$$Q_{nm} = \frac{-2d}{\ell n(b_1/a)} \left\{ \frac{U_1(k_m d)}{k_m} D_{nm} + \frac{k_o}{j\omega\mu_o} U_o(k_m d)\, E_{nm} \right\} , \quad m \leqslant \ell ;$$

$$= \frac{-2d}{\ell n(b_1/a)} \left\{ \frac{V_1(k_m d)}{k_m} D_{nm} + \frac{k_o}{j\omega\mu_o} V_o(k_m d)\, E_{nm} \right\} , \quad m \geqslant \ell+1 ;$$

$$B_n = \frac{2d}{\ell n(b_1/a)} \left\{ \frac{k_o}{j\omega\mu_o} \int_0^W F^i(d,\varphi'=0,z')\hat{\varphi} \cdot \underline{M}^{(4)}_{eop}(k_o\underline{r}')dz' \right. \qquad (4.14)$$

$$\left. + j\omega\varepsilon_o \int_0^W G^i(d,\varphi'=0,z')\hat{z} \cdot \underline{N}^{(4)}_{eop}(k_o\underline{r}')dz' \right\} ;$$

$$D_{nm} = j\omega\varepsilon_o \int_0^W \cos\left(\frac{m\pi z'}{W}\right) \hat{z} \cdot \underline{N}^{(4)}_{eop}(k_o\underline{r}')dz' ;$$

$$E_{nm} = \int_0^W \cos\left(\frac{m\pi z'}{W}\right) \hat{\varphi} \cdot \underline{M}^{(4)}_{eop}(k_o\underline{r}')dz'p$$

where ξ_2 is the arc length along curve C between points Q_1 and Q_2 (see Fig. 4.4); $p = 2n-1$; and $\underline{N}^{(4)}_{eop}$ and $\underline{M}^{(4)}_{eon}$ are vector spherical wave functions (given in Appendix I).

4.3.1 Admittance and Current Distributions

The approach described in section 2.3 of chapter 2 to the end-loaded dipole antenna not only leads to a single equation, (4.13), but also allows easy evaluation of Otto's (1967) admittance expression which takes the form

$$Y = \frac{2\pi}{V\ \ell n(b_1/a)} \int_a^{b_1} H_\varphi(\rho,\varphi,0)\, d\rho ; \qquad (4.15)$$

for the end-loaded dipole antenna with $b_o = a$ (cf. eqn (3.32)). This is discussed fully in section 3.3.1. Because a complete description of the field in the parallel plate region V_1 (see

Fig. 4.4) is expressed most conveniently in cylindrical wave functions, (4.15) becomes

$$Y = \frac{-4j\pi\omega\varepsilon_o}{V\{\ell n(b_1/a)\}^2}\left\{-\sum_{m=0}^{\ell}\frac{F_m}{k_m^2}U_o(k_m b_1) + \sum_{m=\ell+1}^{\infty}\frac{F_m}{|k_m|^2}V_o(k_m b_1)\right.$$

$$+\frac{j\pi V}{8W}\sum_{m=0}^{\ell}\frac{\varepsilon_m}{k_m^2}\left[H_o^{(2)}(k_m b_1)U_o(k_m b_1) - \frac{j4}{\pi}\ell n(b_1/a)\right]$$

$$\left.+\frac{V}{W}\sum_{m=\ell+1}^{\infty}\frac{1}{|k_m|^2}\left[K_o(|k_m|b_1)V_o(k_m b_1) - \ell n(b_1/a)\right]\right\}. \quad (4.16)$$

The derivation of (4.16) is given in section V.2.2 of Appendix V. The last two summations in (4.16) contain no unknown quantities and can be evaluated accurately. Note that the part of the antenna admittance related to these two summations is simply the admittance of a monopole radiating into an infinite parallel plate region (cf. Otto, 1967, eqn. 39). The first two summations in (4.16) contain the unknown $\{F_m\}$ which is obtained by solving integral equation (4.13).

The surface current density $K(\xi)$ on the part of curve C which borders on the parallel plate region V_1 is also derived in Appendix V. As the expressions, (V.33, V.35, and V.36) of Appendix V, for the surface currents are lengthy, they are not repeated here. Unlike the thick dipole antenna problem in chapter 3, the rapidly varying behaviour of $K(\xi)$ near $\xi = 0$ represents no difficulty and requires only a little extra effort in evaluating the last summation in (V.33).

4.4 NUMERICAL SOLUTION

Equation (4.13) can be solved numerically for $K(\xi)$ and $\{F_m\}$ by the method of moments outlined in Appendix II (Morse and Feshbach, 1953, Sect. 8.3; Harrington, 1968, chap. 1). Equation (4.13) is written again as

$$\int_{\xi_2}^{L} Z_n(\xi)\, K(\xi)\, d\xi + \sum_{m=0}^{\infty} Q_{nm} F_m = B_n, \quad n = 1,2,3,\ldots; \qquad \text{METHOD 2A} \qquad (4.17)$$

where $Z_n(\xi)$, Q_{nm}, B_n, are given by (4.14).

Assume that $K(\xi)$ in (4.17) can be approximated accurately by a finite number M_1 of basis functions $\varphi_m(\xi | \xi_2 < \xi < L)$ with unknown expansion coefficients K_m such that

$$K(\xi) = \sum_{m=1}^{M_1} K_m\, \varphi_m(\xi). \qquad (4.18)$$

Equation (4.17) then becomes a system of linear algebraic equations for the members of $\{K_m\}$ and $\{F_m\}$ when (4.18) is substituted for $K(\xi)$ in (4.17), viz.

$$\sum_{m=1}^{M_1} Z_{nm} K_m + \sum_{m=0}^{\infty} Q_{nm} F_m = B_n, \quad n = 1,2,3,\ldots \qquad (4.19)$$

$$Z_{nm} = \int_{\xi_2}^{L} Z_n(\xi)\, \varphi_m(\xi) d\xi \qquad (4.20)$$

Assume further that the infinite series in $Q_{nm}F_m$ can be approximated accurately by the truncated series;

$$\sum_{m=1}^{M_1} Z_{nm} K_m + \sum_{m=0}^{M_2} Q_{nm} F_m = B_n, \quad n = 1,2,3,\ldots \qquad (4.21)$$

This latter assumption is reasonable if the two infinite series in (4.9) and (4.10), which represent the field

components E_z and H_ρ on the surface γ (see Fig. 4.4), converges rapidly.

By defining

$$M = M_1 + M_2 + 1; \quad F_m = K_{M_1+1+m};$$

$$Z_{nm} = Z_{nm}, \quad 1 \leqslant m \leqslant M_1; \tag{4.22}$$

$$Z_{nm} = Q_{n(m-M_1-1)}, \quad M_1 < m \leqslant M;$$

equation (4.21) can be written as (cf. eqn (II.6) in Appendix II)

$$\sum_{m=1}^{M} Z_{nm} K_m = B_n, \quad n = 1,2,3,... \tag{4.23}$$

By choosing n to take values 1,2,...,M, the matrix equation

$$[Z_{nm}][K_m] = [B_n], \; m = 1,2,...,M; \quad n = 1,2,...,M; \tag{4.24}$$

can be written for (4.23). $[Z_{nm}]$ is a square matrix with an inverse $[Z_{nm}]^{-1}$ if it is not singular. The solution to (4.24) is then

$$[K_m] = [Z_{nm}]^{-1}[B_n]. \tag{4.25}$$

4.4.1 Antenna Configuration

The configuration of the end-loaded dipole antenna, for which the numerical results are presented in section 4.6, is shown in Fig. 4.5. The central conductor is of radius a and semi-height W. τ is the radius of curvature of the edges of the endplates. When $\tau = 0$, the endplates are circular discs of diameter 2A. The total dipole semi-height is $H = W+2\tau$. The distance of the surface γ from the z-axis can be varied in the range $b_1 < d \leqslant A$. The inner and outer radii of the

magnetic frill source are respectively $b_0 = a$ and b_1.

4.4.2 Choice of Basis Functions

The surface current density $K(\xi)$ on the part of curve C between $\xi = \xi_2$ and $\xi = L$, i.e. between points Q_2 and Q_3, is approximated by a finite number M_1 of basis functions $\varphi_m(\xi)$ (see eqn (4.18)). In Table 4.1, three basis function sets $\{\varphi_m(\xi) : \xi_2 < \xi < L;\ m = 1,2,3,\ldots\}$ together with their functional forms are given. Forms number 1 and 2, which are the Fourier sine function and the Tchebyshev polynomial, are used in computations when $\tau \geqslant 0.02\lambda$. Form number 3, the wedge Bessel function, is chosen to approximate the current when the endplates are discs ($\tau = 0$). If the factors $(L-\xi)(\xi-\xi_2+d)$ are removed, then $\varphi_m(\xi)$ is one of the wavefunctions exactly applicable to a half plane (wedge of zero angle).

4.5 COMPUTATIONAL CONSIDERATIONS

The computer program, which is written in Fortran IV, is organised into two phases. The first phase evaluates the M x M elements of the matrix $[Z_{nm}]$ in equation (4.24) for a specific antenna configuration in Fig. 4.5. The second phase computes and outputs current distributions and admittances for different magnetic frill sources applied to the antenna. All three basis function sets in Table 4.1 are included in the one program.

The M x M matrix elements Z_{nm}, given by (4.24), are evaluated by numerical integration. To evaluate the Z_{nm} to an accuracy which ensures that the elements K_m in (4.25) are computed, for different magnetic frill sources, to better than 1% accuracy, the procedure described in section 3.5 of

chapter 3 is adopted. Let N denote the number of significant figures to which the Z_{nm} are evaluated by Simpson's quadrature rule, and $[K_m]_N$ be the column matrix $[K_m]$ (see eqn (4.25)) computed for a particular magnetic source when the Z_{nm} are evaluated to N significant figures. The procedure, described in section 3.5, then consists of increasing N by one significant figure at a time until the corresponding elements of $[K_m]_{(N-1)}$ and $[K_m]_N$ agree to within 1%. Since intermediate integration quantities are stored in this procedure, core storage limits the largest value of M that can be handled to 12. This restriction on the size of M means that both the dimensions, A and H, of the end-loaded dipole in Fig. 4.5 have to be less than 0.5λ if numerical convergence is to be achieved.

A numerical solution is defined here to be practicable for a specific end-loaded dipole antenna if (a) the matrices $[Z_{nm}]$ are sufficiently well-conditioned so that the Z_{nm} need be evaluated to at most seven significant figures; and (b) numerical convergence is achieved with $M \leqslant 12$. A test for numerical convergence is described in section 4.6.1.

4.6 NUMERICAL RESULTS

4.6.1 General Discussion

Computations, which use the three sets of basis functions listed in Table 4.1, are carried out for electrically thin ($a < 0.015\lambda$) cylindrical dipoles end-loaded with endplates of varying thickness.

In section 3.5 of chapter 3, a convergence number M_c is defined to give a quantitative measure of the rate of numerical convergence of a solution. But this is not convenient for the end-loaded dipole, as is illustrated by the admittances, which are computed at various values of M_1 and M_2 (see (4.18) and (4.19)), of a particular dipole antenna with endplates $\tau = 0.0375\lambda$ (see Table 4.2). Table 4.2 shows that it is not possible to say that numerical convergence is achieved if M_1 and M_2 are greater than certain values. A different test of convergence is adopted. From a group of 10 computed admittance values (at different values of M_1 and M_2), a mean admittance $\overline{Y} = \overline{G} + j\overline{B}$ is calculated. If the "difference bound" D_b, which is defined to be the difference between $\overline{G}$ (or $\overline{B}$) and the largest or smallest member of the group of 10 conductance (or susceptance) values, is less than 5% of the mean admittance $\overline{Y}$, numerical convergence is considered achieved. The mean admittance and difference bounds are $\overline{G}$ = 1.33 millimhos with D_b = 0.05 millimho, and $\overline{B}$ = 1.69 millimhos with D_b = 0.1 millimho, in Table 4.2.

The position of the fictitious surface γ (see Fig. 4.5) affects numerical solutions. This is illustrated in Tables 4.3 and 4.4, where the normalised determinants $||Z||$ (defined in Appendix II) with $M_1 = 8$ and $M_2 = 3$, and the mean admittances $\overline{Y}$ with their associated difference bounds D_b, are given for two end-loaded dipoles. Table 4.3, where the endplates are thick ($\tau = 0.0375\lambda$), shows that, as the distance d of the surface γ from the z-axis is decreased, $||Z||$ decreases also and $\overline{Y}$ changes by about 0.2 millimho. A distance d that

is only slightly less than A, is thus preferred. Table 4.4, where the endplates are discs (τ = 0), shows that, as d is decreased, (i) $||Z||$ decreases and then increases as do the D_b; and $\overline{Y}$ can vary by about 0.50 millimho. The behaviour of $||Z||$ and the D_b suggests that the surface γ should be placed at d = (A-0.1)λ.

4.6.2 Dependence on H/A

Table 4.5 applies to end-loaded dipole antennas with A = 0.24375λ, τ = 0.0375λ, a = 0.0119λ and a magnetic frill source b_1 = 2.3a. Computations for the results in Table 4.5 use d = 0.1875λ. The $||Z||$ in Table 4.5 decrease as H = (W+τ) increases, but the difference bounds D_b are largest for the smallest value of H. The smallness of the $||Z||$ restricts practicable numerical solutions to dipole antennas loaded with thick ($\tau \geqslant 0.02\lambda$) endplates in the range $0.25 < \tau/A < H/A < 2.0$, and $A < 0.5\lambda$. CPU times required to compute the results in Table 4.5 are between 6 minutes to 10 minutes.

Table 4.6 applies to disc-loaded dipole antennas with H = W = 0.1λ, τ = 0, a = 0.01λ and a magnetic frill source b_1 = 2.3a. The surface γ is situated at d = (A-0.1λ) in the computations carried out for the results in Table 4.6. The table shows that, as A/λ is increased, (i) $||Z||$ increases and then decreases; and (ii) D_b increases. From the results in Table 4.6, numerical solutions to disc-loaded dipole antennas are practicable in the range $0.25 < H/\lambda < 0.4$, $A < 0.4\lambda$ only. CPU times required to compute the results in Table 4.6 vary between 12 minutes to 25 minutes.

Tables 4.5 and 4.6, which apply to antennas with about the same overall dimensions show that the different dependence

on H/A is related to the smallness of the $||Z||$, which is much smaller for the disc-loaded dipole.

4.6.3 Plots of Current Distribution

Representative plots of total current, $I(\xi) = 2\pi\rho'(\xi)K(\xi)$ in eqn (4.7), on two dipole antennas are shown in Figs. 4.6 and 4.7. The current distribution in Fig. 4.6, which applies to a dipole with thick endplates ($\tau = 0.0375\lambda$), is computed by using Tchebyshev polynomial basis functions with $M_1 = 7$ and $M_2 = 3$. It agrees with the other distributions computed with $(M_1,M_2) = (7,1)$, $(7,2)$, $(8,1)$, $(8,2)$, and $(8,3)$ to within 1.5%, and $(M_1,M_2) = (6,1)$ and (6.2) to within 3% of the maximum current value.

The current distribution shown in Fig. 4.7 applies to a disc-loaded dipole ($\tau = 0$), and is computed by using wedge Bessel functions (see Table 4.1). $M_1 = 7$ and $M_2 = 2$ are used in the computations. The distribution agrees with those which are computed with $(M_1,M_2) = (7,1)$, $(7,3)$, $(8,1)$, $(8,2)$ and $(8,3)$ to within 2% of the maximum current value. Its agreement with those computed with $(M_1,M_2) = (6,1)$, $(6,2)$ and $(6,3)$ is to within 5%.

4.6.4 Comparison with Experimental Results

By using conventional slotted line techniques (Montgomery, 1947, chap. 8; Jasik, 1961, Sect. 34.2), the admittances of some top-loaded monopoles, which were mounted on a ground plane and driven by a 50-ohm coaxial line, have been measured. In Tables 4.7 and 4.8, the measured admittance values are compared with the mean admittance values computed by using METHOD 2A. Although the conductances agree to better than 0.2 millimho or 4%, the susceptances differ by as much as 1.2

millimhos. It is suspected that the larger differences in the susceptances is due to the assumption in the computations that the radial component of the electric intensity in the coaxial aperture in the ground plane (see Fig. 4.2a) has the same radial (ρ) dependence as the dominant TEM mode in the coaxial line. The assumption is explicitly given in (4.2) as

$$E_\rho(\rho,\varphi,0) = \frac{V}{\rho\ \ell n(b_1/a)}\ , \qquad a = b_o < \rho < b_1. \tag{4.2}$$

As there is a tendency for E_ρ to be rapidly varying near the edge at $\rho = b_1$, $z = 0$ (Jones, 1964, Sect. 9.2), expression (4.2) is at least erroneous in this respect.

Differences of about 1.0 millimho in the measured and computed susceptances of cylindrical monopoles, driven by a coaxial line and radiating into an infinite parallel-plate region, have been observed by Otto (1967).

4.7 COMPARISON WITH PUBLISHED RESULTS

Kalafus (1971) has recently used the method of Mautz and Harrington (1969; see also equation 1.24) to compute the current distributions on electrically small end-loaded dipoles of maximum dimension 0.08λ. For the disc-loaded dipole, computations were carried out (Kalafus, 1971) for a wide range of H/A (H and A are defined in section 4.4.1). However, the current distribution presented applies to an antenna with $H = A = 0.0283\lambda$ and for which METHOD 2A does not lead to a practicable solution. This distribution was obtained by using a 14 x 14 solution matrix. Note that the current distribution shown in Fig. 4.7 for a dipole of maximum dimension 0.54λ has been computed by using a 12 x 12

solution matrix in METHOD 2A. It is therefore expected that, in the range of H/A for which METHOD 2A is practicable, smaller solution matrices are required by using METHOD 2A than by Kalafus's (1971) method.

Table 4.1: Basis functions $\varphi_m(\xi)$ used for expanding $K(\xi)$ in eqn (4.18)

Identification number of basis function	Name of basis function	Functional form of basis function	Remarks
1	Fourier sine function	$\sin(m\pi[L-\xi]/(2[L-\xi_2]))$	only used for $\tau \neq 0$
2	Tchebyshev polynomial	$T_{2m-1}([L-\xi]/[L-\xi_2])$ $= \cos([2m-1]\arccos([L-\xi]/[L-\xi_2]))$	ditto
3	Wedge Bessel function	$[L-\xi]J_{(n-1)/2}(k_o(\xi-\xi_2-A+d))$; $\xi > \xi_2+A-d$ $[\xi-\xi_2+d](-)^{n-1}J_{(n-1)/2}(k_o(\xi_2+A-d-\xi))$; $\xi < \xi_2+A-d$	only used when $\tau = 0$

Table 4.2: Computed admittances Y = G + jB in millimhos for end-loaded dipole antenna with A = 0.24375λ, H = 0.30λ, τ = 0.0375λ, d = 0.1875λ, a = 0.0119λ and b_1 = 2.3a. Tchebyshev polynomial basis functions used in METHOD 2A.

Admittance Y	conductance G				susceptance B			
M_1 \ M_2	2	3	4	5	2	3	4	5
3	1.31	1.33	1.33	1.30	1.68	1.63	1.59	1.42
4	1.31	1.34	1.37	1.38	1.80	1.71	1.66	1.65
5	1.27	1.31	1.33	1.35	1.78	1.73	1.70	1.69
6	1.34	0.80	1.35	1.35	2.05	5.93	1.65	1.68
Mean admittance $\bar{Y}$ = G+jB; $\underline{G}$ = 1.33±0.05 & $\bar{B}$ = 1.69±0.10								

Table 4.3: Behaviour of $||Z||$ and $\overline{Y}$ with d for end-loaded dipole antenna with A = 0.24375λ, H = 0.150λ, τ = 0.0375λ, a = 0.0119λ, b_1 = 2.3a. METHOD 2A used.
Legend: O($||Z||$) order of magnitude of normalised determinant $||Z||$ with M_1 = 8 and M_2 = 3; $\overline{Y} = \overline{G} + j\overline{B}$ mean admittance in millimhos; and d = distance of surface from z-axis (see Fig. 4.5).

Basis function set $\{\varphi_m\}$ as in Table 4.1	sine			Tchebyshev		
d/λ	O($\|\|Z\|\|$)	$\overline{G}$	$\overline{B}$	O($\|\|Z\|\|$)	$\overline{G}$	$\overline{B}$
0.24375	10^{-13}	2.56±0.05	-10.2±0.10	10^{-9}	2.55±0.05	-10.18±0.05
0.2250				10^{-9}	2.55±0.05	-10.2±0.02
0.1875	10^{-18}	2.60±0.02	-10.27±0.10	10^{-12}	2.60±0.02	-10.3±0.10
0.1500	10^{-24}	2.62±0.05	-10.37±0.10	10^{-16}	2.60±0.05	-10.4±0.10

Table 4.4: Behaviour of $||Z||$ and $\overline{Y}$ with d for disc-loaded dipole antenna with A = 0.3λ, H = W = 0.1λ, τ = 0, a = 0.01λ and b_1 = 2.285a. METHOD 2A used.

Legend: $O(||Z||)$ order of magnitude of normalised determinant $||Z||$ with M_1 = 8 and M_2 = 3;

$\overline{Y} = \overline{G} + j\overline{B}$ mean admittance in millimhos; and

d = distance of surface γ from z-axis (see Fig. 4.5).

Basis function set $\{\varphi_m\}$ as in Table 4.1	Wedge Bessel		
d/λ	$O(\|\|Z\|\|)$	$\overline{G}$	$\overline{B}$
0.25	10^{-30}	1.40±0.20	-5.50±0.50
0.20	10^{-25}	1.40±0.10	-5.40±0.20
0.15	10^{-27}	1.54±0.10	-6.00±0.50
0.10	10^{-35}	-	-

Table 4.5: Behaviour of $||Z||$ and $\overline{Y}$ with antenna semi-height H for end-loaded dipole antennas with $A = 0.24375\lambda$, $\tau = 0.0375\lambda$, $d = 0.1875\lambda$, $a = 0.0119\lambda$, and $b_1 = 2.3a$. METHOD 2A used. Legend: $O(||Z||)$ order of magnitude of normalised determinant $||Z||$; $\overline{Y} = \overline{G} + j\overline{B}$ mean admittance in millimhos.

Basis function set $\{\varphi_m\}$ as in Table 4.1	Sine					Tchebyshev				
H/λ	$O(\|\|Z\|\|)$	M_1	M_2	$\overline{G}$	$\overline{B}$	$O(\|\|Z\|\|)$	M_1	M_2	$\overline{G}$	$\overline{B}$
0.1225	10^{-17}	8	3	3.89±0.10	-26.80±0.30	10^{-12}	8	3	3.88±0.10	-26.70±0.30
0.1500	10^{-18}	8	3	2.60±0.02	-10.27±0.10	10^{-12}	8	3	2.60±0.02	-10.30±0.10
0.2250	10^{-21}	7	4	1.74±0.05	- 1.84±0.05	10^{-16}	7	4	1.72±0.05	- 1.85±0.05
0.3000	10^{-24}	6	5	1.32±0.05	1.70±0.10	10^{-21}	6	5	1.33±0.05	1.67±0.10

Table 4.6: Behaviour of $||Z||$ and $\overline{Y}$ with disc radius A for disc-loaded dipole antennas with $H = W = 0.1\lambda$, $\tau = 0$, $d = A - 0.10\lambda$, $a = 0.01\lambda$ and $b_1 = 2.3a$. METHOD 2A used.

Legend: $O(||Z||)$ order of magnitude of normalised determinant $||Z||$ with $M_1 = 8$ and $M_2 = 3$; and $\overline{Y} = \overline{G} + j\overline{B}$ mean admittance in millimhos.

Basis function set $\{\varphi_m\}$ as in Table 4.1	Wedge Bessel		
A/λ	$O(\|\|Z\|\|)$	$\overline{G}$	$\overline{B}$
0.20	10^{-35}		
0.25	10^{-28}	1.60±0.10	-6.65±0.20
0.30	10^{-28}	1.40±0.10	-5.40±0.20
0.35	10^{-30}	1.30±0.20	-4.60±0.30
0.40	10^{-36}		

Table 4.7: Comparison of computed mean admittances $\overline{Y} = \overline{G} + j\overline{B}$ and measured admittances $Y_m = G_m + jB_m$ in millimhos for top-loaded monopole antennas with A = 6.5 cm, τ = 1.0 cm, d = 5 cm, a = 0.318 cm and $b_1 = 2.3a$. Tchebyshev polynomial basis functions used in METHOD 2A with $M_1 = 8$ and $M_2 = 3$.

H(cm)	frequency (GHz)	$\overline{G}$	$\overline{B}$	G_m	B_m
3	1.123	3.89±0.10	-26.80±0.30	4.0±0.20	-28.2±0.20
3	1.485	2.80±0.05	-16.20±0.20	2.8±0.20	-17.0±0.20
3	1.875	3.80±0.20	- 7.40±0.30	3.7±0.20	- 8.6±0.20
4	1.123	2.60±0.02	-10.30±0.10	2.5±0.20	-11.1±0.20
4	1.485	2.20±0.02	- 5.15±0.10	2.2±0.10	- 5.8±0.10
4	1.875	3.55±0.12	- 0.70±0.10	3.6±0.10	- 1.8±0.05

Table 4.8: Comparison of computed mean admittances $\overline{Y} = \overline{G} + j\overline{B}$ and measured admittances $Y_m = G_m + jB_m$ in millimhos (at 1.078GHz) for disc-loaded monopole antennas with H = W = 0.1λ, τ = 0, d = A - 0.1λ, a = 0.01λ and $b_1 = 2.3a$. Computations carried out in METHOD 2A with $M_1 = 8$ and $M_2 = 3$. Note: the discs used in the measurements are about 0.002λ thick.

A/λ	$\overline{G}$	$\overline{B}$	G_m	B_m
0.30	1.40±0.10	-5.4±0.20	1.6±0.20	-5.8±0.10
0.35	1.30±0.20	-4.6±0.30	1.4±0.20	-4.8±0.10

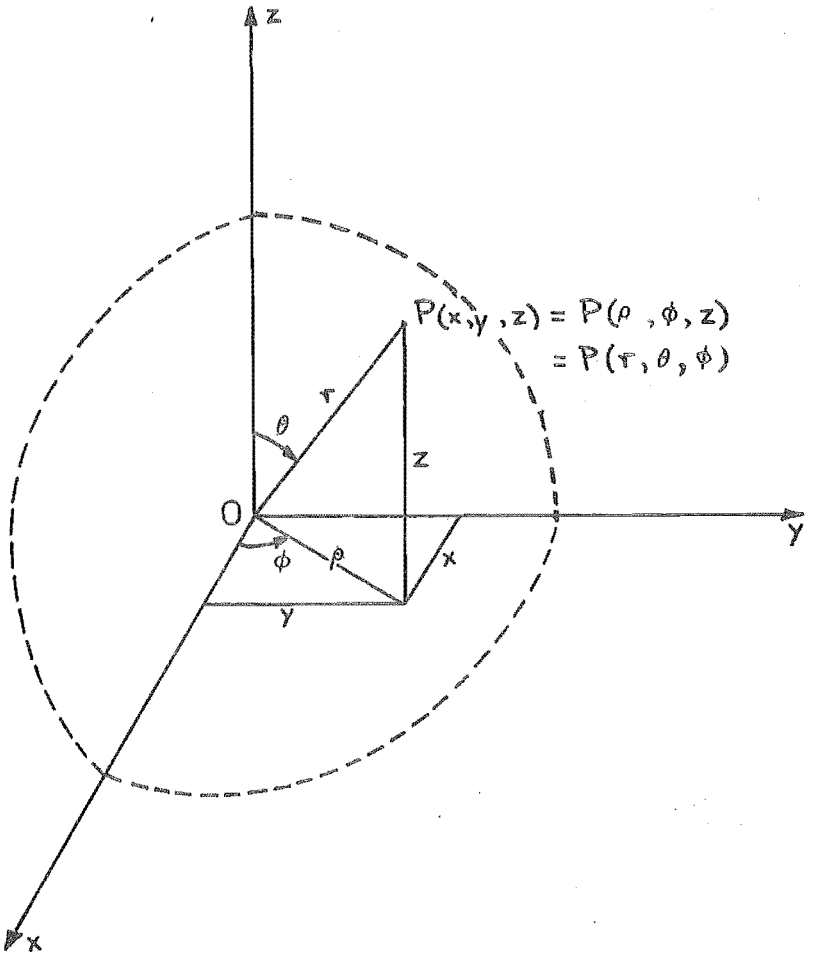

Fig. 4.1: Cartesian, cylindrical and spherical polar coordinate systems.

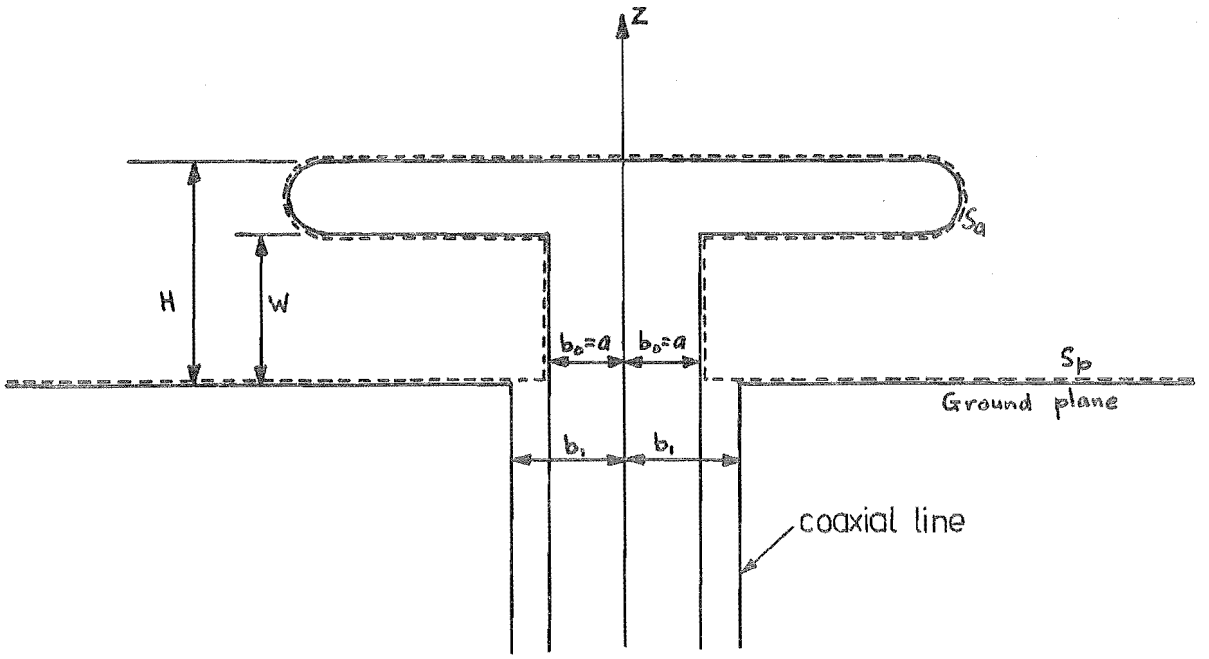

Fig. 4.2a: Top-loaded cylindrical monopole mounted on a ground plane and driven by a coaxial line

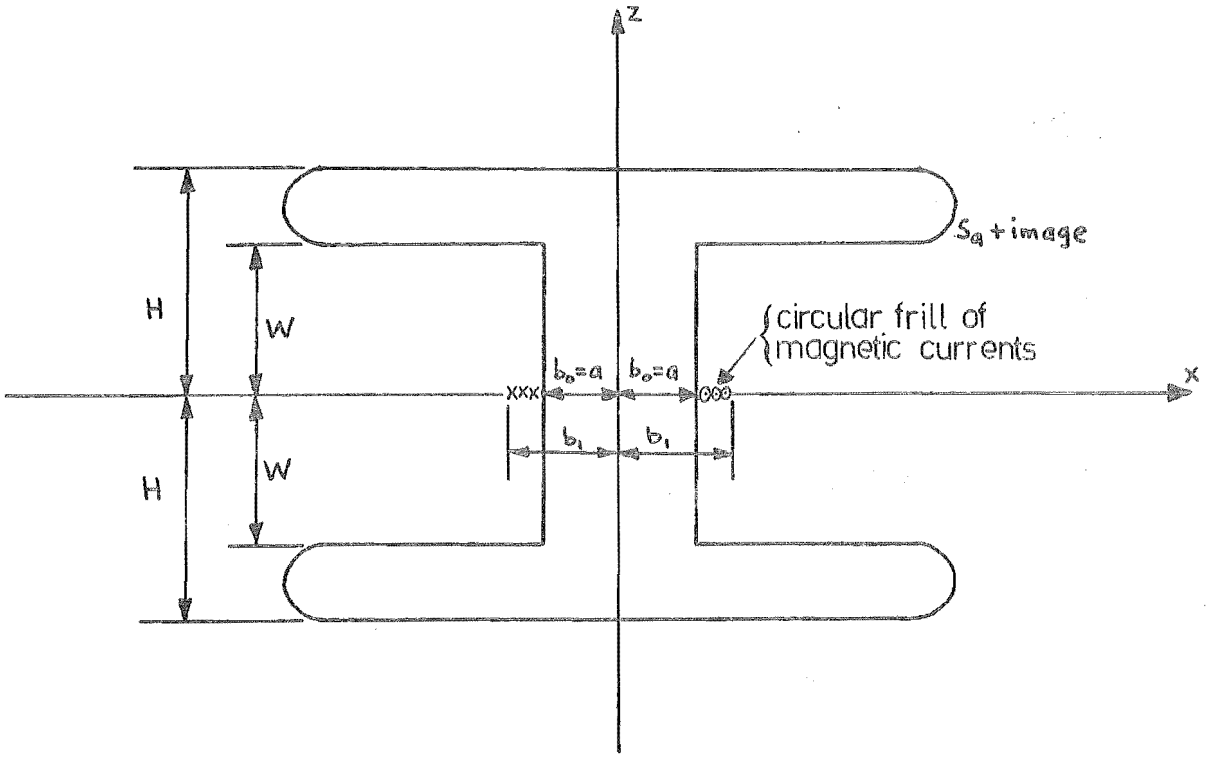

Fig. 4.2b: End-loaded dipole antenna equivalent to that shown in Fig. 4.2a.

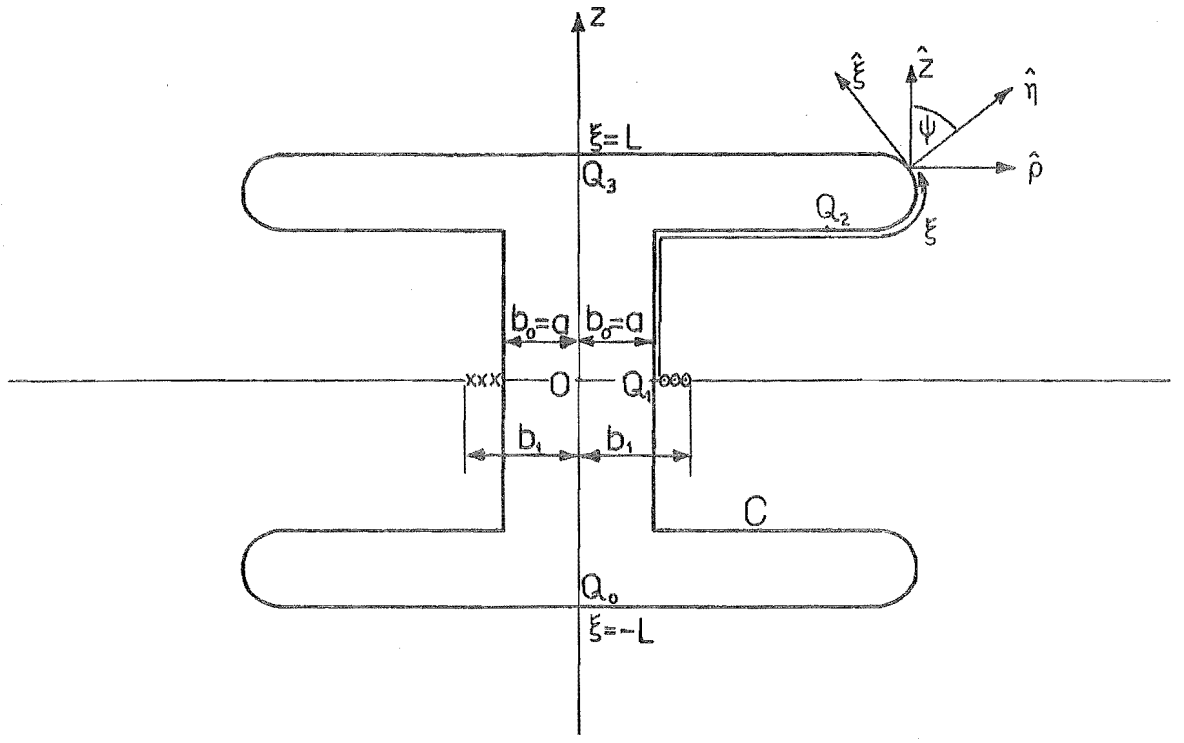

Fig. 4.3: Local surface coordinate system (η, φ', ξ) on the end-loaded dipole.

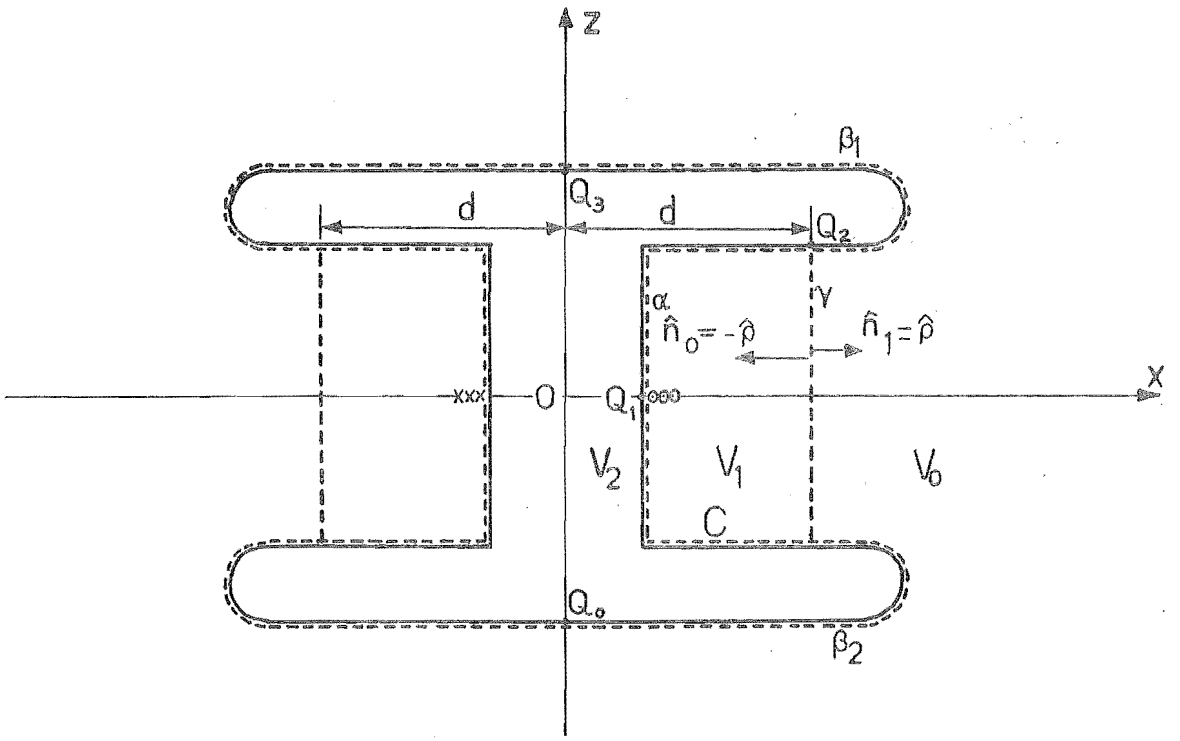

Fig. 4.4: Fictitious surfaces α, β_1, β_2 and γ, and volume regions V_0, V_1 and V_2 referred to in equation (4.8).

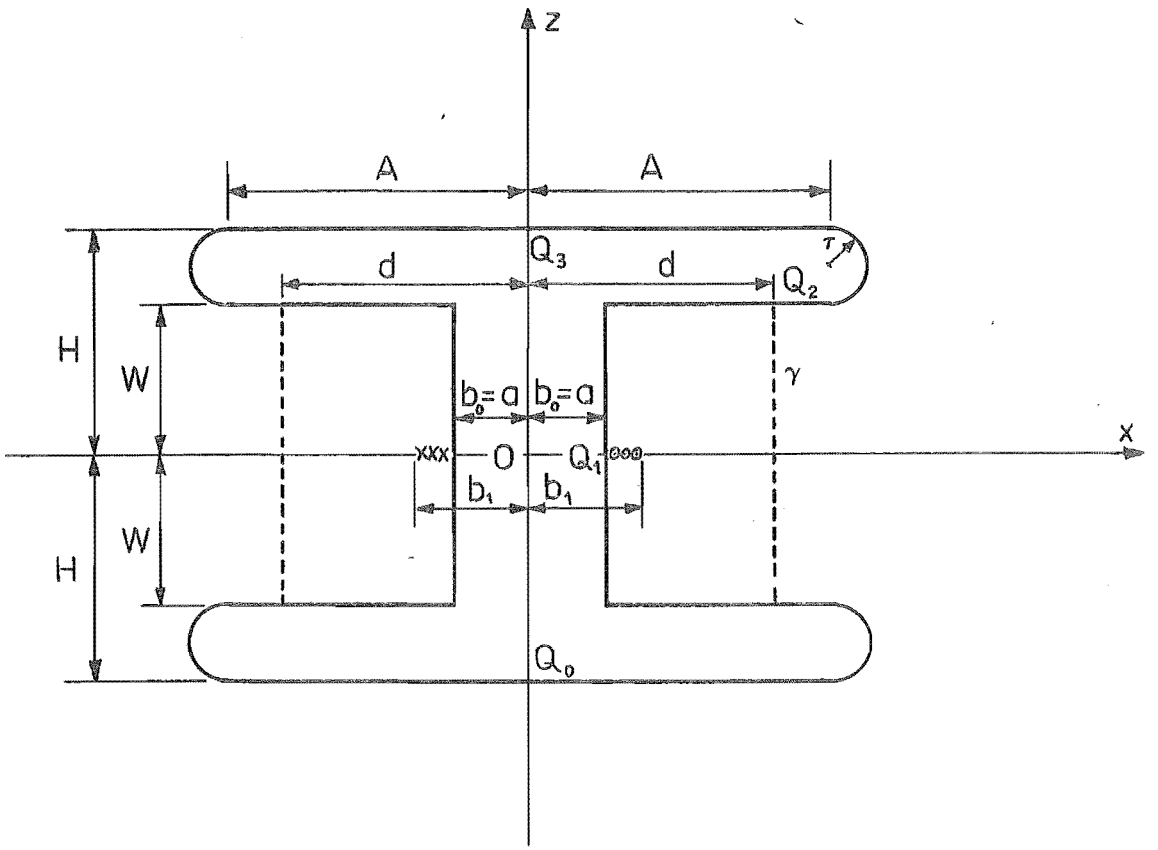

Fig. 4.5: End-loaded dipole antenna configuration to which the results of section 4.6 apply.

Legend: a = central conductor radius;

A = end-plate radius;

b_0, b_1 = inner and outer radii of coaxial line;

d = distance of fictitious surface γ from z-axis;

H = antenna semi-height;

2W = end-plate separation;

2τ = end-plate thickness.

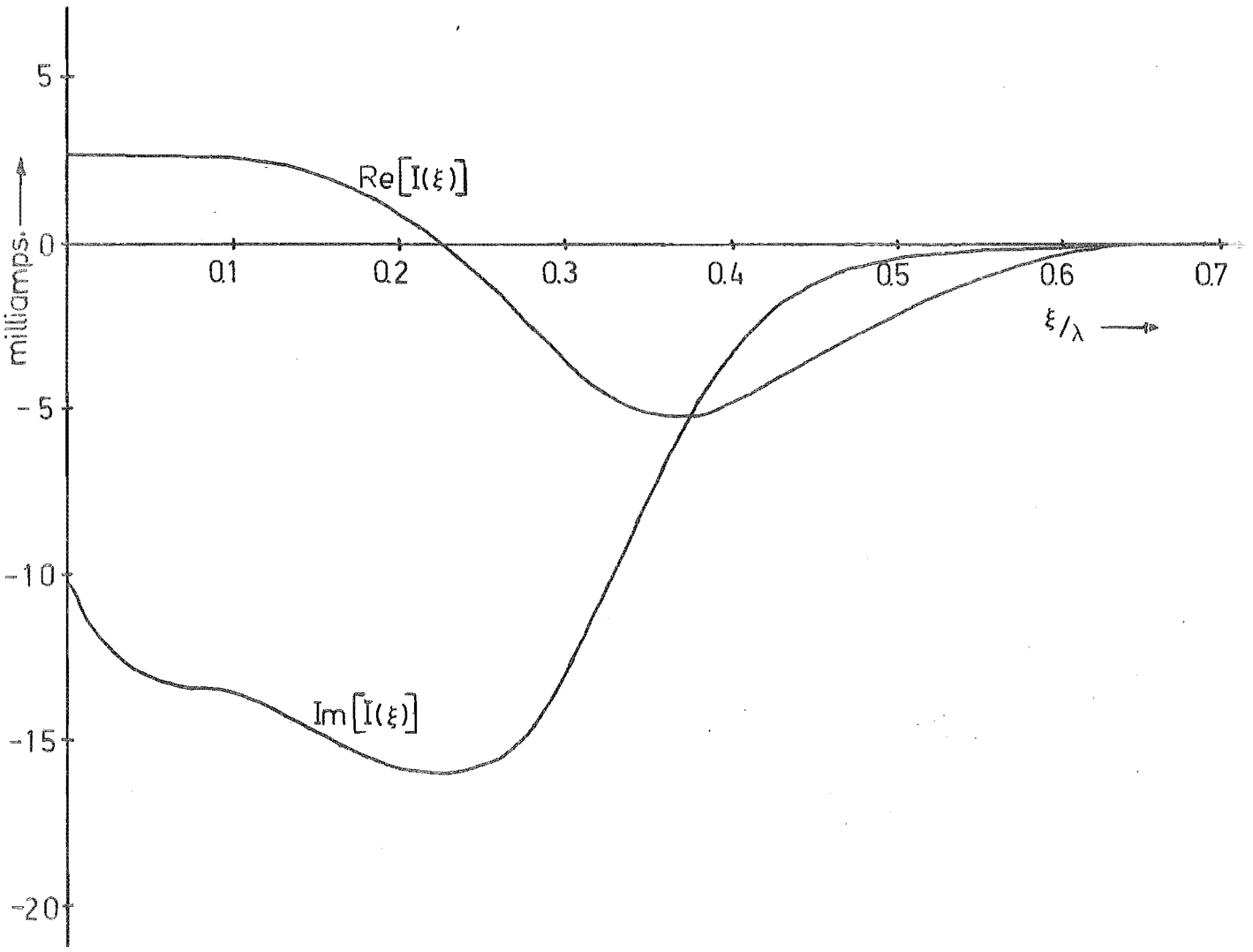

Fig. 4.6: Total current $I(\xi)$ on an end-loaded dipole with $A = 0.24375\lambda$, $H = 0.15\lambda$, $\tau = 0.0375\lambda$, $d = 0.1875\lambda$, $a = 0.0119\lambda$, and $b_1 = 2.3a$. Tchebyshev polynomial basis functions used in METHOD 2A with $M_1 = 7$ and $M_2 = 3$ in eqn (4.21).

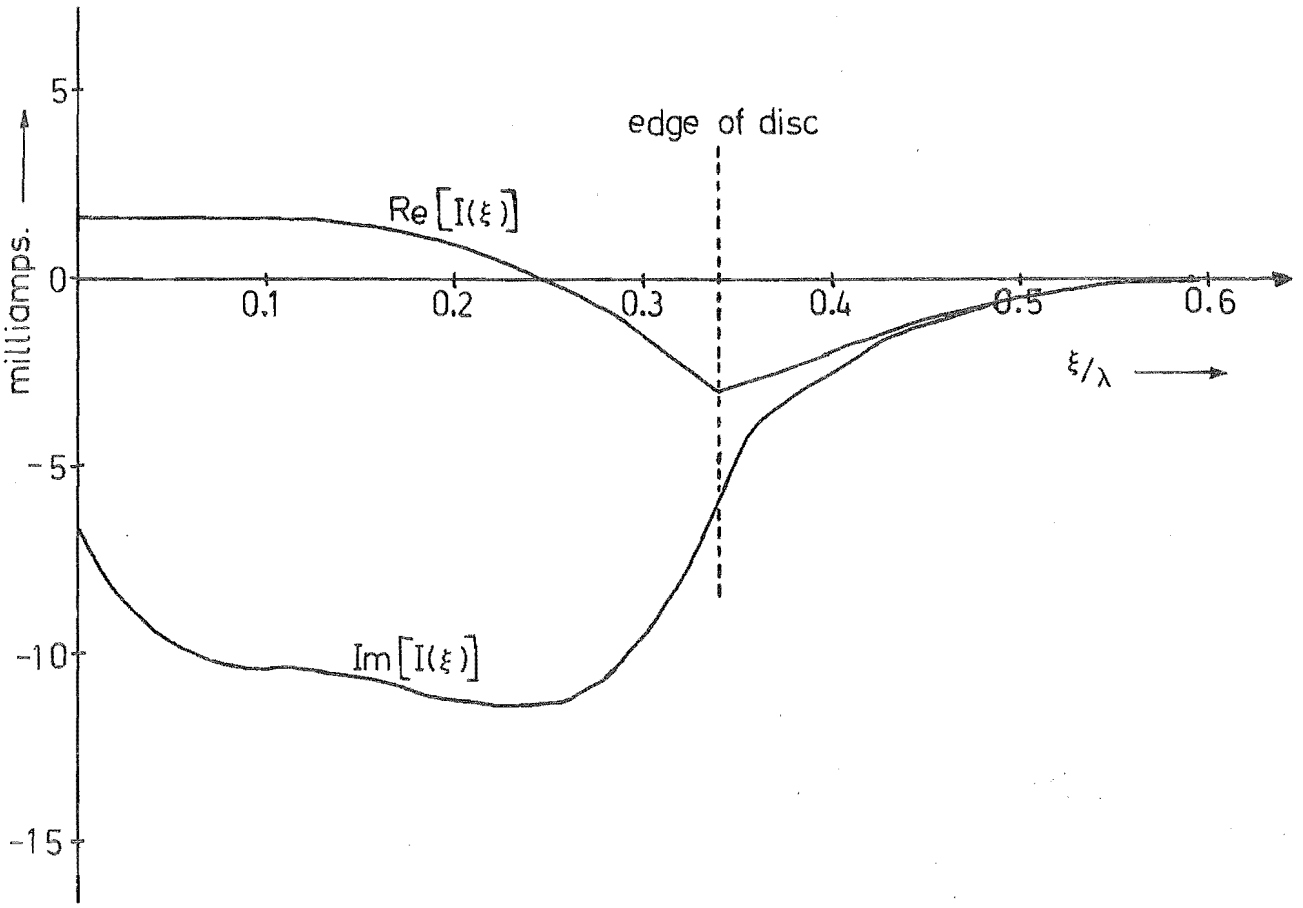

Fig. 4.7: Total current $I(\xi)$ on a disc-loaded dipole with $A = 0.25\lambda$, $H = W = 0.10\lambda$, $\tau = 0$, $d = A - 0.10\lambda$, $a = 0.01\lambda$, and $b_1 = 2.3a$. Wedge Bessel basis functions used in METHOD 2A with $M_1 = 7$ and $M_2 = 2$ in eqn (4.21).

CHAPTER 5

CONCLUSIONS AND SUGGESTIONS FOR FURTHER RESEARCH

5.1 CONCLUSIONS

In this thesis the extended integral equation formulation is applied to two symmetrically fed, axially symmetric solid antennas, viz. the thick and the circular end-loaded cylindrical dipole antenna. The extended integral equations obtained have simple non-singular kernels and involve single line integrals of finite extent. These two properties of the equations make computer programming relatively simpler and numerical solutions probably faster than in the existing methods (Vasil'ev, 1959; Vasil'ev and Seregina, 1963; Vasil'ev et al., 1967a; Mautz and Harrington, 1969; Harrington and Mautz, 1971a,b; Kalafus, 1971) which have integral equations involving double integrals and/or singular kernels. Another advantage over these methods is the practicability of expanding the surface current density in terms of a variety of sets of continuous functions, or more interestingly, functions which have analytic properties suitable for any surface discontinuities on the dipole body.

Numerical solutions using METHODS 1 and 2 (chapter 3) are found to be practicable in the range $0.25 < H/A < 25$, $a < 0.5\lambda$, where a and H are respectively the dipole radius and semi-height.

Numerical solutions using METHOD 2A (chapter 4) are practicable for end-loaded dipole antennas with thick and disc end-plates in the ranges $H/A < 2, A < 0.5\lambda$ and $0.25 < H/A < 0.4$,

$A < 0.4\lambda$, respectively. A and H are respectively the radii of the end-plate and the antenna semi-height.

5.2 SUGGESTIONS FOR FURTHER RESEARCH

5.2.1 Further Applications for the Extended Integral Equation Formulation

The use of METHOD 1 in chapter 3 leads to practicable numerical solutions for the thick solid dipole antenna with a semi-height-to-radius (H/a) ratio in the range $1.0 < H/a < 25$, $a < \lambda/2$. It is expected that METHOD 1, and METHOD 1A described in Appendix VI, are suitable for treating the end-loaded dipole antenna whose central conductor and endplate diameters are smaller than the total antenna height.

Both the analysis and numerical investigation in chapter 4 apply to the end-loaded dipole antenna with free space medium in the parallel-plate region (see Fig. 4.3). They can be straightforwardly extended to treat the same antenna but with an arbitrary medium (complex permittivity ε', permeability μ, and wavenumber $k = \omega(\mu\varepsilon')^{\frac{1}{2}}$) in the parallel-plate region as shown in Fig. 5.1.

5.2.1.1 Monopole fed by a radial transmission line: Fig. 5.2 shows a cylindrical solid monopole mounted on a ground plane and driven, via a radial line, by an incoming TEM mode in the coaxial line. A simple numerical solution to this antenna problem, valid for moderately thick monopoles ($a < 0.1\lambda$) and small radial line gaps ($u \ll \lambda$), has been obtained by Otto (1968b). The problem is treated by Otto (1968b) in two parts. The first deals with the monopole which has a uniform longitudinal electric intensity (E_z) applied across the circumferential slot at $\rho = a$, $0 < z < u$. The second part

transfers the admittance at the slot, found in the first part to the coaxial aperture in the ground plane. For an electrically large radial line gap ($u > 0.05\lambda$), this splitting of the total problem into two independent parts becomes less satisfactory because the monopole-radial line coupling is no longer negligible. METHODS 1A and 2A described respectively in Appendix VI and chapter 4 could be used to supplement Otto's (1968b) method when $u > 0.05\lambda$. No modification is required to the integral equations in Appendix VI and chapter 4.

5.2.1.2 Design of broad-band coaxial feeds: It appears that the design of input regions for the broad-band coaxial feeding of conical monopoles has not been attempted. Consider the infinite conical monopole shown in Fig. 5.3. It is mounted on an infinite ground plane and fed by a coaxial line. For the input region to possess broad-band characteristics, the transition from the coaxial line to the "conical line" should be gradual. The fictitious surfaces, α and β in Fig. 5.3, are respectively situated inside the coaxial and the conical line. By using Love's field equivalence principle (Harrington, 1961, Sect. 3.5), the electromagnetic problems posed in Fig. 5.3 and 5.3a can be shown to be equivalent. Extended integral equations can then be derived by requiring the total field to be zero outside the region bounded by the surfaces α, β, γ and Γ shown in Fig. 5.3a.

5.2.1.3 Hollow monopole driven by a coaxial line: The extended integral equation formulation can also be applied to the hollow cylindrical monopole shown in Fig. 5.4, where the interior of the hollow monopole is short circuited by a

perfectly conducting plate at $z = z_p$, $-\infty < z_p < H$. This monopole has so far been treated for only two cases: (i) the shorting plate is flush ($z_p = 0$) with the ground plane (Chang, 1968a,b); or (ii) it is well inside ($z_p = -\infty$) the central conductor of the coaxial line (Bach Andersen, 1968, 1971; Bach Andersen and Yee, 1969).

The following procedure converts the hollow monopole antenna problem into one suitable for setting up extended integral equations. In Fig. 5.4a, fictitious surfaces α and β envelop the monopole surface, and surface Γ lies over the ground plane and coaxial aperture. Surfaces α and γ completely bound a cylindrical region V_1, in which the field can be represented by cylindrical wave functions (Jones, 1964, Sect. 4.14; Ramo et al., 1965, Sect. 7.16). The field in region V_o is identical to that of the monopole shown in Fig. 5.4b, where the tangential field on γ is the same as that in Fig. 5.4a. Application of Love's equivalence principle (Love, 1901; Harrington, 1961; Sect. 3.5; Otto, 1965, 1967) as described in section 3.2 of chapter 3 shows that the problem of the dipole antenna in Fig. 5.4c is equivalent to that in Fig. 5.4.b. Extended integral equations can then be obtained by using equations (2.5a,b) of chapter 2 for the antenna problem in Fig. 5.4c.

The procedure just described can be applied straightforwardly to the dielectric-filled hollow monopole shown in Fig. 5.5. Ting and King (1970) have treated such monopoles, but assumed that the dielectric medium extends from the shorting plate at $z_p = 0$ to infinity.

5.2.2 Application of Einarsson's Method to the Monopole in a Parallel-Plate Region

Figs 5.6 and 5.7, respectively, show a cylindrical tubular and solid monopole driven by a coaxial line and radiating into an infinite parallel plate region. The method of Einarsson (1966) (cf. Otto, 1968b) can be used to treat both of the antenna problems shown in Fig. 5.6 and 5.7. In Appendix VII, an associated hollow dipole symmetrically driven by a delta gap source is analysed, and the integral equation (VII.19) obtained is closely related to Einarsson's (1966) eqn 13, i.e. equation 1.3 in chapter 1. It should be interesting to solve (VII.19) numerically.

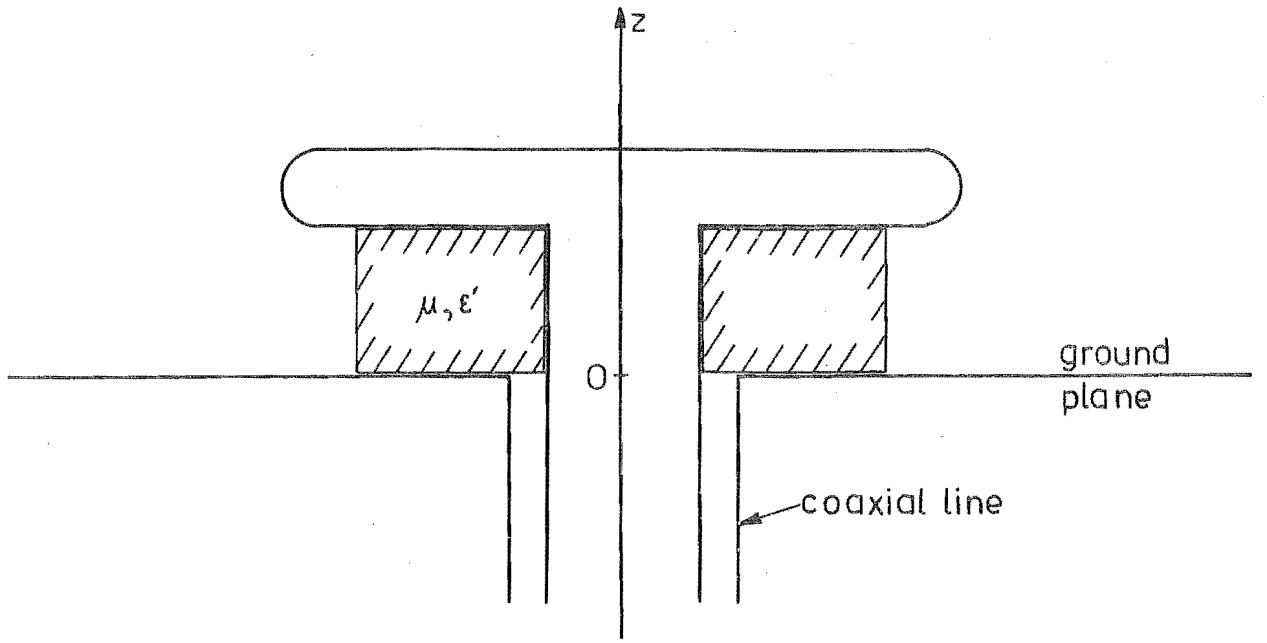

Fig. 5.1: End-loaded dipole driven by a coaxial line. Parallel-plate region filled with a non-conducting medium.

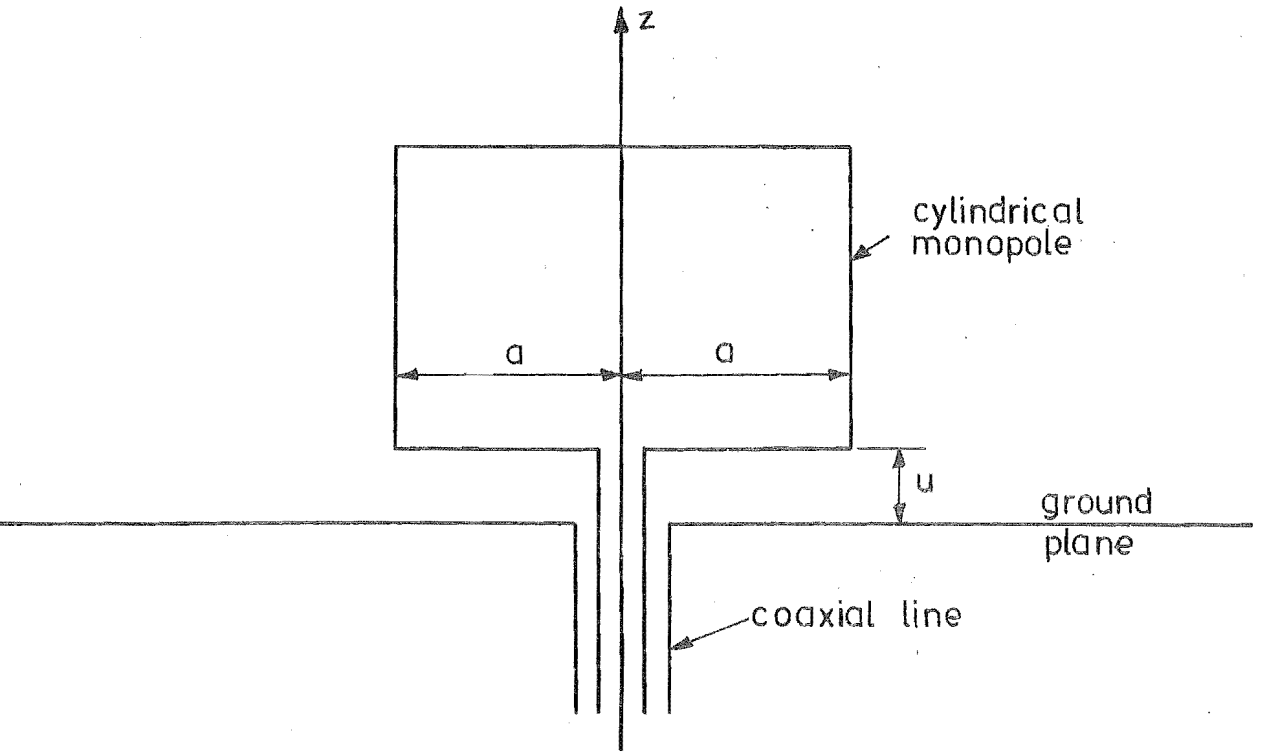

Fig. 5.2: Solid cylindrical monopole driven, via a radial transmission line, by a coaxial line.

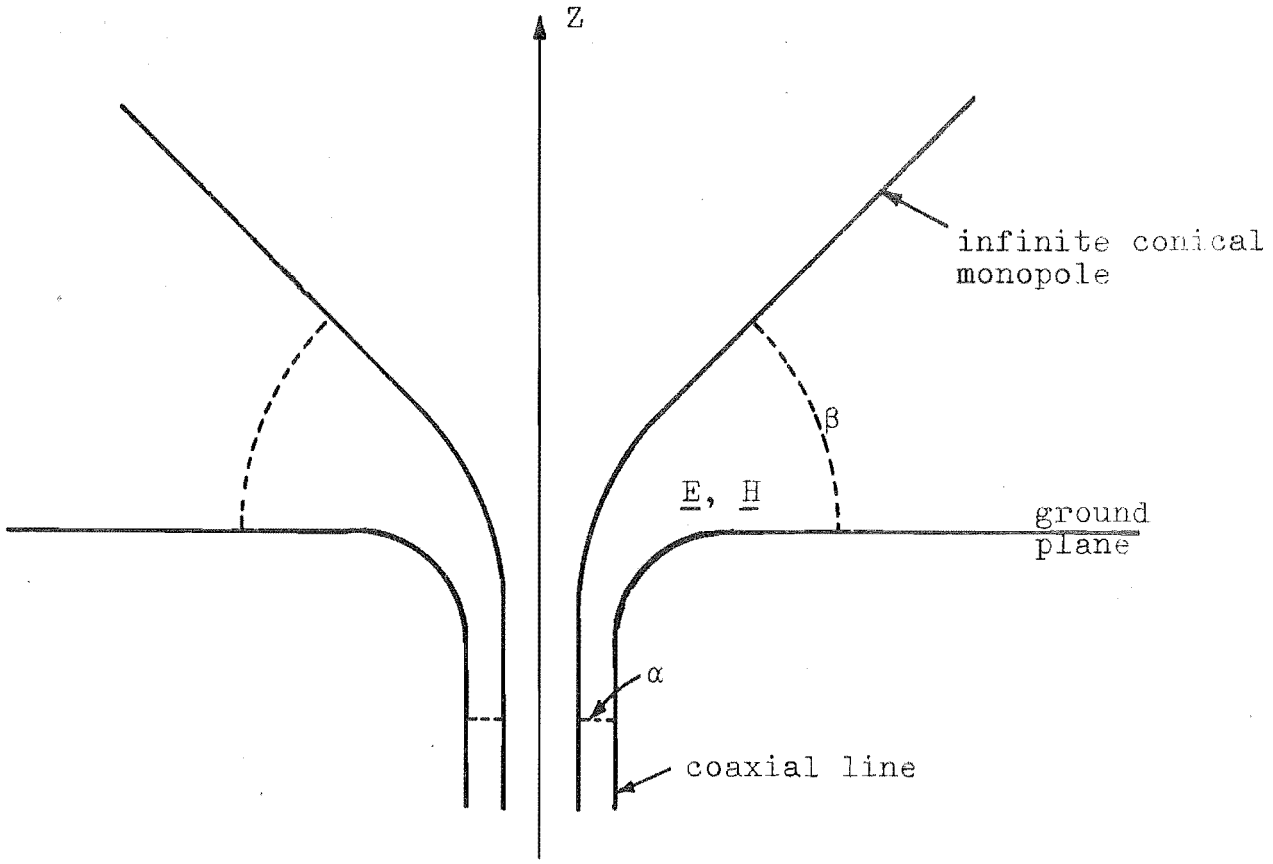

Fig. 5.3: Input region of a coaxially-fed infinite conical monopole. The surfaces α and β are fictitious.

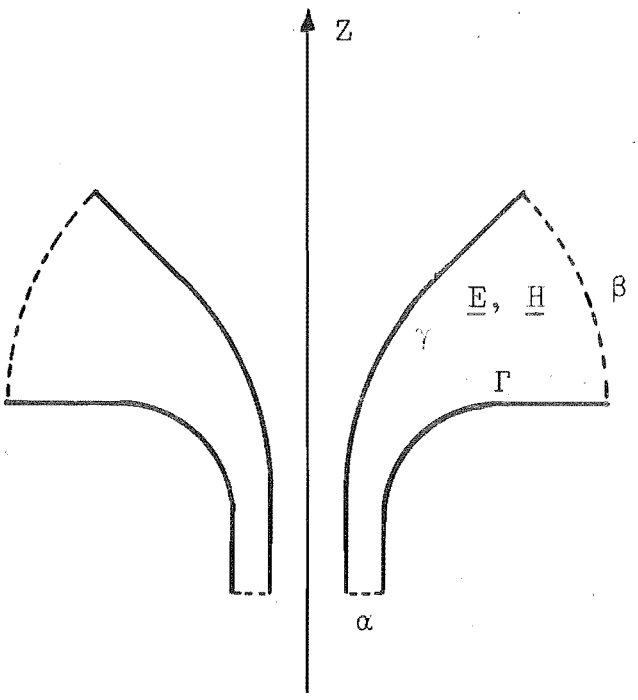

Fig. 5.3a: Electromagnetic problem equivalent to that posed in Fig. 5.3.

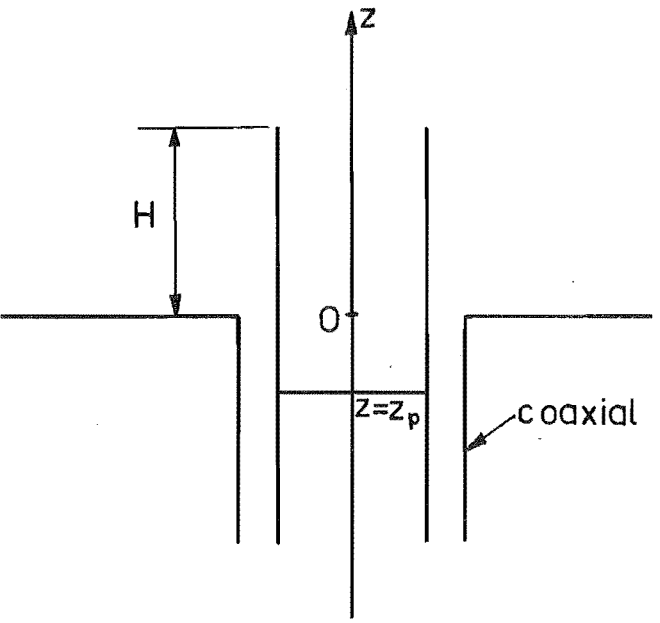

Fig. 5.4: Coaxial line driven hollow cylindrical monopole with interior short-circuited at $Z = Z_p$.

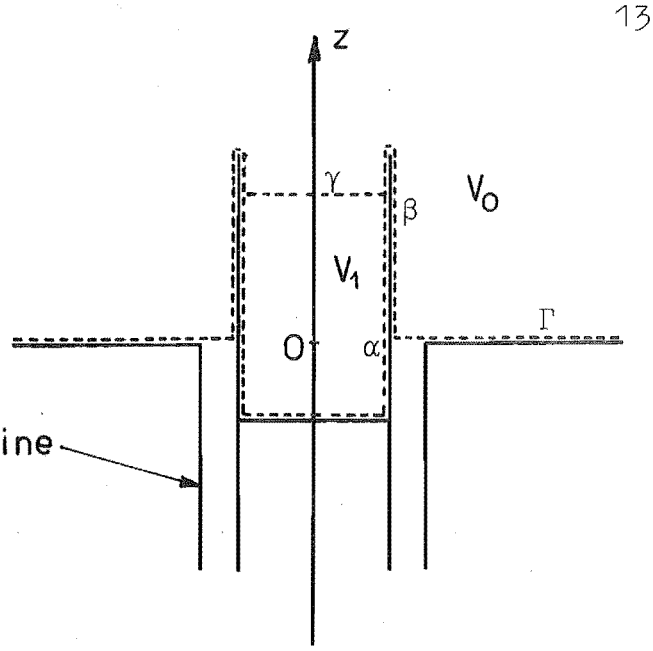

Fig. 5.4a: Fictitious surfaces α, β, γ and Γ.

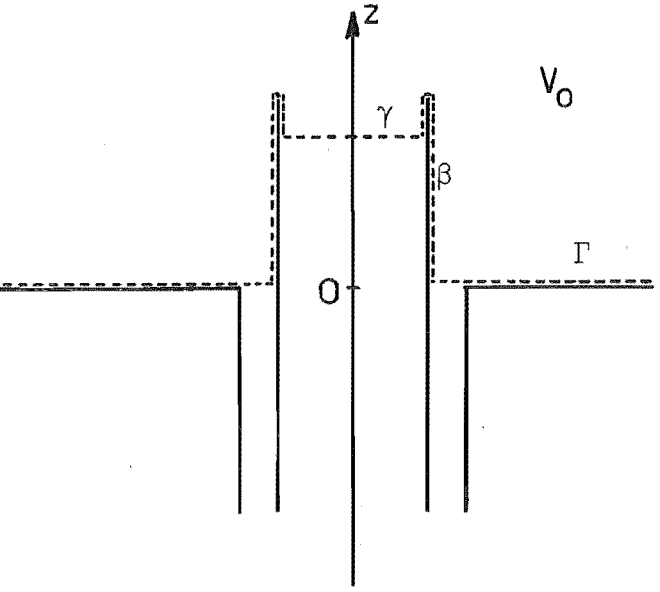

Fig. 5.4b: Antenna problem corresponding to that shown in Fig. 5.4a.

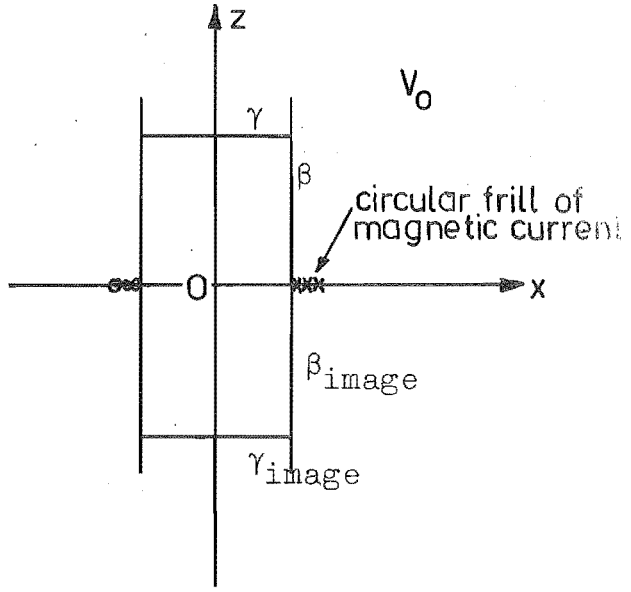

Fig. 5.4c: Dipole antenna equivalent to that shown in Fig. 5.4b.

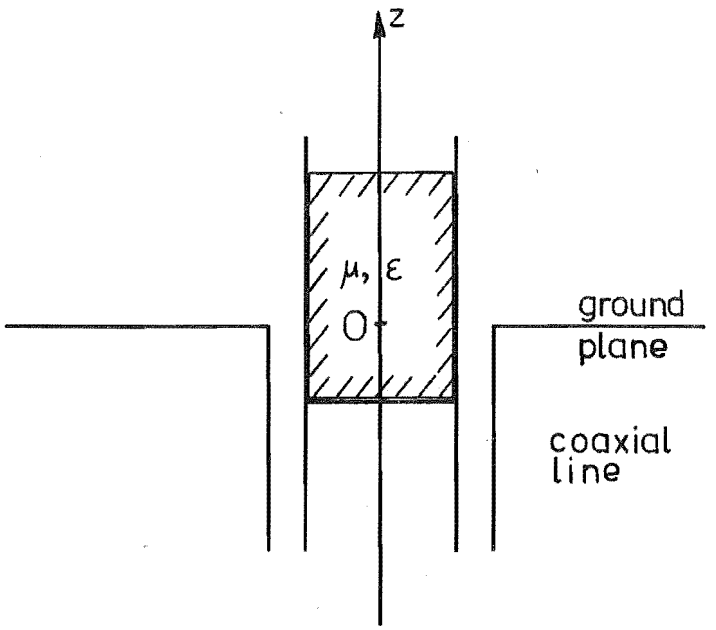

Fig. 5.5: Hollow cylindrical monopole filled with an arbitrary medium.

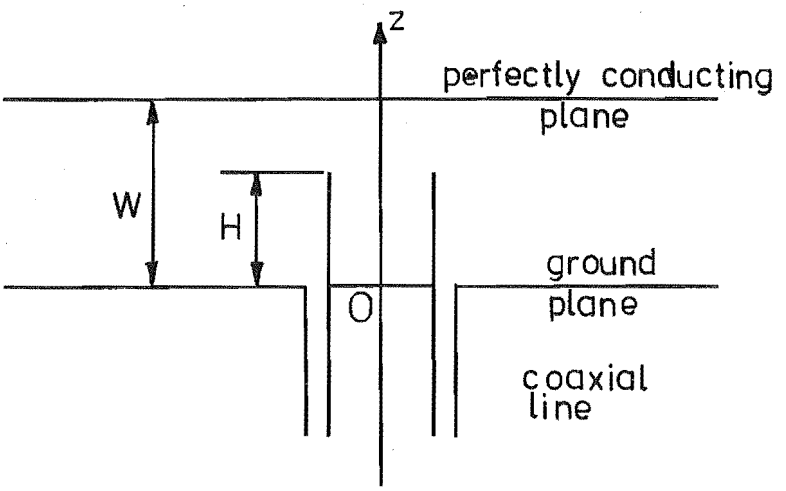

Fig. 5.6: Hollow cylindrical monopole radiating into an infinite parallel-plate region.

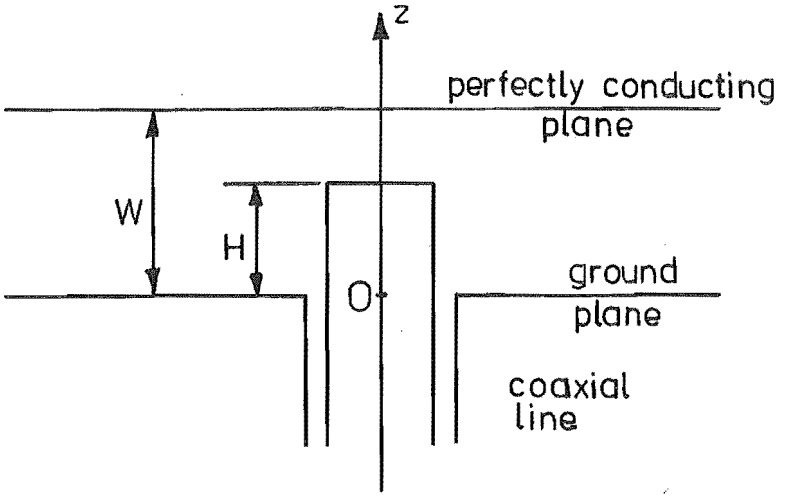

Fig. 5.7: Solid cylindrical monopole with plane ends and radiating into an infinite parallel-plate region.

A P P E N D I C E S

Appendix I: Spherical Vector Wave Functions

Within a source-free region with permittivity ε and permeability μ, the electric and magnetic intensities satisfy the vector Helmholtz wave equation

$$\nabla^2 \underline{U} + k^2 \underline{U} = 0 \tag{I-1}$$

where $k = \omega(\mu\varepsilon)^{\frac{1}{2}}$, the field $\underline{U}$ is assumed to be harmonic with the time factor $\exp(j\omega t)$ understood. In spherical coordinates (r,θ,φ) independent vector solutions of this equation are constructed as (Morse and Feshbach, 1953, p.1865)

$$\underline{L}^{(q)}_{\substack{e\\o}mn}(k\underline{r}) = \frac{1}{k} \nabla P^m_n(\cos\theta)\, z^{(q)}_n(kr) \begin{matrix}\cos\\ \sin\end{matrix} m\varphi, \tag{I-2}$$

$$\begin{aligned}\underline{M}^{(q)}_{\substack{e\\o}mn}(k\underline{r}) &= \underline{L}^{(q)}_{\substack{e\\o}mn}(k\underline{r}) \wedge \underline{r} \\ &= \frac{1}{k} \nabla \wedge \underline{N}^{(q)}_{\substack{e\\o}mn}(k\underline{r}),\end{aligned} \tag{I-3}$$

$$\underline{N}^{(q)}_{\substack{e\\o}mn}(k\underline{r}) = \frac{1}{k} \nabla \wedge \underline{M}^{(q)}_{\substack{e\\o}mn}(k\underline{r}) \tag{I-4}$$

where $\underline{r}$ is a point (r,θ,φ) from the origin

$P^m_n(\cos\theta)$ is the associated Legendre function,

$z^{(1)}_n(kr) = j_n(kr)$ is the spherical Bessel function,

$z^{(2)}_n(kr) = y_n(kr)$ is the spherical Neumann function,

$z^{(3)}_n(kr) = h^{(1)}_n(kr)$ is the Hankel function of the first kind, and

$z^{(4)}_n(kr) = h^{(2)}_n(kr)$ is the Hankel function of the second kind.

The subscript $\begin{matrix}e\\o\end{matrix}$ takes value e or o, indicating whether the

upper or lower φ variation is specified. The integers n and m have ranges $0 \leqslant n < \infty$ and $0 \leqslant m \leqslant n$ respectively.

The first set, $\underset{o}{\underline{L}}^{(q)}_{emn}$, of these solutions corresponds to the longitudinal part and the other two sets correspond to the transverse solutions of (I-1). They have the properties (Stratton, 1941, Sect. 7.1 and Sect. 7.11; Morse and Feshbach, 1953, p.1865):

$$\nabla \wedge \underset{o}{\underline{L}}^{(q)}_{emn} = 0; \tag{I-5}$$

$$\nabla\nabla \cdot \underset{o}{\underline{L}}^{(q)}_{emn} = -k^2 \underset{o}{\underline{L}}^{(q)}_{emn} ; \tag{I-6}$$

$$\nabla \cdot \underset{o}{\underline{M}}^{(q)}_{emn} = \nabla \cdot \underset{o}{\underline{N}}^{(q)}_{emn} = 0; \tag{I-7}$$

$$\int_0^{2\pi} \underset{o}{\underline{M}}^{(q)}_{emn}(k\underline{r})d\varphi = 0 \quad , m \neq 0$$
$$= 2\pi \, \underset{o}{\underline{M}}^{(q)}_{emn}(k\underline{r})\Big|_{\varphi=0} \quad , m = 0; \tag{I-8}$$

$$\int_0^{2\pi} \underset{o}{\underline{N}}^{(q)}_{emn}(k\underline{r})d\varphi = 0 \quad , m \neq 0$$
$$= 2\pi \, \underset{o}{\underline{N}}^{(q)}_{emn}(k\underline{r})\Big|_{\varphi=0}, \quad m = 0; \tag{I-9}$$

and form a complete orthogonal set over any constant spherical surface centred at the origin.

Appendix II: The General Method of Moments

A general procedure of reducing integral equations into a system of simultaneous linear algebraic equations, which are solved by standard matrix methods, is the method of moments (Morse and Feshbach, 1953, Sect. 8.3; Harrington, 1968, Chap. 1). The formal procedure and some relevant notes are given in this appendix.

II.1 Formal Procedure

Consider the inhomogeneous integral equation of the first kind

$$\int_a^b Z(y,x)F(x)dx = B(y), \qquad c \leqslant y \leqslant d \tag{II-1}$$

where the kernal $Z(y,x)$ and the source function $B(y)$ are known, and $F(x)$ is to be determined. Let $w_1, w_2, \ldots, w_N$ be a finite set of testing functions which are at least linearly independent in the interval $c \leqslant y \leqslant d$. Application of the testing functions to (II-1) leads to a set of integral equations,

$$\int_a^b Z_n(x)F(x)dx = B_n, \qquad n = 1,2,\ldots,N; \tag{II-2}$$

$$Z_n(x) = \int_c^d w_n(y)\, Z(y,x)dy; \tag{II-3}$$

$$B_n = \int_c^d w_n(y)\, B(y)dy. \tag{II-4}$$

If it is assumed that $F(x)$ can be approximated accurately by a finite number, M, of basis functions $\varphi_m(x)$, then

$$F(x) = \sum_{m=1}^{M} F_m \varphi_m(x), \qquad \text{(II-5)}$$

where the F_m are unknown expansion coefficients and the φ_m are at least linearly independent in $a \leqslant x \leqslant b$. Substituting (II-5) into (II-2) gives a system of N linear algebraic equations,

$$\sum_{m=1}^{M} Z_{nm} F_m = B_n \ ; \qquad \text{(II-6)}$$

$$Z_{nm} = \int_a^b Z_n(x) \varphi_m(x) \, dx. \qquad \text{(II-7)}$$

(II-6) is written in the matrix notation

$$[Z_{nm}][F_m] = [B_n] \ ; \ m = 1,2,3,\ldots,M; \ n = 1,2,3,\ldots,N. \qquad \text{(II-8)}$$

Both (II-6) and (II-8) represent N independent equations to determine the M unknown F_m constants.

When $N < M$, the solution of (II-6) or (II-8) is non-unique (Kreyszig, 1962, Sect. 7.7). When $N = M$, $[Z_{nm}]$ is a square matrix with an inverse $[Z_{nm}]^{-1}$ if the matrix is non-singular. The column vector $[F_m]$ is given by

$$[F_m] = [Z_{nm}]^{-1} [B_n]. \qquad \text{(II-9)}$$

II.2 Notes

If G is known to be a good approximation of F, the remainder $\overline{F} = F - G$ can be obtained in the same way as for F in section II.1. Rewriting (II-1) as

$$\int_a^b Z(y,x) \overline{F}(x) \, dx = \overline{B}(y), \qquad \text{(II-10)}$$

$$\overline{B}(y) = B(y) - \int_a^b Z(y,x) G(x) \, dx; \qquad \text{(II-11)}$$

gives an integral equation for $\overline{F}$ in the same form as (II-1).

The matrix $[Z_{nm}]$ should be well-conditioned for numerical solution to be practicable. A measure of the conditioning is given by the normalised determinant of $[Z_{nm}]$ (Conte, 1965, Sect. 5.4) which is defined as

$$||Z|| = \text{determinant}\left(Z_{nm}/\sqrt{\sum_{q=1}^{M}|Z_{nq}|^2}\right) . \qquad \text{(II-12)}$$

$||Z|| < 1$ unless $[Z_{nm}]$ has only diagonal elements so that $||Z|| = 1$. When $||Z|| \ll 1$ the solution vector $[F_m]$ in (II-9) is sensitive to errors in the matrix elements Z_{nm} and B_n. As these elements are to be evaluated by numerical integration (see II-3, II-4, II-7), the high accuracy required when $||Z|| \ll 1$ makes computations protracted and expensive.

The testing functions w_n are chosen such that the $Z_n(x)$ and B_n are strongly linearly independent and easily evaluated. A strong linear independence in the $Z_n(x)$ generally leads to a matrix $[Z_{nm}]$ which is well-conditioned. When $Z(y,x)$ is a complicated kernel, the simplest set of w_n which makes $Z_n(x)$ and B_n easily evaluated is the Dirac delta functions $\delta(y-y_n)$ that match (II-1) at discrete points y_n on $c \leqslant y \leqslant d$. With this 'point-matching' procedure, $[Z_{nm}]$ will necessarily become singular as N tends to infinity, and the smoother $Z(y,x)$ is in y the faster is the rate of decrease in $||Z||$. For some kernels, the integration in (II-3) can be performed analytically with particular sets of w_n.

The basis functions φ_m are chosen to make the number M (see II-5) small and/or Z_{nm} easily computed. The method of subsections, where each φ_m exists only over one or two

subsections of the interval $a \leqslant x \leqslant b$, is particularly suited for easy numerical evaluation of the integral in (II-7) because the subsectional intervals of integration are short. The φ_m commonly used with the method of subsections are pulse, triangle, or parabolic functions corresponding to a piece-wise constant, linear or parabolic approximation respectively to F(x).

The computations are successful only if numerical convergence is achieved. The only known method of determining whether numerical convergence is occurring is the obvious (brute force) procedure: increase M until, at a number of closely spaced points on $a \leqslant x \leqslant b$, the F(x) display negligible change with increasing M.

Appendix III: A Physical Optics Approximation

When a cylindrical dipole is excited by a magnetic ring source electrically close to the dipole surface (see Fig. 3.6), the dipole surface currents near the ring source vary rapidly along the meridians. This behaviour can be deduced from the physical optics approximation to the surface currents.

Consider, first, a perfectly conducting plane of infinite extent and illuminated by a uniform line source of negative x-directed magnetic current as shown in Fig. III-1. With the cylindrical polar coordinates (ρ,φ,x) defined in the figure, the magnetic intensity due to the line source at a point P is,

$$\underline{H}^{i}(P) = \hat{x}\,\frac{k_o V}{4Z_o}\,H_o^{(2)}\,(k_o\rho) \qquad \text{(III-1)}$$

where $k_o = 2\pi/\lambda$; Z_o is the intrinsic impedance and is about 120π ohms for free space; and $H_o^{(2)}$ is the zeroth order Hankel function of the second kind. The surface current density on the plane is just the physical optics current given by

$$\underline{K}_s^{P.O.} = 2\,\hat{n}\wedge\underline{H}^{i} = \hat{n}\wedge\hat{x}\,\frac{k_o V}{2Z_o}\,H_o^{(2)}\,(k_o\rho) \qquad \text{(III-2)}$$

where $\hat{n}$ is a unit vector normal to the plane surface.

Consider the infinite perfectly conducting cylinder in Fig. III.2, where the excitation source is a uniform ring of negative φ-directed magnetic current. With the cylindrical polar coordinates (ρ,φ,z) defined in Fig. III.2, the physical optics current density, deduced from (III.2) and Fig. III.1 on the cylinder is

$$\underline{K}_s^{P.O.}(a,\varphi,z) = \hat{z}\,\frac{k_o V}{2Z_o}\,H_o^{(2)}\left(k_o\sqrt{z^2+(b-a)^2}\right) \qquad \text{(III-3)}$$

$I_z^{P.O.}(z)$, the total current along the cylinder, is defined as

$$I_z^{P.O.}(z) = \pi a\,\frac{k_o V}{Z_o}\,H_o^{(2)}\left(k_o\sqrt{z^2+(b-a)^2}\right) \qquad \text{(III-4)}$$

When $(b-a) \ll \lambda$ and $z \ll \lambda$, the small argument expansion of the Hankel function gives

$$I_z^{P.O.}(z) \approx \frac{\pi a k_o V}{Z_o}\left[1 - j\,\frac{2}{\pi}\,\ell n\left(k_o\sqrt{z^2+(b-a)^2}\right)\right] \qquad \text{(III-5)}$$

which is rapidly varying (logarithmic-type) near the ring source.

If $(b-a) = 0$, (III-5) reduces to

$$I_z^{P.O.}(z) = \frac{\pi a k_o V}{Z_o}\left[1 - j\,\frac{2}{\pi}\,\ell n(k_o z)\right]. \qquad \text{(III-6)}$$

The logarithmic behaviour of the imaginary part of the current is identical to that which has been obtained by Fourier transform methods (Duncan and Hinchey, 1960, eqn 3.18; Chang, 1967).

In chapter 3, the unknown surface current density $K(\xi)$ on the dipole antenna shown in Fig. 3.7 is obtained from the integral equations (3.21) and (3.25) by the moment method described in Appendix II. With reference to the basis functions listed in Table 3.1, the Fourier sine functions of low orders of m are smoothly varying in the neighbourhood of $\xi = 0$ (see Fig. 3.7). It is to be expected that, when the ring source is electrically close ($b-a < \lambda/20$) to the dipole surface, many sine functions would be required to accurately approximate $K(\xi)$, which has a logarithmic type behaviour near $\xi = 0$ given by (III-5). The slow numerical convergence can

sometimes be accelerated by "subtracting out" the logarithmic term from $K(\xi)$ and then proceeding with the moment method of solution as described in Appendix II, section II-2. From (III-3), the logarithmic behaviour comes from the Neumann function Y_o part of $H_o^{(2)}$. Let

$$K^{P.O.}(\xi) = -j \frac{k_o}{2Z_o} Y_o \left(k_o\sqrt{\xi^2 + (b-a)^2}\right), \quad 0 < \xi < H-\tau \tag{III-7}$$

so that the remainder $\overline{K}(\xi)$ of $K(\xi)$, with $K^{P.O.}(\xi)$ subtracted out, is

$$\begin{aligned} \overline{K}(\xi) &= K(\xi) - K^{P.O.}(\xi) , \quad 0 < \xi < H-\tau \\ &= K(\xi) \qquad\qquad , \quad H-\tau < \xi < L \end{aligned} \tag{III-8}$$

But $\overline{K}(\xi)$ is discontinuous at $\xi = H-\tau$. A better choice for the term to be subtracted out is

$$Q(\xi) = \frac{-jk_o}{2Z_o} Y_o \left(k_o\sqrt{\xi^2 + (b-a)^2}\right) \frac{\left[1 + \sin\left(\frac{\pi}{2} + \frac{2\pi}{d}\right)\right]}{2},$$

$$0 < \xi < d < H-\tau \tag{III-9}$$

where $d^2 = \chi_1^2 - (b-a)^2$, and χ_1 is the first zero of $Y_o(\chi) = 0$. The new $\overline{K}(\xi)$ is

$$\begin{aligned} \overline{K}(\xi) &= K(\xi) - Q(\xi) , \quad 0 < \xi < d < H-\tau \\ &= K(\xi) \qquad\qquad , \quad d < \xi < L. \end{aligned} \tag{III-10}$$

which is continuous and has only small discontinuous derivatives at $\xi = d$. Note that (III-10) is applicable only if $H-\tau \geqslant d$.

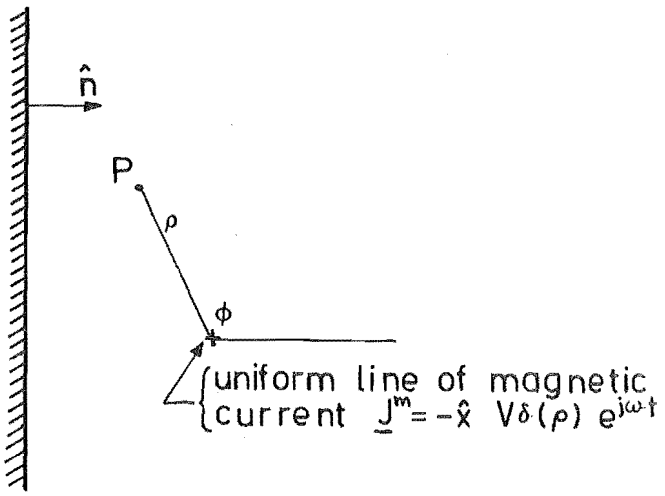

Fig. III.1: An infinite perfectly conducting plane illuminated by a uniform line of magnetic current.

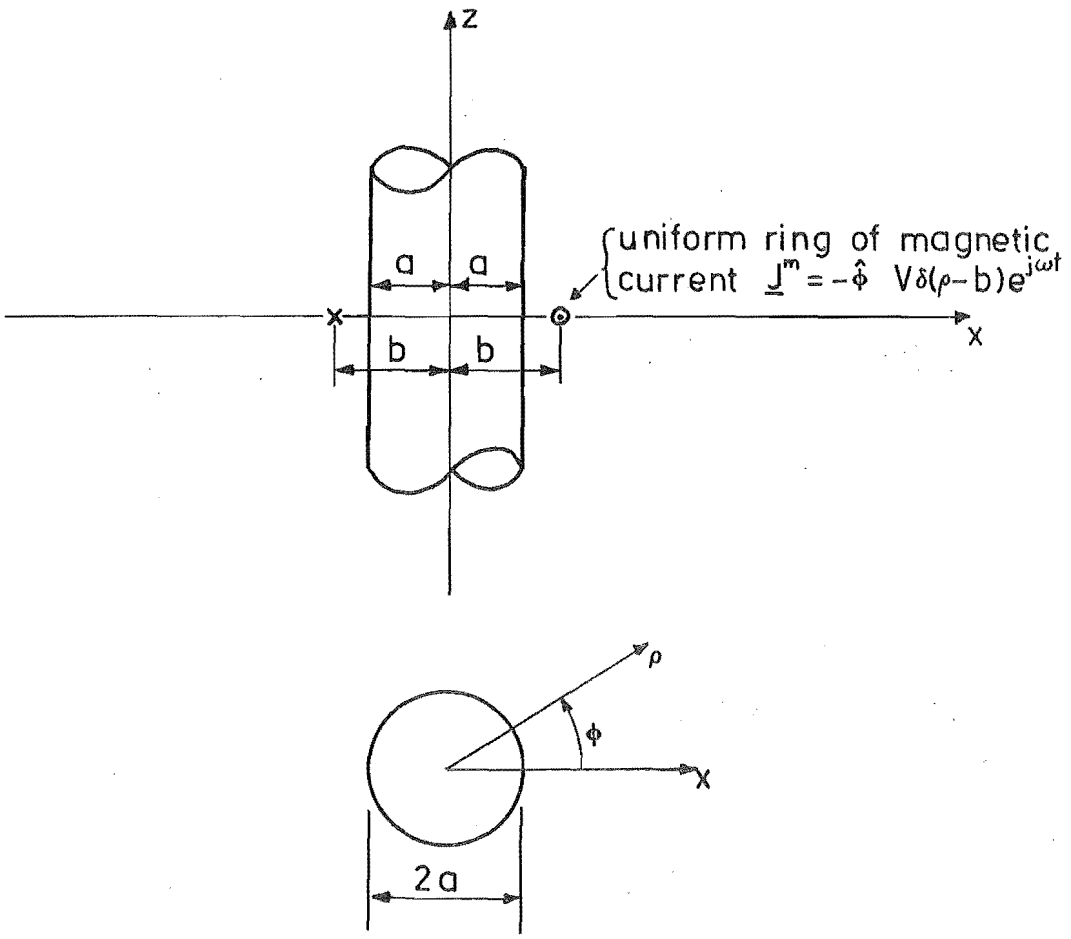

Fig. III.2: An infinite perfectly conducting cylinder illuminated by a uniform ring of magnetic current.

Appendix IV: Electric Surface Field Measurements on a Thick Monopole

Much of the design and construction of the experimental apparatus, and the measurements described in this appendix were performed by Anderson (1971), Gulab (1971) and Williamson (1971) as part of the practical laboratory work required in the final year of their Bachelor of Engineering degree.

Measurements were carried out on a thick cylindrical monopole to obtain confirmatory experimental results for the computational methods discussed in chapter 3. Although Prasad and Rama Rau (1964), Holloy (1968), Chang (1968b), Ting (1969) and Otto (1970) have reported experimental results on thick cylindrical monopoles, only Chang's (1968b) apply antennas with radii greater than one-tenth of the free space wavelength. Unfortunately the antennas considered by Chang are hollow (tubular) monopoles, for which the methods in chapter 3 are not applicable.

Measurements on symmetrically fed thick cylindrical antennas (Holly, 1968; Chang, 1968b; Ting, 1969; Otto, 1970) have generally been carried out on a monopole that forms an extension above ground of the centre conductor of a coaxial line as shown in Fig. IV.1. A major experimental difficulty associated with such an antenna measurement is the existence of unwanted modes (other than the TEM mode) in the coaxial line, caused either by the method of excitation or by irregularities in the coaxial-line structure (Chang, 1968b; Otto, 1970). Because of the high cost in time, material and

equipment involved in setting up this antenna measurement system (cf. Chang, 1968b), a different system for obtaining the confirmatory experimental results was adopted. In our system, the normal component of the electric intensity on a 4-inch diameter copper tube, which was closed at the top end, was measured by an electric field probe. The copper tube, which forms a thick monopole, was mounted centrally on a 6 x 6 foot square aluminium sheet, and was illuminated by a thin excitation monopole some distance away. The physical and electrical dimensions of the thick and the thin monopole at an operating frequency of 0.9732 GHz (i.e. λ =0.30805 metre) are shown in Fig. IV.2.

IV.1 Theoretical considerations

In this section a relation is established between the normal component of the electric intensity, averaged over a circumferential circle, and the circularly symmetric, meridionally-directed current on a thick monopole computed by the methods in chapter 3.

Let (ρ,φ,z) form a cylindrical polar coordinate system which has its origin at the centre of the base circle of the thick dipole (see Fig. IV.2). The induced surface electric currents $\underline{K}_s$ on the thick monopole, which is assumed perfectly conducting, have both meridionally- and circumferentially-directed components. Because of the symmetry of the problem, the surface currents can be expressed as (cf. Kao, 1970b) a Fourier series with respect to φ;

$$\underline{K}_s(\rho=a,\varphi,z) = \hat{z} \sum_{m=0}^{\infty} \varepsilon_m K_{z,m}(z)\cos m\varphi - \hat{\varphi} \sum_{m=1}^{\infty} m K_{\varphi,m}(z)\sin m\varphi; \tag{IV.1}$$

$$\underline{K}_s(\rho,\varphi,z=H) = -\hat{\rho} \sum_{m=0}^{\infty} \varepsilon_m K_{\rho,m}(\rho)\cos m\varphi + \hat{\varphi} \sum_{m=1}^{\infty} \varepsilon_m K_{\varphi,m}(\rho)\sin m\varphi; \tag{IV.2}$$

where ε_m is the Neumann factor; and the subscripts on the current strengths K denote respectively the direction and the order of the Fourier series coefficient. By using Maxwell's equations, the electric intensity normal to the surface is obtained from (IV.1) and (IV.2) as

$$j\omega\varepsilon_o E_\rho(\rho=a,\varphi,z) = \sum_{m=1}^{\infty} m\varepsilon_m \frac{K_{\varphi,m}(z)}{a} \cos m\varphi - \sum_{m=0}^{\infty} \varepsilon_m \frac{dK_{z,m}(z)}{dz} \cos m\varphi; \tag{IV.3}$$

$$j\omega\varepsilon_o E_z(\rho,\varphi,z=H) = -\sum_{m=0}^{\infty} \varepsilon_m \frac{1}{\rho} \frac{\partial}{\partial\rho}[\rho K_{\rho,m}(\rho)] \cos m\varphi - \sum_{m=1}^{\infty} m\varepsilon_m K_{\varphi,m}(\rho) \cos m\varphi; \tag{IV.4}$$

where ε_o is the free space permittivity. Integration of (IV.3) and (IV.4) along a circumference then leads to

$$j\omega\varepsilon_o \int_0^{2\pi} E_\rho(\rho=a,\varphi,z)d\varphi = -2\pi \frac{d}{dz} K_{z,o}(z); \tag{IV.5}$$

$$j\omega\varepsilon_o \int_0^{2\pi} E_z(\rho,\varphi,z=H)d\varphi = -2\pi \frac{1}{\rho} \frac{d}{d\rho} (\rho K_{\rho,o}(\rho)). \tag{IV.6}$$

Thus, the averaged normal component of the electric intensity is proportional to the differentials, along the meridian, of the zeroth harmonic of the meridional component of the surface currents.

Consider the problem of a thick dipole illuminated by a thin dipole, which is driven by a uniform circular frill of magnetic currents as shown in Fig. IV.3. By using image theory and Love's equivalence principle (Love, 1901; Harrington, 1961, Sect. 3.5; Otto, 1965, 1967) in the manner described in section 3.2 of chapter 3, it can be shown that the antenna problems posed in Figs IV.2 and IV.3 are equivalent.

Two assumptions about the radiations from the thin dipole and the magnetic frill source have been made; (1) the current on the thin dipole has a sinusoidal distribution with constant phase (King, 1956, Sect. II.25), and (2) the radiation from the magnetic frill source is negligible compared to that from the thin dipole. An approximate analysis, which uses thin cylindrical antenna theory (King, 1956, Sect. II.25 and Sect. II.38), shows that the frill source radiation is less than 0.1% of the thin dipole.

It can be shown that the zeroth harmonic of the meridionally-directed surface current on the thick dipole in Fig. IV.3 is proportional to that on an identical dipole which is illuminated by an infinite array of thin excitation dipoles situated on a circle around the z-axis. Computations have been carried out for the latter symmetrically-fed, thick dipole antenna problem by using wedge Bessel basis functions (see Table 3.1) in METHOD 2 (see chapter 3).

That the averaged normal component of the electric intensity is simply related to the circularly symmetric, meridionally-directed current on a thick monopole represents a positive benefit because electric field probes are more

easily made than magnetic field probes. Although a magnetic probe in the form of a shielded half-loop (Barzilai, 1949; Morita, 1950; Whiteside and King, 1964; Chang, 1968b; Jamieson and Bates, 1971, 1972) can give the surface currents directly, constructional difficulties usually limit its practical use to operating frequencies below 1.0 GHz (Otto, 1970). In contrast, an electric probe in the form of a monopole (Barzilai, 1949; Plonsey, 1962; Mei and Mobery, 1965; Jamieson and Bates, 1971, 1972) can be made much smaller than a magnetic probe.

The electric probe used in the measurements was a monopole of length 0.026λ (i.e. 8 mm) and diameter 0.0033λ (i.e. 1 mm). Supporting evidence for believing that this monopole does not cause serious distortion of the original field can be found in Plonsey (1962), where probes with radii 0.0024λ and lengths of 0.062λ and 0.099λ were used. A comparison of the normalised signal strengths received by these two probes shows that agreement is to within 2% (Plonsey, 1962, Tables I and II). Because the probe used in our measurements is shorter than Plonsey's, the distortion is estimated to be about 1%.

IV.2 Measurements

A schematic diagram of the experimental apparatus is shown in Fig. IV.4. Details of the design and construction of the thick monopole, the base template, the thin excitation monopole, and the measuring electric probe can be found in Gulab (1971) and Williamson (1971), With reference to Fig. IV.4, a circular copper cylinder of height H = 0.280 λ and

diameter $2a = 0.34\lambda$ was set in a circular groove cut in the base template. The circular groove provided a positive and uniform electrical contact, and also maintained the copper cylinder true as it was rotated about its axis. Rigid attachment of the template to the aluminium ground plane, 5.9λ square, was secured by sixteen equispaced screws. The cylinder was illuminated by a thin excitation monopole (height $h = 0.13\lambda$ and diameter $0.0033\ \lambda$) situated a distance $R = 0.532\lambda$ from the axis of the cylinder. Eleven holes were tapped along a meridian on the cylindrical wall of the cylinder and plugged. The experiment was performed in a laboratory of about 35 x 20 x 8 metre^3 volume space.

During the measurements the electric probe replaced each plug in turn. By rotating the cylinder in 10° steps, a total of 11 sets of 36 samples of the normal component of the electric intensity were obtained. A vector voltmeter (Hewlett Packard 8405A) displayed the magnitude and phase of each sample relative to a constant reference signal. Averaging each set of samples by Simpson's quadrature rule gave the distribution of the zeroth harmonic of the electric intensity normal to the cylindrical wall.

The accuracy of the experimental results is influenced by the physical sizes of the electric probe and ground plane, the positioning of the electric probes, the rotation of the cylinder in 10° steps, the accuracy of the voltmeter readings, the averaging process over each set of 36 samples, and the reflections from the surroundings. Table IV.1 shows estimates of the errors due to these identified sources of experimental errors. The error due to the ground plane

(5.9x5.9λ square) has not been assessed, but it is expected to be small because of the averaging process over each set of samples. Fig. IV.5 shows the variation of the measured electric intensity on the thick monopole as it was rotated a full circle. Since the measured electric intensity varies smoothly with respect to $0 < \varphi < 2\pi$ (see Fig. IV.5), the error due to the averaging process has been estimated by applying the averaging process to a known function, which has the same "order" of variation as the electric intensity. For the sine function, $\sin(\frac{5\varphi}{2})$, $0 < \varphi < 2\pi$, the error has been found to be less than 0.5%. Lastly, the error due to the reflections from the surroundings has been obtained by repeating the measurements with the ground plane placed in various positions and orientations in the laboratory.

Table IV.1 shows that the dominant source of error comes from the reflections from the surroundings. Note that the errors are sufficiently small so that "small-error" analysis (Menzel, 1960, Sect. 2.12, 2.13, 2.14) can be used to obtain error bars for the measured, averaged, normal component of the electric intensity.

Table IV.1: Estimates of experimental errors.

Note: Percentage figures are computed with reference to the maximum magnitude of the sample signal.

Source of error	Error estimates for individual samples	
	Magnitude	Phase (electrical)
Physical size of electric probe	±1%	-
Physical size of ground plane	-	-
Position of probe along cylinder wall	±1%	±0.1°
Rotation of cylinder in 10° steps	±0.5%	±0.5°
Voltmeter readings	± 2%	±1.0°
Reflections from surroundings	±6%	±4.0°

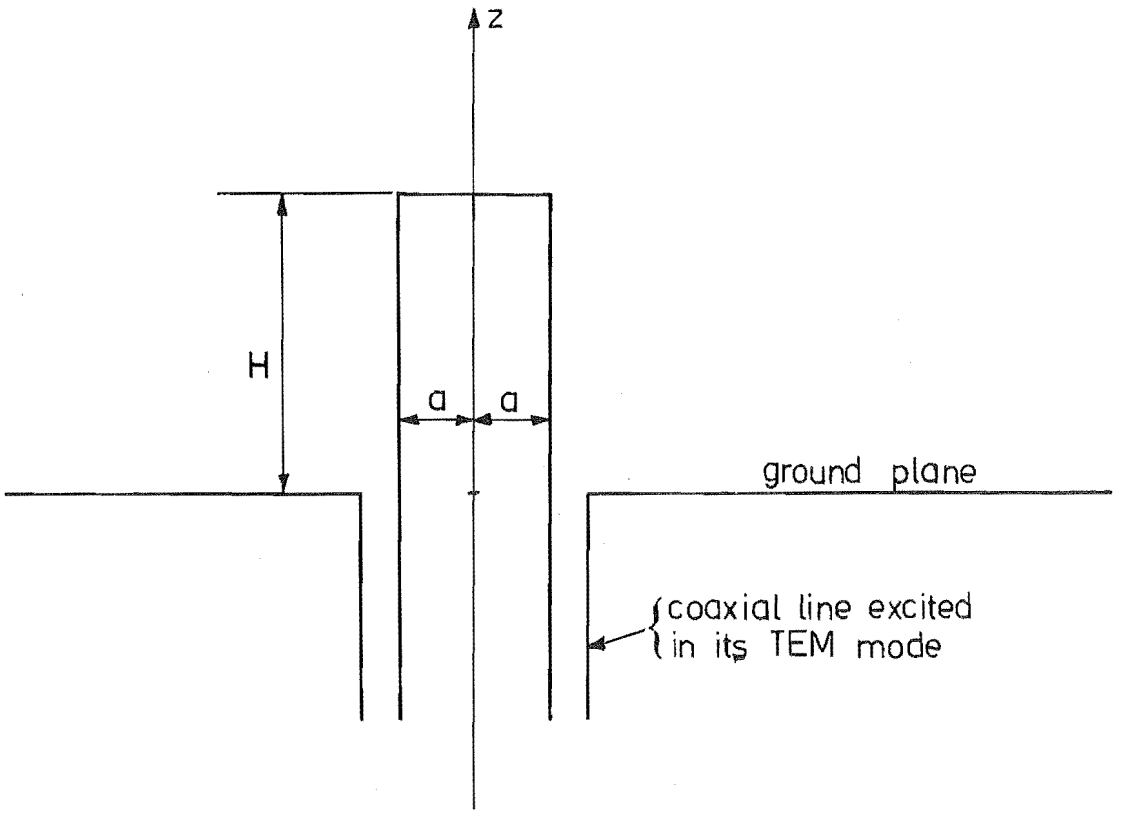

Fig. IV.1: Thick cylindrical monopole mounted on a ground plane and driven by a coaxial line, which is excited in its TEM mode.

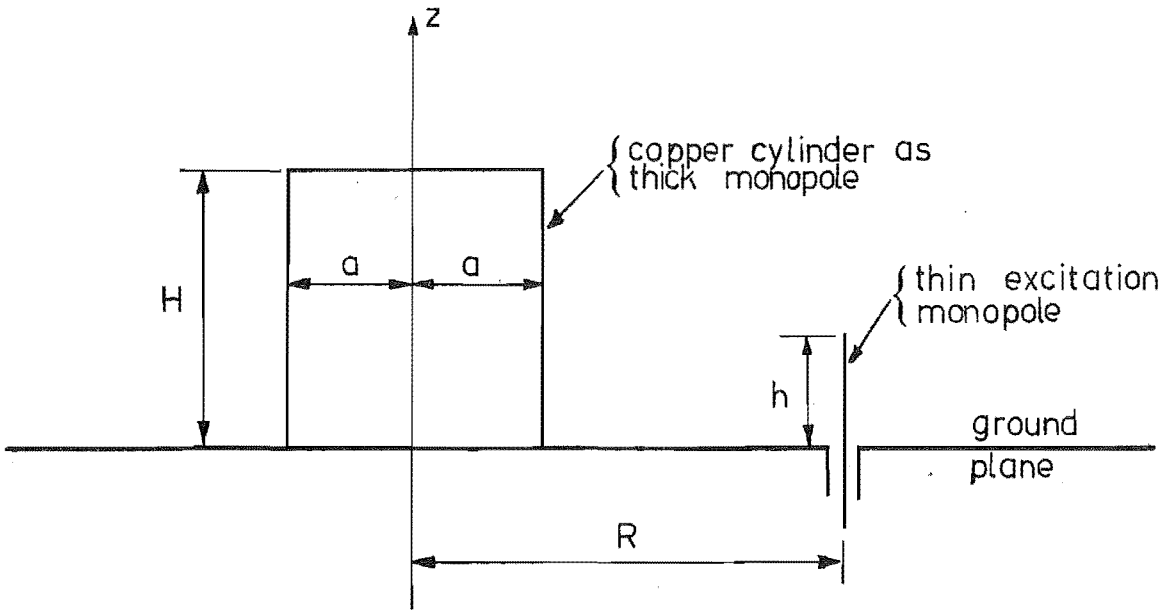

(a) Cross-sectional view

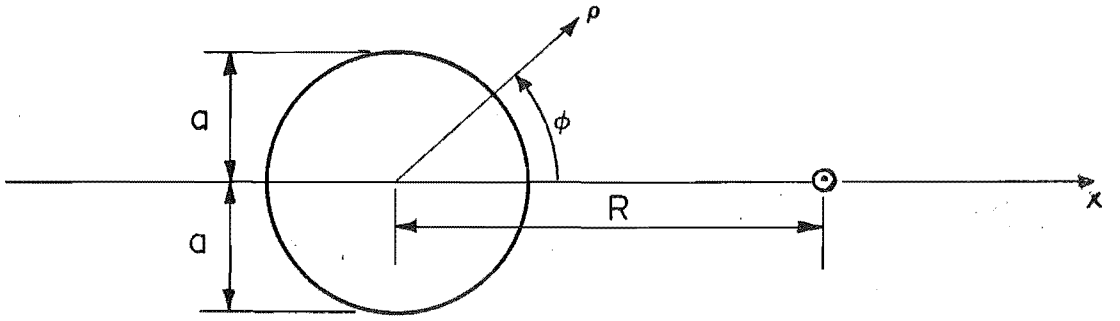

(b) Top view

Fig. IV.2: Thick copper cylinder illuminated by a nearby thin excitation monopole. Operating frequency is at 0.9732 GHz. (λ = 0.30805 metre)

2a = 0.1047 metre = 0.34λ
h = 0.04 metre = 0.13λ
H = 0.0865 metre = 0.28λ
R = 0.164 metre = 0.532λ

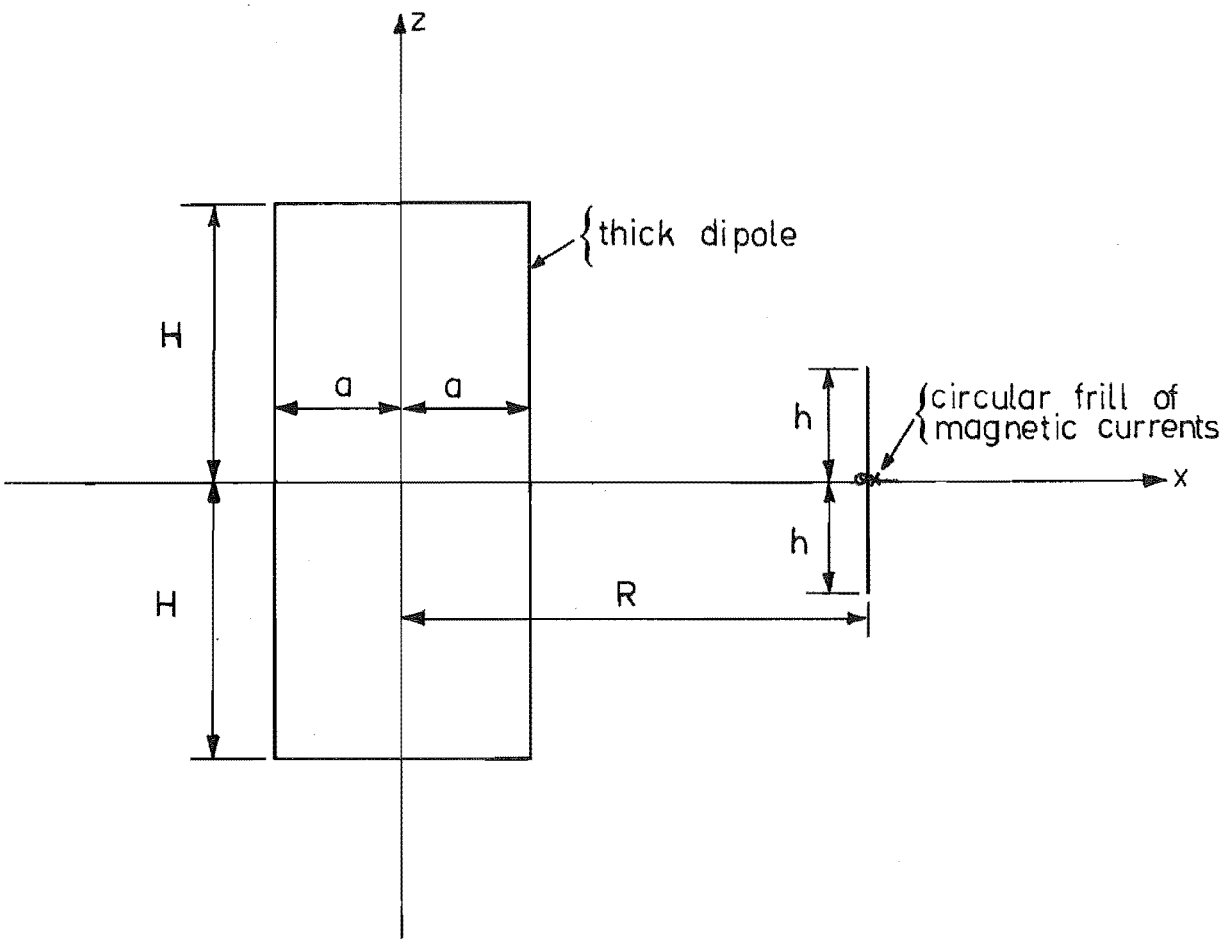

Fig. IV.3: Dipole antenna equivalent to that shown in Fig. IV.2.

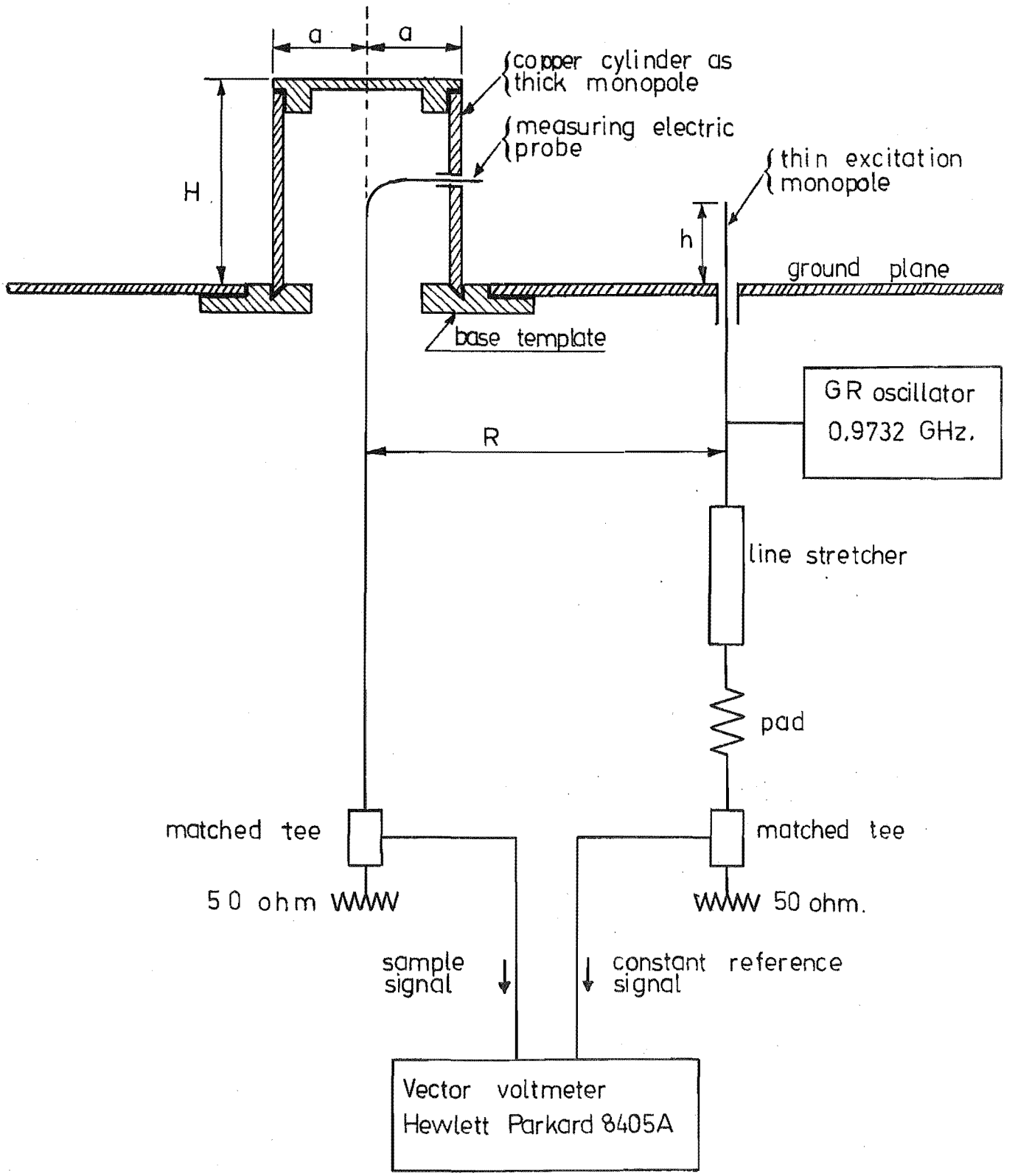

Fig. IV.4: Apparatus for measuring surface electric intensity on a thick monopole.

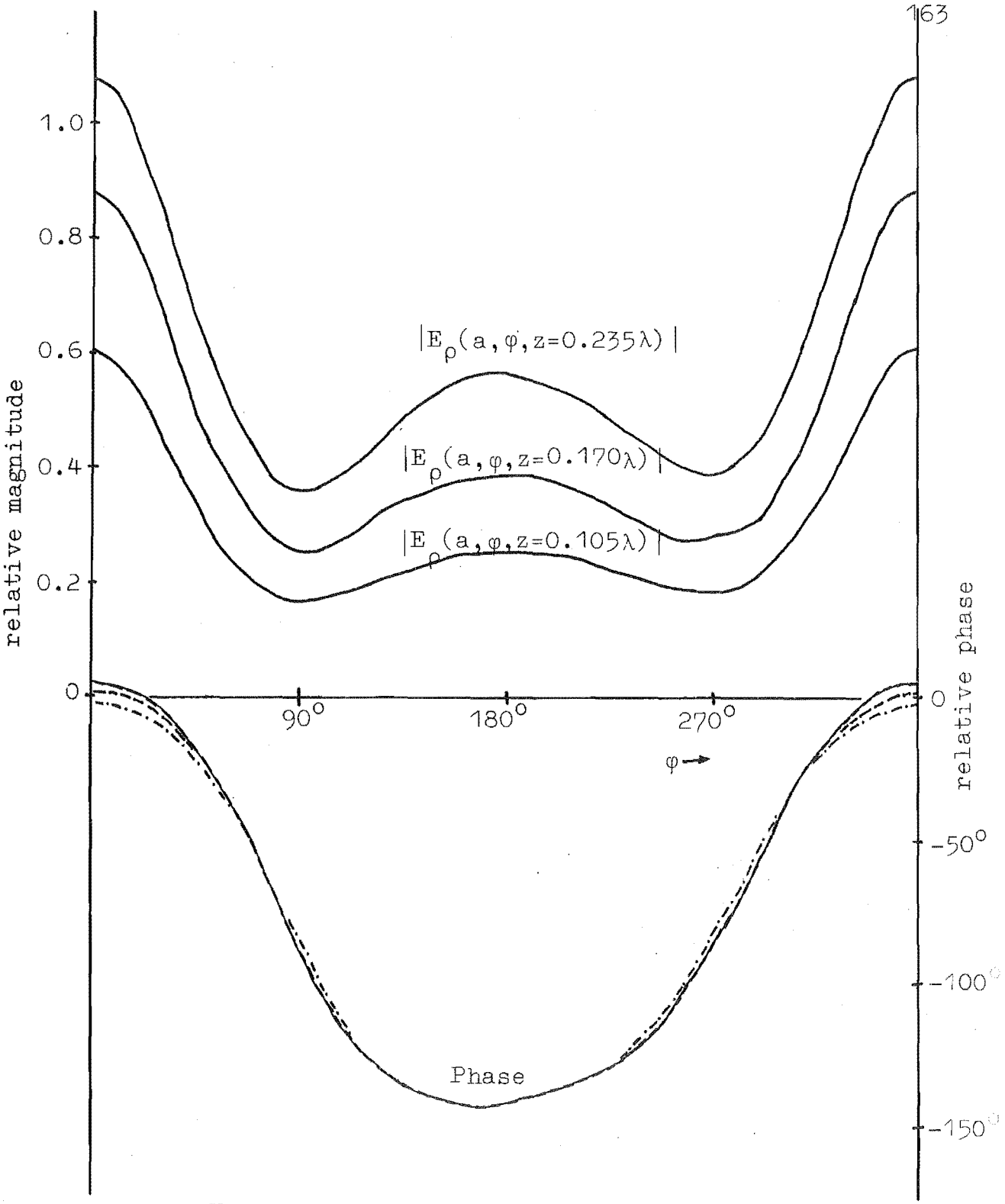

Fig. IV.5: Variation of the measured normal component of electric intensity $E_\rho(a,\varphi,z)$ on the thick monopole shown in Figs IV.2 and IV.4. Legend for the phase of $E_\rho(a,\varphi,z)$: ——— $z = 0.105\lambda$; ----- $z = 0.170\lambda$; and -·-·-·- $z = 0.235\lambda$.

Appendix V: The Field in the Parallel-Plate Region of an End-loaded Dipole Antenna

The analysis here follows closely Bach Andersen's (1971, Appendix 1, Sect. A1.1) derivation of the transformed equations for an infinite rod which is excited by a magnetic ring source. It has some similarity with Otto's (1967) treatment of a dipole antenna radiating into an infinite parallel-plate region.

V.1 The End-loaded Dipole Excited by a Magnetic Ring Source

Consider the perfectly conducting, axially symmetric end-loaded dipole shown in Fig. V.1. It is immersed in free space (permittivity ε_o and permeability μ_o) and is excited by a uniform ring of magnetic current of angular frequency ω,

$$\underline{J}^m = \hat{\varphi}\ \delta(\rho-b)\ \delta(z), \tag{V.1}$$

where ρ,φ,z are cylindrical polar coordinates. A time factor $\exp(j\omega t)$ is suppressed throughout. Let regions I and II refer to the coaxial annular regions,

$$\begin{aligned} &\text{Region I :} \quad a < \rho < b, \ |z| < W; \\ &\text{Region II:} \quad b < \rho < d, \ |z| < W; \end{aligned} \tag{V.2}$$

as shown in Fig. V.1.

Maxwell's equations take the following form for time-harmonic fields and magnetic current sources

$$\nabla \wedge \underline{E} = -j\omega\mu_o \underline{H} - \underline{J}^m, \tag{V.3}$$

$$\nabla \wedge \underline{H} = j\omega\varepsilon_o \underline{E}\ ; \tag{V.4}$$

where $\underline{J}^m$ is given by (V.1). Because of the circular symmetry of the antenna and the excitation source, the only non-zero field components are E_ρ, E_z and H_φ, and (V.3) and (V.4) reduce to

$$\frac{\partial E_\rho}{\partial z} - \frac{\partial E_z}{\partial \rho} = -j\omega\mu_o H_\varphi - \delta(\rho-b)\,\delta(z), \tag{V.5}$$

$$-\frac{\partial H_\varphi}{\partial z} = j\omega\varepsilon_o E_\rho, \tag{V.6}$$

$$\frac{1}{\rho}\frac{\partial}{\partial \rho}(\rho H_\varphi) = j\omega\varepsilon_o E_z. \tag{V.7}$$

The source term in (V.5) gives a discontinuous E_z across the common boundary of regions I and II at $\rho = b$. By integrating in ρ from $b-\Delta$ to $b+\Delta$, (V.5) becomes

$$\lim_{\Delta\to 0}\,[E_z(b+\Delta) - E_z(b-\Delta)] = \delta(z). \tag{V.8}$$

When E_z is found, (V.6) and (V.7) can be used to give E_ρ and H_φ.

In the source-free regions I and II, E_z satisfies the partial differential equation

$$(\nabla^2 + k_o^2)\,E_z = 0 \tag{V.9}$$

where $k_o = \omega(\mu_o\varepsilon_o)^{\frac{1}{2}}$. Because E_z has no φ-variation (V.9) reduces to

$$\frac{1}{\rho}\frac{\partial}{\partial \rho}\left(\rho\,\frac{\partial E_z}{\partial \rho}\right) + \frac{\partial^2 E_z}{\partial z^2} + k_o^2 E_z = 0. \tag{V.10}$$

Use of the standard separation of variables method and the even symmetry of E_z about the xy-plane, $z = 0$ lead to the general solution,

$$E_z = \sum_{m=0}^{\infty} E_m(\rho) \cos\left(\frac{m\pi z}{W}\right) ; \qquad (V.11)$$

$$E_m(\rho) = A_m[H_o^{(1)}(k_m\rho) + B_m H_o^{(2)}(k_m\rho)], \quad |k_m| > 0; \qquad (V.12)$$

$$= A_m[I_o(|k_m|\rho) + B_m K_o(|k_m|\rho)], \quad |k_m| < 0; \qquad (V.13)$$

where $k_m^2 = k_o^2 - (\frac{m\pi}{W})^2$; $H_o^{(1)}$ and $H_o^{(2)}$ are zeroth order Hankel functions; and I_o and K_o are modified Bessel functions of zeroth order. Note that (V.11) gives an E_ρ which automatically satisfies $E_\rho\ (\rho,\varphi,z = \pm W) = 0$.

The expressions of E_z in the regions I and II written in full and involving different arbitrary constants are

Region I:

$$E_z = \sum_{m=0}^{\ell} A_m[H_o^{(1)}(k_m\rho) + B_m H_o^{(2)}(k_m\rho)] \cos\frac{m\pi z}{W} + \sum_{m=\ell+1}^{\infty} A_m[I_o(|k_m|\rho) + B_m K_o(|k_m|\rho)] \cos\frac{m\pi z}{W} ; \qquad (V.14)$$

Region II:

$$E_z = \sum_{m=0}^{\ell} C_m[H_o^{(1)}(k_m\rho) + D_m H_o^{(2)}(k_m\rho)] \cos\frac{m\pi z}{W} + \sum_{m=\ell+1}^{\infty} C_m[I_o(|k_m|\rho) + D_m K_o(|k_m|\rho)] \cos\frac{m\pi z}{W}; \qquad (V.15)$$

where $\ell < \frac{k_o W}{\pi} < \ell+1$. There are four sets of unknown constants $\{A_m\}$, $\{B_m\}$, $\{C_m\}$, and $\{D_m\}$. The B_m can be determined from the boundary condition $E_z = 0$ on the surface of the central dipole, i.e. on $\rho = a$, $|z| < W$. This condition applied to (V.14) gives

$$B_m = -\frac{H_o^{(1)}(k_m a)}{H_o^{(2)}(k_m a)} , \quad m \leqslant \ell;$$

$$= -\frac{I_o(|k_m|a)}{K_o(|k_m|a)} , \quad m > \ell. \qquad (V.16)$$

Equation (V.8), which shows the E_z to be discontinuous at $\rho = b$, $|z| < W$, reduces the remaining sets $\{A_m\}$, $\{C_m\}$, and $\{D_m\}$ to one set, viz. $\{C_m\}$. First the source term in (V.8) is expanded in a Fourier cosine series appropriate to the parallel-plate region, i.e.

$$\delta(z) = \sum_{m=0}^{\infty} \frac{\varepsilon_m}{2W} \cos \frac{m\pi z}{W} \ . \qquad (V.17)$$

where $\varepsilon_m = 1$ when $m = 0$, and 2 when $m \neq 0$. Substitution of (V.17) into (V.8) leads to the relationships,

$$[C_m - A_m]H_o^{(1)}(k_m b) + [C_m D_m - A_m B_m]H_o^{(2)}(k_m b) = \frac{\varepsilon_m}{2W} , \qquad m \leqslant \ell ; \qquad (V.18)$$

$$[C_m - A_m]I_o(|k_m|b) + [C_m D_m - A_m B_m]K_o(|k_m|b) = \frac{1}{W} , \qquad m > \ell . \qquad (V.19)$$

By utilising the Wronskians,

$$H_o^{(1)}(x)\, H_1^{(2)}(x) - H_1^{(1)}(x)\, H_o^{(2)}(x) = \frac{j4}{\pi x} ;$$

$$I_o(x)\, K_1(x) + I_1(x)\, K_o(x) = \frac{1}{x} ,$$

(V,18) and (V.19) give

$$A_m = C_m + j\pi \frac{\varepsilon_m k_m b}{8W} H_1^{(2)}(k_m b),$$

$$C_m D_m = C_m B_m + j\pi \frac{\varepsilon_m k_m b}{8W} [H_1^{(1)}(k_m b) + B_m H_1^{(2)}(k_m b)], \qquad m \leqslant \ell ; \qquad (V.20)$$

$$A_m = C_m - \frac{|k_m|b}{W} K_1(|k_m|b),$$

$$C_m D_m = C_m B_m + \frac{|k_m|b}{W} I_1(|k_m|b) - B_m K_1(|k_m|b) , \qquad m > \ell . \qquad (V.21)$$

The final expressions for the field components, except E_ρ for which there is no interest, in regions I and II are

Region I:

$$E_z = \sum_{m=0}^{\ell} C_m[H_o^{(1)}(k_m\rho) + B_m H_o^{(2)}(k_m\rho)]\cos(\frac{m\pi z}{W})$$

$$+ \sum_{m=\ell+1}^{\infty} C_m[I_o(|k_m|\rho) + B_m K_o(|k_m|\rho)]\cos(\frac{m\pi z}{W})$$

$$+ \sum_{m=0}^{\ell} \frac{j\pi\varepsilon_m k_m b}{8W} H_1^{(2)}(k_m b)[H_o^{(1)}(k_m\rho) + B_m H_o^{(2)}(k_m\rho)]\cos(\frac{m\pi z}{W})$$

$$- \sum_{m=\ell+1}^{\infty} \frac{|k_m|b}{W} K_1(|k_m|b)[I_o(|k_m|\rho) + B_m K_o(|k_m|\rho)]\cos(\frac{m\pi z}{W}); \quad (V.22)$$

$$H_\varphi = j\omega\varepsilon_o \sum_{m=0}^{\ell} \frac{C_m}{k_m}[H_1^{(1)}(k_m\rho) + B_m H_1^{(2)}(k_m\rho)]\cos(\frac{m\pi z}{W})$$

$$+ j\omega\varepsilon_o \sum_{m=\ell+1}^{\infty} \frac{C_m}{|k_m|}[I_1(|k_m|\rho) - B_m K_1(|k_m|\rho)]\cos(\frac{m\pi z}{W})$$

$$- \frac{\omega\varepsilon_o\pi b}{8W} \sum_{m=0}^{\ell} \varepsilon_m H_1^{(2)}(k_m b)[H_1^{(1)}(k_m\rho) + B_m H_1^{(2)}(k_m\rho)]\cos(\frac{m\pi z}{W})$$

$$- \frac{j\omega\varepsilon_o b}{W} \sum_{m=\ell+1}^{\infty} K_1(|k_m|b)[I_1(|k_m|\rho) - B_m K_1(|k_m|\rho)]\cos(\frac{m\pi z}{W}); \quad (V.23)$$

Region II:

$$E_z = \sum_{m=0}^{\ell} C_m[H_o^{(1)}(k_m\rho) + B_m H_o^{(2)}(k_m\rho)]\cos(\frac{m\pi z}{W})$$

$$+ \sum_{m=\ell+1}^{\infty} C_m[I_o(|k_m|\rho) + B_m K_o(|k_m|\rho)]\cos(\frac{m\pi z}{W})$$

$$+ \frac{j\pi b}{8W} \sum_{m=0}^{\ell} \varepsilon_m k_m[H_1^{(1)}(k_m b) + B_m H_1^{(2)}(k_m b)]H_o^{(2)}(k_m\rho)\cos(\frac{m\pi z}{W})$$

$$+ \frac{b}{W} \sum_{m=\ell+1}^{\infty} |k_m|[I_1(|k_m|b) - B_m K_1(|k_m|b)]K_o(|k_m|\rho)\cos(\frac{m\pi z}{W}); \quad (V.24)$$

$$H_\varphi = j\omega\varepsilon_o \sum_{m=0}^{\ell} \frac{C_m}{k_m}[H_1^{(1)}(k_m\rho) + B_m H_1^{(2)}(k_m\rho)]\cos(\frac{m\pi z}{W})$$

$$+ j\omega\varepsilon_o \sum_{m=\ell+1}^{\infty} \frac{C_m}{|k_m|}[I_1(|k_m|\rho) - B_m K_1(|k_m|\rho)]\cos(\frac{m\pi z}{W})$$

$$- \frac{\omega\varepsilon_o \pi b}{8W} \sum_{m=0}^{\ell} \varepsilon_m[H_1^{(1)}(k_m b) + B_m H_1^{(2)}(k_m b)]H_1^{(2)}(k_m\rho)\cos(\frac{m\pi z}{W})$$

$$- \frac{j\omega\varepsilon_o b}{W} \sum_{m=\ell+1}^{\infty} [I_1(|k_m|b) - B_m K_1(|k_m|b)]K_1(|k_m|\rho)\cos(\frac{m\pi z}{W}); \qquad (V.25)$$

by utilising (V.7) to deduce H_φ from E_z. The B_m are given by (V.16). The third and fourth series in (V.24) and (V.25) represent the radially outgoing waves in the case where the end plates in Fig. V.1 are infinite, i.e. d tends to infinity.

V.2 The End-loaded Dipole excited by a Magnetic Frill Source

In this section the results from Section V.1 are used to derive expressions for the field in the parallel-plate region when the excitation source is a uniform circular frill of magnetic currents. With reference to Fig. V.2, the magnetic frill source is given by eqn (4.3) of chapter 4 as

$$\underline{J}^m = -\hat{\varphi}\,\frac{2\,V\,\delta(z)}{\rho\,\ell n(b_1/a)} \quad , \qquad a = b_o < \rho < b_1 \qquad (V.26)$$

By considering the frill as being made up of rings of magnetic current, the field components, E_z and H_φ, in the parallel-plate region are related to those in section V.1 by

$$E_z = \frac{-2V}{\ell n(b_1/a)} \left[\int_a^{\rho} \frac{E_z^{II,ring}}{b}\, db + \int_{\rho}^{b_1} \frac{E_z^{I,ring}}{b}\, db \right],$$

$$H_\varphi = \frac{-2V}{\ell n(b_1/a)} \left[\int_a^{\rho} \frac{H_\varphi^{II,ring}}{b}\, db + \int_{\rho}^{b_1} \frac{H_\varphi^{I,ring}}{b}\, db \right],$$

$$a < \rho < b_1; \qquad \text{(V.27)}$$

$$E_z = \frac{-2V}{\ell n(b_1/a)} \int_a^{b_1} \frac{E_z^{II,ring}}{b}\, db,$$

$$H_\varphi = \frac{-2V}{\ell n(b_1/a)} \int_a^{b_1} \frac{H_\varphi^{II,ring}}{b}\, db,$$

$$b_1 < \rho; \qquad \text{(V.28)}$$

where $E_z^{I,ring}$, $H_\varphi^{I,ring}$, $E_z^{II,ring}$ and $H_\varphi^{II,ring}$ are respectively given by (V.22) to (V.25). For convenience the following terms are defined,

$$U_o(k_m\rho) = H_o^{(1)}(k_m\rho) + B_m H_o^{(2)}(k_m\rho),$$

$$U_1(k_m\rho) = H_1^{(1)}(k_m\rho) + B_m H_1^{(2)}(k_m\rho),$$

$$m \leqslant \ell; \qquad \text{(V.29)}$$

$$V_o(k_m\rho) = I_o(|k_m|\rho) + B_m K_o(|k_m|\rho),$$

$$V_1(k_m\rho) = I_1(|k_m|\rho) - B_m K_1(|k_m|\rho),$$

$$m > \ell; \qquad \text{(V.30)}$$

$$F_m = V \int_a^{b_1} \frac{C_m}{b}\, db. \qquad \text{(V.31)}$$

The final form of equation (V.27) is, for $a = b_o < \rho < b_1$,

$$E_z = \frac{-2}{\ell n(b_1/a)} \left\{ \sum_{m=0}^{\ell} F_m U_o(k_m\rho)\cos\left(\frac{m\pi z}{W}\right) + \sum_{m=\ell+1}^{\infty} F_m V_o(k_m\rho)\cos\left(\frac{m\pi z}{W}\right) \right.$$

$$- \frac{j\pi V}{8W} \sum_{m=0}^{\ell} \varepsilon_m H_o^{(2)}(k_m b_1)\, U_o(k_m\rho)\, \cos\left(\frac{m\pi z}{W}\right)$$

$$\left. + \frac{V}{W} \sum_{m=\ell+1}^{\infty} K_o(|k_m|b_1)\, V_o(k_m\rho)\, \cos\left(\frac{m\pi z}{W}\right) \right\}; \qquad \text{(V.32)}$$

$$H_\varphi = \frac{-2j\omega\varepsilon_o}{\ell n(b_1/a)} \left\{ \sum_{m=0}^{\ell} \frac{F_m}{k_m} U_1(k_m\rho)\cos(\frac{m\pi z}{W}) + \sum_{m=\ell+1}^{\infty} \frac{F_m}{|k_m|} V_1(k_m\rho)\cos(\frac{m\pi z}{W}) \right.$$

$$- \frac{j\pi V}{8W} \sum_{m=0}^{\ell} \frac{\varepsilon_m}{k_m} \left[H_o^{(2)}(k_m b_1)\, U_1(k_m\rho) + \frac{j4}{\pi k_m \rho} \right] \cos(\frac{m\pi z}{W})$$

$$\left. + \frac{V}{W} \sum_{m=\ell+1}^{\infty} \frac{1}{|k_m|} [K_o(|k_m|b_1)\, V_1(k_m\rho) - \frac{1}{|k_m|\rho}] \cos(\frac{m\pi z}{W}) \right\} . \qquad (V.33)$$

For the region $\rho > b_1$, E_z and H_φ are given by, (from (V.28)),

$$E_z = \frac{-2}{\ell n(b_1/a)} \left\{ \sum_{m=0}^{\ell} F_m U_o(k_m\rho)\cos(\frac{m\pi z}{W}) + \sum_{m=\ell+1}^{\infty} F_m V_o(k_m\rho)\cos(\frac{m\pi z}{W}) \right.$$

$$- \frac{j\pi V}{8W} \sum_{m=0}^{\ell} \varepsilon_m U_o(k_m b_1) H_o^{(2)}(k_m\rho)\cos(\frac{m\pi z}{W})$$

$$\left. + \frac{V}{W} \sum_{m=\ell+1}^{\infty} V_o(k_m b_1)\, K_o(|k_m|\rho)\, \cos(\frac{m\pi z}{W}) \right\} ; \qquad (V.34)$$

$$H_\varphi = \frac{-2j\omega\varepsilon_o}{\ell n(b_1/a)} \left\{ \sum_{m=0}^{\ell} \frac{F_m}{k_m} U_1(k_m\rho)\cos(\frac{m\pi z}{W}) + \sum_{m=\ell+1}^{\infty} \frac{F_m}{|k_m|} V_1(k_m\rho)\cos(\frac{m\pi z}{W}) \right.$$

$$- \frac{j\pi V}{8W} \sum_{m=0}^{\ell} \frac{\varepsilon_m}{k_m} U_o(k_m b_1)\, H_1^{(2)}(k_m\rho)\, \cos(\frac{m\pi z}{W})$$

$$\left. - \frac{V}{W} \sum_{m=\ell+1}^{\infty} \frac{1}{|k_m|} V_o(k_m b_1)\, K_1(|k_m|\rho)\, \cos(\frac{m\pi z}{W}) \right\} . \qquad (V.35)$$

V.2.1 Surface current density

The surface current density $\underline{K}_s$ on the antenna surface which borders the parallel-plate region is obtained from (V.33) and (V.35) as

$$\underline{K}_s = \hat{z}\, H_\varphi(a,\varphi,z) \quad , \text{ on the central dipole surface;}$$

$$= \hat{\rho}\, H_\varphi(\rho,\varphi,\pm W) \quad , \text{ on the end plates.} \qquad (V.36)$$

V.2.2 Admittance

Otto (1967) showed that the admittance of a monopole antenna mounted on a ground plane and driven by a coaxial line is related to the integrals of the tangential fields in the coaxial aperture in the ground plane. A discussion of the use of Otto's (1967) admittance expression is given in sections 3.2 and 3.3.1 of chapter 3. The admittance expression is written for the present end-loaded dipole antenna as

$$Y = \frac{2\pi}{V\ \ell n(b_1/a)} \int_a^{b_1} H_\varphi(\rho,\varphi,0)\, d\rho. \qquad (V.37)$$

Substituting (V.33) into (V.37),

$$Y = -\frac{4j\pi\omega\varepsilon_o}{V\{\ell n(b_1/a)\}^2} \left\{ -\sum_{m=0}^{\ell} \frac{F_m}{k_m^2} U_o(k_m b_1) + \sum_{m=\ell+1}^{\infty} \frac{F_m}{|k_m|^2} V_o(k_m b_1) \right.$$

$$+ \frac{j\pi V}{8W} \sum_{m=0}^{\ell} \frac{\varepsilon_m}{k_m^2} [H_o^{(2)}(k_m b_1) U_o(k_m b_1) - \frac{j4}{\pi} \ell n(b_1/a)]$$

$$\left. + \frac{V}{W} \sum_{m=\ell+1}^{\infty} \frac{1}{|k_m|^2} [K_o(|k_m| b_1) V_o(k_m b_1) - \ell n(b_1/a)] \right\}. \qquad (V.38)$$

The third and last series in (V.38) are identical to those of Otto's (1967, eqn 39) used in computing the admittance for an infinite parallel-plate antenna.

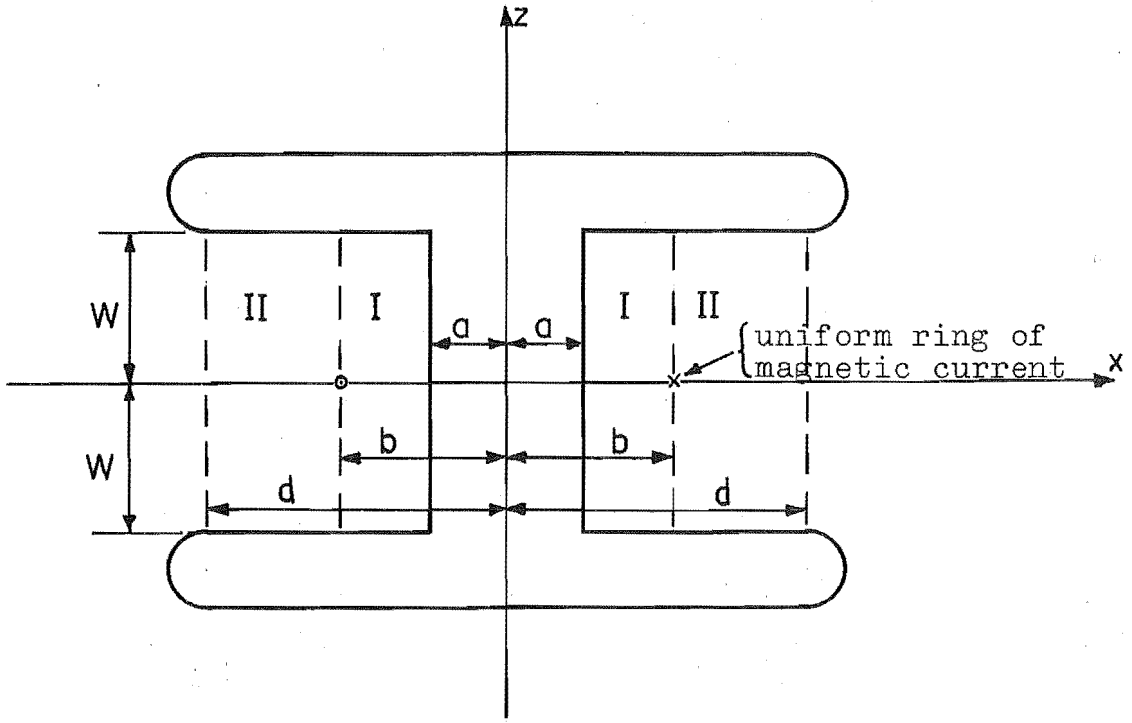

Fig. V.1: End-loaded dipole driven by a uniform ring of magnetic current.

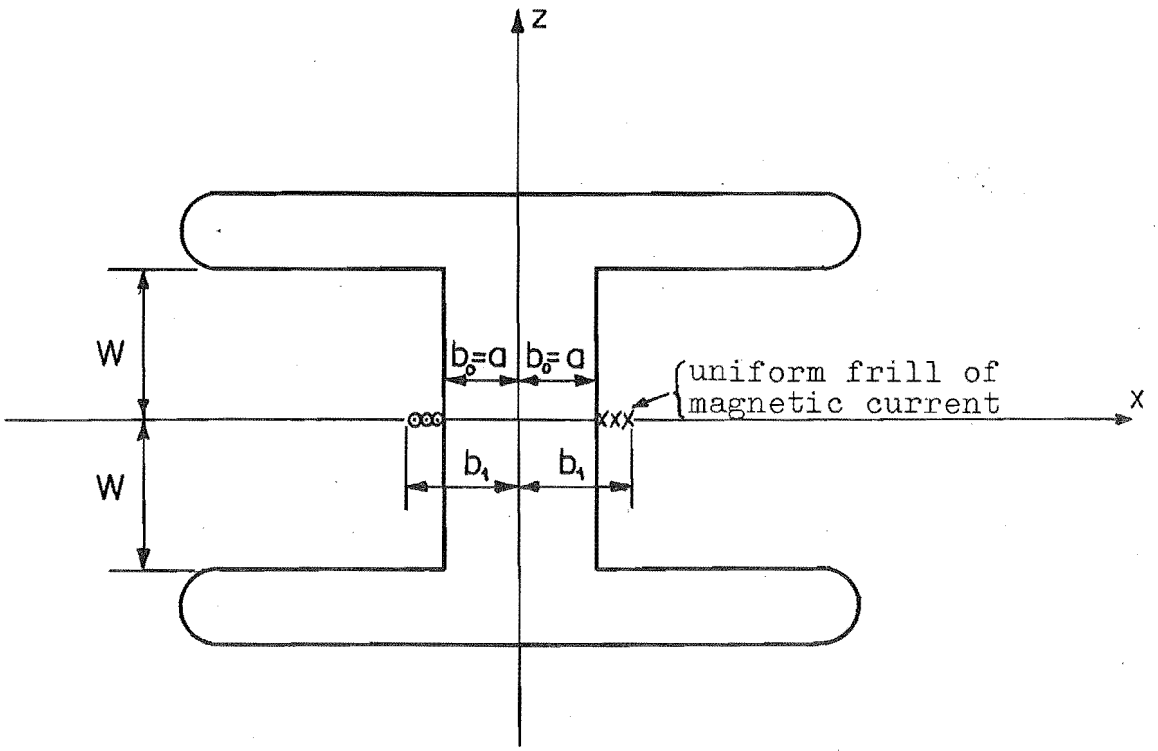

Fig. V.2: End-loaded dipole driven by a uniform frill of magnetic current.

Appendix VI: METHOD 1A

Another integral equation, which has a close correspondence to that of METHOD 1 in chapter 3 (see eqns 3.21 and 3.34), can be derived for the circular end-loaded dipole examined in chapter 4. By applying the extended boundary condition on the z-axis inside the dipole, equation (4.8) together with (4.9) and (4.10) becomes, after some manipulation,

$$\int_{\xi_z}^{L} Z(z,\xi)K(\xi)d\xi + \sum_{m=0}^{\infty} Q_m(z)F_m = B(z), \quad |z| < H; \text{ METHOD 1A;} \tag{VI.1}$$

$$Z(z,\xi) = \frac{\rho'(\xi)}{j\omega\varepsilon_o}\left\{\left[\sin\phi\left(\frac{\partial^2 G_o}{\partial z^2} + k_o^2 G_o\right) + \cos\phi\,\frac{\partial^2 G_o}{\partial z\,\partial\rho'}\right] + \left[\sin\phi\left(\frac{\partial^2 G_o}{\partial z^2} + k_o^2 G_o\right) + \cos\phi\,\frac{\partial^2 G_o}{\partial z\,\partial\rho'}\right]_{\xi=-\xi}\right\}_{\rho=0};$$

$$Q_m(z) = \frac{2d}{\ell n(b_1/a)}\left[\frac{jU_1(k_m d)}{\omega\varepsilon_o k_m} D_m(z) - U_o(k_m d)E_m(z)\right]; \quad m \leqslant \ell$$

$$= \frac{2d}{\ell n(b_1/a)}\left[\frac{jV_1(k_m d)}{\omega\varepsilon_o |k_m|} D_m(z) - V_o(k_m d)E_m(z)\right]; \quad m \geqslant \ell+1 \tag{VI.2}$$

$$B(z) = \frac{2}{\ell n(b_1/a)}\left\{\frac{1}{j\omega\varepsilon_o}\int_{-W}^{W} G^i(d,\varphi'=0,z')\left(\frac{\partial^2 G_o}{\partial z^2} + k_o^2 G_o\right)dz' - \int_{-W}^{W} F^i(d,\varphi'=0,z')\left.\frac{\partial G_o}{\partial\rho'}\right|_{\rho'=d} dz'\right\}_{\rho=0};$$

$$D_m(z) = \left\{\int_{-W}^{W}\cos\left(\frac{m\pi z'}{W}\right)\left(\frac{\partial^2 G_o}{\partial z^2} + k_o^2 G_o\right)dz'\right\}_{\rho=0};$$

$$E_m(z) = \left\{\int_{-W}^{W}\cos\left(\frac{m\pi z'}{W}\right)\left.\frac{\partial G_o}{\partial\rho'}\right|_{\rho'=d} dz'\right\}_{\rho=0};$$

where ξ_z is the distance of the point Q_z from Q_1 measured along curve C (see Fig. 4.4); ϕ is the angle which the surface

normal vector $\hat{\eta}$ makes with the z-axis.

Equation (VI.1) can be solved numerically by the method of moments described in section 4.4 for solving equation (4.13) of METHOD 2A. By point-matching (VI.1) at N discrete points on the z-axis in the dipole, (VI.1) becomes

$$\int_{\xi_z}^{L} Z_n(\xi)\, K(\xi)\, d\xi + \sum_{m=0}^{\infty} Q_{nm} F_m = B_n, \quad n = 1,2,3,\ldots,N; \qquad \text{METHOD 1A} \qquad \text{(VI.3)}$$

$$Z_n(\xi) = Z(z_n,\xi);$$

$$B_n = B(z_n) \; ; \qquad \text{(VI.4)}$$

$$Q_{nm} = Q_m(z_n) \; ;$$

where $Z(z,\xi)$, $B(z)$ and $Q_m(z)$ are given by (VI.2). Equation then has the same form as (4.17) in section 4.4 so that the moment method for solving (4.17) can be straightforwardly applied.

Appendix VII: Hollow Dipole in a Parallel-Plate Region

The analysis here parallels Einarsson's (1966) derivation of an integral equation for a hollow cylindrical dipole driven by a delta gap source.

Consider the hollow perfectly conducting dipole placed centrally in an infinite parallel plate region (width 2W) as shown in Fig. VII.1. Its radius and semi-height are a and H respectively. An applied electric field of angular frequency ω is maintained across a circumferential slot of infinitesimal width at the centre of the dipole, i.e.

$$E_z(\rho=a, |z| < H) = -\delta(z); \qquad \text{(VII.1)}$$

where (ρ,φ,z) are cylindrical polar coordinates. The medium in the parallel plate region is free space with permittivity ε_o, permeability μ_o, and wavenumber $k_o = \omega(\mu_o\varepsilon_o)^{\frac{1}{2}} = 2\pi/\lambda$. With reference to Fig. VII.1, region I refers to the cylindrical volume $\rho<a, |z| < W$, and region II is the space $\rho>a$, $|z| < W$.

Rotational symmetry requires that the only non-vanishing components of the electromagnetic field are H_φ, E_ρ and E_z and that these components have no φ-variation. In the source free regions I and II, E_z satisfies the scalar Helmholtz equation

$$(\nabla^2 + k_o^2)E_z = 0 \; ; \qquad \text{(VII.2)}$$

which reduces to

$$\frac{1}{\rho}\frac{\partial}{\partial\rho}\left(\rho\frac{\partial E_z}{\partial\rho}\right) + \frac{\partial^2 E_z}{\partial\rho^2} + k_o^2 E_z = 0, \qquad \text{(VII.3)}$$

because E_z has no φ-variation. Use of the standard separation of variables method and the even symmetry of E_z about the xy-plane (z=0) leads to the following general solution to eqn (VII.3),

$$E_z = \sum_{m=0}^{\infty} E_m(\rho) \cos\left(\frac{m\pi z}{W}\right), \quad |z| < W; \tag{VII.4}$$

$$E_m(\rho) = A_m H_o^{(1)}(k_m\rho) + B_m H_o^{(2)}(k_m\rho), \quad |k_m| > 0; \tag{VII.5}$$

$$= A_m I_o(|k_m|\rho) + B_m K_o(|k_m|\rho), \quad |k_m| < 0; \tag{VII.6}$$

where $k_m^2 = k_o^2 - (\frac{m\pi}{W})^2$; $H_o^{(1)}$ and $H_o^{(2)}$ are zeroth order Hankel functions; and I_o and K_o are zeroth order modified Bessel functions of the first and second kind respectively.

In region I the field is finite so that $B_m = A_m$ in (VII.5) and $B_m = 0$ in (VII.6). Therefore

$$E_z^I(\rho,z) = \sum_{m=0}^{\ell} A_m J_o(k_m\rho)\cos\left(\frac{m\pi z}{W}\right) + \sum_{m=\ell+1}^{\infty} A_m I_o(|k_m|\rho)\cos\left(\frac{m\pi z}{W}\right); \tag{VII.7}$$

where $\ell < \frac{k_o W}{\pi} < \ell+1$, J_o is a zeroth order Bessel function, and the superscript I denotes region I. It is convenient to write (VII.7) as

$$E_z^I(\rho,z) = \sum_{m=0}^{\ell} C_m(a) \frac{J_o(k_m\rho)}{J_o(k_m a)} \cos\left(\frac{m\pi z}{W}\right) + \sum_{m=\ell+1}^{\infty} C_m(a) \frac{I_o(|k_m|\rho)}{I_o(|k_m|a)} \cos\left(\frac{m\pi z}{W}\right); \tag{VII.8}$$

$$C_m(a) = A_m J_o(k_m a), \quad m \leqslant \ell;$$
$$= A_m I_o(|k_m|a), \quad m > \ell. \tag{VII.9}$$

An examination of equation (VII.7) or (VII.8) shows that $C_m(a)$ is the m^{th} expansion coefficient of $E_z^I(a,z)$ in a Fourier cosine series, i.e.

$$E_z^I(a,z) = \sum_{m=0}^{\infty} C_m(a) \cos\left(\frac{m\pi z}{W}\right) , \qquad |z| < W \quad ; \qquad \text{(VII.10)}$$

$$C_m(a) = \frac{\varepsilon_m}{2W} \int_{-W}^{W} E_z^I(a,z) \cos\left(\frac{m\pi z}{W}\right) dz \quad ; \qquad \text{(VII.11)}$$

where ε_m is the Neumann factor. The magnetic intensity is obtained from (VII.7) and Maxwell's equations, such that

$$H_\varphi^I(\rho,z) = j\omega\varepsilon_o \left\{ \sum_{m=0}^{\ell} \frac{C_m(a)}{k_m} \frac{J_1(k_m a)}{J_o(k_m a)} \cos\left(\frac{m\pi z}{W}\right) + \sum_{m=\ell+1}^{\infty} \frac{C_m(a)}{|k_m|} \frac{I_1(|k_m|\rho)}{I_o(|k_m|a)} \cos\left(\frac{m\pi z}{W}\right) \right\} . \qquad \text{(VII.12)}$$

In region II, the field has to satisfy the radiation condition at infinity so that $A_m = 0$ in both (VII.5) and (VII.6). Following the procedure from equations (VII.7) to (VII.12), the expressions for the field in region II are

$$E_z^{II}(\rho,z) = \sum_{m=0}^{\ell} C_m(a) \frac{H_o^{(2)}(k_m\rho)}{H_o^{(2)}(k_m a)} \cos\left(\frac{m\pi z}{W}\right) + \sum_{m=\ell+1}^{\infty} C_m(a) \frac{K_o(|k_m|\rho)}{K_o(|k_m|a)} \cos\left(\frac{m\pi z}{W}\right) \quad ; \qquad \text{(VII.13)}$$

$$H_\varphi^{II}(\rho,z) = j\omega\varepsilon_o \left\{ \sum_{m=0}^{\ell} \frac{C_m(a)}{k_m} \frac{H_1^{(2)}(k_m\rho)}{H_o^{(2)}(k_m a)} \cos\left(\frac{m\pi z}{W}\right) - \sum_{m=\ell+1}^{\infty} \frac{C_m(a)}{|k_m|} \frac{K_1(|k_m|\rho)}{K_o(|k_m|a)} \cos\left(\frac{m\pi z}{W}\right) \right\} \quad ; \qquad \text{(VII.14)}$$

where the continuity of E_z across the cylindrical surface $\rho=a$, $|z| < W$, i.e. $E_z^I(a-0,z) = E_z^{II}(z+0,z)$ has been used.

The total current $I(z)$ on the hollow dipole is given by

$$I(z) = 2\pi a \left[H_{\varphi}^{II}(a+0,z) - H_{\varphi}^{I}(a-0,z)\right] , \quad |z| < H \qquad \text{(VII.15)}$$

where $H_{\varphi}^{II}(a+0,z)$ and $H_{\varphi}^{I}(a-0,z)$ are obtained from (VII.14) and (VII.12) respectively. Across the cylindrical surface $\rho = a$, $H < |z| < W$, the magnetic intensity is continuous, i.e.

$$H_{\varphi}^{I}(a-0,z) = H_{\varphi}^{II}(a+0,z), \quad H < |z| < W. \qquad \text{(VII.16)}$$

Substituting (VII.12) and (VII.14) into (VII.16) for H_{φ}^{I} and H_{φ}^{II}, respectively, gives

$$\sum_{m=0}^{\ell} \frac{j2C_m(a)}{\pi a k_m^2} \frac{\cos(\frac{m\pi z}{W})}{H_o^{(2)}(k_m a)J_o(k_m a)}$$

$$- \sum_{m=\ell+1}^{\infty} \frac{C_m(a)}{a|k_m|^2} \frac{\cos(\frac{m\pi z}{W})}{I_o(|k_m|a)K_o(|k_m|a)} = 0, \quad H < |z| < W. \qquad \text{(VII.17)}$$

Since $E_z(a,z) = -\delta(z)$ when $|z| < H$ and is unknown when $H < |z| < W$, the coefficients $C_m(a)$ can be obtained from equation (VII.11) as

$$C_m(a) = \frac{\varepsilon_m}{2W} \left\{ -1 + 2 \int_H^W E_z(a,z) \cos(\frac{m\pi z}{W}) \, dz \right\} . \qquad \text{(VII.18)}$$

Equation (VII.17) then becomes

$$\int_H^W E_z(a,\zeta) \cdot \left\{ \sum_{m=0}^{\ell} \frac{j2\varepsilon_m}{\pi a k_m^2} \frac{\cos(\frac{m\pi z}{W})\cos(\frac{m\pi \zeta}{W})}{H_o^{(2)}(k_m a)J_o(k_m a)} \right.$$

$$\left. - \sum_{m=\ell+1}^{\infty} \frac{\varepsilon_m \cos(\frac{m\pi z}{W})\cos(\frac{m\pi \zeta}{W})}{a|k_m|^2 I_o(|k_m|a)K_o(|k_m|a)} \right\} d\zeta$$

$$= \sum_{m=0}^{\ell} \frac{j\varepsilon_m \cos(\frac{m\pi z}{W})}{\pi a k_m^2 H_o^{(2)}(k_m a)J_o(k_m a)} - \sum_{m=\ell+1}^{\infty} \frac{\varepsilon_m \cos(\frac{m\pi z}{W})}{a|k_m|^2 J_o(|k_m|a)K_o(|k_m|a)}$$

$$H < |z| < W \qquad \text{(VII.19)}$$

which is an integral equation for $E_z(a,z)$, $H < |z| < W$. An undesirable feature of this integral equation is the slowly converging series on both sides of the equation (see VII.19), i.e. the terms decrease as m^{-2}. A suggested series of basis functions for expanding $E_z(a,z)$ is

$$E_z(a,z) = \sum_{n=0}^{N} A_n \left(\frac{[z-H]}{[W-H]}\right)^{n-\frac{1}{2}} ; \qquad \text{(VII.20)}$$

where the A_n are unknown expansion coefficients and N is a finite positive integer. Expansion (VII.20) satisfies the electromagnetic edge conditions at the dipole ends (Jones, 1964, Sect. 9.2) at $z = \pm H \pm 0$. After substituting (VII.20) in (VII.19), for $E_z(a,\zeta)$, the integral in (VII.19) can be carried out in terms of Fresnel integrals (Abramowitz and Stegun, 1965, Sect. 7.3).

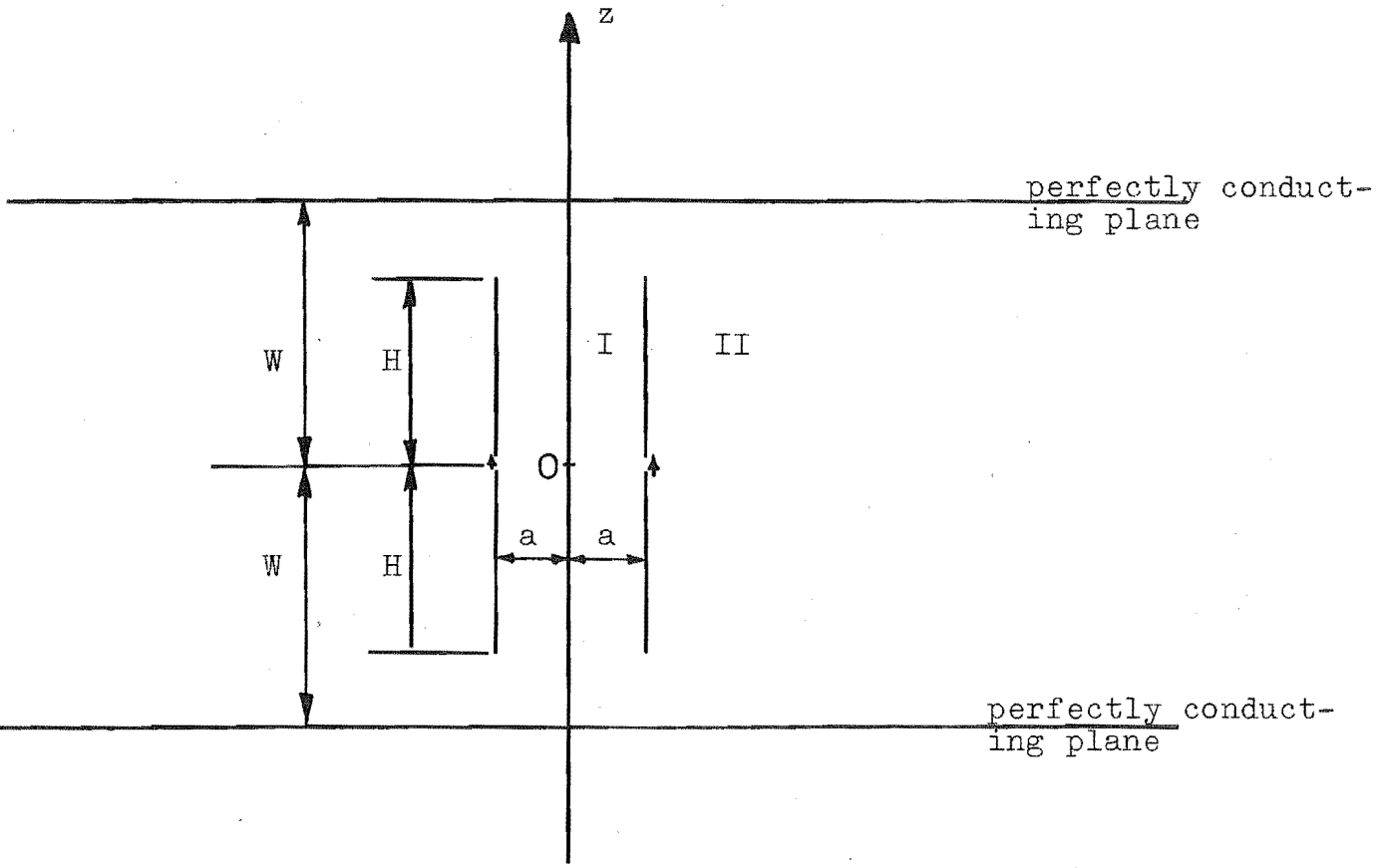

Fig. VII.1: Hollow cylindrical dipole fed by a delta gap source and situated centrally between two perfectly conducting infinite parallel plates.

a = dipole radius

H = dipole semi-height

2W = separation between the plates.

REFERENCES

Abeyaskere, W.D.M. (1972), "An introduction to the algorithmic Albert-Synge antenna equation", Proc. IREE, 33, 90-97.

Abramowitz, M. and Stegun, I.A. (1965), Handbook of Mathematical Functions, Dover, New York.

Albert, G.E. and Synge, J.L. (1948), "The general problem of antenna radiation and the fundamental integral equation, with application to an antenna of revolution - Part I", Q. App. Math., 6, 117-131.

Anderson, C.L. (1971), "Equivalent circuit of feed for electrically thick monopoles", Final year B.E.(Hons) project, Electrical Engineering Dept, University of Canterbury, New Zealand.

Andreasen, M.G. (1965), "Scattering from bodies of revolution", IEEE Trans. AP-13, 303-310.

Andrews, C.L. (1968), "Surface measurements of disk antennas", IEEE Trans., AP-18, 600-601.

Avetisyan, A.A. (1970), "A generalized method of separation of variables and diffraction of electromagnetic waves at bodies of revolution", Radiotekn i Electron (USSR) 15, 3-? [Radio Eng. Electron. (USSR) 15, 1-9].

Bach Andersen, J. (1968), "Admittance of infinite and finite cylindrical metallic antenna", Radio Science 3 (New Series), 607-621.

Bach Andersen, J. (1971), Metallic and Dielectric Antennas, Polyteknisk Forlag.

Bach Andersen, J. and Yee, H.Y. (1969), "Ray-optical techniques applied to antenna admittance theory", IEEE Trans., AP-17, 368-369.

Bakhrakh, L.D., Pistol'kors, A.A. and Fel'd, Y.N. (1967), "Developments in antenna technology", Radio Eng. & Elec. Phys. 12, 1787-1813.

Bates, R.H.T. (1968), "Modal expansions for electromagnetic scattering from perfectly conducting cylinders of arbitrary cross-section", Proc. IEE (London), 115, 1443-1445.

Bates, R.H.T. (1969), "The theory of the point-matching method for perfectly conducting waveguides and transmission lines", IEEE Trans., MTT-17, 294-301.

Barzilai, G. (1949), "Experimental determination of the distribution of current and charge along cylindrical antennas", Proc. IRE 37, 825-829.

Chang, D.C. (1967), "On the electrically thick cylindrical antenna", Radio Science 2 (New Series), 1043-1060.

Chang, D.C. (1968a), "On the electrically thick monopole Part I - theoretical solution", IEEE Trans., AP-16, 58-64.

Chang, D.C. (1968b), "On the electrically thick monopole Part II - experimental study", IEEE Trans., AP-16, 64-71.

Chang, D.C. and Wu, T.T. (1968), "A note on the theory of end-corrections for thick monopoles", Radio Science 3, (New Series), 639-641.

Chen, Y.M. and Keller, J.B. (1962), "Current on and input impedance of a cylindrical antenna", J. Res. NBS 66D, 15-21.

Collin, R.E. (1969), "Radiation from apertures", in Collin, R.E. and Zucker, F.J. (editors), Antenna Theory: Part I, McGraw Hill, New York, 61-92.

Conte, S.D. (1965), Elementary Numerical Analysis, McGraw-Hill, New York.

Copley, L.G. (1967), "Integral equation method for radiation from vibrating bodies", J. Acoust. Soc. Am. 41, 807-816.

Duncan, R.H. and Hinchey, F.A. (1960), "Cylindrical antenna theory", J. Res. NBS 64D, 569-584.

Einarsson, O. (1963), "The current distribution on cylindrical antennas of arbitrary length", Trans. Roy. Inst. Technol., no.216.

Einarsson, O. (1966), "A comparison between tube-shaped and solid cylinder antennas", IEEE Trans., AP-14, 31-37.

Faddeeva, V.N. (1959), Computational Methods of Linear Algebra, Dover, New York.

Fenlon, F.H. (1969), "Calculation of the acoustic radiation field at the surface of a finite cylinder by the method of weighted residuals", Proc. IEEE, 57, 291-306.

Galejs, J. (1964), "Capacitor type biconical antenna", Radio Science, J. Res. NBS 68D, 165-172.

Garbacz, R.J. and Turpin, R.H. (1971), "A generalised expansion for radiated and scattered fields", IEEE Trans., AP-19, 348-358.

Garbacz, R.J. (1965), "Modal expansions for resonance scattering phenomena", Proc. IEEE, 53, 856-864.

Gardner, F. (1969), "Reflection of circularly polarized waves from imperfect spheres", Proc. IEEE, 57, 844-846.

Gavorun, N.N. (1959), Dokl. Akad. Nauk, SSSR, 126, 49-52.

Gavorun, N.N. (1962), "The numerical solution of an integral equation of the first kind for the current density in an antenna body of revolution", [Translated from Zh. vych. mat., 1, 664-679, 1961].

Gulab, A. (1971), "Current distribution on electrically thick monopoles", Final year B.E.(Hons) project, Electrical Engineering Dept, University of Canterbury, New Zealand.

Hallen, E. (1938), "Theoretical investigation into the transmitting and receiving qualities of antennae", Nova Acta Regiae Soc. Sci. Upsaliensis (4) 11, 1-44.

Hallen, E. (1953), Elektricitetslära, Stockholm.

Hallen, E. (1956), "Exact treatment of antenna current wave reflection at the end of a tube-shaped cylindrical antenna", IRE Trans., AP-4, 479-491.

Hallen, E. (1961), "Exact solution of the antenna equation", Trans. Roy. Inst. Techn. No. 183.

Hallen, E. (1962), Electromagnetic Theory, Chapman and Hall, London.

Hansen, J. and Larsen, T. (1962), "The electric field at the ground plane near a disk-loaded monopole", J. Res. Radio Prop. 66D, 205-210.

Harrington, R.F. (1961), Time-Harmonic Electromagnetic Fields, McGraw Hill, New York.

Harrington, R.F. (1968), Field Computation by Moment Methods, Macmillan, New York.

Harrington, R.F. and Mautz, J.R. (1971a), "Theory of characteristic modes for conducting bodies", IEEE Trans., AP-19, 622-628.

Harrington, R.F. and Mautz, J.R. (1971b), "Computation of characteristic modes for conducting bodies", IEEE Trans., AP-19, 629-639.

Harrington, R.F., Mautz, J.R. and Chang, Y. (1972), "Characteristic modes for dielectric and magnetic bodies", IEEE Trans., AP-20, 194-198.

Holly, S. (1968), "Experimental study of electrically thick monopole antennas", Ph.D. dissertation, Harvard University, Cambridge, Mass.

Hönl, H., Maue, A.W. and Westpfahl, K. (1961), Theory of Diffraction, Handbuch der Physik, Vol. 25/1, Springer-Verlag (Berlin).

Hunter, J.D. (1972), "The surface current density on perfectly conducting polygonal cylinders", Can. J. Phys., 50, 139-150.

Hunter, J.D. and Bates, R.H.T. (1970), "Computation of scattering from a class of bodies of unrestricted size", J. Engrg. Math., 4, 119-128.

Hunter, J.D. and Bates, R.H.T. (1972), "Secondary diffraction from close edges on perfectly conducting bodies", Int. J. Electronics, 32, 321-333.

Hurd, R.A. (1964), "Variational solution for the admittance of a long cyoindrical antenna", Radio Science, J. Res. NBS 66D, 311-315.

Hurd, R.A. (1966), "Admittance of a long linear antenna", Can. J. Phys., 44, 1723-1744.

Hurd, R.A. (1969), "The antenna admittance problem", The Technical University of Denmark, Laboratory of Electromagnetic Theory.

*Hizal, A. and Marincic, A. (1970), "New rigorous formulation of electromagnetic scattering from perfectly conducting bodies of arbitrary shape", Proc. IEE, 117, 1639-1647.

Jacobsen, J. and Hurd, R.A. (1970), "Admittance of a thick antenna", Can. J. Phys., 48, 2201-2209.

Jamieson, A.R. (1971), "Aperture antennas", Ph.D. thesis, University of Canterbury.

Jamieson, A.R. and Bates, R.H.T. (1971), "Near field method for inferring aperture antenna radiation patterns", paper deposited in IEE library.

Jamieson, A.R. and Bates, R.H.T. (1972), "Experimental determination of higher-order modes in a circular aperture antenna", Proc. IEE, to appear.

Jasik, H. (1961), Antenna Engineering Handbook, McGraw-Hill, New York.

Jones, D.S. (1964), The Theory of Electromagnetism, Pergamon Press, London.

Kalafus, R.M. (1971), "Broad-band dipole design using the method of moments", IEEE Trans., AP-19, 771-773.

Kao, C.C. (1970a), "Electromagnetic scattering from a finite tubular cylinder: Numerical solutions", Radio Science 3, 617-623.

Kao, C.C. (1970b), "Measurements of surface currents on a finite circular tube illuminated by electromagnetic wave", IEEE Trans., AP-18, 569-573.

Kao, C.C. (1971), "First order admittance of coaxially driven infinite monopole", IEEE Trans., AP-19, 782-784.

King, R. (1955), "The end correction for a coaxial line when driving an antenna over a ground screen", IRE Trans., Ant. and Prop. AP-3, 66-72.

King, R.W.P. (1956), The Theory of Linear Antennas, Harvard University Press, Cambridge, Massachusetts.

King, R.W.P. (1967), "The linear antenna - eighty years of progress", Proc. IEEE, 55, 2-16.

King, R.W.P. and Wu, T.T. (1967), "The thick tubular transmitting antenna", Radio Science 2 (New Series), 1061-1065.

Kreyszig, E. (1962), Advanced Engineering Mathematics, Wiley, New York.

Kummich, R. (1958), "Der Fusspunktswiderstand zylindrischer am Fusspunkt konisch zugespitzter Antennen", Zeitschrift Für Schwingungs Und Schwachstromtechnik, 12, 369-379.

Lee, S.W. and Mittra, R. (1969), "Admittance of a solid cylindrical antenna", Can. J. Phys., 47, 1959-1970.

Lewin, L. (1959), "A contribution to the theory of cylindrical antennas - radiation between parallel plates", IRE Trans. AP-7, 162-168.

Love, A.E.H. (1901), "The integration of the equations of propagation of electric waves", Phil. Trans. Roy. Soc. London, Ser. A, 197, 1-45.

Mautz, J.R. and Harrington, R.F. (1969), "Radiation and scattering from bodies of revolution", Appl. Sci. Res., 20, 405-435.

Mei, K. and M$_o$berg, M. (1965), "Measurement of surface current distributions on cylindrical obstacles", Proc. IEEE 53, 1104-1105.

Mentzer, J.R. (1955), Scattering and Diffraction of Radio Waves, Pergamon Press, London.

Menzel, D.H. (1960), Fundamental Formulas of Physics, Dover, New York.

Montgomery, C.G. (1947), Technique of Microwave Measurements, McGraw Hill, New York.

Morita, T. (1950), "Current distributions on transmitting and receiving antennas", Proc. IRE 38, 898-904.

Morse, P.M. and Feshbach, H. (1953), Methods of Theoretical Physics, Part 1, McGraw Hill, New York.

Morse, P.M. and Feshbach, H. (1953), Methods of Theoretical Physics, Part 2, McGraw Hill, New York.

Ng, F.L. and Bates, R.H.T. (1972), "Null field method for waveguides of arbitrary cross section", IEEE Trans., Microwave Theory Tech., in press.

Noble, B. (1958), Methods Based on the Wiener-Hopf Technique for the Solution of Partial Differential Equations, Pergamon Press, London.

Otto, D.V. (1965), "The theory of cylindrical antennas", Antenna Theory Report, University of Auckland, Radio Research Centre, Auckland, New Zealand.

Otto, D.V. (1967), "The admittance of cylindrical antennas driven from a coaxial line", Radio Science, 2 (New Series), 1031-1042.

Otto, D.V. (1968a), "A note on the mathematical representation of the source for tubular transmitting antennas", Radio Science 3 (New Series), 862-864.

Otto, D.V. (1968b), "Fourier transform method in cylindrical antenna theory", Radio Science 3 (New Series), 1050-1057.

Otto, D.V. (1969), "The admittance of infinite cylindrical antennas," IEEE Trans., AP-17, 234-235.

Otto, D.V. (1970), "A precision technique for measuring surface currents at U.H.F. and microwave frequencies", Nelcon 1970 Conference, N.Z.

Papadopoulos, V.M. (1969), "Wave propagation in a coaxial line system", Quart. App. Math. 17, 423-436.

Plonsey, R. (1962), "Surface current measurements with an electric probe", IRE Trans. MTT-10, 214-217.

Prasad, S. and Rama Rau, Y.N. (1964), "Experimental investigation of thick, cylindrical antenna", New Mexico State University, University Park, N.M., Tech. Rept. 22.

Rama Rao, B. (1965), "Current distribution and impedance of an antenna in a parallel-plate region", Proc. IEE, 112, 259-268.

Ramo, S., Whinnery, J.R. and Van Duzer, T. (1965), Fields and Waves in Communication Electronics, John Wiley and Sons, New York.

Richmond, J.H. (1965), "Digital computer solutions of the rigorous equations for scattering problems", Proc. IEEE 53, 796-804.

Ross, G.R. and Fenster, P. (1968), "Members of the class of TEM-mode wire antennas with a TLIR", IEEE Intl. PGAP Symposium, Boston, Massachusetts.

Schelkunoff, S.A. (1952), Advanced Antenna Theory, John Wiley & Sons, London.

Schenck, H.A. (1967), "Improved integral formulation for acoustic radiation problems", J. Acoust. Soc. Am., 44, 41-58.

Otto, D.V. (1970), "A precision technique for measuring surface currents at U.H.F. and microwave frequencies", Nelcon 1970 Conference, N.Z.

Papadopoulos, V.M. (1969), "Wave propagation in a coaxial line system", Quart. App. Math. 17, 423-436.

Plonsey, R. (1962), "Surface current measurements with an electric probe", IRE Trans. MTT-10, 214-217.

Prasad, S. and Rama Rau, Y.N. (1964), "Experimental investigation of thick, cylindrical antenna", New Mexico State University, University Park, N.M., Tech. Rept. 22.

Rama Rao, B. (1965), "Current distribution and impedance of an antenna in a parallel-plate region", Proc. IEE, 112, 259-268.

Ramo, S., Whinnery, J.R. and Van Duzer, T. (1965), Fields and Waves in Communication Electronics, John Wiley and Sons, New York.

Richmond, J.H. (1965), "Digital computer solutions of the rigorous equations for scattering problems", Proc. IEEE 53, 796-804.

Ross, G.R. and Fenster, P. (1968), "Members of the class of TEM-mode wire antennas with a TLIR", IEEE Intl. PGAP Symposium, Boston, Massachusetts.

Schelkunoff, S.A. (1952), Advanced Antenna Theory, John Wiley & Sons, London.

Schenck, H.A. (1967), "Improved integral formulation for acoustic radiation problems", J. Acoust. Soc. Am., 44, 41-58.

Sinclair, G. (1959), "The numerical solution of antenna and scattering problems", IRE Trans. Ant. and Prop. AP-7, 5402-5405.

Smythe, W.R. (1956), "Charged right circular cylinder", J. Appl. Phys., 27, 917-920.

Smythe, W.R. (1960), "Charged sphere in cylinder", J. Appl. Phys., 31, 553-556.

Stratton, J.A. (1941), Electromagnetic Theory, McGraw-Hill, New York.

Synge, J.L. (1948), "The general problem of antenna radiation and the fundamental integral equation, with application to an antenna of revolution - Part II", Q. App. Math. 6, 133-156.

Ting, C.Y. (1969), "Theoretical study of a cylindrical antenna with a hemispherical cap", IEEE Trans., AP-17, 715-721.

Ting, C.Y. and King, R.W.P. (1970), "The dielectric-filled tubular monopole", IEEE Trans., AP-18, 604-610.

Vasil'ev, E.N. (1959), "Excitation of a smooth perfectly conducting solid of revolution - I & II", Iz. VUZ., Radiofizika, 2, 588-601.

Vasil'ev, E.N. (1965), "A function encountered in diffraction theory", [Translated from Zh. vychisl. Mat. mat. Fiz., 5, 841-851].

Vasil'ev, E.N. and Seregina, A.R. (1963), "The excitation of a thick cylinder of finite length", Radiotekh. Electron., 8, 1972-1979.

Vasil'ev, E.N., Malushkov, G.D. and Falunin, A.A. (1967a), "Integral equations of the first kind in some problems of electrodynamics", Soviet Phys. - Tech. Phys., 12, 303-310 [Translated from Zhurnal Tekhnicheskoi Fiziki, 37, 421-429] .

Vasil'ev, E.N., Malushkov, G.D. and Falunin, A.A. (1967b), "Excitation of an impedance structure in the form of a solid of revolution", Soviet Phys. - Tech. Phys., 12, 311-317 [Translated from ZhTF, 37, 431-439].

Wait, J.R. (1959), "Earth currents near a monopole antenna with symmetrical top-loading", J. Research NBS 62D, 247-255.

Wait, J.R. (1969a), "Electromagnetic radiation from conical structures", in Collin, R.E. and Zucker, F.J. (editors), Antenna Theory: Part I, McGraw Hill, New York, 483-559.

Wait, J.R. (1969b), "Characteristics of antennas over lossy earth", in Collin, R.E. and Zucker, F.J. (editors), Antenna Theory: Part II, McGraw Hill, New York, 386-437.

Wallenberg, R.F. and Harrington, R.F. (1969), "Radiation from apertures in conducting cylinders of arbitrary cross section", IEEE Trans. AP-17, 56-62.

Waterman, P.C. (1965), "Matrix formulation of electromagnetic scattering", Proc. IEEE 53, 805-812.

Waterman, P.C. (1969a), "Scattering by dielectric obstacles", Alta Frequenza, 38, (Speciale), 348-352.

Waterman, P.C. (1969b), "New formulation of acoustic scattering", J. Acoust. Soc. Am. 45, 1417-1429.

Waterman, P.C. (1971), "Symmetry, unitarity, and geometry in electromagnetic scattering", Phys. Rev. D-3, 825-839.

Watt, A.D. (1967), V.L.F. Radio Engineering, Pergamon, Oxford.

Whiteside, H. and King, R.W.P. (1964), "The loop antenna as a probe", IEEE Trans., AP-12, 291-297.

Williamson, J.O. (1971), "Impedance measurements on electrically thick monopoles", Final year B.E.(Hons) project, Electrical Engineering Dept, University of Canterbury, New Zealand.

Wu, T.T. (1962), "Input admittance of infinitely long dipole antennas driven from coaxial lines", J. Math. Phys., 3, 1298-1301.

Wu, T.T. (1963), "Input admittance of linear antennas driven from a coaxial line", J. Res. NBS 67D, 83-89.

ADDITIONAL REFERENCES (UNQUOTED)

Harrington, R.F. and Mautz, H.R. (1972), "Radiation and scattering from loaded bodies of revolution", Appl. Sci. Res., 25, in press.

Jong, G. de (1972), "Scattering by a perfectly conducting cylindrical obstacle in a rectangular waveguide", Int. J. Electronics, 32, 153-167.

Knepp, D.L. and Goldhirsh, J. (1972), "Numerical analysis of electromagnetic radiation properties of smooth conducting bodies of arbitrary shape", IEEE Trans., AP-20, 383-388.

Vasil'ev, E.N. and Seregina, A.R. (1971), "A method of calculating the near field of a dipole antenna", Radio Engineering & Electronic Physics 16, 930-935 (English Translation).